Université de Montréal

Déterminants structuraux et moléculaires de la sélectivité fonctionnelle du récepteur β2-adrénergique

par Louis-Philippe Picard

Département de biochimie et médecine moléculaire

Faculté de Médecine

Thèse présentée
en vue de l'obtention du grade de Philosophiae Doctor (Ph.D.)

en biochimie

Janvier, 2019

Résumé

Les récepteurs couplés aux protéines G (RCPGs) forment la plus grande famille de récepteurs membranaires. En raison de leur grande variété de ligands ainsi que leur capacité à activer plusieurs voies de signalisation, ils sont impliqués dans une grande variété de processus biologiques et sont par conséquent des cibles thérapeutiques de choix pour plusieurs conditions pathologiques. Il a été démontré que le même RCPG peut activer plusieurs voies de signalisation et que différents ligands, du même RCPG, peuvent différentiellement activer ces dernières; concept connu sous le nom de signalisation biaisée du ligand. Ces découvertes ouvrent la possibilité de développer des médicaments qui activent de façon spécifique les voies de signalisation thérapeutiques tout en évitant celles menant aux effets secondaires. Cependant, les mécanismes qui gouvernent la signalisation biaisée du ligand demeurent mal connus.

Le premier objectif de ma thèse fut de développer un capteur de conformation pour le récepteur β2-adrénergique (β2AR), un RCPG prototypique, ainsi que de caractériser les changements conformationnels induits par différents ligands et effecteurs. Les résultats ont démontré la stabilisation de différents ensembles de conformations pour les ligands non biaisés et les ligands biaisés contre la β-arrestine.

Le deuxième objectif de ma thèse fut d'identifier les points de contact entre le récepteur et son ligand responsable de la sélectivité fonctionnelle. Pour ce faire, nous avons comparé les interactions entre le récepteur et le ligand complet épinéphrine et ceux entre le récepteur et le ligand partiel et biaisé salmétérol dans les structures cristallines du β2AR. À partir de cette analyse, nous avons identifié un réseau d'interactions polaires différent entre les deux ligands

et confirmé le rôle de ce réseau dans la signalisation biaisée du ligand via une étude de mutagenèse.

Le dernier objectif de ma thèse fut d'étudier le rôle de résidus connectant des motifs structuraux importants pour l'activation des RCPGs, connus sous le nom de « microswitchs », dans la signalisation biaisée. Plus spécifiquement, l'étude s'est portée sur le résidu L124$^{3.43}$ du β2AR qui forme des interactions avec le motif PIF et le motif NPxxY. Les résultats ont démontré qu'une perte des interactions entre cette position et les deux motifs se traduit par un gain d'activité constitutive pour Gs et une perte de recrutement de la β-arrestine ainsi qu'une perte de changement de conformation induit par les ligands. Par contre, le gain d'interactions entre la position 124 et les motifs PIF et NPxxY se traduit par un gain de recrutement de la β-arrestine et de changements conformationnels induits par les ligands biaisés. Ces données suggèrent que le lien entre le PIF et NPxxY est important pour la sélection des voies de signalisation engagées par le ligand.

L'ensemble de ces résultats ont permis d'identifier des changements conformationnels différents entre les ligands non biaisés et biaisés ainsi que d'identifier deux régions importantes pour l'activation spécifique de voies de signalisation menant à une meilleure compréhension des mécanismes régulant la signalisation biaisée.

Mots clés : récepteurs couplés aux protéines G (RCPGs), récepteur β2-adrénergique (β2AR), signalisation cellulaire, structure, signalisation biaisée, biocapteur.

Abstract

G proteins-coupled receptors (GPCRs) form the largest family of membrane receptor. Due to their variety of ligands and their capacity to activate several signaling pathways, they are involved in various biological processes and are a target of choice for the development of drugs in many clinical indications. It has been shown that a given GPCR can activate several pathways and that different ligands of the same GPCR can differentially activate these pathways, a concept known as ligand biased signaling. These discoveries open the possibility to generate drugs that selectively activate the therapeutically relevant pathways while avoiding the one leading to side effects. However, the mechanisms leading to bias signaling remains unclear.

The first objective of my thesis was to develop a conformational sensor of the β2-adrenergic receptor (β2AR), a prototypical GPCR and to characterize the conformational changes induced by different ligands and effectors. The results have shown the stabilization of different conformation ensembles for unbiased ligands and ligands biased against β-arrestin.

The second objective of my thesis was to identify the interactions between the receptor and the ligand leading to functional selectivity. To achieve that objective, we did a structural comparison between the epinephrine and salmeterol bound crystal structures. The analysis has revealed a network of polar interactions that might help stabilize the binding pocket contraction. The role of these residues has been confirmed by a mutagenesis study.

The last objective of my thesis was to study the role of residues connecting structural motifs important for GPCR activation, known as “microswitches”, for ligand biased signaling. More specifically, the study was on the residue L124$^{3.43}$ of the β2AR that forms interactions with the

PIF and NPxxY motifs. The results have shown that a loss of interaction between the position 124 and the two motifs lead to a gain of constitutive activation of Gs and a loss of β-arrestin recruitment and observed conformational changes upon ligand stimulation. In contrast the gain of interaction between the two motifs and the position 124 lead to increased β-arrestin recruitment and observed conformational changes induced by bias ligands. These data suggest that the link between the PIF and NPxxY motifs is important for the selection of which pathways are activated by the receptor.

The results of the three projects have allowed the identification of different conformational changes between unbiased and biased ligands and the identification of two regions playing an important role for specific activation of β-arrestin leading to a better understanding of mechanisms governing ligand bias signaling.

Key words: G proteins-coupled receptors (GPCRs), β2-adrenergic receptor (β2AR), structure, ligand biased signaling, biosensors, cell signaling.

Table des matières

Liste des Figures

Liste des abréviations

AKP	Phosphatase alkaline
AKT	Protéine Kinase B
AMPc	Adénosine monophosphate cyclique
AP2	Protéine adaptatrice de type 2
ARF	ADP-ribosylation factor
ASK1	Apoptosis signal-regulating kinase 1
ATP	Adénosine triphosphate
BRET	Transfer d'énergie de bioluminescence
CDK	Kinase dépendante des cyclines
COLT	Coltérol
c-RAF	RAF proto-oncogene serine/threonine protein kinase
CRYO-EM	Microscopie cryo-électronique
c-SRC	Proto-oncogene tyrosine-protein kinase SRC
C-ter	Parti Carboxi-terminal d'une chaine peptidique
CyOFP	Protéine fluorescente orange-cyan (Cyan-Orange Fluorescent Protein)
CyRFP	Protéine fluorescente rouge-cyan (Cyan-Red Fluorescent Protein)
DAG	Diacylglycérol
DEER	Double electron electron resonance
eBFP	Protéine fluorescente bleu (Blue Fluorescent Protein)
ECL	Boucle extracellulaire
EGFR	Récepteur à l'EGF(Epidermal Growth Factor)
EPAC	Protéine d'échange directement activée par l'AMPc
EPI	Épinéphrine
EPR	Résonance électronique paramagnétique
ERK	Extracellular signal-regulated kinase
FRET	Transfer d'énergie de fluorescence

GAP	Protéine activatrice de l'activité GTPase
GDP	Guanosine diphosphate
GEF	Facteur d'échange du guanosine
GIRK	G protein-coupled inwardly-rectifying potassium channel
GPCRdb	Banque de donnée GPCRdb. Il s'agit d'une ressource en ligne.
GRK	Protéine Kinase des récepteurs couplés aux protéines G
GTP	Guanosine triphosphate
H8	Hélice 8
ICL	Boucle intracellulaire
IGFR	Insulin-like growth factor receptor
IP3	Ionositol-1,4,5-triphosphate
ISO	Isoprotérénol
JNK	c-Jun N-terminal kinase
LSD	Acide lysergique diéthylamine
MAPK	Mitogen-activated protein kinase
Mdm2	Mouse double minute 2 homolog
MEK1	MAPK/ERK kinase
MKK	MAPK kinase
Nb	Nanobody
Nluc	Nano-luciférase
N-term	Parti Amino-terminal d'une chaine peptidique
PDB	Protein data bank
PDE	Phosphodiesterase
PDGFR	Platelet-derived growth factor receptor
PI3K	Phosphoinositide 3-kinase
PIP2	Phosphatidylinosital-4,5-diphosphate
PKA	Protéine kinase A
PKC	Protéine kinase C

PLC	Phospholipase C
PP2A	Protéine Phosphatase 2A
PP2B	Protéine Phosphatase 2B
Rab	Protéine de liaison associé à Ras
RCPG	Récepteur couplé aux protéines G
RGS	Régulateurs de la signalisation des protéines G
RhoGEF	Facteur d'échange du guanosine de la protéine Rho
Rluc	Luciférase provenant de *Renilla*
RMN	Résonance Magnétique Nucléaire
RTK	Récepteur à activité tyrosine kinase
SALB	Salbutamol
SALM	Salmétérol
SNX1	Sorting nexin family member 1
TM	Domaine transmembranaire
YFP	Protéine fluorescente jaune (Yellow Fluorescent Protein)

Récepteurs couplés aux protéines G

$5HT_{2B}$	récepteur de la sérotonine $5HT_{2B}$
A2AR	récepteur de l'adénosine de type A2a
AT1R	récepteur de l'angiotensine II de type 1
CB1R	récepteur canabinoide de type 1
D2R	récepteur dopaminergique de type 2
M2R	récepteur muscarinique de type 2
PAR1	récepteur activé par les protéases de type 1
V2R	récepteur de la vasopressine de type 2
β2AR	récepteur β2 adrénergique

Acide aminé	code à trois lettres	code à une lettre
Alanine	Ala	A
Arginine	Arg	R
Asparagine	Asn	N
Aspartate	Asp	D
Cystéine	Cys	C
Glutamine	Gln	Q
Glycine	Gly	G
Histidine	His	H
Isoleucine	Ile	I
Leucine	Leu	L
Lysine	Lys	K
Méthionine	Met	M
Phénylalanine	Phe	F
Proline	Pro	P
Sérine	Ser	S
Thréonine	Thr	T
Tryptophane	Trp	W
Tyrosine	Tyr	Y
Valine	Val	V

Remerciements

Je tiens tout d'abord à remercier le Dr. Michel Bouvier de m'avoir accueilli dans son laboratoire et m'avoir fourni tout le soutien dont j'ai eu besoin pour réaliser mes projets.

Par la suite, je voudrais remercier tous les membres du laboratoire que j'ai côtoyé lors de ma thèse. Ce parcourt ne se fait pas seul et être accompagné par des gens toujours prêts à aider simplifie beaucoup la vie et aide à garder la bonne humeur malgré les différents échecs que nous rencontrons.

Je tiens aussi à remercier plus particulièrement Christian Le Gouill pour nos discussions scientifiques et ces conseils, qui m'ont permis de prendre du recul et d'avoir une meilleure vision globale sur mes projets. C'est un modèle pour tout scientifique.

Je voudrais aussi remercier le Dr. Brian Kobilka ainsi que les membres de son laboratoire. Une partie de cette thèse n'aurait pas été envisageable sans cette collaboration.

Finalement, j'aimerais remercier les organismes qui ont financé mes recherches tout au long de ma thèse via différentes bourses d'excellences; le Fond de recherche du Québec- Santé (FRQS), la faculté des études supérieures et postdoctorales de l'Université de Montréal (FESP) et les instituts de rechercher en santé du Canada (IRSC).

Introduction

Récepteurs couplés aux protéines G

Généralités

Les récepteurs couplés aux protéines G (RCPG), aussi appelés récepteur à sept domaines transmembranaires, sont des protéines membranaires capables de transmettre des stimuli du milieu extracellulaire vers le milieu intracellulaire. Cette transduction de signal se produit, de manière simplifiée par la liaison de ligands qui stabilisent les changements conformationnels menant à l'activation de protéines G trimériques et la production de seconds messagers, menant à une réponse cellulaire.

Les RCPGs forment la plus grande famille de récepteurs membranaires avec un peu plus de 800 membres dans le génome humain, soit environ 4% de ce dernier[1]. Cette grande variété de récepteurs permet de répondre à une grande variété de stimuli incluant les photons, ions, hormones aminergiques, lipides, peptides et même à de petites protéines. Cette grande variété de ligands potentiels confère au RCPGs un rôle central dans plusieurs processus biologiques tels que la vision, le goût, l'odorat, la chimiotaxie, les processus de neurotransmission, les fonctions cardiaques et autres. Par conséquent, un grand nombre de pathologies sont reliées à des dysfonctionnements des RCPGs et leur signalisation incluant les troubles métaboliques, reproductifs et, immunologiques ainsi que les maladies cardiovasculaires et les cancers[2]. Ainsi, environ 30% des médicaments sur le marché ciblent les RCPGs.

L'étude des mécanismes moléculaires des RCPGs a commencé dans les années 70 et 80 alors que les nouvelles techniques biochimiques et de biologie moléculaire ont permis la purification[3-7] et le clonage [8-11]des premiers RCPGs. Ces innovations ont permis l'étude au niveau moléculaire des RCPGs, notamment par l'expression des récepteurs en système hétérologue[12] menant à notre compréhension actuelle des RCPGs. Tout d'abord, le clonage du récepteur β2-adrénergique (β2AR) a révélé des similarités de séquence avec la rhodopsine suggérant la présence d'une famille de récepteurs membranaires. Par la suite, le séquençage du génome humain a permis l'identification de plusieurs autres RCPGs. Plus tard dans les années 2000 les avancés dans le domaine de la biologie structurale a permis la résolution des structures cristallographiques de la rhodopsine (2000) et du β2AR (2007) toute deux dans la forme inactive des récepteurs permettant de reconnaitre les similarités entre les deux protéines qui ont servi de modèle pour l'étude structurale des RCPGs (voir section Structure des RCPGs). Depuis, plus de 260 structures cristallographiques de RCPGs (GPCRdb.org) ont été résolues dans les formes inactives et actives pour différents récepteurs permettant une meilleure compréhension structurale de cette famille de récepteurs membranaires jouant un rôle central dans les divers processus biologiques.

Classification

Modèle de Kolakowski

Avec plus de 800 récepteurs différents, plusieurs systèmes de classification des RCPGs ont été utilisés. Le modèle de Kolakowski a été développé en 1994 et fut un des premiers systèmes de classification des RCPGs et est basé sur les similarités de séquences. Dans ce système de classification, les RCPGs sont regroupés en sept groupes A-F et O[13]. Les classes D-E et O ne

sont pas présentes chez les mammifères et ne seront pas discutées dans cette section. La classification de Kolakowski a servi de base pour plusieurs modèles subséquents, dont celle de la banque de données GPCRdb[14], où de nouvelles connaissances ont été prises en considération.

La classe A « Rhodopsin-like » est la plus grande classe de RCPG et comprend environ 80% de ces derniers. Les récepteurs faisant partie de cette classe se caractérisent par un domaine N-term assez court et par la présence de séquence consensus formant des motifs d'activation bien définis, tel que le motif E/DRY au bas du TM3 et le motif NPxxY dans le TM7 (ces motifs seront détaillés dans une autre section). En générale, les récepteurs de cette classe se lient à des ligands de petite taille tels que les lipides, les hormones aminergiques telles que l'adrénaline et la dopamine ou encore à de petits peptides. La position du site de liaison des différents ligands est conservée et est présente du côté extracellulaire des 7 TMs. Dû à l'abondance de cette classe, elle est la plus étudiée et les sections subséquentes de la thèse porteront uniquement sur celle-ci.

La classe B peut se sous-diviser en deux sous-classes soit les « Secretine-like » qui lient des peptides de grande taille, tels que le glucagon, et les récepteurs d'adhésion. L'homologie observée pour ces récepteurs avec les récepteurs de classe A est plutôt faible. D'ailleurs, les motifs retrouvés chez les récepteurs de classe A sont absents. Toutefois, différents motifs d'activation ont aussi été identifiés dans ces récepteurs et ont un rôle similaire à ceux observés dans la classe A. Une autre caractéristique des récepteurs de classe B est un domaine N-term relativement long formant une structure tridimensionnelle conservée impliquée dans la liaison du ligand.

La classe C « Metabotropic Glutamate receptors-like » comprend les récepteurs du glutamate, du calcium, les récepteurs GABAergiques. La principale caractéristique de ces récepteurs est la présence d'un très grand domaine N-term qui se replie en deux lobes formant ainsi le site de liaison du ligand. Contrairement aux récepteurs de classe A et B, la dimérisation des récepteurs de classe C est essentielle pour leur activation.

Finalement, la dernière classe présente chez l'humain, la classe F, est composée des récepteurs homologues aux protéines « Frizzled/Smoothened ». Ces protéines sont impliquées dans le contrôle de la voie Wnt et par conséquent de nombreux processus tels que la polarité cellulaire et le développement embryonnaire. Durant plusieurs années, ces récepteurs ont été considérés comme non RCPG, puisque leur couplage aux protéines G n'avait pas été démontré. Ce n'est que tout récemment que ce problème a été résolu[15].

Modèle GRAFS

Le modèle de classification GRAFS repose sur une analyse phylogénétique des RCPG du génome humain [16]. Cette analyse considère le degré de similarité des différents RCPG au niveau de leurs TMs. Dans ce système, les récepteurs sont classifiés en cinq familles différentes, soit Glutamate (G), Rhodopsine (R), Adhésion (A), Frizzled (F) et Sécrétine (S). Cette classification diverge de la classification de Kolakowski par deux caractéristiques principales. Premièrement, la séparation de la classe B en deux familles distinctes, soit Sécrétine (S) et Adhésion (A). Deuxièmement, par la division de la famille de la Rhodopsine en quatre sous-branches : α, β, γ et δ.

Signalisation

Signalisation Canonique des RCPGs par les protéines G hétérotrimériques

La signalisation classique des RCPGs repose sur la liaison d'un agoniste qui va stabiliser les changements conformationnels du récepteur au niveau cytoplasmique menant à l'activation des protéines G hétérotrimérique. Les protéines G hétérotrimériques sont composées de trois sous-unités : α, β et γ. Le complexe est associé lorsqu'il est inactif et la sous-unité Gα est liée au GDP (guanosine diphosphate). Lors du processus d'activation le récepteur agit en tant que GEF (facteur d'échange du guanosine) en catalysant l'échange du GDP pour le GTP (guanosine triphosphate). Suivant cet échange, les sous-unités Gβγ se dissocient de la sous-unité Gα. La protéine G étant activée, chacune de ses deux sous-unités, Gα et Gβγ peuvent réguler divers effecteurs et déclencher ainsi différentes voies de signalisations. La protéine G est désactivée par son activité GTPase de la sous-unité Gα permettant l'hydrolyse du GTP en GDP suivie de la reformation de l'hétérotrimère inactif. Différentes protéines régulatrices des diverses voies de signalisation peuvent réguler l'activité GTP de la sous-unité Gα et ainsi moduler la signalisation de cette dernière. C'est notamment le cas des régulateurs de la signalisation des protéines G (RGS) qui agissent en tant que protéine activatrice de l'activité GTPase (GAP) en accélérant l'activité GTPase de la sous-unité Gα.

Signalisation des sous-unités Gα

Dans le génome humain, il existe 16 gènes pour les différentes sous-unités Gα. Ces gènes sont divisés en quatre familles en fonction de la similarité de séquence, et par conséquent leur fonction : la famille Gs, la famille Gi/o, la famille Gq et la famille G12/13.

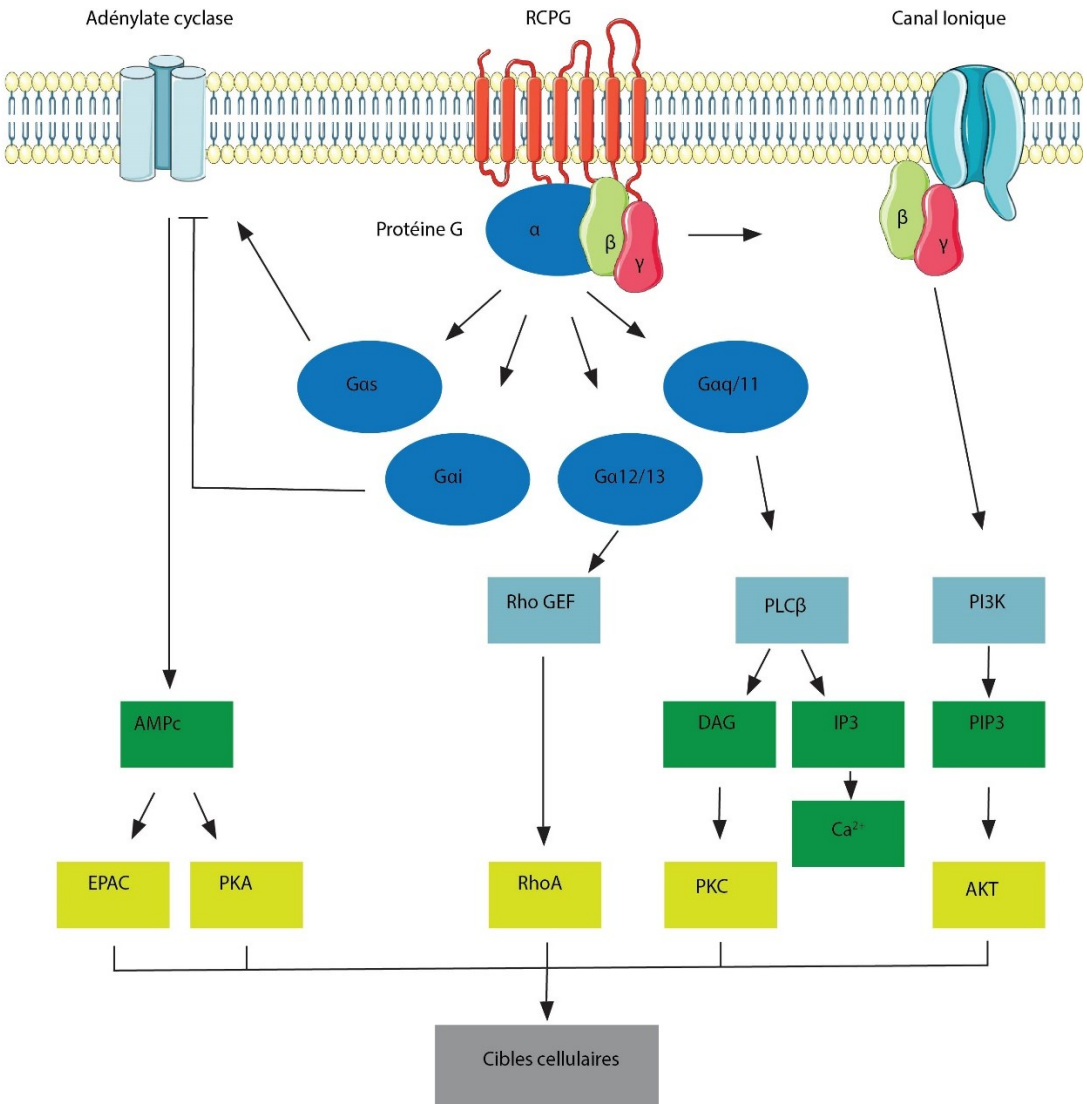

Figure 1. Illustration schématique de la signalisation des protéines G. Les différentes familles de protéine G activent différents effecteurs qui définissent les voies de signalisation engagées. Les différents effecteurs primaires activés par les protéines G sont illustrés en bleu pâle. Ces derniers font mener à la production de seconds messagers, illustrés en vers. Finalement, les seconds messagers activent différents effecteurs, en jaune, menant à différentes réponses cellulaires.

Tout d'abord, la famille Gs (stimulatrice) est composée de Gαs et Gαolf. Ces deux sous-unités Gα activent l'adénylate cyclase, une enzyme qui catalyse la production d'adénosine monophosphate cyclique (AMPc) à partir d'adénosine triphosphate (ATP)[17]. L'AMPc sert de second messager et peut activer plusieurs effecteurs tels que la protéine kinase A (PKA) qui

phosphoryle plusieurs cibles dont les RCPGs[18,19], pour la désensibilisation, et active d'autres régulateurs du métabolisme[20]. L'AMPc active aussi l'EPAC (exchange protein directly activated by cAMP) qui agit comme GEF pour l'activation de petites protéines G[21].

La famille Gi/o(inhibitrice) est composée de Gαi1, Gαi2, Gαi3, GαO, Gαz, Gαt et Gαgust. Ces sous-unités Gα inhibent la production d'AMPc. Cependant, à l'inverse de la famille Gs où les différents membres ont le même mécanisme d'action, la stimulation de l'adénylate cyclase, l'inhibition peut se faire de manière différente. Dans le cas de Gαi1, Gαi2, Gαi 3, GαO et GαZ le mécanisme moléculaire est une inhibition directe de l'adénylate cyclase[22,23]. Finalement, Gαt et Gαgust régulent l'activité de cGMP-phosphodiestérase (cGMP-PDE)[24-26].

La famille Gq, composée de Gαq, Gα11, Gα14 et Gα15, active la phospholipase C β (PLCβ)[27]. PLCβ est une enzyme qui clive le phosphatidylinosital-4,5-diphosphate (PIP2) en diacylglycérol (DAG) et ionositol-1,4,5-triphosphate (IP3). DAG et IP3 servent de seconds messagers en induisant la relâche des réserves de calcium du réticulum endoplasmique et en activant la protéine kinase C(PKC).

Finalement, la famille G12/13 est composée de Gα12 et Gα13. Ces sous-unités Gα activent RhoGEF permettant la régulation des petites GTPase de la famille RhoA[28]. Le rôle principal des RhoA est la régulation du cytosquelette d'actine pour l'adhésion et la migration cellulaire[29].

Signalisation des sous-unités Gβγ

Chez l'Homme, il y a 5 différentes sous-unités Gβ et 12 différentes sous-unités Gγ, donnant la possibilité de former une énorme variété de dimères Gβγ[30]. Originalement, le dimère Gβγ était considéré comme une sous-unité inhibitrice de la sous-unité Gα[31]. Cependant, de nombreux travaux ont démontré que la sous-unité Gβγ, une fois la protéine G activée, possède la capacité d'activer de nombreuses voies de signalisation indépendamment de la sous-unité Gα. Notamment, le rôle de la sous-unité Gβγ a été démontré pour l'activation des canaux GIRK[32], menant à la production d'un courant potassique, mais aussi dans l'inhibition des canaux calcique[33] et potassique[34], dans l'activation de PLC[35], de PI3K[36], des MAPK[35] et de l'adénylate cyclase[36,37].

Protéines kinases de RCPGs (GRK)

Les protéines kinases des RCPGs (GRKs) forment une famille d'enzyme qui phosphoryle les RCPGs suite à leur activation ainsi que d'autres cibles cellulaires[38]. La phosphorylation des RCPGs se fait sur certains résidus sérines ou thréonines de la troisième boucle intracellulaire (ICL3) et de la queue C-term du récepteur. La famille des GRKs est formée de sept protéines différentes classées en trois sous-familles en fonction de leur homologie de séquence.

Les GRKs ont une structure conservée formée de trois domaines. En N-term de la protéine, il a y a un domaine d'homologie aux RGS (RH), puis le domaine catalytique au centre de la séquence, tous deux impliqués dans la désensibilisation et l'endocytose des RCPGs[39-44], et un domaine C-term servant à la localisation des GRKs. Les domaines C-term sont variables et la localisation des différentes GRK est déterminée par différents mécanismes.

Le domaine C-term de la sous-famille de GRK1 contient un site de farnésylation permettant de les ancrer à la membrane [45].

Les GRKs de la sous-famille de la GRK2 sont majoritairement cytoplasmiques. Elles sont recrutées à la membrane grâce à leur domaine PH qui interagit avec la sous-unité Gβγ des protéines G suite à leur activation ainsi qu'avec le PIP2[46]. L'activation de la protéine G hétérotrimérique menant à la séparation des sous-unités Gα et Gβγ a longtemps été considérée essentielle pour le recrutement de GRK2-3 aux RCPGs. Cependant, il a été démontré récemment que GRK2 ne nécessite pas l'activation de la protéine G hétérotrimérique ou du dimère Gβγ pour phosphoryler le récepteur de la dopamine de type 2 (D2R)[47].

Finalement, les GRKs de la sous-famille GRK4 sont elles aussi ancrées à la membrane plasmique. Pour GRK4 et GRK6, leur localisation à la membrane se fait via un site de palmitoylation [48,49] tandis que pour GRK5 la localisation à la membrane plasmique dépend d'un motif polybasique[50] .

L'activité kinase des GRK peut être modulée par différent mécanisme. Tout d'abord, PKA peut phosphoryler GRK2 en position S685 ce qui diminue l'affinité de cette dernière pour Gβγ et ainsi inhibe la phosphorylation des RCPGs par GRK2[51]. Par la suite, ERK1/2 peut augmenter l'affinité entre GRK2 et Gβγ en phosphorylant le résidu S670[52,53]. Finalement, différentes protéines peuvent lier directement certaines GRKs et moduler leur fonction. C'est notamment le cas pour PKC [54], c-Src[55] , CDK2[56] et mdm2[57].

Les arrestines

La famille de protéines arrestines est formée par quatre gènes différents chez l'humain: arrestine 1-4. Les arrestines 1 et 4 sont exprimées dans le système visuel tandis que les arrestines 2 et 3, aussi appelées β-arrestine 1 et 2 respectivement, sont ubiquitaires. Initialement, ces protéines ont été identifiées comme régulateur de l'activité des RCPGs[58,59], plus particulièrement pour la désensibilisation et l'internalisation des récepteurs. Plus récemment, il a aussi été démontré que les arrestines peuvent servir de protéines d'échafaudage pour nombre de voies de signalisation indépendante des protéines G tel que l'activation des MAPKs[60].

Signalisation des arrestines

Le premier effecteur des β-arrestines à avoir été identifié est la protéine kinase c-Src. L'association entre c-Src et la β-arrestine1 résulte de l'interaction du domaine catalytique de c-Src avec le domaine SH3 (domaine d'interaction homologue aux Scr de type 3) de la β-arrestines[61]. La liaison de cette protéine à la β-arrestine suite à l'activation d'un RCPG mène à l'activation de ERK1/2[61,62], une protéine de la famille des MAPK. Plusieurs RCPGs activent la voie des MAPK via les β-arrestines. Cette activation résulte de la formation de complexes entre les MAPK et la β-arrestine. Par exemple, l'AT1R et le β2AR induisent la formation d'un complexe entre la β-arrestine2 et le complexe de signalisation MAPK, c-Raf1-MEK1-ERK1/2 [63-65]. De plus, la formation d'un complexe entre la β-arrestine2 et MAPK, ASK1-MKK4-JNK3 peut être induit par le récepteur AT1R[66].

Il a aussi été démontré que les β-arrestines peuvent activer les récepteurs à activité tyrosine kinase (RTK), représentant une autre façon d'activer les MAPKs. Parmi les différents RTKs activés par les β-arrestines, on retrouve les récepteurs PDGFR[67], EGFR[68] et IGFR[69]. Parmi les mécanismes d'activation des RTKs par les arrestines, on retrouve l'engagement de c-Src aux arrestines[70-73] et l'activation de métalloprotéases de la matrice extracellulaire (MMP) qui clivent les protoligands des RTKs[74].

Non seulement la transactivation des RTKs par la β-arrestine peut mener à l'activation des MAPKs, mais cette transactivation peut aussi induire l'activation de PI3K via l'IGFR[75] et l'endocytose de ce dernier[76]. L'activation de PI3K, mène à l'activation de AKT. L'activation de AKT par les RCPGs a été démontrée pour plusieurs récepteurs dont le récepteur de la ghréline[77] et PAR1[78]. Il a aussi été démontré que la β-arrestine peut aussi interagir directement avec AKT en formant un complexe avec c-SRC et AKT ce qui est important pour l'activation de AKT par le récepteur à l'insuline[79]. Il a été proposé que l'activation de AKT par la β-arrestine se fait via le recrutement du complexe arrestine-c-Src-AKT au RTK[79].

Non seulement les arrestines peuvent activer la voie PI3K/AKT via les RTKs, mais elles pourraient aussi inhiber cette même voie de signalisation. En effet, il a été démontré que la β-arrestine interagit avec PP2A[80] et que cette interaction se retrouve dans un complexe protéique β-arrestine-ATK-PP2A[81]. Par conséquent, il a été proposé que ce complexe mène à la déphosphorylation de AKT par PP2A. De plus, il a aussi été démontré que la β-arrestine interagit avec PTEN et augmente l'activité catalytique de celle-ci[82].

De plus, la β-arrestine peut interagir avec plusieurs autres protéines membranaires et les réguler. C'est notamment le cas avec les échangeurs Na+/H+ de type 1 et 5 [83,84], les canaux calciques de type v [85] et d'autres canaux ioniques[86].

Hypothèse du code de phosphorylation

Une des hypothèses les plus répandues pour expliquer la signalisation différentielle des β-arrestines est le code de phosphorylation. Suivant l'activation des RCPGs par leurs ligands, ceux-ci peuvent être phosphorylés par différentes kinases, dont celle de la famille de protéines kinase des RCPGs (GRKs). Les différentes kinases phosphorylent les domaines intracellulaires des RCPGs à différents site[87]. De plus, plusieurs études ont démontré que la phosphorylation des RCPGs par différentes GRKs, aux différents sites de phosphorylation, mène à l'activation de différentes voies de signalisation[87-91]. Par exemple, la phosphorylation du récepteur de la vasopressine de type 2 (V2R) et du récepteur de l'angiotensine II de type 1 (AT1R) par GRK2-3 favorise l'endocytose et la désensibilisation des RCPGs tandis que celle induite par GRK5-6 mène à la signalisation dépendante des β-arrestines[92,93]. Par conséquent, il a été proposé que les différents motifs de phosphorylation peuvent induire différentes conformations des β-arrestines menant à différentes voies de signalisation[94].

Régulation de la signalisation des RCPGs

Désensibilisation dépendante de la phosphorylation

Historiquement, la désensibilisation des RCPGs réfère à l'arrêt de la signalisation des protéines G hétérotrimériques où la β-arrestine joue un rôle crucial. Cependant, nous savons aujourd'hui

que les RCPGs peuvent signaliser via d'autres protéines telles que la β-arrestine (voir section signalisation des arrestines). Par conséquent, la désensibilisation des RCPGs peut être interprétée comme une transition entre la signalisation des protéines G et la signalisation des arrestines. La désensibilisation des RCPGs peut se faire via plusieurs mécanismes. Tout d'abord par la phosphorylation du récepteur. Les récepteurs peuvent être phosphorylés par deux classes de kinases soit les GRKs ou les kinases activées par les seconds messagers tels que PKA ou PKC.

Les GRKs phosphorylent spécifiquement les récepteurs activés dans la ICL3 ou en C-term (voir section protéines kinases des RCPGs), ce phénomène est connu sous le nom de désensibilisation homologue et est dépendant de la β-arrestine[95]. Suite à la phosphorylation du récepteur par les GRKs, le découplage aux protéines G hétérotrimérique se fait via le recrutement de la β-arrestine au récepteur par encombrement stérique du site de liaison des protéines G[96]. Dans ce contexte, la phosphorylation du récepteur sert à augmenter l'affinité de ce dernier pour la β-arrestine[97]. La β-arrestine ainsi activée par le récepteur peut alors recruter à son tour des enzymes qui vont dégrader les seconds messagers. Parmi ces enzymes, il y a DACK[98] et des phosphodiestérases[99] pour la dégradation de DAG et AMPc respectivement.

Les kinase PKA et PKC phosphorylent les RCPGs suivant leur activation par ces derniers. Cependant, en contraste avec les GRKs où la désensibilisation est spécifique pour les récepteurs activés, PKA et PKC peuvent phosphoryler des récepteurs inactifs et ainsi désensibiliser les vagues subséquentes de stimuli; ce qui est connu sous le nom de désensibilisation hétérologue[95,100,101]. La désensibilisation par les kinases activées par les seconds messagers n'affecte pas autant l'affinité des récepteurs pour la β-arrestine. C'est notamment le cas pour le

récepteur β2-adrénergique (β2AR) où la phosphorylation de GRK augmente de 10 fois l'affinité tandis que la phosphorylation par PKA n'affecte pas l'affinité de l'interaction[97]. De plus, la désensibilisation par les kinases activées par les seconds messagers peut aussi se faire directement en régulant la production de seconds messagers. De cette façon, les adénylate cyclase de type V et VI sont inhibés par le calcium intracellulaire et par leur phosphorylation par PKA[102]. Finalement, il a été suggéré que la phosphorylation dans la ICL3 des récepteurs peut changer le couplage de Gs vers Gi pour certains récepteurs tels que le β1AR et le β2AR[103,104].

Désensibilisation indépendante de la phosphorylation

En plus de provoquer la désensibilisation des RCPGs via la phosphorylation de ces derniers, les GRKs peuvent désensibiliser les RCPGs de façon indépendante de la phosphorylation. Il a été démontré que GRK peut former un complexe avec Gαq et Gβγ en s'insérant entre les deux sous-unités de la protéine Gq. Les changements d'orientation causés par GRK2 dans la protéine Gq découplent cette dernière des RCPGs[41,105]. De plus, GRK2 peut désensibiliser d'autres protéines G telles que Gs[106,107], et Gi[108] sans toutefois former de complexe similaire puisqu'aucune interaction entre GRK2 et Gαs et Gαi n'ont été démontré. Ces données suggèrent d'autres mécanismes de désensibilisation induits par les GRKs.

Les protéines régulatrices de la signalisation des protéines G (RGS) sont une autre famille de protéine participant à la désensibilisation des RCPGs. Ces protéines participent à l'inactivation des protéines Gα en stimulant l'activité GTPase de ces dernières[109,110]. Elles sont parfois recrutées directement au récepteur via l'ICL3 afin de réduire la signalisation de ceux-ci[111,112].

Endocytose

Dans le modèle classique de désensibilisation des RCPGs, suivant leur phosphorylation, ils sont séquestrés de la membrane plasmique via les puits de clathrine[113,114]. Les clathrines servent à former des invaginations membranaires qui sont par la suite détachées par la dynamine afin de compléter l'endocytose du récepteur. Dans ce modèle, les arrestines jouent un rôle crucial, puisque ces dernières servent de protéine d'échafaudage pour le recrutement de la protéine adaptatrice AP2 et la clatherine[115-117].

En plus, de ce modèle classique, certains RCPGs peuvent interagir directement avec la protéine AP2 qui recrute par la suite les clathrines. L'interaction directe entre AP2 et les RCPGs peut se faire via un motif tyrosine d'endocytose[118] ou un segment de huit arginines[118,119], situé en C-term du récepteur.

L'endocytose des récepteurs peut être modulée par des petites protéines G monomériques contrôlant la formation et le mouvement des vésicules. Plusieurs exemples sont disponibles. Tout d'abord, Rab5 peut participer à la formation des cages de clathrine de certains RCPGs ainsi que leur translocation aux endosomes précoces[120]. C'est notamment le cas pour le récepteur de l'angiotensine II de type 1 (AT1R), où Rab5 est directement activé par le C-term du récepteur[121]. De plus, ARF6 agit aussi en favorisant l'endocytose des RCPGs. Il a été démontré que l'activation d'une GAP de ARF6 réduit l'endocytose des RCPGs[122]. Tandis que l'activation d'une GEF de ARF6 augmente l'endocytose des RCPGs[123].

Les RCPGs peuvent aussi être internalisés de manière indépendante des clathrines. Un mécanisme alternatif se fait via la voie des calvéolines qui sont responsables de l'invagination de la membrane plasmique[124-128]. Tout comme les puits tapissés de clatherine, la séparation de ces structures de la membrane plasmique implique la dynamine afin de compléter l'endocytose. Il a été démontré que plusieurs RCPGs peuvent être internalisés via la voie des clathrines et celles des cavéolines[129-135].

Resensibilisation

Suite à la désensibilisation et endocytose des RCPGs, ceux-ci peuvent se recoupler aux protéines G, cependant, ils doivent tout d'abord être déphosphorylés et réacheminés à la membrane plasmique[136]. Cette resensibilisation nécessite la participation de nombreuses protéines telles que les AKP et les arrestines qui servent de protéine d'échafaudage pour le recrutement de phosphatase telles que PP2A et PP2B[137,138].

Adressage post-endocytique des RCPGs

Suite à l'endocytose des récepteurs, l'adressage de ces derniers doit être effectué afin de réguler leur activité. De façon générale, il y a deux possibilités, soit le recyclage de ces derniers à la surface pour une vague subséquente de stimulation, soit l'adressage vers les lysosomes pour la dégradation des récepteurs. Il a été proposé que l'affinité du récepteur pour les β-arrestines serait un des déterminants régulant l'adressage des RCPGs suite à leur internalisation[139]. Par conséquent, les RCPGs ont été classés dans la classe A ou la classe B correspondant respectivement, à une faible et forte affinité pour les β-arrestine. Les récepteurs de classe A ont une tendance à être recyclé plus facilement que ceux de classe B qui eux vont plus souvent vers la dégradation. La différence d'affinité pour les β-arrestines viendrait de la différence de

phosphorylation du domaine C-term des récepteurs[140]. De façon générale, les récepteurs de classe A démontrent une préférence pour la β-arrestine2 tandis que les récepteurs de classe B ne démontrent pas de préférence entre la β-arrestine1 et la β-arrestine2 suggérant un rôle distinct entre les différentes β-arrestines dans l'adressage post-endocytique des RCPGs. Cependant, la préférence entre les deux β-arrestine ne dicte pas de façon stricte l'adressage d'un récepteur suivant son internalisation. Plusieurs exemples où une différence entre le recrutement de β-arrestine et l'adressage du récepteur a été démontrée dans la littérature. Par exemple, l'adressage du récepteur PAR1 au lysosome ne dépendant pas de son interaction avec la β-arrestine1, mais de son interaction avec SNX1[141,142]. La β-arrestine a aussi été identifiée pour son rôle dans le recyclage des RCPGs[143-145].

En plus des β-arrestines dans l'adressage post-endocytique des RCPGs, une autre famille de protéines a été identifiée comme joueur clé de ce phénomène. Il s'agit des petites protéines G monomériques de la famille des Rabs (Ras-associated binding protein) qui peuvent lier les RCPGs[121,146-149]. Rab 4 a été identifié dans le recyclage rapide des récepteurs, tandis que Rab11 dans le recyclage lent de ces derniers[150-152]. Rab7 a été identifié pour la dégradation des récepteurs en contrôlant l'adressage vers les lysosomes[153].

Pharmacologie

La question fondamentale de la pharmacologie est la relation entre la concentration d'un ligand et son effet biologique. Pour ce faire, plusieurs modèles ont été mis de l'avant selon les connaissances de chaque époque. Ces modèles sont des outils importants pour notre compréhension des mécanismes moléculaires entourant l'activation des RCPGs. Par conséquent, la section suivante présente les modèles importants qui ont mené à notre compréhension actuelle des mécanismes d'activations des RCPGs.

Modèles analytiques

Modèle de Clark-Gaddum-Stephenson.

Ce modèle, aussi connu sous le nom de théorie de l'occupation, a été utilisé durant de nombreuses années pour expliquer l'effet d'une hormone sur son récepteur. Les hypothèses de ce modèle sont que la vitesse d'association d'un ligand est proportionnelle à la quantité de ligands et de récepteurs libre et que la vitesse de dissociation est dépendante du nombre de complexes ligand-récepteur. Dans la première étude de Clark, il a proposé que la fraction de récepteur occupé est égale à la fraction de la réponse maximale et par ce fait que la réponse maximale provient uniquement d'une occupation maximale du récepteur [154]. Cependant, en 1956, Stephenson a démontré que la réponse maximale peut varier entre différents ligands, malgré l'occupation maximum des récepteurs [155]. Ces nouveaux résultats étant en désaccord avec le modèle de Clark viennent le modifier en ajoutant que l'effet maximal d'un agoniste peut être obtenu en dessous de l'occupation maximale, que la réponse ne forme pas une relation linéaire avec le nombre de récepteurs occupés et que différents ligands peuvent avoir des

efficacités distinctes. De ce modèle, la notion d'agoniste partiel est née. Par la suite, de nombreuses recherches ont permis de modifier le modèle afin de correspondre avec les nouvelles données expérimentales. L'équation de ce modèle est donnée par la formule suivante :

$$\frac{E}{Emax} = f(\frac{[L]x\varepsilon[Rt]}{[L] + kd})$$

Où
E= efficacité du ligand
f = efficacité de couplage en fonction du stimulus
ε = efficacité intrinsèque de l'agoniste
[L] = concentration de ligand libre
[Rt] = concentration de récepteur totale
Kd = constante de dissociation

Modèle opérationnel

En 1983, Black et Leff proposent une alternative au modèle de Clark-Gaddum-Stephenson. Ce modèle repose sur le fait que la quantité de complexes ligand-récepteur ainsi que la réponse biologique observable sont saturables. Conséquemment, ils choisissent pour le développement de leur modèle une fonction hyperbolique rectangle pour bâtir leur modèle. Dans ce modèle, l'efficacité de couplage à une voie de signalisation est donnée par la constante de couplage, Ke[156]. Plus cette constante de dissociation est petite, moins de complexes ligand-récepteur sont nécessaires pour transduire la réponse. L'équation de ce modèle en incluant la loi d'action de masse est donnée par l'équation suivante:

$$E = \frac{[L]x[Rt]xEmax}{[L]([Rt] + Ke)(KdxKe)}$$

Où
E= efficacité du ligand
Emax = efficacité maximale
[L] = concentration de ligand libre
[Rt] = concentration de récepteur totale
Ke = constante de couplage du complexe ligand-récepteur
Kd = constante de dissociation

Cependant, la forme la plus utilisée de ce modèle est la forme simplifiée de l'équation où le ratio de transduction, τ, correspondant à la concentration totale de récepteur sur la constante de couplage, Ke. Le ratio de transduction est une composante intégrale du modèle et provient directement de la saturation de l'activité du complexe ligand-récepteur.

$$E = \frac{[L]x\ \tau\ xEmax}{[L](\tau + 1) + kd}$$

Où
E= efficacité du ligand
Emax = efficacité maximale
[L] = concentration de ligand libre
τ = ratio de transduction [Rt] /Ke
Kd = constante de dissociation

Le modèle peut alors être interprété en fonction du ratio de transduction où plus le ratio est élevé, plus le couplage du complexe ligand-récepteur à la voie de signalisation est important. Un des avantages de ce modèle est que la valeur relative du ratio de transduction est constante entre les différents agonistes ce qui le rend extrêmement utile pour comparer différents

ligands[157]. De plus, ce modèle sera modifié pour calculer le biais de signalisation entre différentes voies de signalisation (voir section sur la signalisation biaisée).

Modèles mécanistiques

Modèle à deux étapes

Ce modèle repose sur la notion qu'un changement de conformation du récepteur a lieu suite à la liaison du ligand. En 1957, Del Castillo et Katz s'inspirent du modèle enzymatique de Michaelis-Menten et proposent la formation d'un complexe intermédiaire ligand-récepteur inactif [158]. La réponse obtenue dépend alors de la vitesse des réarrangements conformationnels du récepteur induit par le ligand.

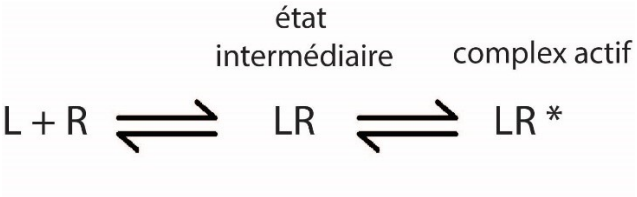

Figure 2. Modèle à deux étapes. Le principe du modèle à deux étapes comprend le ligand (L) qui s'associe avec son récepteur (R) afin de former le complexe intermédiaire (LR). Des changements structuraux sont alors nécessaires afin d'atteindre le complexe active (LR*). Ce modèle reprend les équations du modèle enzymatique de Michaelis-Menten. Figure adaptée de [158]

Modèle à deux états

Les équations de ce modèle sont basées sur la théorie de l'allostérie développée par Monod, Wyman et Changeux[159]. Le modèle à deux états repose sur la notion que les récepteurs sont en équilibre entre une conformation inactive et une conformation active. Selon ce modèle, un agoniste possède une plus grande affinité pour la conformation active que la conformation

inactive stabilisant ainsi la conformation active. Par conséquent, la puissance et l'efficacité sont dépendantes des vitesses de changement de conformation entre la forme active et la forme inactive ainsi que de l'affinité de l'agoniste pour ces deux conformations. Par conséquent, l'efficacité d'un ligand dépend de l'affinité relative de la forme active par rapport à la forme inactive. Ce modèle développé pour les canaux ioniques a été validé pour les RCPGs par plusieurs études[160].

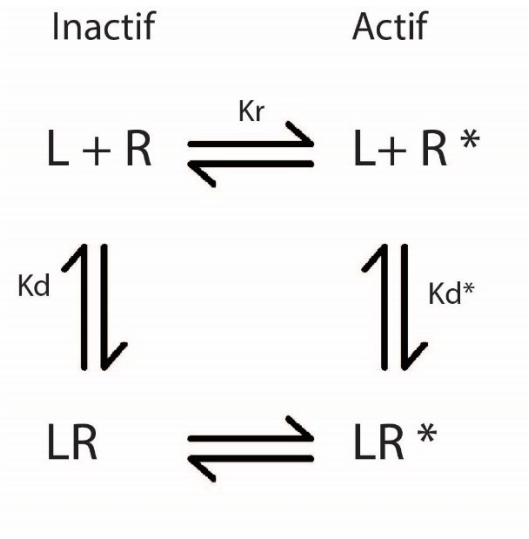

Figure 3. Modèle à deux états. Dans le modèle à deux états, le récepteur possède deux conformations différentes. La conformation R inactive et la conformation R* active. Ces deux conformations sont à l'équilibre selon la constante Kr. Les ligands peuvent alors lier le récepteur directement dans un ou l'autre de ces deux états selon les constantes Kd et Kd*. La différence d'affinité pour l'état actif ou inactif définit alors la nature du ligand. Figure adaptée de [160]

Modèles complexe ternaire

Modèle ternaire simple

Dans les années 70, plusieurs découvertes viennent perturber les modèles classiques précédents. Parmi ces découvertes, il y a l'engagement d'effecteurs au récepteur [18], l'inhibition de la réponse par le GDP [18,161,162], un site de haute et basse affinité pour les agonistes sensibles au nucléotide

guanine[163]. Avec ces nouvelles connaissances, un modèle, où l'effet du GTP et GDP est causé par la modulation allostérique d'un effecteur liant ces derniers, est proposé. Ce modèle peut être schématisé comme suit :

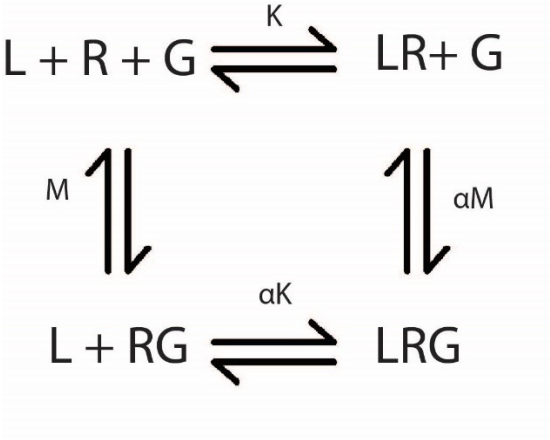

Figure 4. Modèle ternaire simple. Dans ce modèle, le ligand (L) ainsi que la protéine G (G) se lient au récepteur (R) afin de former des complexes. Les différents états possibles sont en équilibre selon les constantes K et M. L'effet allostérique entre la protéine G et le ligand est décrit par le facteur α. Figure adaptée de [162]

Tel que visualisé dans la figure 4, le récepteur forme des complexes avec le ligand et l'effecteur en fonction des constantes K et M[162]. L'effet allostérique de l'effecteur est décrit par facteur α. Selon ce modèle, l'activité constitutive peut être expliquée selon la formation du complexe récepteur-effecteur. De plus, le site de haute affinité est expliqué par la formation du complexe ternaire entre le ligand, le récepteur et l'effecteur.

Modèle ternaire étendu et cubique

Suite à la découverte de mutants rendant le récepteur constitutivement actif [164]et des agonistes inverses[165,166], une nouvelle classe de ligand inhibant l'activité constitutive des récepteurs, le

modèle ternaire simple devient invalide dû à son incapacité d'expliquer ces phénomènes. De plus, une étude montre notamment que l'association d'un effecteur au récepteur n'est pas essentielle pour le site à haute affinité dans le cas des mutants constitutivement actifs[164]. Ainsi, le modèle ternaire fut modifié pour réintroduire le concept d'activation spontané du récepteur retrouvé dans le modèle à deux états. Cependant, le modèle ternaire simple assume qu'il n'y a pas d'interaction entre le récepteur à l'état inactif et l'effecteur. Un concept qui sera rajouté à ce modèle afin de former le modèle ternaire cubique [167].

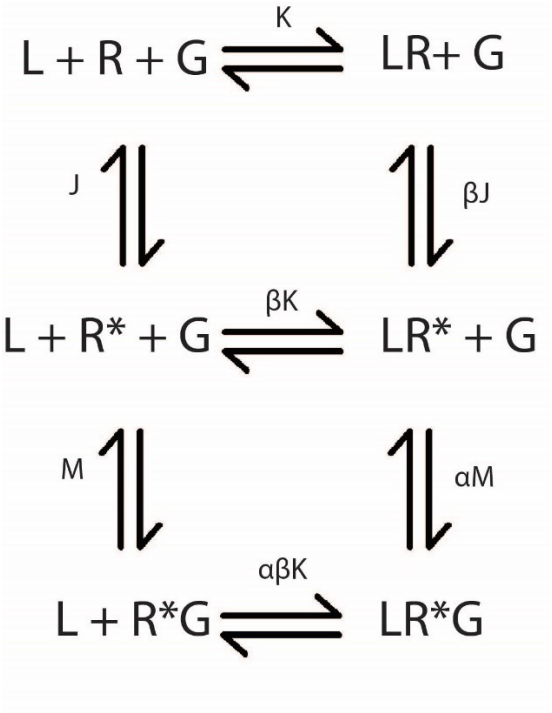

Figure 5. Modèle ternaire étendu. Tout comme le modèle ternaire simple, le récepteur (R) forme des complexes avec le ligand (L) et la protéine G (G) qui sont en équilibre selon les constantes K, M et J représentant la liaison du ligand, la liaison de la protéine G et l'activation spontanée du récepteur. L'effet allostérique entre le ligand et la protéine G est décrit par le facteur α tandis que l'effet allostérique entre la liaison du ligand et l'activité spontanée est décrit par le facteur β. L'efficacité du signal correspond alors au vecteur αβ. Figure adaptée de [164]

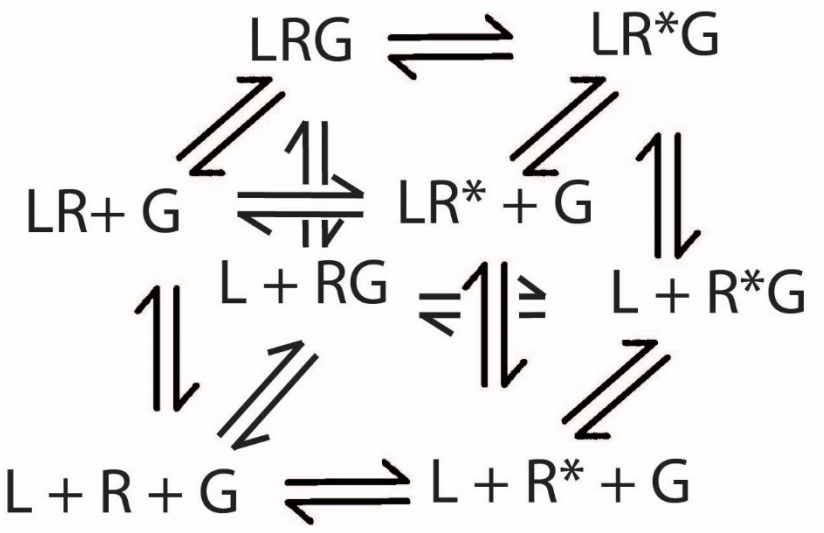

Figure 6. Modèle ternaire cubique. Le modèle est similaire au modèle ternaire étendu, mais avec l'addition des interactions possibles entre la protéine G et le récepteur inactif.

Signalisation biaisée

Les modèles pharmacologiques précédents considèrent que le récepteur est couplé à une seule voie de signalisation ou effecteur. Or, plusieurs études ont démontré que ce n'est pas le cas et qu'un récepteur donné peut être couplé à plusieurs voies de signalisations un concept connu sous le nom de pluridimentionalité fonctionnelle du récepteur [168,169]. Par la suite, il a été démontré que les différentes voies de signalisation sont séparables pharmacologiquement [65,170,171], c'est-à-dire qu'un ligand peut être un agoniste pour une voie de signalisation et un agoniste inverse pour une autre. Ainsi un ligand peut favoriser l'activation de certaines voies de signalisation d'un récepteur au détriment de d'autres. Ce concept est connu sous le nom de sélectivité fonctionnelle ou encore signalisation biaisée du ligand. Cette découverte ouvre aussi la possibilité de développer des médicaments activant uniquement les voies de signalisation ayant un effet thérapeutique en omettant celles qui peuvent mener aux effets secondaires. Pour

cette raison, ce phénomène est un des aspects les plus étudiés aujourd'hui dans le domaine des RCPGs. Pour expliquer la signalisation biaisée, plusieurs études biochimiques et biophysiques ont démontré que les RCPGs peuvent adopter plusieurs conformations distinctes [172-174]. Ainsi l'hypothèse pour expliquer la signalisation biaisée est que différentes conformations sont responsables pour le couplage à différentes voies de signalisations. Ainsi les différents ligands stabilisent différents ensembles de conformations ayant différentes efficacités pour les différentes voies de signalisation. Suivant ce concept, plusieurs nouveaux modèles pharmacologiques ont vu le jour. Tout d'abord, il y a eu l'extension du modèle ternaire cubique pour former le modèle ternaire hypercubique[175]. Ce modèle bien qu'élégant n'est pas viable expérimentalement dû à sa complexité et son grand nombre de variables et est souvent simplifié au modèle ternaire étendue pour l'analyse des résultats.

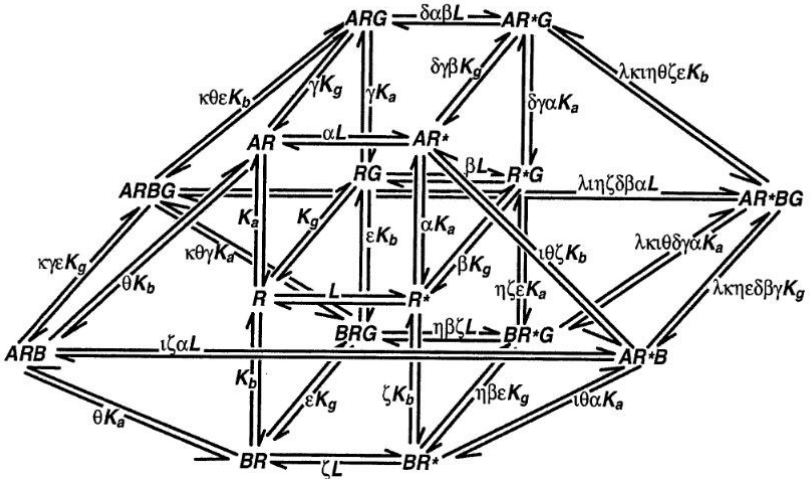

Figure 7. Modèle ternaire hypercubique. Ce modèle représente une superposition de tous les complexes ternaires cubiques possibles entre le récepteur, ses effecteurs ainsi que son ligand. Figure adaptée de [175]

Un autre modèle, qui a émergé, est le modèle probabiliste. Dans ce modèle, le récepteur peut adopter différentes distributions de conformations ayant différentes efficacités en absence de ligand. L'activité d'un ligand dépend alors des sous-ensembles stabilisés par ce dernier générant une nouvelle distribution des conformations du récepteur. Cependant, l'analyse statistique de ces ensembles ne peut être calculée qu'en connaissant les ensembles de distributions stabilisées et est très difficile à utiliser dans le cadre de la signalisation biaisée. Certaines études récentes par résonance magnétique nucléaire (RMN) semblent confirmer ce modèle pour le récepteur d'adénosine de type 2a (A2AR)[176] et le récepteur β2-adrénergique (β2AR)[177].

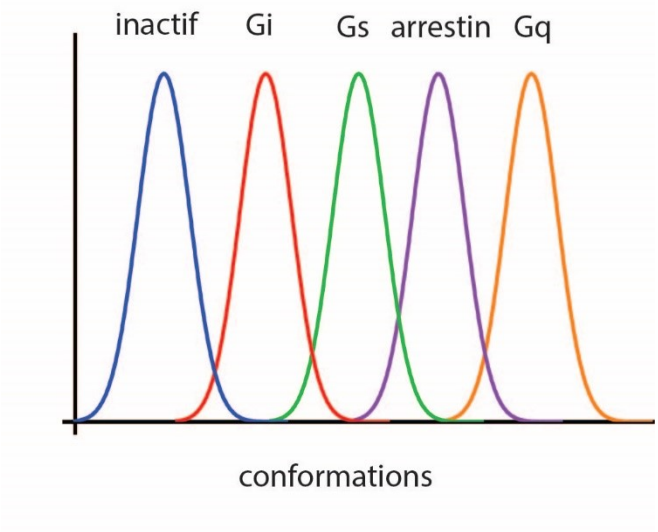

Figure 8. Modèle probabiliste. Dans ce modèle, un ligand va stabiliser différents ensembles de conformation possédant des efficacités distinctes pour les différentes voies de signalisation telles qu'illustrées par les courbes de différentes couleurs. L'efficacité d'un ligand dépendant donc des différentes populations stabilisées par ce dernier. L'intersection entre deux distributions de conformation représente des conformations capables d'activer les deux voies de signalisation.

Une extension du modèle opérationnel a aussi vu le jour afin de calculer, en une seule valeur, le biais de signalisation entre des divers ligands relativement à un ligand de référence ayant la

capacité d'activer toutes les voies de signalisation du récepteur étudié[178]. Ce modèle mathématique est représenté par l'équation suivante :

$$biais = 10^{\Delta\Delta \log\left(\frac{\tau}{Kd}\right) j1-j2}$$

Où

$$\Delta\Delta \log\left(\frac{\tau}{Kd}\right) j1 - j2 = \Delta \log\left(\frac{\tau}{Kd}\right) j1 - \Delta \log\left(\frac{\tau}{Kd}\right) j2$$

Les différents paramètres (τ/Kd) sont identifiés individuellement pour chaque combinaison de ligand et voie de signalisation et la différence est faite selon un ligand de référence. Le paramètre (τ/Kd) est quant à lui évalué selon l'équation classique du modèle opérationnel de Black et Leff (voir section modèle opérationnel).

Structure des RCPGs

L'aspect principal de ma thèse fut de comprendre les mécanismes d'activation des RCPGs menant à l'activation spécifique de certaines voies de signalisations. Dans la section suivante, les aspects structuraux de l'activation des RCPGs ainsi que leur couplage à différents effecteurs vont être explorés. Cette section est la plus pertinente pour la compréhension de ma thèse et des hypothèses soulevées dans celle-ci.

Généralités

Les RCPGs sont des cibles difficiles pour les études de biologie structurale due à leur grande flexibilité qui est importante pour leurs fonctions[179,180]. Les premières évidences de cette flexibilité proviennent d'études où le récepteur avec étiquette fluorescente démontre des changements de conformation suivant la liaison de l'agoniste[181]. Cependant, la cristallisation du complexe agoniste-récepteur ne montre pas de changements conformationnels significatifs en comparaison avec les structures inactives[182]. Des simulations de dynamique moléculaire (MD) ont par la suite confirmé que la conformation active des RCPGs n'est pas la plus stable lorsqu'uniquement l'agoniste est lié au récepteur[182-184]. Ces simulations ont par la suite été confirmées par plusieurs études de spectroscopie, dont des études de spectroscopie RMN et EPR[174,176,177,185]. Afin d'élucider la structure active des RCPGs l'aide de protéine stabilisant celle-ci ont dû être utilisé [186-192]. Il est important de considérer que d'autres conformations existent et ont pu être mises en évidence grâce à des techniques de spectroscopie, mais doivent encore être caractérisées[174,176].

La structure des RCPGs de classe A est composé d'un domaine N-term, de sept domaines transmembranaires (TM1 à TM7) reliés entre eux par 3 boucles intracellulaires (ICL) et 3 boucles extracellulaires (ECL), d'une hélice intracellulaire (H8) suivant le TM7 et d'un domaine non structuré C-term. Deux cystéines sont conservées pour plusieurs RCPGs dans le TM3 et L'ECL2 formant un pont disulfure essentiel au maintien de la fonction de ces RCPGs. Le site de liaison du ligand est formé par une cavité entre les différents TM au niveau extracellulaire. Pour ce qui est du site de liaison des protéines G et de l'arrestine, une cavité similaire est formée au niveau intracellulaire suivant l'activation du récepteur. En plus de la structure générale en 7 TMs, certains motifs structuraux tels que les motifs DRY, PIF/connecteur et NPxxY sont conservés dans cette famille de récepteurs.

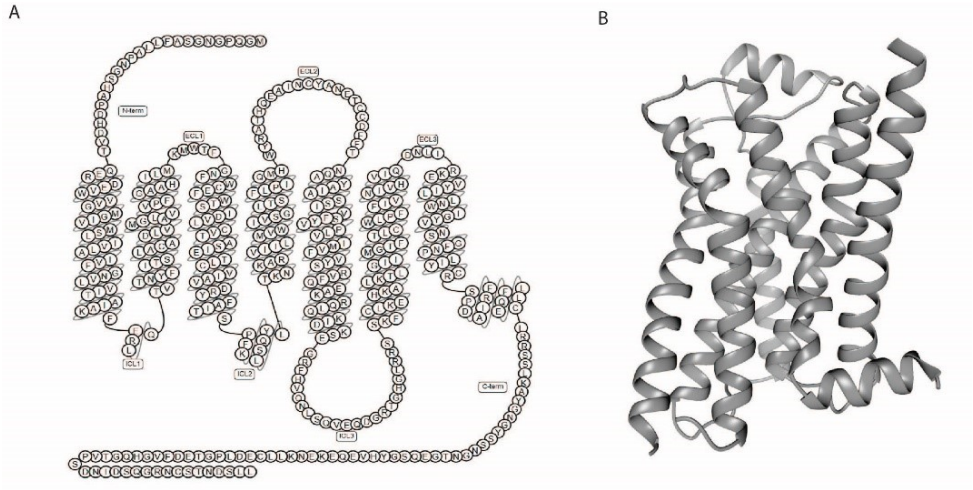

Figure 9. Structure schématique et tridimensionnelle du récepteur β2AR. A) Représentation en serpentin du récepteur β2AR. B) structure tridimensionnelle de la forme inactive du récepteur β2AR (PDB 2RH1) démontrant l'architecture conservée des TMs et H8 des RCPGs

Mécanisme d'activation

En considérant la grande flexibilité des RCPGs, le modèle d'activation le plus accepté aujourd'hui est que la liaison du ligand va permettre l'oscillation entre différentes conformations du récepteur et que le couplage d'un effecteur va stabiliser la conformation active du récepteur pour celui-ci. Par conséquent, le couplage allostérique entre le ligand et les changements conformationnels liés à l'activation est considéré comme étant faible[179], puisqu'il permet la propagation de ces changements structuraux sans pour autant être suffisant pour complètement les stabiliser.

La comparaison des structures cristallines active et inactive de différent RCPGs permet l'appréciation de la conservation structurale de cette famille de récepteurs ainsi que de leur mécanisme d'activation. Les changements structuraux menant à l'activation des RCPGs comprennent, la rotation du TM5 et un mouvement extérieur du TM6 afin de former la cavité permettant le couplage à différents effecteurs tel que les protéines G[186] ou l'arrestine[191]. Non seulement, ces changements structuraux sont conservés dans les structures cristallines des RCPGs de classe A, mais aussi dans celles de classe B récemment obtenus[187,188] suggérant ainsi qu'en dépit d'avoir des motifs structuraux divergeant, les changements conformationnels majeurs menant à l'activation sont conservés.

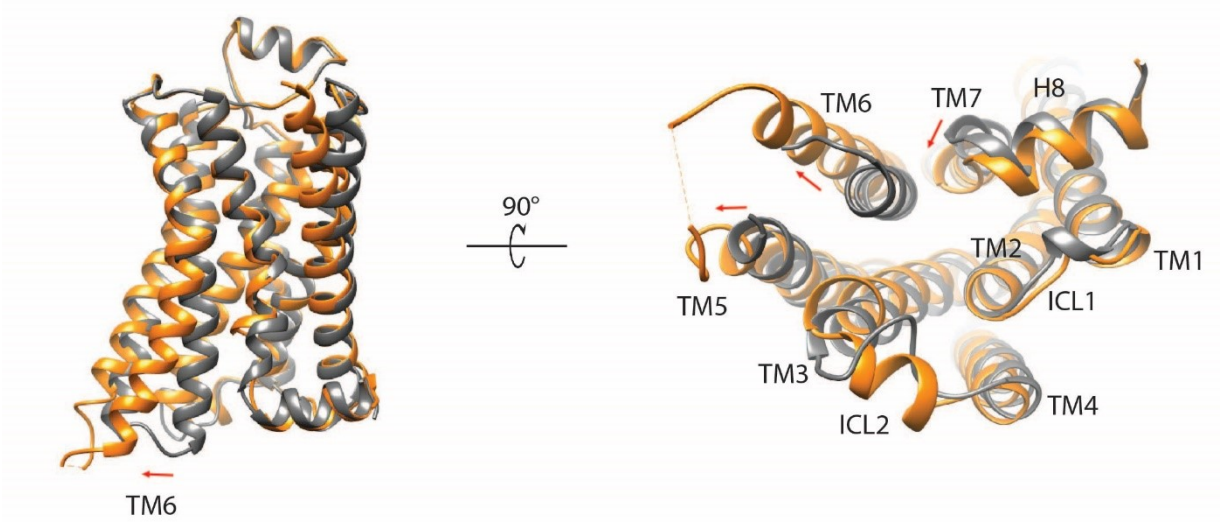

Figure 10. Changements structuraux lors de l'activation des RCPGs. Comparaison structurale entre la conformation inactive (gris; PDB :2RH1) et active (orange; PDB : 4LDE). Les flèches indiquent les changements structuraux importants.

Les motifs structuraux conservés entre les différents RCPGs de classe A jouent un rôle important lors de l'activation de ceux-ci. Tout d'abord, le motif E/DRY situé au bas du TM3 a été proposé pour stabiliser la conformation inactive du récepteur via un pont salin avec le résidu $E^{6.30}$(nomenclature de Ballesteros-Weinstein[193] où le premier chiffre correspond au TM et deuxième à la position du résidu en référence au résidu le plus conservé dans le TM portant le numéro 50 par défaut) du TM6 formant ainsi le *ionic lock*. Plusieurs études de mutagenèse ont démontré l'importance du *ionic lock* comme barrière d'activation, notamment pour la rhodopsine[194]. De plus, des études de RMN du β2AR et A2aR ont démontré deux états inactifs correspondant à la formation et au bris du *ionic lock*[176,177].

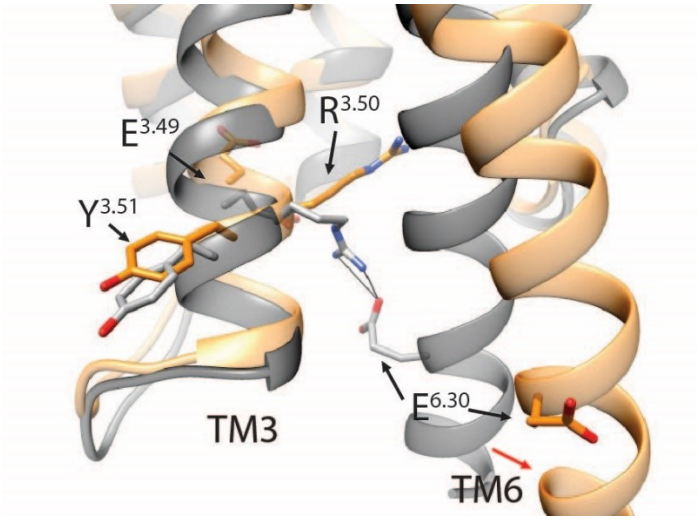

Figure 11. *Ionic lock*. La forme inactive des RCPGs en gris (PDB : 1U19) est stabilisée par la formation d'un pont salin entre les résidus $R^{3.50}$ et $E^{6.30}$ qui est brisé suite au déplacement vers l'extérieur du TM6 observé dans la forme active en orange (PDB : 3PQR). Le mouvement du TM6 est représenté par la flèche rouge et les ponts hydrogène entre les résidus $R^{3.50}$ et $E^{6.30}$ par les lignes noires.

Un autre motif conservé chez les RCPGs de classe A qui a été démontré pour être important dans l'activation, est le motif NPxxY situé au bas du TM7[195-197]. Ce motif permet la stabilisation de la conformation active d'une façon similaire à ce au motif E/DRY pour la conformation inactive. Le résidu $Y^{7.53}$ participe à un réseau d'interaction polaire médié par des molécules d'eau, notamment avec le résidu conservé $Y^{5.58}$ [198]. Dans plusieurs cas, le réseau d'interaction avec les molécules d'eau s'étend avec une interaction entre le résidu $Y^{5.58}$ et $R^{3.50}$ du motif E/DRY tel qu'observer dans les structures actives du récepteur μ-opioïde et de la rhodopsine. Dans le cas de la rhodopsine, des mutations du résidu $Y^{5.58}$ permettent d'augmenter le temps de vie de la conformation active de la métarhodopsineII[198].

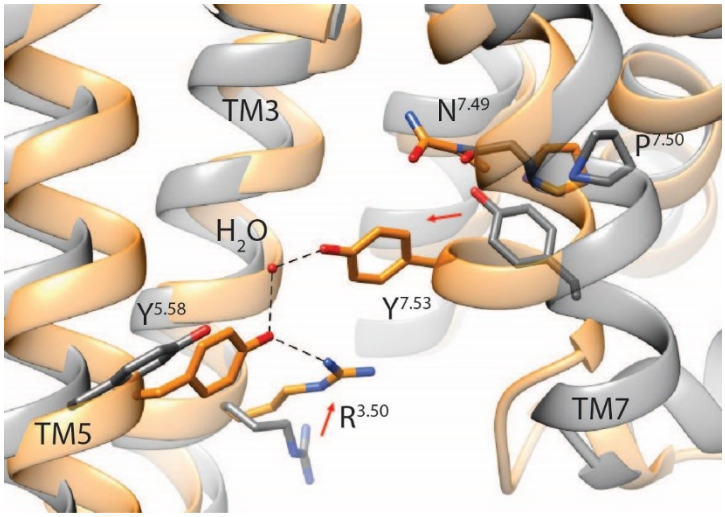

Figure 12. Motif NPxxY. Changements conformationnels observés dans le motif NPxxY entre la conformation inactive (gris; PDB : 4DKL) et active (orange; PDB 5C1M) du récepteur μ-opioïde. Les flèches rouges représentent les changements majeurs et les lignes pointillées les ponts hydrogènes présents.

Un motif a été identifié dans la structure cristalline de la forme active du récepteur β2AR comme étant important pour la transduction du signal provenant de la poche de liaison du ligand. Il s'agit du motif PIF ou encore connecteur. Ce motif tridimensionnel est formé des résidus hydrophobes $P^{5.50}$, $I^{3.40}$ et $F^{6.44}$ [186,199]. Le mouvement du résidu 6.44 est transféré vers le résidu 3.40 permettant une pénétration des changements conformationnels de la poche de liaison du ligand vers le cœur du récepteur. De plus, ce mouvement pourrait être lié avec la contraction de la poche de liaison du ligand qui est une caractéristique des structures actives des RCPGs. Les réarrangements du motif PIF/connecteur ont été observés pour plusieurs récepteurs tels que le β2AR, la rhodopsine, le récepteur d'adénosine A2a et le μ-opioïde[186,189,200]. Cependant, certains récepteurs ne possèdent pas ce motif tel que le récepteur M2 muscarinique (M2R) et le récepteur cannabinoïde de type 1(CB1R) qui possède des résidus plus petits aux positions 3.40 et 6.44, par conséquent les mouvements de ces résidus sont plus modestes[201,202]. Toutefois, la contraction de la poche de liaison est quand même présente chez ces deux récepteurs.

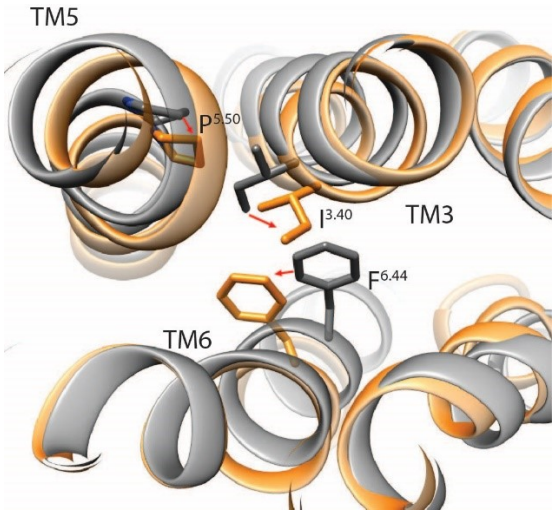

Figure 13. Motif PIF/connecteur. Mouvement observé entre la conformation inactive (gris; PDB :2RH1) et active (orange; PDB :4LDE) dans le motif PIF/connecteur. Le mouvement des différents résidus est illustré par les flèches rouges.

À proximité du motif PIF/connecteur se trouve un site de liaison au sodium, notamment observé dans les structures cristallines du récepteur d'adénosine A2a. Le sodium est un régulateur allostérique négatif des RCPGs[203,204]. Le site de liaison est coordonné par des résidus des TM2, TM3 et TM7 dans la forme inactive du récepteur [205]. Les réarrangements structuraux de ce site suivant l'activation du récepteur requièrent le bris de plusieurs liens avec le sodium.

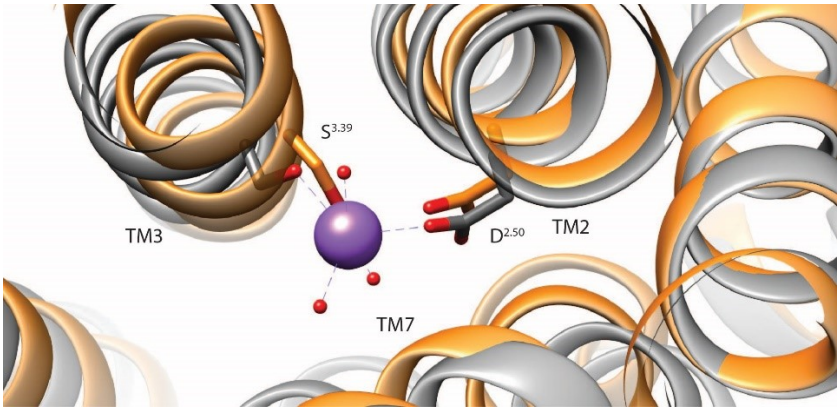

Figure 14. Site de liaison au sodium. L'ion de sodium (mauve) stabilise la conformation inactive du récepteur d'adénosine A2A (gris; PDB :4EIY). Un bris d'interaction avec les résidus S3.39 et D2.50 est nécessaire pour la conformation active (orange; PDB : 5G53).

Dans le contexte de la sélectivité fonctionnel, les déterminants structuraux menant à l'activation de voies de signalisation spécifique demeurent inconnus. Cependant, quelques études récentes ont permis d'avancer certaines hypothèses sur les possibles mécanismes. Tout d'abord, une étude de simulation MD, a proposé que le biais entre différentes protéines G hétérotrimériques puisse être causé par une différence d'ouverture entre le TM3 et le TM6 du récepteur[206]. Cette hypothèse semble être appuyé par les structures en Cryo-EM de complexe entre la protéine Gi et différent récepteur où l'ouverture entre le TM3 et TM6 est en effet plus petite que pour le complexe Gs-β2AR[207,208]. Cependant, une différence d'orientation d'environ 21° est aussi observée pour la protéine G elle-même. De plus, les complexes obtenus pour les récepteurs avec Gi et ceux avec Gs ne sont pas les mêmes, ce qui soulève la question de savoir si ces différences déterminent le couplage à la protéine G ou bien peuvent-elles causé un biais de signalisation sur le même récepteur.

Suivant l'hypothèse généralement acceptée que le biais est causé par la stabilisation de différente conformation par les différents ligands, une étude en FRET de molécule unique du récepteur β2AR a démontré que les ligands ayant différents profils de signalisation stabilisaient différents ensembles de conformations[209]. De plus, des études de RMN sur le β2AR et le récepteur d'adénosine A2a ont pu démontrer des résultats similaires[176,177]. Plus récemment, une structure cristalline active d'un agoniste partiel et biaisé du β2AR a été résolu et démontre une conformation intermédiaire entre la conformation inactive et active du ligand endogène, l'épinéphrine[210].

Une hypothèse alternative à différente conformation pouvant expliquer la sélectivité fonctionnelle est une différence dans les temps de résidence de la conformation active du récepteur. Ce modèle est appuyé par une étude sur le récepteur de la sérotonine $5HT_{2B}$, où la structure cristalline a été résolue en complexe avec le LSD[211]. Dans cette étude, une simulation MD a identifié des résidus permettant de maintenir le ligand dans la poche de liaison en formant un couvercle au-dessus de celle-ci. Les mutations de ces résidus affectent la relâche du ligand sans affecter sa vitesse de liaison. La capacité de ces mutants a activé la protéine G n'a pas changé, mais celle de recruté la β-arrestine a diminué suggérant un rôle du temps de résidence du ligand et par conséquent de celui de la conformation active. Ce modèle est intéressant lorsqu'on considère l'absence de différence majeure dans la conformation de la rhodopsine en complexe avec le peptide de la transducine et celle en complexe avec l'arrestine visuel[191].

Structure des protéines G hétérotrimériques.

Les protéines Gα ont une structure tridimensionnelle conservée formée de deux domaines structuraux : Le domaine GTPase et le domaine hélical [212]. Ces deux domaines sont liés par deux jonctions. Pour ce qui est du domaine GTPase, il est composé d'un feuillet β à cinq brins parallèles et un brin antiparallèle et sept hélices α dont trois formant des jonctions de type cross-over pour relier les brins du feuillet β. Cette architecture est conservée chez les petites GTPase monomériques telles que Rho, car elle définit l'activité catalytique de l'enzyme. Le domaine hélical quant à lui est formé de six hélices α et recouvre le site de liaison des nucléotides.

La sous-unité Gβ possède elle aussi deux domaines; une structure de type β-propeller à sept lames ainsi qu'une hélice α en N-term. La sous-unité Gγ elle est beaucoup plus simple et est formée uniquement de deux hélices α. Le dimère Gβγ est indissociable et les interactions entre les deux sous-unités sont composées d'un dimère de type *coil-coiled* entre l'hélice α N-term de la sous-unité Gβ et l'hélice α C-term de la sous-unité Gγ ainsi que de l'interaction entre les lames 5 et 6 de la sous-unité Gβ et l'hélice N-term de Gγ [213,214]. Dans la conformation inactive, lié au GDP, la sous-unité Gα interagit avec la sous-unité Gβ via les interactions des domaines *switch I/II* de Gα et le domaine *β-propeller* de la sous-unité Gβ pour former l'hétérotrimère Gαβγ [215].

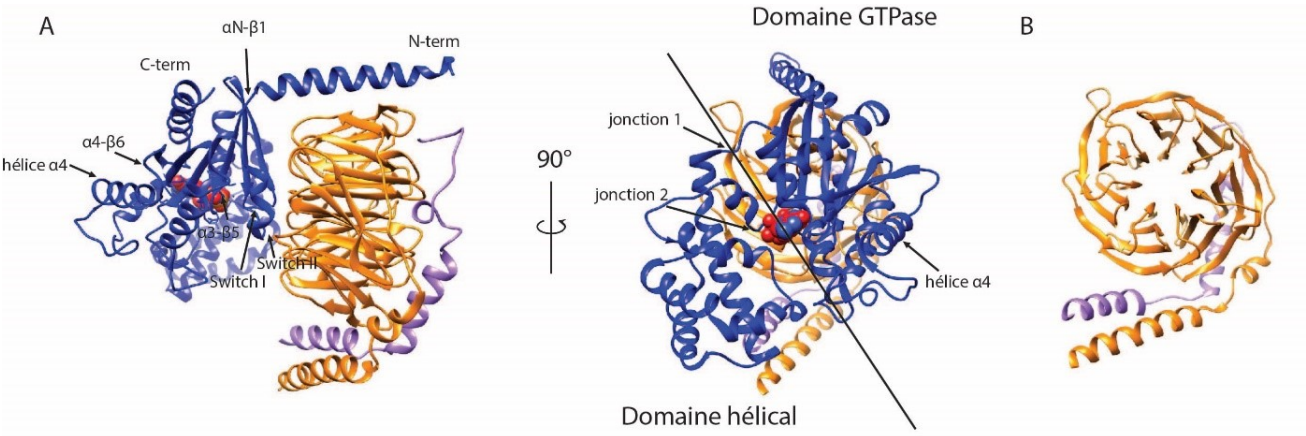

Figure 15.Structure d'une protéine G hétérotrimérique. A) Structure du complexe αi(bleu) β1(orange) γ2(violet). Les domaines importants pour l'activation de la protéine Ga sont annotés. B) Structure en baril de type β-propeller à 7 lames de la sous-unité β1 en orange en complexe avec la sous-unité Gγ2, en violet(PDB 1gg2)

Activation des protéines G

Les RCPGs activent les protéines G hétérotrimérique en catalysant l'échange d'une molécule de GDP pour une molécule de GTP. À partir de la structure inactive de la transducine (Gt), où les domaines hélical et Ras de la sous-unité alpha recouvrent le site de liaison des nucléotides guanines, il a été proposé que l'activation de la protéine G se fait via la séparation des deux domaines menant à l'exposition du site de liaison des nucléotides guanine permettant ainsi l'échange du GDP pour le GTP[216]. Cette étape du mécanisme a été confirmée dans la structure cristalline du complexe entre le récepteur β2-adrénergique (β2AR) et la protéine G hétérotrimérique, Gs, où un large changement conformationnel du domaine hélical est observé [186]. De plus, des études de spectroscopie de double résonnance électron-électron (DEER)[217], et des simulations MD[218,219] ont confirmé l'importance de la séparation entre le domaine hélical et Ras pour l'activation des protéines G. Cependant, contrairement à la conformation observée dans la structure cristalline du complexe β2AR-Gs, des études de microscopie électronique du

même complexe[220] ainsi que la structure en Cryo-EM du complexe entre le récepteur du glucagon-like peptide 1 et Gs[188], ont démontré que le mouvement du domaine hélical et très dynamique et peut adopter différente conformation.

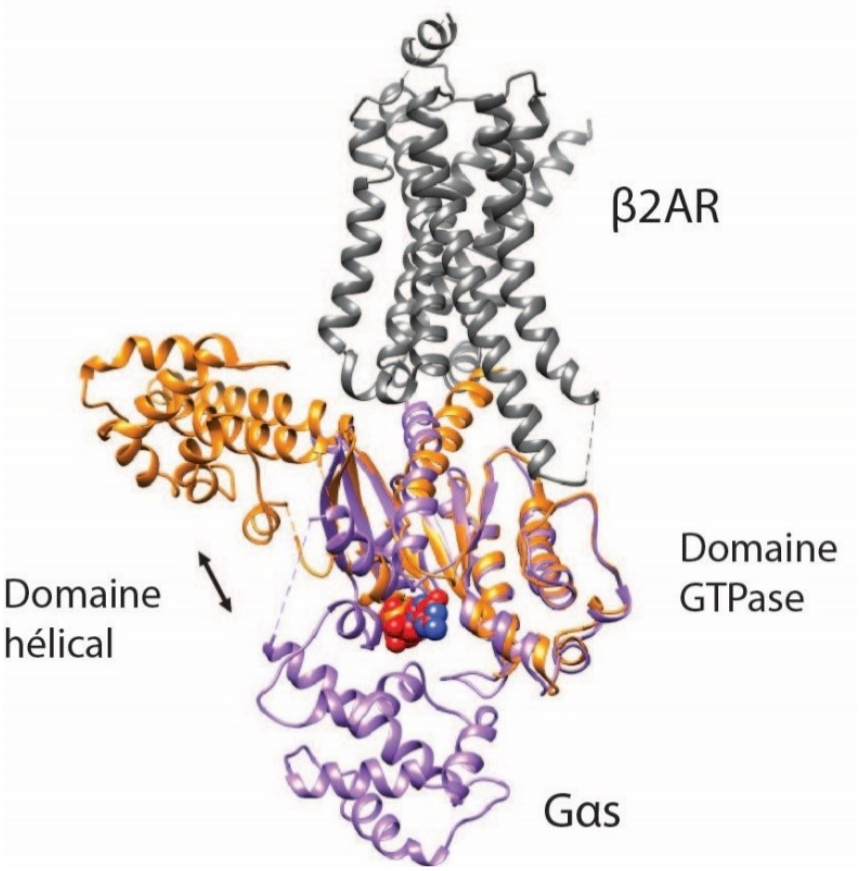

Figure 16. Changements conformationnels de la sous-unité Gα médiés par le récepteur. Comparaison structurale de la conformation liée au GTPγS (violet, PDB: 1ATZ) et de la conformation sans nucléotide (orange) en complexe avec le récepteur β2AR (gris, PDB : 3SN6). Le changement de conformation du domaine hélical est représenté par la flèche noire. Les sous-unités βγ ne sont pas représentées.

Bien que le déplacement du domaine hélical est essentiel pour l'activation des protéines G, il a été démontré que ce déplacement n'est pas suffisant pour induire la relâche du GDP. Une forme tronquée de la protéine G, manquant le domaine hélical, maintient sa capacité de liaison au GDP[221]. D'ailleurs, des simulations en dynamique moléculaire en combinaison avec de la

spectroscopie de type DEER ont démontré que même après la séparation du domaine hélical, le GDP reste lié à la protéine G[219]. Ces données suggèrent un mécanisme d'activation en plusieurs étapes où la séparation des domaines hélical et Ras forment la première étape et que des contacts supplémentaires avec le récepteur sont nécessaires.

Le domaine d'interaction des protéines G interagissant avec les RCPGs le mieux caractérisé sont ceux impliquant l'hélice α5 en C-term de la sous-unité α de la protéine G qui a été démontrée comme étant essentiel pour le couplage avec les RCPGs [222-226]. L'hélice α5 interagit directement avec le corps du récepteur activé en formant des interactions avec le TM3, TM5, TM6, ICL2 et ICL3[186-189]. Ces interactions permettent une rotation et une translation de l'hélice α5 en comparaison avec la forme inactive de la protéine G qui semble affecter la conformation du domaine Ras et son site de liaison des nucléotides. Notamment, la boucle β6-α5 située en N-term de l'hélice α5 qui présente une plus grande flexibilité suivant le changement de conformation de l'hélice α5[223,227]. La boucle β6-α5 contient le motif TCAT, important pour la liaison de l'anneau purine de la guanine et des mutations dans cette boucle peuvent accélérer la relâche du GDP en absence de récepteur [228,229].

En plus, de modifier la conformation de la boucle β6-α5, l'hélice α5 interagit aussi avec les régions α1, β2 et β3 par des interactions hydrophobes qui sont brisées lors de la rotation et translation de l'hélice α5, ce qui a pour conséquence de déstabiliser la région α1 [186-188,227]. La région α1 contient le motif de Walker (GXXXXGK(S/T) responsable pour la liaison du GDP. De plus, cette région interagit avec l'hélice αF du domaine hélical en conformation inactive. Par conséquent, il a été proposé que la déstabilisation de la région α1 accélère la relâche du GDP.

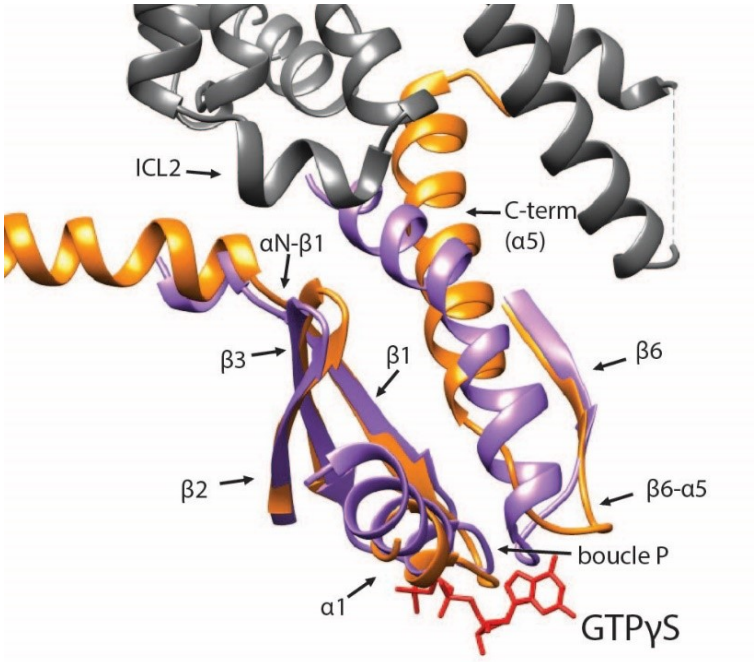

Figure 17. Motif d'activation de la sous-unité Gα. Comparaison structurale de la conformation active liée au GTPγS (violet, PDB: 1ATZ) et de la conformation sans nucléotide (orange) en complexe avec le récepteur β2AR (gris, PDB 3SN6).

En plus de l'hélice α5, la boucle αN-β1 est importante pour la relâche du GDP[226,230,231]. Dans les structures cristallines disponibles, cette boucle interagit avec l'ICL2 du récepteur permettant ainsi une connexion entre l'ICL2 et la boucle P du site de liaison des nucléotides de la protéine G via le brin β1[186-189]. Il a aussi été démontré que la flexibilité de cette région augmente suite au couplage avec le récepteur activé [227]. De plus, des mutations dans l'ICL2 de la rhodopsine affectent la relâche du GDP par la transducine (Gt) sans affecter le couplage de cette dernière au récepteur [230]. Ces données suggèrent une connexion entre l'ICL2 et la boucle P ayant un rôle à jouer lors de l'activation de la protéine G.

Structure des arrestines

La structure des arrestines est conservée entre les quatre membres de la famille. Cette structure est formée de deux lobes (N et C en référence aux domaines N et C term de la protéine) chacun composé d'un sandwich de brin β qui sont connecté entre eux par une région de type *hinge*. À l'interface entre les deux domaines N et C term, on retrouve la boucle C, la boucle finger, la boucle middle et la boucle lariat. Deux boucles sur le côté extérieur du lobe C forment le *Edge* C qui interagit avec les lipides suite à l'activation de l'arrestine[232,233].

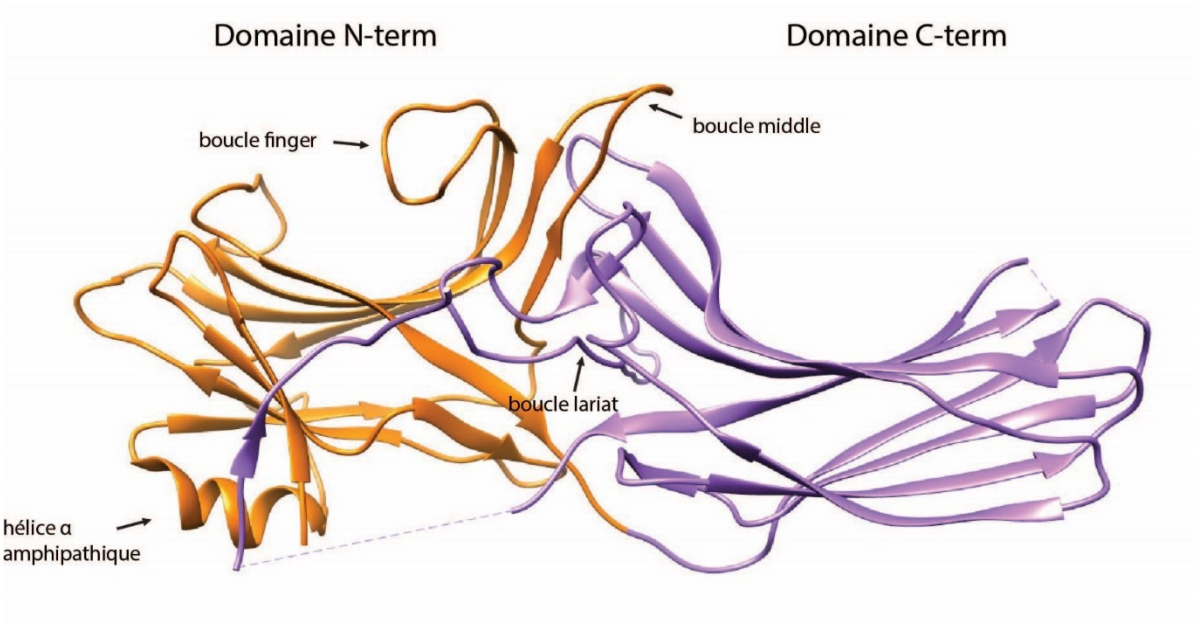

Figure 18. Structure de la β-arrestin1 inactive. Le domaine N-term est en orange tandis que le domaine C-term est en violet. Les régions structurales importantes sont annotées. (PDB 1zsh)

La forme inactive de l'arrestine est stabilisée par deux composantes structurales. Premièrement, le motif à trois éléments, qui est un réseau d'interaction hydrophobe entre la queue C-term et le brin β1 et l'hélice α amphipathique du lobe N-term.

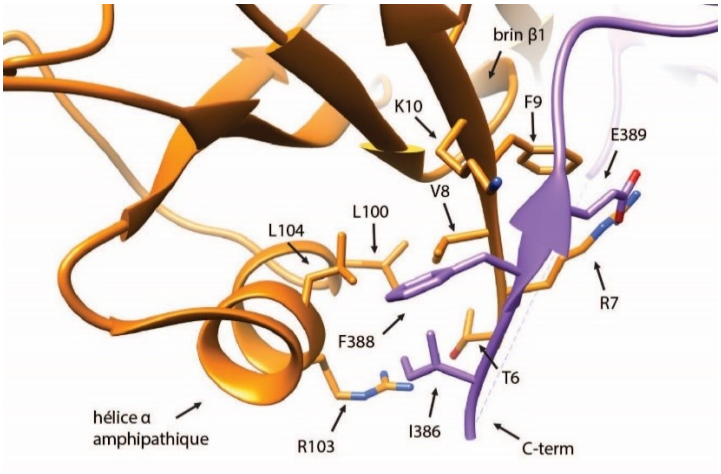

Figure 19. Structure du motif à trois éléments. Le motif à trois éléments est composé d'une série d'interactions hydrophobes entre l'hélice α amphipathique, le brin β1 du lobe N ainsi que le C-term de la β-arrestine (PDB : 1zsh)

La deuxième composante est le cœur polaire. Cet élément est composé de plusieurs interactions de type pont hydrogène entre cinq résidus chargés non exposés au solvant sur les brins β3, β10 du lobe N ainsi que la boucle lariat et la partie distale de la queue C-term. Ces interactions permettent de garder l'interface des lobes C et N compacte et de prévenir l'accès à la cavité chargée positivement du lobe N.

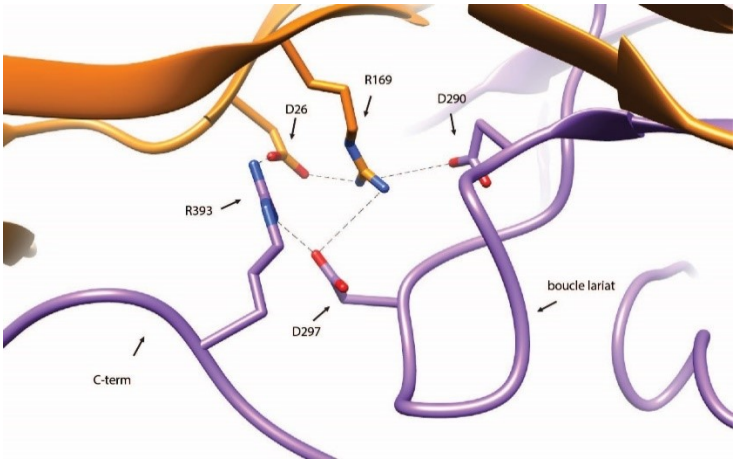

Figure 20. Motif du cœur polaire de la β-arrestine. Ce motif permet de maintenir la β-arrestine dans sa conformation inactive. Les lignes représentent le réseau d'interaction hydrogène (PDB :1zsh).

Couplage aux arrestines

L'activation de l'arrestine par les RCPGs demande plusieurs changements conformationnels permettant de briser les interactions stabilisant la forme inactive de l'arrestine (voir section Structure arrestine). Parmi ces changements majeurs, on retrouve le bris de l'interaction à trois éléments, du cœur polaire, une rotation inter domaine d'environ 20°, la libération de la queue C-term et des réarrangements des boucles finger, middle et lariat [234]. Ces changements permettent l'exposition de l'interface centrale du lobe N ainsi que l'exposition de résidus chargés positivement permettant leur interaction avec les sites phosphorylés en C-term du récepteur.

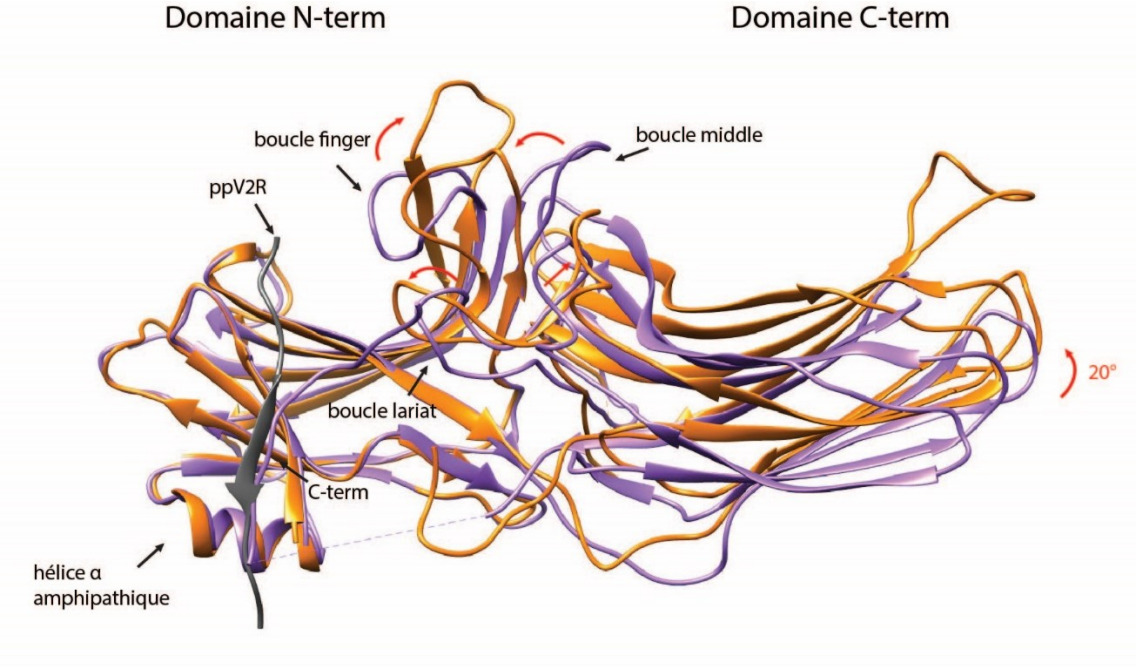

Figure 21.Changements structuraux lors de l'activation de l'arrestine. Comparaison structurale entre la forme inactive de l'arrestine en violet (PDB 1zsh) avec la conformation active en orange couplée au phosphopeptide du récepteur de la vasopressine de type 2 (ppV2R) en gris (PDB 4JQI). Les domaines importants de l'arrestine sont annotés en noir à partir de la structure inactive et les changements structuraux lors de l'activation en rouge.

L'ordre précis de ces changements ainsi que les détails mécanistiques de ceux-ci demeurent aujourd'hui inconnus. Cependant, beaucoup d'informations sur l'interaction directe entre le récepteur et l'arrestine ont pu être résolues grâce à la structure du complexe entre la rhodopsine et l'arrestine visuelle [191]. L'interaction entre le récepteur et l'arrestine se fait via deux régions principales. Premièrement, entre le C-term phosphorylé du récepteur et l'interface centrale du lobe N ou des interactions électromagnétiques sont observées. Deuxièmement, entre le cœur du récepteur et la partie centrale de l'arrestine. Cette deuxième région comprend plusieurs éléments d'interactions. Tout d'abord, la boucle finger de l'arrestine est complètement engagée dans la poche de liaison intracellulaire du récepteur. Ensuite, la région en C-term de la boucle finger et la boucle lariat interagissent avec la partie intracellulaire des TM5 et TM6 et de l'ICL3 du récepteur. Finalement, la crevasse entre la boucle middle, lariat et C de l'arrestine accommode la partie intracellulaire du TM3 et de l'ICL2. Des études de mutagenèse dirigée précédente avaient déjà identifié ces régions d'interactions confirmant ainsi la validité de la structure cristalline [232,235-237].

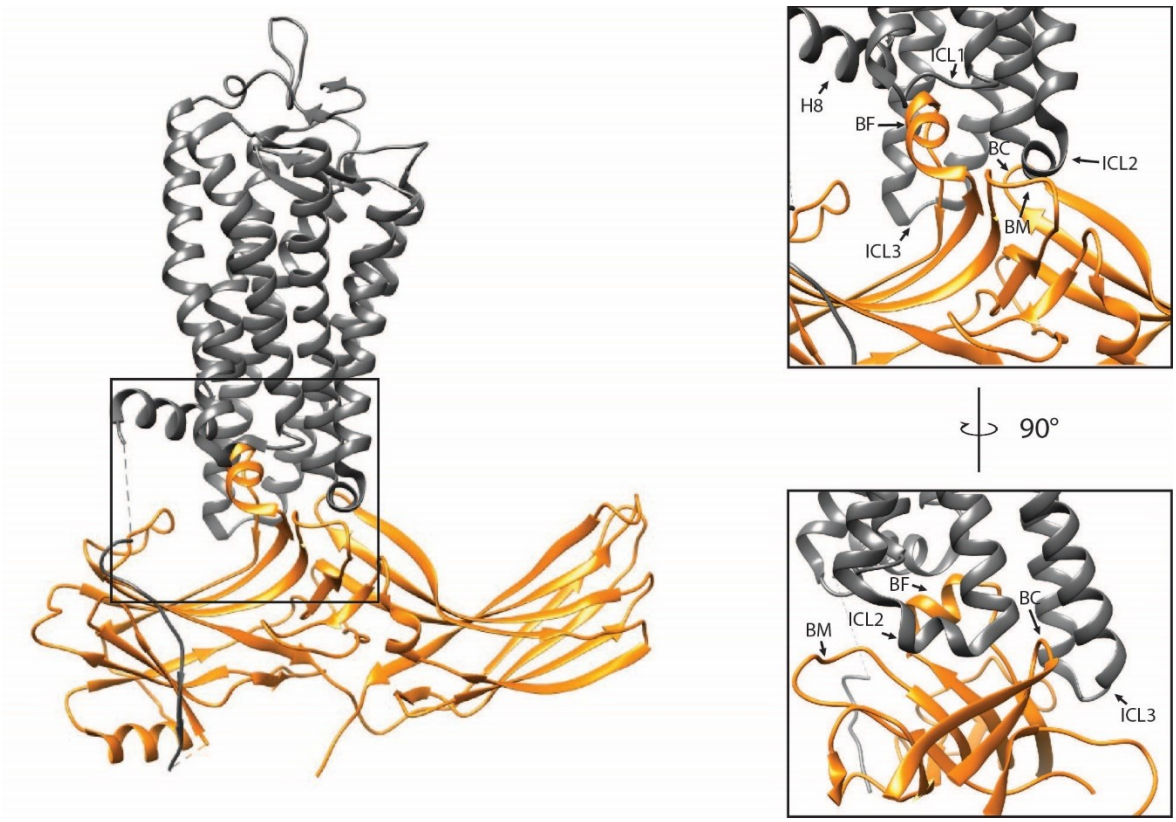

Figure 22. Interface entre le récepteur et l'arrestine. Structure cristalline du complexe entre le récepteur, rhodopsine(gris) et l'arrestine1 (orange). Le rectangle noir représente la région centrale d'interaction où les interactions sont détaillées dans les panneaux à droite entre les différents motifs de l'arrestine : (boucle finger (BF), boucle C (BC) et la boucle middle (BM)) et ceux du récepteur : hélice 8 (H8), boucle intracellulaire (ICL)1,2 et 3 (PDB 5W0P).

Le récepteur β2-adrénergique (β2AR)

Lors de mes travaux de thèse, le récepteur β2-adrénergique (β2AR) a été utilisé comme modèle d'étude. Au début du projet, il représentait le seul récepteur pour lequel les outils nécessaires, tels que la structure cristalline inactive et active ainsi que divers ligands biaisés, étaient disponibles. Ce récepteur est un récepteur prototypique des RCPGs de Classe A (rhodopsine-like) et un des mieux étudiés jusqu'à présent. Ainsi plusieurs voies de signalisation dépendantes et indépendantes des protéines G ont été caractérisées pour ce récepteur. Tout d'abord, la voie de signalisation classique pour ce récepteur est celle dépendante de la protéine Gs qui stimule

l'adénylate cyclase pour la production d'AMPc [18,238] entrainant l'activation de la kinase dépendante de l'AMPc, la PKA. Dans la vision classique d'activation des RCPGs, c'est par cette protéine que les divers effets physiologiques devraient avoir lieu. Cependant, dans le contexte de la sélectivité fonctionnelle du récepteur, il est clair que le β2AR peut activer d'autres voies de signalisation. Par exemple, la PKA peut phosphoryler le récepteur et induire un changement dans le couplage de ce dernier passant de Gs à Gi et ainsi venir activer diverses voies de signalisation dépendante de Gi tel que l'activation de ERK1/2 et l'activation de récepteur tyrosine kinase[103]. De plus, les canaux au calcium peuvent être activés directement par Gs de façon indépendante de la production d'AMPc[239]. Il a aussi été démontré que le β2AR peut activer les échangeurs NA^+/H^+ de type 1 via G13 ou Gi[240]. En plus de ces voies de signalisation dépendante des protéines G, le β2AR peut activer des voies de signalisation indépendante des protéines G tel que l'activation des MAPK (ERK1/ 2, P38, JNK) où le recrutement de la β-arrestine joue un rôle important[241].

Objectifs de la thèse

Au début de ma thèse, en dépit des avancées majeures dans le domaine, les déterminants moléculaires et structuraux de la signalisation biaisée par le ligand étaient mal caractérisés et les outils pour étudier ceux-ci en cellules entières limités. Ainsi, le premier objectif de cette thèse fut de développer un biocapteur du récepteur β2AR permettant de distinguer les ensembles de conformation de ce récepteur dans différentes conditions. Par la suite, les poses des ligands dans le récepteur dictant la signalisation biaisée n'étaient pas connues. Pour ce faire, des études de mutagenèse et caractérisation de ligands ont été effectuées afin de mieux comprendre les composantes du site de liaison du ligand impliquées dans l'activation de voies de signalisation spécifique ce qui constitue le deuxième objectif de la thèse. Le troisième objectif de cette thèse fut de mieux comprendre les différences de transduction de signal impliqué dans l'activation de voies de signalisation spécifique, ce qui a été effectué à l'aide d'étude de mutagenèse et a permis l'identification d'une région du β2AR régulant de manière différente l'activation de Gs et le recrutement de la β-arrestine.

Résultats

Article 1

Bioluminescence resonance energy transfer-based biosensors allow monitoring of ligand- and transducer-mediated GPCR conformational changes

Louis-Philippe Picard, Anne Marie Schönegge, Martin J. Lohse et Michel Bouvier

Publié dans *Communication Biology*, le 7 août 2018

Résumé

Les récepteurs couplés aux protéines G (RCPG) sont des protéines à sept domaines transmembranaires qui méditent une variété de réponses cellulaires ce qui en fait d'eux une cible thérapeutique de choix dans plusieurs indications cliniques. Il est maintenant bien établi que les RCPGs peuvent adopter plusieurs conformations distinctes qui peuvent être différentiellement stabilisées par différents ligands menant à différentes réponses biologiques. Ce concept est connu sous le nom de sélectivité fonctionnelle du ligand. Cependant, à cause de la nature extrêmement hydrophobique des RCPGs, les outils pour étudier les ensembles conformationnels des RCPG sont limités et avec les techniques actuelles de biologie structurale, étudier la dynamique de ces changements demeure un défi. Dans cette étude, nous décrivons un nouveau biocapteur à base de transfert d'énergie de luminescence (BRET) qui peut détecter les réarrangements conformationnels induits par des ligands possédants différente efficacité de signalisation ainsi que l'impact de différents transducteurs tel que Gs et β-arrestin sur ces transitions de conformations. Le design ce type de biocapteur pour d'autres récepteurs devrait

être utile pour l'exploration des composantes structurales de la sélectivité fonctionnelle des RCPG.

Contributions : J'ai effectué le design des expériences, généré les résultats expérimentaux, réalisé l'analyse des résultats et l'interprétation de ceux-ci sous la supervision de mon directeur de thèse. Seul, le clonage du biocapteur a été effectué par Anne Marie Schönegge, sous la supervision du Dr Martin Lohse. J'ai aussi rédigé le manuscrit conjointement avec mon directeur de thèse, Dr Michel Bouvier, et procédé à l'ensemble des révisions.

Bioluminescence resonance energy transfer-based biosensors allow monitoring of ligand- and transducer-mediated GPCR conformational changes

Louis-Philippe Picard[1], Anne Marie Schönegge [1,2], Martin J. Lohse [2,3] and Michel Bouvier [1*]

1 Department of Biochemistry and Molecular Medicine, Institute for Research in Immunology and Cancer, Université de Montreal, Montreal, QC, Canada, H3C 3J7.

2 Department of Pharmacology, Institute of Pharmacology and Toxicology, Würzburg, Germany,97078.

3 Current address: Max Delbruck Center for Molecular Medicine, Berlin, Germany,13125.

Corresponding author: Michel Bouvier, Institute for Research in Immunology and Cancer, Université de Montréal, C.P. 6128 Succursale Centre-Ville, Montréal, Qc. Canada, H3C 3J7. Email : michel.bouvier@umontreal.ca

Abstract:

G proteins coupled receptors (GPCRs) are seven transmembrane proteins that mediate a variety of cellular response which make them a target of choice for drugs development in many indications. It is now well established that GPCRs can adopt several distinct conformations that can be differentially stabilized by various ligands resulting in different biological outcomes; a concept known as functional selectivity. However, du to the highly hydrophobic nature of GPCRs, tools to monitor these conformational ensembles are limited and, addressing their conformation dynamics remains a challenge with current structural biology approaches. Here we describe new bioluminescent resonance energy Transfer (BRET)-based biosensors that can probe the conformational rearrangement promoted by ligands with different signalling efficacies as well as the impact of transducers such as G proteins and β-arrestin on these conformational transitions. The design of such sensors for other receptors should be useful to further explore the structural determinants of GPCR functional selectivity.

Main Text:

Introduction

G protein coupled receptors (GPCRs) form the largest family of membrane proteins involved in signal transduction, play central roles in multiple biological processes and, as such, are the target for the development of drugs in many clinical indications. In their classical representation, GPCRs promote their cellular effect by the engagement and activation of selective G proteins while the engagement of β-arrestin leads to desensitization and internalization[1]. However, in recent years it has been clearly established that individual receptors can engage multiple G protein subtypes and that in addition to it role in desensitization, β-arrestin also lead to intrinsic

signaling activity including MAP kinase activation [2,3]. Recently, the observation that each GPCR can engage multiple signalling pathways[4,5] coupled to the concepts of functional selectivity and ligand-biased signaling[6-8] have raised the possibility of identifying ligands that selectively modulate the therapeutically relevant pathways while avoiding those responsible for undesirable side effects[9,10]. It has been proposed that such ligand-biased signaling results from the stabilization of different receptor conformation ensembles that select distinct signaling partners, such as G proteins or β-arrestin[11-14]. For the β2 adrenergic receptor (β2AR), compounds such as salbutamol and salmeterol have been shown to be efficacious partial agonist for the stimulatory G protein (Gs), while poorly promoting the recruitment of β-arrestin[15] . However, monitoring these ligand-specific conformations remains a challenge, in particular when considering the allosteric nature of the receptor's interaction with cellular tranducers in their native cellular environment. Recently, FRET[16] and FlAsH-FRET[17-19] probes have been introduced in GPCR constructs to monitor the intramolecular conformational changes promoted by ligands with different efficacies. When compared to FRET, BRET-based sensors, such as those developed herein, present several advantages. Notably, because there is no direct activation with light, no artefactual direct excitation of the RET acceptor can occur thus limiting the background. For the same reason, autofluorescence or photobleaching that can limit FRET applications is not an issue with BRET. A direct comparison of conformational BRET and FRET-based sensors is presented in an accompanying paper[20]. FlAsH-BRET has been used to probe conformational rearrangements[18,19]. Although it has the advantage of having an energy acceptor that is smaller than a fluorescent protein, it requires exogenous labelling and extensive washing, which make the assay less convenient. None of these studies assessed the impact of transducers engagement on the conformational ensembles of the receptors. Probing transducers'

influence on receptor conformations is of particular interest when considering the major differences observed between the agonist-bound β2-adrenergic receptor (β2AR) conformations in the presence or absence of Gs[21,22]. Indeed, directly monitoring the dynamics of the conformation ensembles resulting from the engagement of the receptor by both ligands and transducers should prove useful to understand how drugs can selectively promote the engagement of subsets of their downstream transducers.

In the present study, taking advantage of the Oplophorus Gracilirostris-derived luciferase (Nluc) brightness[23], we developed a BRET-based biosensor that can be multiplexed with other BRET-based assays to monitor receptor conformational changes and the engagement of cellular transducers in parallel in living cells.

Results

Biosensors design and characterization

The β2AR, a prototypical class A GPCR was used as a study model since the structures of both inactive and active conformations have been solved. Furthermore, multiple signaling pathways have been characterized for this receptor and several biased ligands are available. To probe the movement associated with receptor conformational rearrangements, Nluc, a luciferase which is brighter and smaller than the traditionally used renillia luciferase (Rluc), was used as the BRET energy donor. it was introduced in the third intracellular loop (ICL3; between positions 251 and 252) and the archetypal BRET1[24,25] or BRET2 [26,27]acceptors, YFP or GFP10, were fused to the C-terminus of the receptor (position 369) (see Methods and Fig. 1a). These positions detect the rotation of TM5 and the outward movement of TM6 that bring ICL3 away from the C termini[16].

Two different energy acceptors, YFP (NY-β2AR) and GFP10 (NG-β2AR) (NY and NG stand for Nluc- YFP or Nluc-GFP10, BRET pairs) were tested. The spectra of the two BRET pairs were obtained using Coelenterazine 400a (Coel.400a) as the Nluc substrate. As shown in Fig. 1b, the YFP construct yielded a more efficient transfer (60% vs 45% for YFP and GFP10, respectively) and a better separation between the donor and acceptor emission peaks (78 nm for YFP vs 50 nm for GFP10).

The NY-β2AR biosensor was then used to probe the activation-induced conformational changes promoted by the full agonist isoproterenol (ISO) in the presence or absence of the antagonist propanolol (PRO) (Fig. 1c-d). The concentration-dependent ISO-promoted decrease in BRET was completely blocked by the addition of PRO, demonstrating that the biosensor detected conformational changes associated with activation that are consistent with a separation between the C-terminus and ICL3, which is observed in the active conformation of the receptor[16,28]. To determine whether the biosensor can detect the distinct conformation ensembles stabilized by ligands with different intrinsic efficacy, the effect of agonists, partial agonists and inverse agonists was tested. The different changes in BRET signal detected for these different ligands (Fig. 1e) correlated well with the known efficacy of the compounds for G□s activation, consistent with the notion that different groups of ligands stabilize distinct conformational ensembles.

Biosensor functionality and multiplexing

To assess the possible impact of the BRET probes on the functionality of the NY-β2AR conformation sensor, its ability to promote cAMP production and β-arrestin recruitment was

compared to that of the wild-type β2AR. Taking advantage of the substrates specificity between Nluc and RlucII (with crossover of less than 3%; Supplementary Fig. 1), Coelenterazine 400a was used to monitor the signal from Nluc and methoxy-e-coelentrazine from RlucII. As seen in Figure 1f-g, at similar expression levels of NY- and wild-type β2AR (Supplementary Fig. 2), both receptor constructs resulted in cAMP production and β-arrestin recruitment, detected by BRET using RlucII-EPAC-GFP10[29] and β-arrestin-RlucII/rGFP-CAAX[30] biosensors, respectively. Although the extent of β-arrestin recruitment detected for NY-β2AR is somewhat smaller than the one observed for wild-type β2AR, the biosensor is functional and can transduce signals.

Using a similar experimental design, we multiplexed the detection of the BRET-based sensors to evaluate in parallel Gαs activation, cAMP production, or β-arrestin engagement on the one hand and the receptor conformational changes on the other. As shown in Supplementary Fig 3, the multiplexing mode shows that the concentration-dependent ISO-promoted conformational change detected by NY-β2AR is accompanied by increases in Gs activation, cAMP accumulation and β-arrestin recruitment. The potency of ISO to promote the conformational change (pEC50: -7.2, -6.9 and -7.2 in the presence of the Gs, cAMP, and β-arrestin biosensors, respectively) was well correlated with its potency to promote Gs activation (pEC50: -7.2) and β-arrestin engagement (pEC50: -7.3). The amplification between the Gs activation and the cAMP is clearly seen by the left shift in the potency of ISO to stimulate cAMP production (pEC50: -8.9). In contrast, SALB, which is a biased ligand[15] activating Gs (albeit to a lower extent than ISO) but only marginally promoting the engagement of β-arrestin, did not induce any conformational changes detectable with NY-β2AR, even at a concentration maximally

occupying the receptor. This difference between ISO- and SALB-promoted conformational changes was also observed in kinetic experiments (Fig. 2a). The observation that SALB was equi-efficacious to ISO in promoting cAMP production (Supplementary Fig. 3d) suggests that the difference in the ability of the two ligands to promote the receptor conformational change did not result from a difference in PKA-mediated phosphorylation of the receptor.

Control experiments confirmed that cross-contamination between the BRET configurations in the multiplexing experiments did not adversely affect the data. Indeed, as shown in Supplementary Fig. 1, no important contribution of the possible transfer from Nluc to GFP10 to the signal detected for the Nluc transfer to YFP occurred in the multiplexed configurations. Similarly, the possible transfer of Rluc to YFP did not contribute to the signal detected for the Rluc transfer to GFP10 in the NY-β2AR/Gs (Gαs117RlucII/Gγ1-GFP10) multiplexed configuration. However, the transfer of energy between the Rluc of the GFP10-linker-RlucII-pβarr2 sensor and the YFP of NY-β2AR contributed to the BRET signal detected for the ISO-promoted recruitment of β-arrestin2 to the NY-β2AR in the multiplexed configuration. This resulted in an amplification of the β-arrestin2 engagement signal observed with NY-β2AR compared to wild-type β2AR (Supplementary Fig 1g). This phenomenon can be advantageously used to increase the signal window for a given sensor. However, it highlights the fact that the possible contamination of one acceptor signal by the other should always be controlled for and taken into consideration when multiplexing BRET sensors and selecting the configuration of the assays.

Evaluation of transducers effect on the conformational sensor

The above results suggest that different conformation ensembles are stabilized by ISO and SALB and raise the possibility that the engagement of Gs and/or β-arrestin may contribute to the conformational changes detected. To test this hypothesis, we evaluated the impact of G proteins and β-arrestin over-expression on the conformational change detected. As shown in Fig. 2b, over-expression of Gs led to significant concentration-dependent conformational changes of NY-β2AR, indicating that coupling to Gs in the absence of agonist is sufficient to induce such changes. The effect of Gs was selective, since over-expression of G12 or Gi had much weaker effects on the conformation (Supplementary Fig. 4). Such ligand-independent conformational changes imposed by the G proteins is consistent with the notion that some receptors may be pre-coupled to G proteins[31-33]. However, we cannot exclude the possibility that such pre-coupling is forced by over-expressing the G proteins.

In the presence of over-expressed Gs, stimulation with ISO promoted additional BRET changes, but to a lower extent than in the absence of over-expressed Gs (Fig.2a and Fig. 2c). Whether the agonist promotes further changes in receptor conformation or stabilizes a larger fraction of the receptors coupling to Gs, remains to be established. However, the fact that the BRET change promoted by Gs (Fig. 2b) is hyperbolic and reaches saturation, supports the former hypothesis. Over-expression of β-arrestin on its own did not affect the conformation of NY-β2AR (Supplementary Fig. 4). However, it potentiated the ISO-promoted BRET change (Fig. 2d), suggesting that β-arrestin modifies the agonist-bound receptor conformational ensembles. This could result either from a larger conformational change promoted by β-arrestin than by Gs or from the stabilization of a greater proportion of the receptor in the agonist-promoted conformation.

The observation that both Gs and β-arrestin modulate the receptor's conformation ensemble detected by NY-β2AR, could suggest that the change is entirely due to the transducer binding. To determine if this is the case or if ISO can promote a conformational change on its own, the conformational change was assessed in cells devoid of Gs or β-arrestin. For this purpose, we took advantage of the Gs and β-arrestin deficient cell lines that were recently generated using CRISPR/Cas9[34,35]. The lack of Gs and β-arrestin was functionally confirmed by the absence of ISO-stimulated cAMP production and β2AR endocytosis in the Gs and β-arrestin deficient cells, respectively, when compared with their parental cells (Supplementary Fig. 5). As shown in Fig 2e and f, the lack of either transducer did not prevent the ISO-promoted conformational changes of the receptor, but the basal BRET observed for the NY-β2AR sensor was higher in the cells lacking functional Gs (Fig. 2h), indicating that native expression levels of Gs may be sufficient to induce a conformational change in NY-β2AR, yielding a reduction of BRET consistent with the effect observed in the presence of over-expressed Gs (Fig. 2b). In cells lacking β-arrestin, treatment with cholera toxin to eliminate the contribution of receptor-bound Gs (cholera toxin leads to a constitutive activation and long term down-regulation of Gs[36]), ISO still promoted NY-β2AR BRET change (Supplementary Fig. 6), indicating that ISO binding on its own is sufficient to change the conformation ensembles of the receptor.

In contrast to ISO, SALB did not promote any significant change in the BRET signal of NY-β2AR for the time period examined (Figures 1e and 2a). Not surprisingly, over-expression of β-arrestin did not influence this lack of response. However, a rapid and sustained decrease in the Gs-promoted conformational response was observed upon SALB stimulation (Fig. 2c). This decrease was not observed in the concentration-response curves presented in Supplementary

Fig. 3, most-likely due to the lower level of Gs expressed in these multiplexing experiments that was not sufficient to significantly affect the conformational ensemble of NY-β2AR. The fact that SALB reduced the conformational change resulting from the constitutive Gs coupling upon over-expression, indicates that the partial agonist changed the equilibrium between Gs-bound and -free receptor. Such reduction in the proportion of receptor in the Gs-induced conformation cannot be compensated by the recruitment of β-arrestin, since SALB does not promote efficient recruitment of β-arrestin (Supplementary Fig. 3). Taken together, these data clearly indicate that the biased partial agonist, SALB, while activating Gs, promotes conformational rearrangements that are clearly distinct from that of ISO and that these conformations are differentially influenced by the receptor's transducers (Fig. 2i). Consistent with the notion that the stabilization of distinct conformational ensembles is a characteristic of the biased and partial agonist nature of SALB, another partial and Gs biased ligand, SALM, failed to promote detectable conformational change on its own and also reduced the Gs-promoted conformational change of the receptor (Supplementary Fig. 7).

Discussion

In summary, we have developed a conformational biosensor for the β2AR that can distinguish between compounds with distinct signalling efficacies in living cells, as well as monitor the impact of transducers on receptor conformation. Such biosensors can be easily combined with other BRET-based sensors to correlate conformational rearrangements with signaling profiles. The generalizability of such biosensors is illustrated in an accompanying paper[20] where similar biosensors were created for the α1AR and PTHR in addition to β2AR. Even though the approach is generalizable, special attention should be given to the design of the biosensors. In

particular, the position in which the biosensor components (energy donors and acceptors) are introduced should be selected with care. Indeed, the insertion of relatively large inserts in the receptor structure could have detrimental effects on the signaling activity of some receptors. Controls experiments to asses such potential impact are therefore required and any alterations in the signaling profile observed should be taken into consideration in the interpretations of the data.

The observation that Gs significantly increased the ISO-promoted decrease in BRET signal observed with the NY-β2AR sensor is in agreement with the previously published study using single molecule FRET[37] between the TM4 and TM6 in which an amplification of the ligand-promoted changes in conformation promoted by epinephrine (EPI) was observed in the presence of Gs. Such amplification of the conformational changes in the presence of Gs is consistent with the crystal structures obtained for the agonist-bound β2AR[28,38]. Indeed, the opening of the TM6 away from the core of the receptor to create a cradle for the C-tail of the G protein α subunit is much larger in the crystals obtain for the agonist-bound receptor in complex either with Gαs [28] or a nanobody mimicking the α subunit of Gs[38]. It follows that the NY-β2AR conformation sensor can be used to probe the allosteric conformational changes promoted by both ligands and transducers in living cells.

In the case of β-arrestin, its overexpression alone does not promote any detectable conformation change. This lack of effect is expected when considering the low constitutive activity of this pathways for the β2AR. The results of the overexpression of β-arrestin upon ligands stimulation demonstrate the difference in activation mechanism of biased ligands such SALB and SALM in

comparison to ISO. In the case of ISO stimulation, the overexpression of β-arrestin amplified the BRET changes detected by the conformation sensor, whereas in the case of SALB and SALM no response was observed. This is in keeping with the fact that the biased ligands SALB and SALM are poor recruiter of β-arrestin, therefore the β-arrestin can not stabilized the ligand-induced response such as observed with ISO. These experiments demonstrate the utility of the conformation sensor in living cells to better probe the structural determinants underlying functional selectivity.

In addition, to probe the activation of the receptors with known ligands and transducers, the BRET-based GPCR conformational sensors should prove useful to probe both ligand and transducer-promoted conformational changes to identify ligands for orphan receptors as well as identifying the transducers coupled to a given receptor. Finally, the sensors could be used to monitor the effect of mutations on the conformation changes of GPCRs upon activation by ligands with different biases to further explore the specific residues and receptor domains involved in ligand-biased signaling.

Methods

Reagents. (-)-Isoproterenol hydrochloride (ISO), (-)-Epinephrine (EPI), (-)-Norepinephrine (NE), Alprenolol hydrochloride (ALP), Labetalol hydrochloride (LAB), (±)-Propanolol hydrochloride (PRO), Metoprolol tartrate (MET), Timolol maleate (TIM) and cholera toxin (CTX) were purchased from Sigma Aldrich. Salbutamol hemisulfate (SALB) and Xamoterol hemifumarate (XAM) were purchased from Tocris Bioscience. Salmeterol xinofoate was

purchased from Selleckchem. Coelenterazine 400a (Coel400a) and methoxy-e-coelenterazine were purchased from NanoLight Technology.

Plasmids. The GFP10-mutEPAC1-RlucII[29], GFP10-linker-RlucII-pβarr2[39], Flag-β2AR[40], Gαs-117-RlucII[40], Gβ1[41], Gβ1-GFP10[41], β-arrestin2-RluII[42] and rGFP-CAAX[30] were previously described. The Gαs, Gαi2, Gα12, Gβ1 and hβarr2 plasmids were purchased from cDNA.org. The pNL1.1 plasmid was purchased from Promega. The NY-β2AR sensor was obtained by Gibson assembly, using the previously published flag-β2AR FRET sensor[16], and replacing the CFP by a Nluc. The YFP was then replaced by a GFP10 to obtain the NG-β2AR version of the sensor.

Cell culture and transfection. HEK293T is the cell line in which BRET-based biosensors have been developed in Dr Bouvier's laboratory and this cell line was used for all the BRET and ELISA experiments. HEK293T cells were grown in Dulbecco's modified Eagle's medium (DMEM) supplemented with 10% newborn calf serum (NCS) at 37°C with 5% CO_2. HEK293-ΔGs and HEK293-Δβarr1/2 were generated by CRISPR/Cas9 gene editing as previously reported[34,35]. HEK293-ΔGs, HEK293-Δβarr1/2 and their respective parental cells were grown in Dulbecco's modified Eagle's medium (DMEM) supplemented with 10% fetal bovine serum (FBS) at 37°C with 5% CO_2. For transfection, cells were detached with trypsin, diluted at a concentration of 500,000 cells per ml, and transfected with 2.5 µg of total DNA for 10^6 cells using linear polyethylenimine (PEI, Polysciences) as transfecting agent with a PEI:DNA ratio of 3:1. Directly after transfection, cells were plated in white 96 well culture plates (Greiner) coated with Poly-L-Ornithine (Sigma-Aldrich) at a concentration of 50,000 cells per well and

were incubated for 48 h before the experiment. Cells were regularly tested for mycoplasma contamination (PCR Mycoplasma Detection kit, abm).

Bioluminescence spectral profiles. HEK293T cells were transfected with the indicated constructs as described above. The luminescence spectra between 360 and 600 nm were acquired with steps of 5 nm, immediately after the addition of 2.5 µM of Coel400a using a FlexStationII microplate reader (Molecular Devices). The bioluminescence is expressed as a percentage of the maximal emission.

BRET measurements. 48 h after transfection, cells were washed with stimulation buffer (Hank's balanced salt solution, HBSS). For the conformational sensor alone (NY-β2AR), Coel400a, diluted in stimulation buffer, was added (2.5 µM final) for 6 min. Increasing concentrations of ISO, diluted in stimulation buffer, or 10 µM of different ligands were then added for 5 min. BRET was monitored with a TriSTAR2 LB 942 microplate reader (Berthold Technologies) equipped with a donor filter 485/20 nm and an acceptor filter 530/25 nm. For the multiplexing, the conformational biosensor (NY-β2AR) was co-transfected with the individual transducer biosensors. The response of the NY-β2AR was measured as described above. The transducer biosensors were measured in separate wells. Methozy-e-coelenterazine (0.25µM) was added for 6 min followed by increasing concentrations of ISO, diluted in stimulation buffer for 5 min (Gs) or 15 min (cAMP production and β-arrestin recruitment). BRET was then monitored with a TriSTAR2 LB 942 microplate reader (Berthold Technologies) equipped with a donor filter of 410/80 nm and an acceptor filter of 515/40 nm. In all cases, BRET ratio was calculated by dividing the acceptor emission over the donor emission.

Conformational sensor. HEK293T, ΔGs, Δβ-arrestin and their respective parental cells were either transfected with the YFP (NY-β2AR) version of the conformational biosensor alone or in combination with specific sensors for different pathways (see below), or in combination with different G proteins (Gαs, Gα12 or Gαi2) or β-arrestin2. BRET was then monitored as described above.

cAMP production. HEK293T cells were co-transfected with the conformational biosensor (NY-β2AR) or the wild-type β2AR and the BRET-based biosensor GFP10-mutEPAC1-RlucII[29]. BRET was then monitored as described above. The conformational change of the GFP10-mutEPAC1-RlucII after cAMP binding leads to a decrease in the BRET ratio.

β-arrestin recruitment. HEK293T cells were co-transfected with the conformational biosensor (NY-β2AR) or the wild-type β2AR and the BRET-based plasma membrane translocation biosensors rGFP-CAAX/βarr2-RlucII[30]. BRET was then monitored as described above. Recruitment of β-arrestin to the receptor induces a change in localisation of the β-arrestin to the plasma membrane that leads to an increase in BRET ratio.

β-arrestin engagement. HEK293T cells were co-transfected with the conformational biosensor (NY-β2AR) or the wild-type β2AR and the plasma membrane anchored BRET-based biosensor GFP10-linker-RlucII-pβarr2[39]. BRET was then monitored as described above. The recruitment of the β-arrestin to the stimulated receptor increases the proximity between RlucII and GFP10, leading to an increase in BRET signal.

Gs activation. HEK293T, Δβ-arrestin or their parental cells were co-transfected with the conformational biosensor (NY-β2AR) and a three-component BRET-based biosensor,

Gαs117RlucII, Gβ1, Gγ1-GFP10[40]. BRET was then monitored as described above. The dissociation of the Gαs and Gβ/Gγ subunits after activation leads to a decrease in BRET ratio.

Endocytosis. Δβ-arrestin and their parental cells were co-transfected with the β2AR-RlucII construct and the FYVE-rGFP biosensor. BRET was then monitored as described above. The translocation of the β2AR-RlucII from the membrane to the early endosomes (marked with the sensor FYVE-rGFP) leads to an increase in the BRET signal.

Kinetics. HEK293T cells were transfected with the YFP version of the conformational biosensor (NY-β2AR) alone or in combination with trimeric Gs or β-arrestin2. Cells were washed with stimulation buffer, HBSS. BRET was monitored 5 min after the addition of 2.5 μM of coel400a, at every 0.72 sec, for a total time of 6 min with an injection of vehicle, 100 μM ISO or 100 μM SALB at the 40 sec time point. The first 40 sec represent the basal state of the biosensor and the mean of these time points was used as 0%, while the last time point stimulated with ISO without co-transfection of Gs or β-arrestin represents 100% of the response. The reading was done on a Mithras LB 940 microplate reader (Berthold Technologies) equipped with a donor filter of 485/20 nm and an acceptor filter of 530/25 nm.

Total Fluorescence measurements. HEK293T cells were transfected with NG-β2AR and GFP10-mutEPAC1-RlucII, as described above. The total fluorescence was monitored using a FlexStationII microplate reader with a combination of excitation at 400 nm and emission at 510 nm, for GPF10, and with excitation at 485 nm and emission at 538 nm, for YFP.

Luciferase measurements. Luminescence of NG-β2AR and GFP10-mutEPAC1-RlucII sensors was monitored 5 min after the addition of 2.5 □M Coel400a or 0.25 □M methoxy-e-coelenterazine, with a TriSTAR2 LB 942 microplate reader equipped with 485/20 nm and

410/80, respectively, corresponding to the filters used for the Nluc and RlucII in BRET experiments. The relative expression of each biosensors was monitored by measuring the fluorescence of the GFP10 of NG-β2AR or GFP10-mutEPAC1-RlucII sensors excited at 410/8 nm.

Cell surface ELISA. HEK293T cells were transfected with the Flag-tagged NG-β2AR and wild-type β2AR constructs, as described above. Cells were washed 2 times with PBS, then fixed with 3% PFA diluted in PBS for 15 min. Fixed cells were washed 3 times with WashB solution (0.5% BSA in PBS). The primary antibody (anti-FLAG M2 Sigma-Aldrich) was added at a dilution of 1/10,000, and cells were incubated for 1 h at 25°C. After the incubation, cells were washed 3 times with WashB solution. The HRP tagged secondary antibody against mouse IgG (GE healthcare) was added at a dilution of 1/1,000 and cells were incubated for 1 h at 25°C. After the incubation, cells were washed 3 times with WashB solution. 50 □L of HBSS was added per well, and 2 min before the reading, 50 µL of ECL (Perkin Elmer) was added. Total bioluminescence was monitored with a TriSTAR2 LB 942 microplate reader.

Data analysis. All data were analysed using Graphpad PRISM (GraphPad Software, La Jolla, CA, USA). A four parameters non-linear logistic equation was used to analyse the concentration-response curves, whereas unpaired or multiple T-test analysis was used to evaluate the statistical difference of single-concentration experiments. All data are represented by the mean ± SEM of multiple independent experiments.

Data availability. The authors declare that all data supporting the findings in this study are presented within the article and its Supplementary Information Files and are available from the corresponding author upon request.

Acknowledgements. This work was supported by grants from the Canadian Institutes for Health Research (CIHR), [MOP11215] and [FDN148431]. L-PP received a scholarship from CIHR and Fonds de la Recherche du Quebec – Santé (FRQS). AMS was supported by a post-doctoral research fellowship from FRQS. MB holds a Canada Research Chair in Signal Transduction and Molecular Pharmacology. We are grateful to Dr. Monique Lagacé for useful discussions and revision of the manuscript.

Author contributions. L-PP and MB designed the study. L-PP performed the experiments, as well as the analysis of the data. AMS designed and constructed the conformational sensors under the supervision of MJL. L-PP and MB interpreted the data and wrote the manuscript.

Competing interests statement. The authors declare that they have no competing financial or non-financial interest**.**

References

1 Lohse, M. J., Benovic, J. L., Codina, J., Caron, M. G. & Lefkowitz, R. J. beta-Arrestin: a protein that regulates beta-adrenergic receptor function. *Science* **248**, 1547-1550 (1990).

2 Luttrell, L. M. *et al.* Beta-arrestin-dependent formation of beta2 adrenergic receptor-Src protein kinase complexes. *Science* **283**, 655-661 (1999).

3 DeFea, K. A. *et al.* beta-arrestin-dependent endocytosis of proteinase-activated receptor 2 isrequired for intracellular targeting of activated ERK1/2. *The Journal of cell biology* **148**, 1267-1281 (2000).

4 Galandrin, S., Oligny-Longpre, G. & Bouvier, M. The evasive nature of drug efficacy: implications for drug discovery. *Trends in pharmacological sciences* **28**, 423-430, doi:10.1016/j.tips.2007.06.005 (2007).

5 Liu, Y. *et al.* Biased signalling: the instinctive skill of the cell in the selection of appropriate signalling pathways. *Biochem J* **470**, 155-167, doi:10.1042/BJ20150358 (2015).

6 Azzi, M. *et al.* Beta-arrestin-mediated activation of MAPK by inverse agonists reveals distinct active conformations for G protein-coupled receptors. *Proceedings of the National Academy of Sciences of the United States of America* **100**, 11406-11411, doi:10.1073/pnas.1936664100 (2003).

7 Pupo, A. S. *et al.* Recent updates on GPCR biased agonism. *Pharmacol Res* **112**, 49-57, doi:10.1016/j.phrs.2016.01.031 (2016).

8 Rankovic, Z., Brust, T. F. & Bohn, L. M. Biased agonism: An emerging paradigm in GPCR drug discovery. *Bioorg Med Chem Lett* **26**, 241-250, doi:10.1016/j.bmcl.2015.12.024 (2016).

9 Kenakin, T. The potential for selective pharmacological therapies through biased receptor signaling. *BMC Pharmacol Toxicol* **13**, 3, doi:10.1186/2050-6511-13-3 (2012).

10 Kenakin, T. & Christopoulos, A. Signalling bias in new drug discovery: detection, quantification and therapeutic impact. *Nature reviews. Drug discovery* **12**, 205-216, doi:10.1038/nrd3954 (2013).

11 Zocher, M., Fung, J. J., Kobilka, B. K. & Muller, D. J. Ligand-specific interactions modulate kinetic, energetic, and mechanical properties of the human beta2 adrenergic receptor. *Structure* **20**, 1391-1402, doi:10.1016/j.str.2012.05.010 (2012).

12 Liu, J. J., Horst, R., Katritch, V., Stevens, R. C. & Wuthrich, K. Biased signaling pathways in beta2-adrenergic receptor characterized by 19F-NMR. *Science* **335**, 1106-1110, doi:10.1126/science.1215802 (2012).

13 Bhattacharya, S., Hall, S. E., Li, H. & Vaidehi, N. Ligand-stabilized conformational states of human beta(2) adrenergic receptor: insight into G-protein-coupled receptor activation. *Biophysical journal* **94**, 2027-2042, doi:10.1529/biophysj.107.117648 (2008).

14 Dror, R. O. *et al.* Activation mechanism of the beta2-adrenergic receptor. *Proceedings of the National Academy of Sciences of the United States of America* **108**, 18684-18689, doi:10.1073/pnas.1110499108 (2011).

15 van der Westhuizen, E. T., Breton, B., Christopoulos, A. & Bouvier, M. Quantification of ligand bias for clinically relevant beta2-adrenergic receptor ligands: implications for

drug taxonomy. *Molecular pharmacology* **85**, 492-509, doi:10.1124/mol.113.088880 (2014).
16 Reiner, S., Ambrosio, M., Hoffmann, C. & Lohse, M. J. Differential signaling of the endogenous agonists at the beta2-adrenergic receptor. *The Journal of biological chemistry* **285**, 36188-36198, doi:10.1074/jbc.M110.175604 (2010).
17 Maier-Peuschel, M. *et al.* A fluorescence resonance energy transfer-based M2 muscarinic receptor sensor reveals rapid kinetics of allosteric modulation. *The Journal of biological chemistry* **285**, 8793-8800, doi:10.1074/jbc.M109.098517 (2010).
18 Devost, D. *et al.* Conformational Profiling of the AT1 Angiotensin II Receptor Reflects Biased Agonism, G Protein Coupling, and Cellular Context. *The Journal of biological chemistry* **292**, 5443-5456, doi:10.1074/jbc.M116.763854 (2017).
19 Sleno, R. *et al.* Designing BRET-based conformational biosensors for G protein-coupled receptors. *Methods* **92**, 11-18, doi:10.1016/j.ymeth.2015.05.003 (2016).
20 Schihada, H. *et al.* A universal bioluminescence resonance energy transfer sensor design enables high-sensitivity screening of GPCR activation dynamics. *Communications Biology* (2018).
21 Ghanouni, P. *et al.* Functionally different agonists induce distinct conformations in the G protein coupling domain of the beta 2 adrenergic receptor. *The Journal of biological chemistry* **276**, 24433-24436, doi:10.1074/jbc.C100162200 (2001).
22 Yao, X. J. *et al.* The effect of ligand efficacy on the formation and stability of a GPCR-G protein complex. *Proceedings of the National Academy of Sciences of the United States of America* **106**, 9501-9506, doi:10.1073/pnas.0811437106 (2009).
23 Hall, M. P. *et al.* Engineered luciferase reporter from a deep sea shrimp utilizing a novel imidazopyrazinone substrate. *ACS Chem Biol* **7**, 1848-1857, doi:10.1021/cb3002478 (2012).
24 Xu, Y., Piston, D. W. & Johnson, C. H. A bioluminescence resonance energy transfer (BRET) system: application to interacting circadian clock proteins. *Proceedings of the National Academy of Sciences of the United States of America* **96**, 151-156 (1999).
25 Angers, S. *et al.* Detection of beta 2-adrenergic receptor dimerization in living cells using bioluminescence resonance energy transfer (BRET). *Proceedings of the National Academy of Sciences of the United States of America* **97**, 3684-3689, doi:10.1073/pnas.060590697 (2000).
26 Bertrand, L. *et al.* The BRET2/arrestin assay in stable recombinant cells: a platform to screen for compounds that interact with G protein-coupled receptors (GPCRS). *J Recept Signal Transduct Res* **22**, 533-541, doi:10.1081/RRS-120014619 (2002).
27 Mercier, J. F., Salahpour, A., Angers, S., Breit, A. & Bouvier, M. Quantitative assessment of beta 1- and beta 2-adrenergic receptor homo- and heterodimerization by bioluminescence resonance energy transfer. *The Journal of biological chemistry* **277**, 44925-44931, doi:10.1074/jbc.M205767200 (2002).
28 Rasmussen, S. G. *et al.* Crystal structure of the beta2 adrenergic receptor-Gs protein complex. *Nature* **477**, 549-555, doi:10.1038/nature10361 (2011).
29 Breton, B. *et al.* Multiplexing of multicolor bioluminescence resonance energy transfer. *Biophysical journal* **99**, 4037-4046, doi:10.1016/j.bpj.2010.10.025 (2010).
30 Namkung, Y. *et al.* Monitoring G protein-coupled receptor and beta-arrestin trafficking in live cells using enhanced bystander BRET. *Nat Commun* **7**, 12178, doi:10.1038/ncomms12178 (2016).

31 Tian, W. N., Duzic, E., Lanier, S. M. & Deth, R. C. Determinants of alpha 2-adrenergic receptor activation of G proteins: evidence for a precoupled receptor/G protein state. *Molecular pharmacology* **45**, 524-531 (1994).
32 Nobles, M., Benians, A. & Tinker, A. Heterotrimeric G proteins precouple with G protein-coupled receptors in living cells. *Proceedings of the National Academy of Sciences of the United States of America* **102**, 18706-18711, doi:10.1073/pnas.0504778102 (2005).
33 Cevheroglu, O., Becker, J. M. & Son, C. D. GPCR-Galpha protein precoupling: Interaction between Ste2p, a yeast GPCR, and Gpa1p, its Galpha protein, is formed before ligand binding via the Ste2p C-terminal domain and the Gpa1p N-terminal domain. *Biochimica et biophysica acta* **1859**, 2435-2446, doi:10.1016/j.bbamem.2017.09.022 (2017).
34 Stallaert, W. *et al.* Purinergic Receptor Transactivation by the beta2-Adrenergic Receptor Increases Intracellular Ca(2+) in Nonexcitable Cells. *Molecular pharmacology* **91**, 533-544, doi:10.1124/mol.116.106419 (2017).
35 Cahill, T. J., 3rd *et al.* Distinct conformations of GPCR-beta-arrestin complexes mediate desensitization, signaling, and endocytosis. *Proceedings of the National Academy of Sciences of the United States of America* **114**, 2562-2567, doi:10.1073/pnas.1701529114 (2017).
36 Milligan, G., Unson, C. G. & Wakelam, M. J. Cholera toxin treatment produces down-regulation of the alpha-subunit of the stimulatory guanine-nucleotide-binding protein (Gs). *Biochem J* **262**, 643-649 (1989).
37 Gregorio, G. G. *et al.* Single-molecule analysis of ligand efficacy in beta2AR-G-protein activation. *Nature* **547**, 68-73, doi:10.1038/nature22354 (2017).
38 Rasmussen, S. G. *et al.* Structure of a nanobody-stabilized active state of the beta(2) adrenoceptor. *Nature* **469**, 175-180, doi:10.1038/nature09648 (2011).
39 Schonegge, A. M. *et al.* Evolutionary action and structural basis of the allosteric switch controlling beta2AR functional selectivity. *Nat Commun* **8**, 2169, doi:10.1038/s41467-017-02257-x (2017).
40 Thomsen, A. R. *et al.* GPCR-G Protein-beta-Arrestin Super-Complex Mediates Sustained G Protein Signaling. *Cell* **166**, 907-919, doi:10.1016/j.cell.2016.07.004 (2016).
41 Gales, C. *et al.* Probing the activation-promoted structural rearrangements in preassembled receptor-G protein complexes. *Nature structural & molecular biology* **13**, 778-786, doi:10.1038/nsmb1134 (2006).
42 Quoyer, J. *et al.* Pepducin targeting the C-X-C chemokine receptor type 4 acts as a biased agonist favoring activation of the inhibitory G protein. *Proceedings of the National Academy of Sciences of the United States of America* **110**, E5088-5097, doi:10.1073/pnas.1312515110 (2013).

Figure legends

Figure 1. Description and functional characterization of the intramolecular β2AR conformational biosensors. a) Schematic representation of the biosensors. b) Bioluminescence emission spectra of the YFP (NY-β2AR) and GFP10 (NG-β2AR) versions of the biosensor. c) Concentration-response curves of the NY-β2AR conformational biosensor following isoproterenol (ISO) stimulation, in the presence or absence of 10 μM propranolol (PRO). The data are express as % of the maximal ISO-promoted response. d) Absolute ΔBRET values of a typical experiment. e) BRET changes in the NY-β2AR induced by ligands with different intrinsic efficacy. Statistical analysis was performed using Student's tests with Holm-Sidak correction for multiple comparison (* p-value <0.05). f-g) Concentration-response curves for cAMP production (f) and recruitment of β-arrestin (g), using GFP10-mutE- PAC1-RlucII (a decrease BRET signal indicates an increase in cAMP production) and rGFP-CAAX/β-arrestin2-RlucII (an increase in BRET indicates a recruitment of β-arrestin to the receptor) BRET sensors, respectively, upon activation of NY-β2AR or the Flag-tagged wild-type β2AR (WT-β2AR) (for equivalent receptor levels; see Supplementary Fig. 2). In all cases, data are expressed as the mean ± SEM from 3 to 5 independent experiments conducted in duplicates.

Figure 2. Effects of Gs and β-arrestin on conformational changes promoted by isoproterenol (ISO) and salbutamol (SALB). a) Kinetics of the changes in BRET signal of the NY-β2AR conformational sensor upon ISO and SALB (100 μM) stimulation in HEK293T cells. Data are expressed as normalized ligand-promoted BRET changes; the maximal response of the biosensor in response to ISO being set as 100%. Although the ISO-promoted conformational

change results in a decrease in BRET, the BRET changes are represented as positive responses. b) Gαs-promoted change in the NY-β2AR conformational sensor BRET signal as a function of the amount of Gαs co-transfected. Data are expressed as percentage of ISO response in the absence of overexpressed G protein. The response to ISO in the absence of over-expressed Gs is represented by the square symbol on the Y axis. c-d) Effect of co-transfection of Gs or β-arrestin (500 ng per 10^6 cells) on the kinetics of ISO- and SALB-promoted conformational changes of the NY-β2AR sensor. Data are expressed as percentage of ISO-promoted response in the absence of Gs and β-arrestin overexpression (Fig. 2A), the dotted line corresponding to the basal BRET signal observed in the presence of overs-expressed Gs or β-arrestin in the absence of ligand. e-f) Concentration-response curves of the ISO-stimulated NY-β2AR response in HEK293 cells lacking β-arrestin vs their parental cells (e) or in HEK293 cells lacking Gs vs their parental cells (f). g-h) Basal BRET levels observed in the different cell lines. Statistical analysis was performed using an unpaired Student's test (* p-value <0.05). Data are expressed as percentage of ISO response for the parental

cell lines and represent the mean ± SEM of at least 3 independent experiments conducted in duplicates. i) Schematic cartoon of ISO- vs SALB-induced conformational changes.

Supplementary Figure 1. Comparison of NLuc (NY-β2AR and NG-β2AR) and Rluc (EPAC) luminescence emission in the presence of their appropriate substrate. a) Total fluorescence of Rluc-EPAC-GFP10 and NG-β2AR expressed as a percentage of the EPAC signal. b-c) Luminescence in cells expressing either Rluc-EPAC-GFP10 or NG-β2AR was measured 5 minutes after the addition of methoxy-e-coelenterazine(b) or coelenterazine 400a(c). Data are expressed as a percentage of the luminescence emitted in the channel corresponding to the

wavelengths associated with each of the substrates (400 nm for methoxy-e-coelenterazine and 480 nm for Coel-400). d) Theoretical emission spectra of RlucII, Nluc, GFP10, and YFP with the passing bands of the filters used for their detection (dotted rectangles). e-f) Evaluation of the transfer from Nluc to GFP10 (e) and from RlucII to YFP (f) in the multiplexing experiments to assess the possible contaminating emission of GFP10 and YFP upon excitation by Nluc/Coel-400 and Rluc/methoxy-e-coelenterazine, respectively. The transfer from Nluc to GFP10 was monitored by measuring the ratio of the emission in the GFP10 channel (515/40 nm) over the emission in the YFP channel (530/25 nm) after the addition of Coel-400, in the presence or absence of ISO. The transfer from RlucII to YFP was monitored by measuring the ratio of the emission in the YFP channel (530/25 nm) over the emission in the GFP channel (515/40 nm) after addition of methoxy-e-coelenterazine, in the presence or absence of ISO. This ratio in the multiplex condition was divided by the one obtained in a mock condition were the second sensor was not present. The equation used to assess the cross contamination between the multiplexed signals is shown at the bottom of panel (d). A ratio of 1 represents no detectable cross-transfer. g) Concentration-response curves for ISO stimulation of NY-β2AR sensor compared with WT-β2AR for β-arrestin recruitment assessed using the GFP10-linker-RlucII-pβarr2 sensor. Results show an increased signal for the NY-β2AR sensor compared with the WT due to the transfer of the RlucII to the YFP. Data represent the mean ± SEM of 3 independent experiments conducted in duplicates. The red dots and squares in a,b,c,e and f indicate the individual data points obtained in each of the independent experiments. Overall, the results show that essentially no cross-contaminating emission of the Nluc emission into the Rluc channel (less than 1%) or reciprocally of the Rluc emission in the Nluc channel (less than 3%) was detected when Coel-400 and methoxy-e-coelenterazine were used respectively as substrates (b-c). The data also

show that possible contamination transfer from Nluc to GFP10 does not contribute to the signal detected for the Nluc transfer to YFP in the multiplexed configurations (ratios between 1.01 and 1.02 for the various conditions(e)). Similarly, no significant contribution of the transfer of Rluc to YFP to the signal detected for Rluc transfer to GFP10 occurred in the NY-β2AR/Gs multiplexed configuration (Ratios between 0.99 and 1.04(f)). However, the transfer of energy between the Rluc attached to βarr-2 (GFP10-linker-RlucII-pβarr2) and the YFP of the NY-β2AR sensor contributed to the BRET signal detected for the βarr2 recruitment to the NY-β2AR in the multiplexed configuration in the presence of ISO (ratio of 1.28) as would be expected from the presence of the NYβ2AR and GFP10-linker-RlucII-pβarr2 in the same complex upon stimulation with ISO. This explains the higher βarr2 engagement response observed with NY-β2AR compared to WT β2AR.

Supplementary Figure 2. Cell surface expression levels of Flag-tagged NY-β2AR conformational sensor and WT β2AR assessed by ELISA. Data are expressed as a % of the expression level of the WT-β2AR. Data represent the mean ± SEM of 3 independent experiments conducted in duplicates. The red dots represent the individual data points obtained in each of the independent experiments. The results show similar levels of receptor on cells expressing either construct.

Supplementary Figure 3. Parallel (multiplexed) detection of the conformational biosensor signals and downstream transducer responses. Concentration-response curves were obtained for isoproterenol (ISO) and salbutamol (SALB) in cells co-expressing NY-β2AR and the individual downstream transducer sensors. Ligand-promoted NY-β2AR responses (a-c-e) alongside Gs

activation (bimolecular G protein activity sensor Gαs117RlucII/Gγ1-GFP10; b), cAMP production (unimolecular cAMP detecting sensor GFP10-mutEPAC1-RlucII; d) and β-arrestin engagement (unimolecular GFP10-linker-RlucII-pβarr2; f). The signal of the conformational sensor was monitored after addition of coelenterazine 400a and detected using 485 nm (donor)/535 nm (acceptor) emission filters, whereas Gs, EPAC and β-arrestin sensor signals were monitored after the addition of methoxy-e-coelenterazine using 400 nm (donor)/510 nm (acceptor) emission filters. Data represent the mean ± SEM of 4 independent experiments conducted in duplicates.

Supplementary Figure 4. Different G protein induced distinct conformational changes in NY-β2AR. G protein-promoted changes in the NY-β2AR conformational sensor BRET signal, as a function of the amount of co-transfected Gα12 (a) , Gαi2 (b) and β-arrestin2 (c). Data are expressed as normalized G protein-promoted BRET changes, the maximal response of the biosensor in response to ISO in the absence of over-expressed G protein being set as 100%. Data represent the mean ± SEM of 3 independent experiments conducted in duplicates.

Supplementary Figure 5. Functional characterization of cells in which Gs or β-arrestin were inactivated using the CRISPR/Cas9 gene editing system. a) Endocytosis of the β2AR in parental cells and β-arrestin-deficient cells. b) cAMP production by the β2AR upon ISO stimulation in parental cells and Gs-deficient cells. Data are represented as the mean ± SEM of 3 independent experiments. The results confirm the inactivation of Gs and β-arrestin.

Supplementary Figure 6. ISO-promoted NY-β2AR BRET signal changes in the absence of funtional Gs and β-arrestin. Concentration-response curves of isoproterenol (ISO)-stimulated

NY-β2AR expressed in HEK293 cells lacking β-arrestin and pre-treated with cholera toxin (CTX) (200 ng/mL for 18 h) to remove the influence of Gs (a). To control the inactivation of Gs by the CTX treatment, the receptor promoted Gs activation was assessed in the same cell background using the bimolecular G protein activity sensor Gαs117RlucII/Gγ1-GFP10, in the presence and absence of CTX treatment (b). Data are expressed as % response of untreated cells (no CTX). Data represent the mean ± SEM of 3-4 independent experiments conducted in duplicates and indicate that ISO can induce conformational changes independently of Gs and β-arrestin engagement.

Supplementary Figure 7. Effect of Gs and β-arrestin overexpression on the NY-β2AR conformational sensor response upon stimulation with SALB and SALM. Conformational changes in the NY-β2AR sensor upon stimulation with a saturating concentration (10 μM) of ISO, SALB and SALM. Data are expressed as percentage of ISO-promoted response in the absence of Gs and β-arrestin overexpression and represent the mean ± SEM of 5 independent experiments conducted in duplicates. Results demonstrate that SALM and SALB do not induce detectable conformational changes in cells overexpressing β-arrestin. However, in the presence of overexpressed Gs, both ligands reduce the Gs-promoted response of the NY-β2AR sensor, suggesting stabilization of a similar receptor conformational ensemble by the two ligands for the Gs-bound receptor.

Figure 1

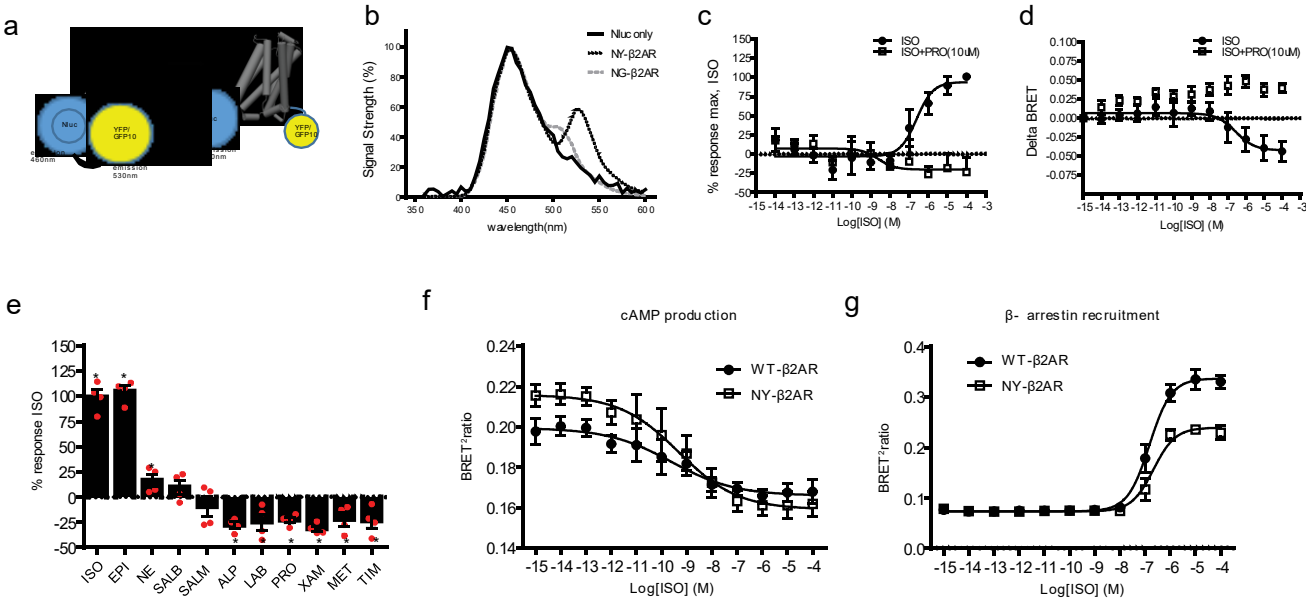
a
b
Nluc only
NY-β2AR
NG-β2AR
Signal Strength (%)
wavelength(nm)
c
ISO
ISO+PRO(10uM)
% response max, ISO
Log[ISO] (M)
d
ISO
ISO+PRO(10uM)
Delta BRET
Log[ISO] (M)
e
% response ISO
ISO
EPI
NE
SALB
SALM
ALP
LAB
PRO
XAM
MET
TIM
f
cAMP production
WT-β2AR
NY-β2AR
BRET²ratio
Log[ISO] (M)
g
β- arrestin recruitment
WT-β2AR
NY-β2AR
BRET²ratio
Log[ISO] (M)

Figure 2

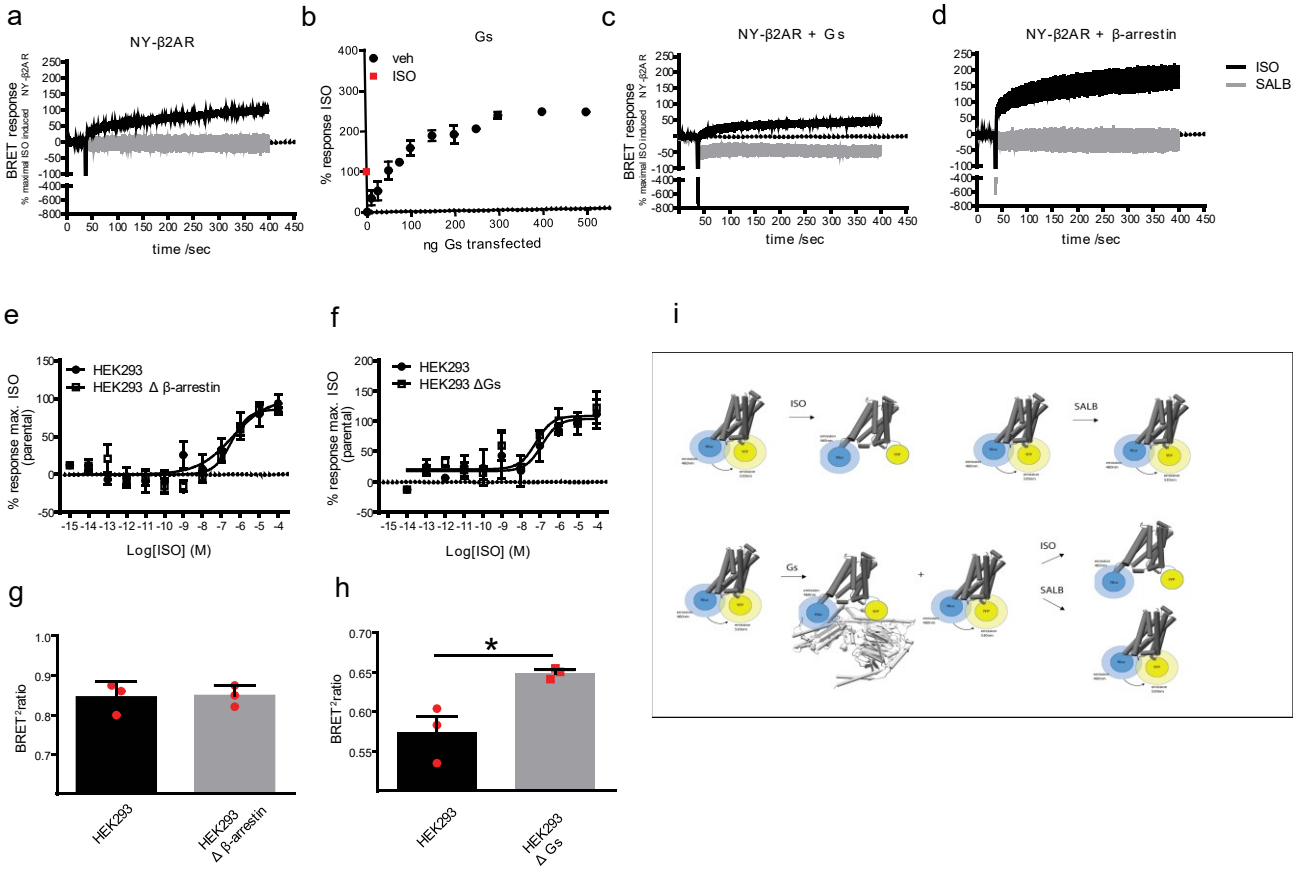
a
NY-β2AR
BRET response
% maximal ISO induced NY-β2AR
time /sec
b
Gs
veh
ISO
% response ISO
ng Gs transfected
c
NY-β2AR + Gs
BRET response
% maximal ISO induced NY-β2AR
time /sec
d
NY-β2AR + β-arrestin
ISO
SALB
time /sec
e
HEK293
HEK293 Δ β-arrestin
% response max. ISO (parental)
Log[ISO] (M)
f
HEK293
HEK293 ΔGs
% response max. ISO (parental)
Log[ISO] (M)
i
ISO
SALB
Gs
ISO
SALB
g
BRET²ratio
HEK293
HEK293 Δ β-arrestin
h
BRET²ratio
*
HEK293
HEK293 Δ Gs

Supplementary Figure 1

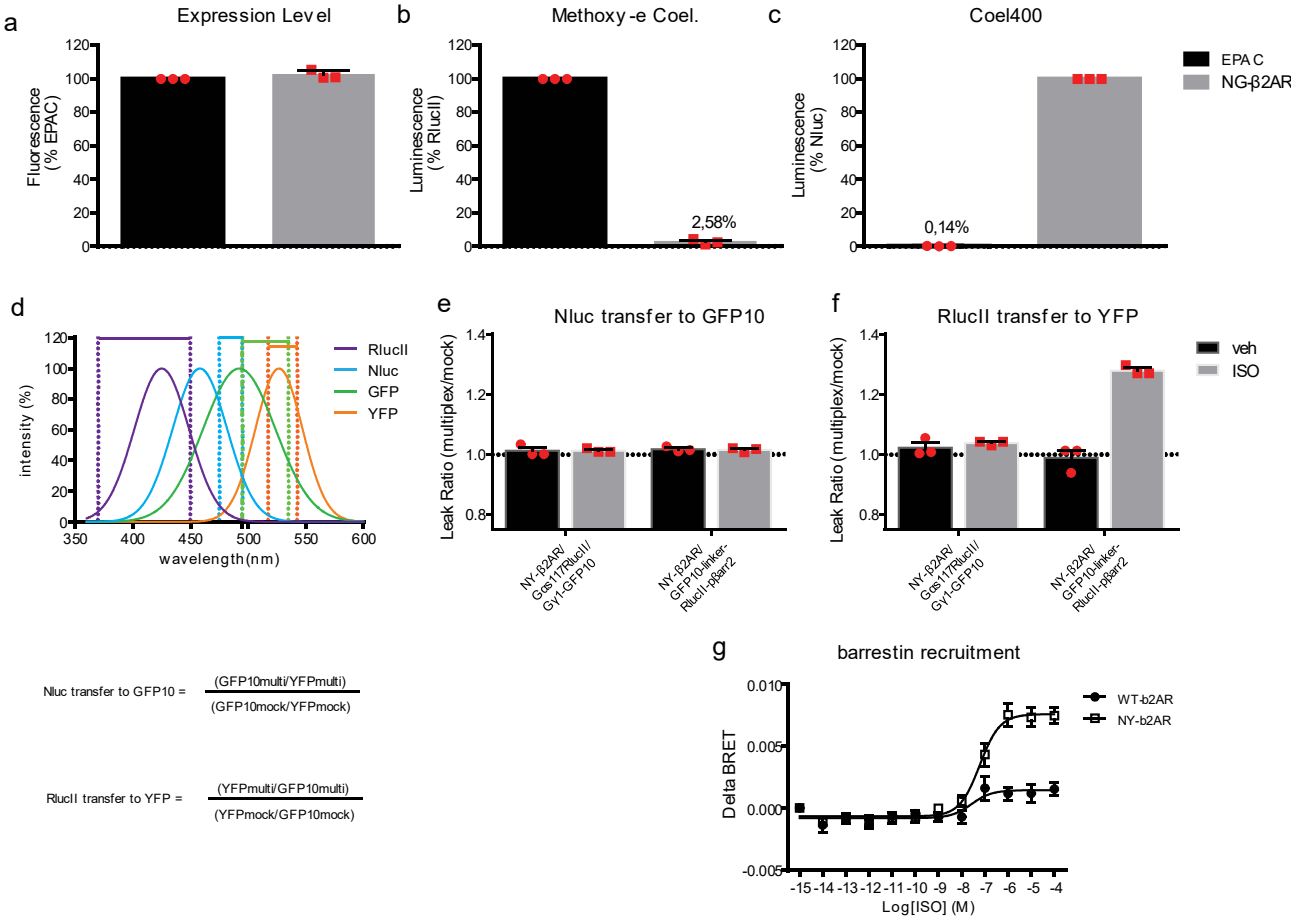

Supplementary Figure 2

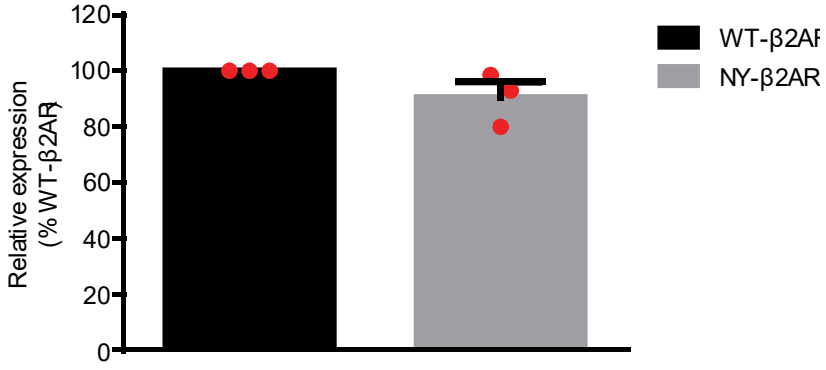

Supplementary Figure 3

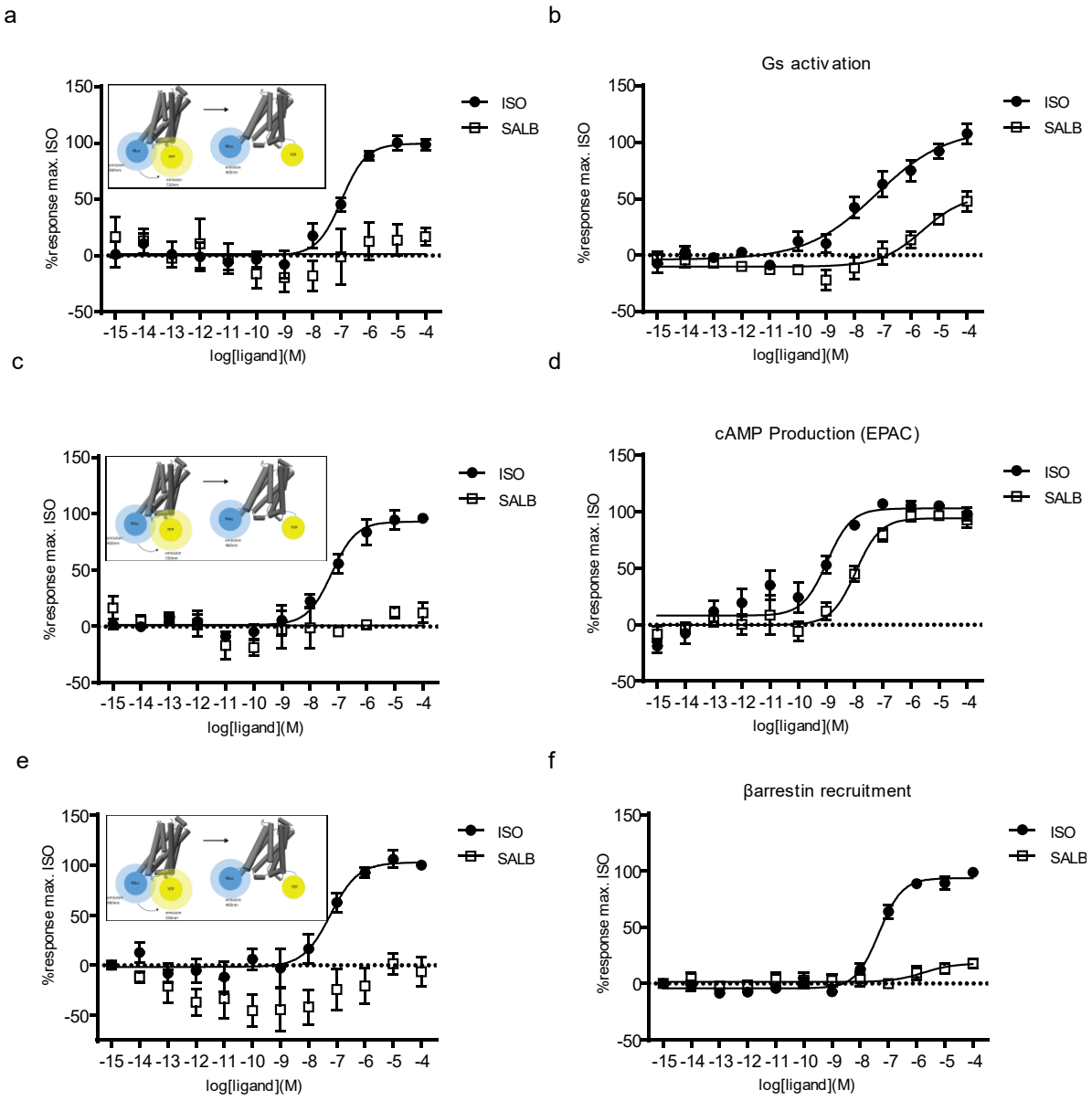

Supplementary Figure 4

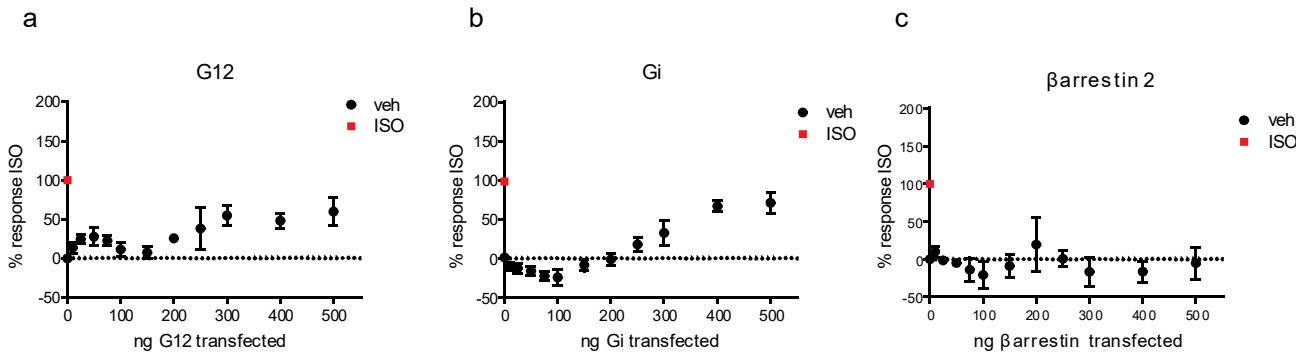

Supplementary Figure 5

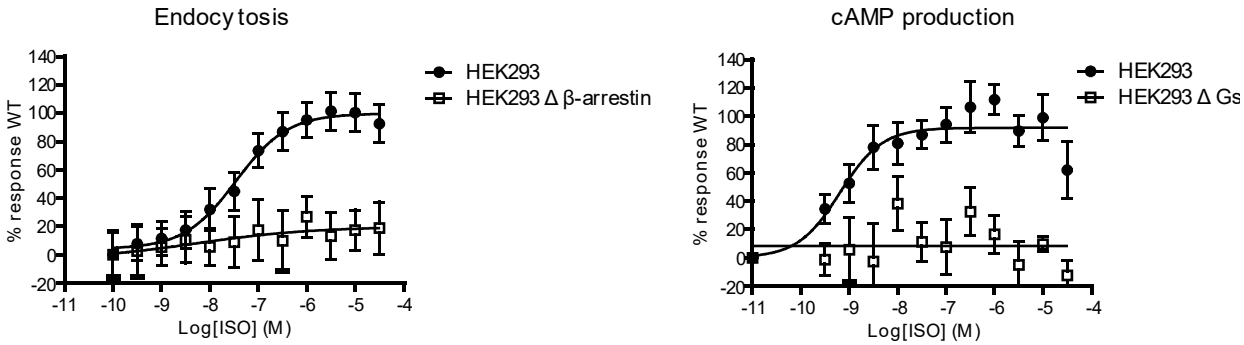

Supplementary Figure 6

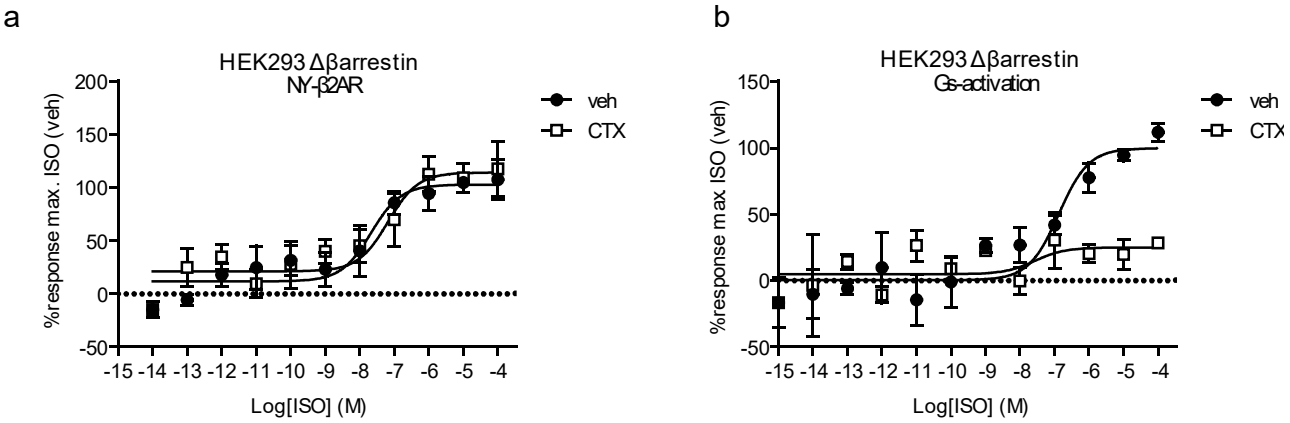

Supplementary Figure 7

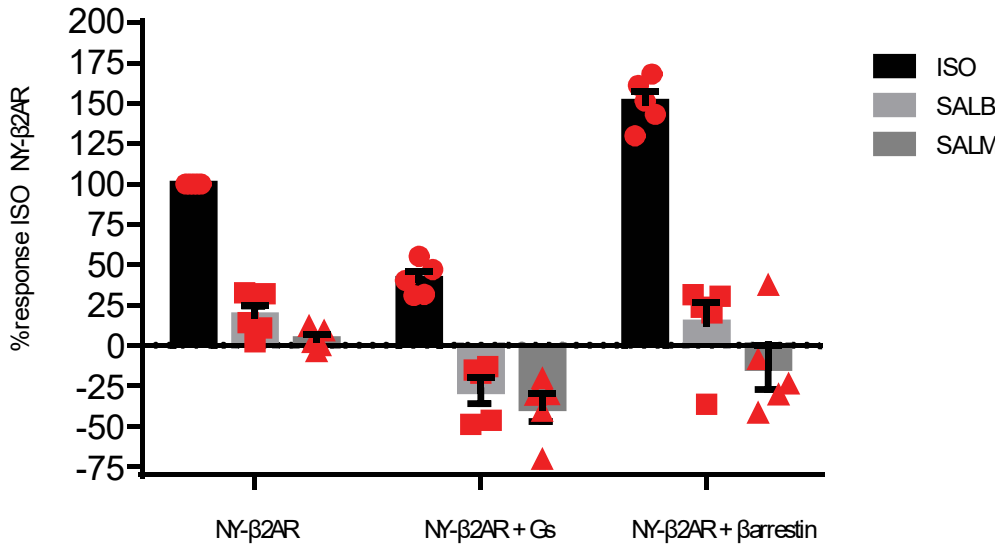

Article 2

Structural insights into binding specificity, efficacy and bias of a β2AR partial agonist

Matthieu Masureel*, Yaozhong Zou*, **Louis-Philippe Picard**, Emma van der Westhuizen, Jacob P. Mahoney, João P.G.L.M. Rodrigues, Thomas J. Mildorf, Ron O. Dror, David E. Shaw, Michel Bouvier, Els Pardon, Jan Steyaert, Roger K. Sunahara, William I. Weis, Cheng Zhang & Brian K. Kobilka
(* Contributions équivalentes des auteurs)

Publié dans *Nature Chemiacal Biology,* le 14 novembre 2018

Résumé

Le Salmétérol est un agoniste partiel du récepteur β2-adrénergique (β2AR), et le premier agoniste à longue action à être vastement utilisé en clinique pour le traitement de l'asthme et des maladies pulmonaires obstructives chroniques. Le salmétérol a été sujet à des controverses tant pour son innocuité que pour son mécanisme d'action. Pour comprendre son action pharmacologique inhabituelle et son activité agonisme partiel, nous avons obtenu la structure cristalline du β2AR lié au salmétérol en complexe avec un nanobody qui stabilise la conformation active du récepteur. La structure a révélé la location de l'exosite, où les séquences du β1AR et β2AR divergent expliquant la spécificité pour le sous-type de récepteur. De plus, une comparaison structurale entre la structure du β2AR lié à l'agoniste complet, l'épinéphrine, a révélé des différences dans le réseau de ponts hydrogènes impliquant les résidus Ser204$^{5.43}$ et Asn 293$^{6.55}$. Les études de mutagenèse et biophysique effectuées suggèrent que ces interactions mènent à une forme active distincte qui est responsable pour l'efficacité partielle sur l'activation de Gs et l'absence de recrutement de β-arrestin pour le salmétérol.

Contributions. J'ai effectué le design, les expériences et l'analyse de l'étude de mutagenèse qui a permis l'identification des résidus S204 et N293 comme potentiel point de contact pour

le biais observé pour le salmétérol sous la supervision de mon directeur de thèse. De plus, j'ai effectué la caractérisation des profils de signalisation de l'épinéphrine, l'isoprotérénol, le salbutamol et le salmétérol pour le récepteur de type sauvage en mesurant l'activation de Gs et le recrutement de la β-arrestine en plus de valider les changements conformationnels engagés par ces différents ligands dans des cellules entières en utilisant le biocapteur de l'article 1. Finalement, j'ai contribué avec mon directeur de thèse et l'équipe du Dr. Kobilka à l'écriture et aux révisions du manuscrit.

Structural insights into binding specificity, efficacy and bias of a β2AR partial agonist

Matthieu Masureel1,13, Yaozhong Zou1,12,13, Louis-Philippe Picard2, Emma van der Westhuizen2,12, Jacob P. Mahoney3,12, João P.G.L.M. Rodrigues1,4,5, Thomas J. Mildorf6,12, Ron O. Dror6,12, David E. Shaw6,7, Michel Bouvier2, Els Pardon8,9, Jan Steyaert8,9, Roger K. Sunahara10, William I. Weis1,5, Cheng Zhang11* & Brian K. Kobilka1*

1Department of Molecular and Cellular Physiology, Stanford University School of Medicine, Stanford,California, USA. 2Department of Biochemistry, Institute for Research in Immunology and Cancer, Université de Montreal, Montreal, Québec, Canada. 3Department of Pharmacology, University of Michigan, Ann Arbor, Michigan, USA. 4Department of Computer Science, Stanford University,Stanford, California, USA. 5Department of Structural Biology, Stanford University, Stanford, California, USA. 6D. E. Shaw Research, New York, NY 10036, USA. 7Department of Biochemistry and Molecular Biophysics, Columbia University, New York, New York, USA. 8Structural Biology Brussels, Vrije Universiteit Brussel, Brussels, Belgium. 9Structural Biology Research Center, VIB, Brussels, Belgium. 10Department of Pharmacology, University of California San Diego School of Medicine, La Jolla, California, USA. 11Department of Pharmacology and Chemical Biology, University of Pittsburgh, Pittsburgh, Pennsylvania, USA.

12Present addresses: Y.Z.: Geneus Technologies, Ltd, Chengdu, Sichuan, People's Republic of China. E.W.: Monash Institute for Pharmaceutical Sciences, Monash University, Victoria, Australia; J.P.M.: Department of Molecular and Cellular Physiology, Stanford University School of Medicine, Stanford, California, USA. T.M.: Dropbox, New York, New York, USA; R.O.D.: Department of Computer Science and Institute for Computational and Mathematical Engineering, Stanford University, Stanford, California, USA.

13These authors contributed equally.
* To whom correspondence should be addressed: chengzh@pitt.edu, kobilka@stanford.edu

Abstract

Salmeterol is a partial agonist for the β2 adrenergic receptor (β2AR), and the first long acting β2AR agonist (LABA) to be widely used clinically for the treatment of asthma and chronic obstructive pulmonary disease. Salmeterol has been controversial both for its safety and mechanism of action. To understand its unusual pharmacological action and partial agonism, we obtained the crystal structure of salmeterol-bound β2AR in complex with an active-state stabilizing nanobody. The structure reveals the location of the salmeterol exosite, where sequence differences between β1AR and β2AR explain the high receptor subtype selectivity. A structural comparison with the β2AR bound to the full agonist epinephrine reveals differences in the hydrogen bond network involving residues Ser $204^{5.43}$ and Asn $293^{6.55}$. Mutagenesis and biophysical studies suggest that these interactions lead to a distinct active-state conformation that is responsible for the partial efficacy of G protein activation and the limited β-arrestin recruitment for salmeterol.

Introduction

G-protein coupled receptors (GPCRs) are able to respond to a large variety of ligands with different efficacy profiles for specific signaling pathways[1]: full agonists that maximally stimulate; partial agonists that produce submaximal stimulation even at fully saturating concentrations; inverse agonists that suppress the basal signaling; and neutral antagonists that bind to the receptor without stimulating or inhibiting basal signaling. Among these categories, partial agonists are often better tolerated as therapeutics compared with full agonists[2].

Salmeterol is a partial agonist for the human β2-adrenergic receptor (β2AR). As a potent bronchodilator, it is among the most prescribed drugs for the treatment of asthma and chronic obstructive pulmonary disease (COPD)[3]. Compared to some other β2AR agonists such as isoproterenol and salbutamol, salmeterol exhibits two desirable pharmacological properties. First, salmeterol is able to distinguish β2AR from β1AR for selective stimulation (1400- to 3000-fold selectivity)[4], thereby minimizing cardiac toxicity[5]. Second, salmeterol belongs to the class of long-acting β2AR agonists (LABAs) with a duration of action up to 12 hours, in contrast to the short-acting β2AR agonists such as salbutamol with only a 4-6 hour duration of action[6-8]. Those pharmacological properties of salmeterol have contributed to its successful use in treating asthma and COPD for more than two decades. However, LABAs used alone, especially salmeterol, have been implicated, in several clinic trials, to be associated with increased mortality in asthmatics. This liability is mitigated when LABAs are combined with an inhaled corticosteroid[9-11].

The high selectivity and long-acting properties of salmeterol have been attributed to its unusual bitopic structure. In addition to the saligenin ethanolamine pharmacophore that replaces the catecholamine structure of the endogenous β2AR ligand epinephrine (also known as adrenaline), salmeterol contains an extra moiety of an aryloxyalkyl tail consisting of a phenol ring with an eleven-atom ether chain (**Fig. 1a**). While the pharmacophore binds to the orthosteric site responsible for receptor activation, the aryloxyalkyl tail is proposed to bind to an additional site (exosite), providing additional interactions responsible for the high receptor-subtype selectivity and the slow dissociation rate contributing to its long duration of action[12]. Previous mutagenesis and biochemical studies to locate the exosite have led to conflicting results[4,12-16]. Salmeterol is also of interest in being a functionally selective β2AR partial agonist with a 5- to 20-fold bias towards Gs over arrestin[17,18]. Previous studies revealed that, compared to isoproterenol, activation of the β2AR by salmeterol leads to slower initial rates of G protein-coupled receptor kinase (GRK) phosphorylation with similar maximal degrees of phosphorylation[19,20], but strongly reduced arrestin-mediated receptor internalization and desensitization[17,21,22], contributing to the prolonged therapeutic effect of salmeterol in bronchial dilation as a result of β2AR stimulation. This signaling bias may contribute to the advantageous therapeutic profile of salmeterol by maintaining bronchodilation through Gs-mediated signaling while minimizing arrestin-mediated β2AR desensitization, and avoiding arrestin-dependent pro-inflammatory effects[23,24] .

Recent progresses in the structural characterization of β adrenergic receptors, especially the crystal structures of active β2AR bound to full agonists BI-167107 or epinephrine (also known as adrenaline), with either a Gs protein or active-state stabilizing nanobody, as well as

the crystal structures of inactive avian β1AR bound to a variety of full and partial agonists, have greatly advanced our understanding of the pharmacology and activation of β adrenergic receptors[25-29]. In an effort to further understand the molecular basis for the unusual pharmacological properties of salmeterol and its partial agonism, we obtained the crystal structure of salmeterol-bound human β2AR in an active state stabilized by a conformation specific nanobody, Nb71. The structure reveals the location of the exosite and provides a structural explanation for the high receptor-subtype selectivity and distinct signaling behavior of salmeterol.

Results

Nanobody Nb71 stabilizes the salmeterol-bound β2AR

It has been shown for the β2AR and the μ-opioid receptor (μOR) that agonists alone are not sufficient to stabilize the receptors in active conformational states[27,30-32]. As a result, the active-state structures of the β2AR and μOR have required either a G protein or conformation specific camelid antibody fragments (nanobodies) to stabilize the active states of the receptors[25,26,29]. The first active-state structure of a hormone-activated GPCR was obtained using a nanobody named Nb80, which was obtained from a llama immunized with β2AR bound to the ultra high-affinity full agonist BI-167107 reconstituted into phospholipid vesicles[25]. The structures of β2AR in the β2AR-Nb80 complex and the β2AR-Gs complex are very similar[25,26]. However, evidence from biophysical studies suggest that partial agonists may stabilize distinct states[33], so Nb80 may not be the best candidate to stabilize salmeterol bound β2AR.

While Nb80 preferentially binds to agonist-occupied β2AR over antagonist-occupied β2AR[25], Octet Red studies show that Nb80 also preferentially binds to β2AR bound to BI-167107 and epinephrine over β2AR bound to salmeterol (**Supplementary Table 1**). Moreover, Nb80 has a greater effect on enhancing the binding affinity of the agonist isoproterenol than on the partial agonist salmeterol (**Supplementary Fig. 1**). We therefore selected another nanobody, Nb71, generated from the same immunization that produced Nb80. Nb71 preferentially binds to agonist-occupied β2AR[34], but in contrast to Nb80, has no preference for these catecholamines over salmeterol (**Supplementary Table 1, Supplementary Fig. 1**). Therefore, we chose Nb71 to stabilize the salmeterol-bound β2AR for structural characterization.

Structural features of Nb71-stabilized β2AR

We used an engineered β2AR with T4 lysozyme (T4L) fused to its N-terminal region and a truncated intracellular loop3 (referred to as T4L-β2AR-ΔICL3 hereafter) to crystallize β2AR bound to salmeterol. Previous studies have demonstrated that T4L-β2AR-ΔICL3 exhibits similar ligand binding and G protein activating properties as the wild type β2AR[37]. Using this construct, we obtained crystals of the β2AR-salmeterol-Nb71 complex by the lipidic cubic phase (LCP) method[35]. A complete data set was obtained by merging data from 23 crystals and the structure was determined to a resolution of 3.0 Å (**Fig. 1b,c; Supplementary Table 2**). Like Nb80, Nb71 binds to the cytoplasmic surface of the receptor with its third complementarity-determining region (CDR3) loop inserted into a hydrophobic cavity formed by residues from

transmembrane helices (TMs) 3, 5, 6 and 7 (**Fig. 1b, Supplementary Fig. 2**), yet Nb71 stabilizes a conformation that is distinct from that stabilized by Nb80 (**Supplementary Fig. 2**).

The active-state conformation of the receptor in the β2AR-salmeterol-Nb71 complex resembles that of the BI-167107-bound β2AR in complex with Nb80 (PDB ID 3P0G, rmsd = 1.0 Å) or with Gs (PDB ID 3SN6, rmsd = 1.3 Å) more than the inactive-state conformation of the receptor in the inverse agonist carazolol-bound β2AR structure (PDB ID 2RH1, rmsd = 1.9 Å)[25,26]. Indeed, the structural features associated with receptor activation[25], including the outward movement of TM6 at the cytoplasmic side associated with the conformational changes of the core triad residues Pro $211^{5.50}$, Ile $121^{3.40}$ and Phe $282^{6.44}$, as well as the slightly contracted ligand-binding pocket at the extracellular side, are all observed in the structure of β2AR-salmeterol-Nb71 complex when compared to the inactive β2AR (**Fig. 2a-c**). However, the Nb71-stabilized β2AR shows some distinct structural features compared to the Nb80- and Gs-stabilized β2AR. Relative to the inactive β2AR, the Nb71-stabilized β2AR displays a smaller outward movement of the cytoplasmic end of TM6 (8Å) than the Nb80-stabilized β2AR (11Å) or Gs-stabilized β2AR (13Å) (**Fig. 2a**). There is also a slightly smaller counter-clockwise rotation of TM6 in the Nb71-stabilized β2AR when viewed from the cytoplasmic surface, as shown by the position of Glu268 (**Fig. 2b**). While this current structure clearly shows an active-state conformation of β2AR, the smaller conformational rearrangements observed for TM6 upon activation compared to the changes seen for the active-state stabilized β2AR bound to Nb80 or Gs suggest a less active or a partially active conformational state of β2AR stabilized by Nb71. It is tempting to speculate that such partially active conformational state may closely resemble a salmeterol-stabilized conformation of β2AR that is less efficient at coupling to Gs. However,

the conformation of TM6 is primarily stabilized by interactions with Nb71 and may not reflect the conformation stabilized by salmeterol alone.

Exosite binding of salmeterol

The location and the molecular details of the exosite for the aryloxyalkyl tail of salmeterol are of great interest because of its association with the high receptor selectivity, high affinity and long-lasting action properties of salmeterol. The clear electron density map of salmeterol based on our structure allowed us to unambiguously define the structural basis of the exosite (**Figs. 3a,b & Supplementary Figs. 3,4**). The crystal structure shows that the aryloxyalkyl tail of salmeterol extends towards the extracellular surface of the receptor, occupying a cleft formed by residues from extracellular loop2 (ECL2), ECL3 and the extracellular ends of TM6 and TM7. Interactions between salmeterol and the exosite are mediated primarily through extensive van der Waals and hydrophobic interactions (**Fig. 3c**). The phenol ring of the tail also forms π-π interactions with the surrounding aromatic residues Phe 194ECL2, Tyr $308^{7.35}$ and His $296^{6.58}$ (Ballesteros-Weinstein numbers), in agreement with previous studies reporting a 5- to 18-fold decrease of salmeterol affinity caused by mutating those residues4. In addition, the ether oxygen atom of the tail forms a hydrogen bond with the main chain amide group of residues Phe 193 ECL2 (**Fig. 3a**). It acts as a 'hinge' point where the tail of salmeterol bends almost 90° to fit the exosite. Previous studies indicated that shifting the ether oxygen in the aryloxyalkyl tail or removing it substantially reduces the affinity of salmeterol for β2AR[21], suggesting an important role of this hydrogen bond in the exosite binding (**Supplementary Fig. 5**). All those additional interactions in the exosite contribute to the 1000-

fold higher affinity of salmeterol compared to salbutamol, a short-acting β2AR agonist (SABA) which shares the same orthosteric pharmacophore as salmeterol but lacks the long aryloxyalkyl tail36 (**Fig. 1a**).

The exosite binding also explains the very high selectivity of salmeterol for β2AR over β1AR (>3000-fold)[36]. β1AR and β2AR share a very high overall structural similarity (rmsd of carazolol-bound avian β1AR and human β2AR = 0.58 Å, PDB IDs 2YCW & 2RH1, respectively) and sequence similarity (92% in TM segments for human β1AR and β2AR, **Supplementary Fig. 6**). In particular, all residues that form the orthosteric binding pocket, with the exception of Y308 are identical in β1AR and β2AR. In contrast, the exosite is relatively divergent in those two receptors. Salmeterol achieves high receptor selectivity by sampling this divergent region with its long aryloxyalkyl tail (**Fig. 3d, Supplementary Fig. 6)**. Such selectivity determinants do not apply to salbutamol, which only has about 20-fold selectivity for β2AR over β1AR[36]. Our results are in agreement with extensive chimeric receptor and site-directed mutagenesis studies recently reported by Baker et al.[7], who observed the K305D and H296K mutations in the β2AR to have a substantial effect on salmeterol affinity while having little effect on salbutamol affinity.

The salmeterol exosite in β2AR is reminiscent of the well-defined allosteric site in the M2 muscarinic receptor (M2R)[37]. The M2R represents one of the most extensively characterized model systems for allosteric regulation. **Fig. 3e** shows a comparison of the exosite in the β2AR and the binding site for the positive allosteric modulator LY2119620 revealed by the active-state crystal structure of M2R bound to the orthosteric agonist iperoxo and LY211962037. The

similarity between those two sites suggests the potential for allosterically regulating β2AR activity by small molecules that target the exosite. On the other hand, the bitopic nature of salmeterol with two-site binding on β2AR supports the feasibility of developing highly selective bitopic compounds for other GPCRs including muscarinic receptors38.

Polar interactions within the orthosteric binding site

While the interactions between the aryloxyalkyl tail of salmeterol and the exosite in the extracellular vestibule of β2AR confer the high affinity and selectivity of salmeterol, they are not responsible for its efficacy and signaling bias. Salmeterol and salbutamol exhibit similar signaling properties including partial agonism and the selective activation of Gs over arrestin and Gi (**Supplementary Fig. 7**)[17], despite their differences in affinity and receptor selectivity. Considering that salmeterol and salbutamol only share the saligenin ethanolamine pharmacophore (**Fig. 1a**), the interactions between this shared pharmacophore and the receptor within the orthosteric binding pocket are likely to be responsible for their shared signaling properties. In the orthosteric binding site, the alkylamine and β-hydroxyl groups of salmeterol form hydrogen-bonding interactions with Asp $113^{3.32}$ and Asn $312^{7.39}$ and the saligenin group forms hydrogen-bonding interactions with Ser $203^{5.42}$ and $Ser207^{5.46}$, similar to those observed for β2AR bound to the full agonist epinephrine (**Figs. 4a,b**). In the structure of β2AR bound to epinephrine, the hydrogen bonding interactions with Ser $203^{5.42}$ and $Ser207^{5.46}$ are associated with the inward movement of TM5 around those two serine residues, which is further linked to the rearrangement of the core triad residues and the outward movement of the cytoplasmic end of TM6[29]. For salmeterol, the two saligenin hydroxyl groups also form direct hydrogen bonding

interactions with Ser 203$^{5.42}$ and Ser 207$^{5.46}$. However, compared to epinephrine, these interactions with salmeterol may have a weaker effect on stabilizing the inward movement of TM5 because of the additional methylene between the meta position hydroxyl group and the phenyl ring.

In epinephrine-bound β2AR, Asn 293$^{6.55}$ forms a hydrogen bond with Ser 204$^{5.43}$ and the meta-hydroxyl of epinephrine. This polar network is not observed in salmeterol-bound β2AR. Asn 293$^{6.55}$ and Ser 204$^{5.43}$ have previously been shown to be important for the binding of epinephrine but not for the binding of antagonists[39,40]. To further investigate the possible role of these polar networks in ligand efficacy, we used molecular dynamics simulations to characterize the stability of specific ligand-receptor hydrogen bonds that would be expected to stabilize the inward movement of TM5 and the rotation of TM6 observed in active state structures of the β2AR (**Fig. 5a**). These simulations show that salmeterol forms less stable hydrogen bonds with Asn293$^{6.55}$ and Asn312$^{7.39}$ than does epinephrine. Salmeterol forms a more stable hydrogen bond with Ser203$^{5.42}$, but apparently only because its longer hydroxymethyl group can maintain this hydrogen bond better than epinephrine's hydroxyl group even when TM5 moves away from its crystallographic position. Thus, while the salmeterol-bound crystal structure captured a binding pocket conformation similar to that observed for full agonist, molecular dynamics simulations suggest that this active conformation is stabilized less by salmeterol than by epinephrine, with the most dramatic difference observed for Asn293$^{6.55}$. To further characterize the role of Asn 293$^{6.55}$ and Ser 204$^{5.43}$ interactions, we examined the effects of mutating these residues on β-arrestin2 recruitment and Gs activation by bioluminescence resonance energy transfer (BRET) between membrane anchored GFP and luciferase-tagged arrestin or luciferase-tagged Gs and

GFP-tagged Gβ1/Gγ1, respectively[41,42](**Fig. 5b,c & Supplementary Table 3**). For all the mutations we tested in the presence of isoproterenol, a catecholamine similar to epinephrine, we observe a dramatic reduction in β-arrestin2 recruitment (**Fig. 5b, left panel**), and a more moderate reduction in Gs activation (**Fig. 5c, left panel**). This suggests an important role of these two residues in regulating bias, either by directly modulating arrestin coupling, or by altering GRK phosphorylation and hence arrestin binding. Interestingly, the same mutations, with the exception of S204T, had a less pronounced effect on the ability of salmeterol to activate Gs (**Fig. 5c, right panel**), and all mutants showed very little or no salmeterol-induced arrestin recruitment, similar to wild-type β2AR (**Fig. 5b, right panel**). Thus, the absence of the hydrogen bonds between Asn $293^{6.55}$ and salmeterol may account for the weak β-arrestin recruitment, as well as the lower efficacy in Gs activation of salmeterol-bound β2AR compared to β2AR bound to full agonist.

Spectroscopic insights into salmeterol-bound β2AR

The differences in efficacy and signaling bias between salmeterol and the full agonist epinephrine suggest that salmeterol may stabilize a distinct conformation. Previous single molecule Förster resonance energy transfer (FRET) studies suggested a smaller outward displacement of TM6 in β2AR bound to salmeterol compared to β2AR bound to epinephrine or BI16710743. In addition, cellular assays using a BRET-based β2AR conformational sensor44 confirmed the reduced propensity of salmeterol to promote the outward movement of TM6 (**Supplementary Fig. 8**). Nevertheless, these RET studies cannot distinguish the following two mechanistic possibilities: 1- salmeterol stabilizes the same conformation of TM6 as epinephrine,

but for a smaller receptor population; 2- salmeterol stabilizes a distinct TM6 conformation. To further investigate the differences at the cytoplasmic end of TM6 upon activation between salmeterol-bound and epinephrine-bound β2AR in the absence of conformation-stabilizing nanobodies, we performed steady-state spectroscopic studies on purified, labeled receptor in detergent with two different reporter systems (**Supplementary Fig. 9a**). We used β2AR labeled at Cys 265 with the fluorophore monobromobimane (mBBr or bimane), which we previously used as a conformational reporter of β2AR activation[31,45], and developed a new fluorescent reporter system using an engineered β2AR labeled at residue 266 with the fluorophore Atto655.

The bimane fluorophore has been extensively used to report on activation of β2AR[25,45,46] as well as other GPCRs[47,48,] as it is very sensitive to its chemical environment. In the inactive state, bimane attached at the cytoplasmic end of TM6 is in a hydrophobic environment. Upon receptor activation, the intracellular end of TM6 undergoes an outward and "unwinding" motion (**Fig. 6a**) that shifts bimane to a more polar and solvent-exposed environment, resulting in a decrease in fluorescence intensity and a red-shift in λmax. Agonists alone produce a 10-20% decrease in intensity and ~10 nm red-shift in λmax. Further changes are observed upon G protein coupling. Using this reporter system, we find that even though salmeterol has a higher binding affinity to β2AR than epinephrine[6], epinephrine causes a larger reduction in intensity and red-shift in λmax of bimane compared to salmeterol when both ligands are used at saturating concentrations (**Fig. 6b**). This suggests that salmeterol stabilizes β2AR in conformations with on average a smaller outward movement or rotation of TM6. In addition, we observe that Gs induces a similar bimane response with salmeterol as with epinephrine (**Fig. 6b**, "+Gs" curves), indicating that once coupled to Gs, the β2AR adopts a similar TM6 conformation no matter what agonist is bound

at the extracellular region, consistent with previous single molecule FRET studies[33]. Nevertheless, the extent to which salmeterol-bound receptor couples to Gs appears to be slightly lower, as the change in λmax and fluorescence intensity is slightly less pronounced compared to epinephrine-bound receptor.

To complement the bimane-based measurements, we developed a new, distance sensitive fluorescent reporter. Rather than relying on FRET, where stoichiometric and specific labeling of donor and acceptor is required to faithfully report on distance changes in bulk measurements, we employed a single-dye reporter system. In photo induced electron transfer (PET), fluorophores such as Atto655 can be quenched by a tryptophan in close proximity, through the formation of weakly fluorescent or non-fluorescent dye-tryptophan ground-state complexes[49] (**Fig. 6c**). Owing to the strong distance-dependence of PET, small-scale conformational changes result in "on–off" switching of fluorescence, yielding a change in fluorescence intensity but no shift in λmax over a small distance range, typically about 5-10Å[49].

To report only on the outward motion of TM6, we chose to label Leu 266 mutated to cysteine instead of the native Cys 265, as the former does not undergo inward to outward rotations upon activation, but points outwards in both active and inactive structures (**Supplementary Fig. 9a**). Based on the inactive and active β2AR crystal structures and dye simulations (**Supplementary Fig. 9b**), we speculated that a tryptophan residue introduced at the intracellular end of TM5 (L230W) would quench the fluorescence of Atto655 in the inactive, but considerably less in the active state, as the distance range and change between TM5 and TM6 that occurs upon activation should be compatible with PET-induced quenching. By

simulating the conformational ensembles of Atto655 bound to Cys 266 in the inactive and active β2AR structures, we found an average dye-Trp 230 distance change of about ~5 Å upon receptor activation (**Supplementary Fig. 9b**), compatible with the reported quenching distance. We thus introduced mutations L230W and L266C into a minimal cysteine background β2AR[33] and verified that the detergent-purified, Atto655-labeled β2ARΔ6 L230W:L266C construct retained wild-type ligand binding properties (**Supplementary Fig. 10**).

When measuring the steady-state fluorescence emission of Atto655-labeled β2ARΔ6 L230W:L266C, referred to as Atto-β2AR from here on, in the presence of saturating concentrations of epinephrine, we observe a ~30% increase in fluorescence intensity compared to unliganded receptor, compatible with an outward motion of TM6 and an increased distance between Atto655 and the Trp 230 quencher on TM5 (**Fig. 6d, Supplementary Fig. 11a**). Given the short distance over which PET-quenching occurs, this observation likely reflects a TM6 displacement of ~5Å or more in approximately 30% of epinephrine-bound receptor. This is consistent with the fraction of receptor in an active conformation observed in double electron-electron resonance spectroscopy studies[31]. Interestingly, we observed a much smaller difference (<10%) between unliganded and salmeterol-bound receptor (**Fig. 6d, Supplementary Fig. 11a**), suggesting that TM6 did not move sufficiently far away from TM5 in salmeterol-bound β2AR to reduce Atto655 quenching by Trp230. Based on the efficacy of salmeterol in G protein activation (60% of isoproterenol, **Supplementary Fig. 7c**) we would expect a much larger change in Atto-β2AR fluorescence in response to salmeterol if salmeterol and isoproterenol stabilized the same active state. Addition of Gs to salmeterol- and isoproterenol-bound Atto-β2AR led to a 1.8- and 2.2-fold increase in fluorescence intensity, respectively, compared to

unliganded receptor (**Fig. 6d**, "+Gs" curves). This is consistent with the G protein stabilizing an active conformation in a larger fraction of receptor. Control measurements on a construct without the engineered L230W mutation showed little intensity change upon addition of agonists alone or together with Gs (**Supplementary Fig 11b**). In line with the difference in TM6 outward motion between the Nb80- and Nb71-bound structures, the Atto response in the presence of Nb80 is much larger than in the presence of Nb71, both for epinephrine and salmeterol (**Supplementary Fig. 11c**). This is similar to what we observed in the presence of Gs (**Fig. 6b, d**): when both ligand and Gs or nanobody are present, the TM6 receptor conformation is mainly stabilized by the intracellular binding protein and not the ligand. However, both of our fluorescence-based approaches in the absence of nanobody clearly suggest a difference in TM6 conformation between epinephrine- and salmeterol-bound receptors.

Discussion

β2ARs expressed in airway smooth muscle and epithelial cells mediate bronchodilation and fluid clearance, respectively, and are thus well-established targets for the treatment of asthma and COPD[50]. The unusual pharmacological characteristics of salmeterol including the extremely high selectivity for β2AR and the long duration of action, which can be attributed to its long aryloxyalkyl tail, make it among the most commonly prescribed LABAs for treating asthma and COPD. Our structure revealed an additional site in the extracellular vestibule of β2AR, the exosite, for the binding of the aryloxyalkyl tail, thus providing a structural basis for the prominent pharmacological action of salmeterol. It also resolves a long-standing debate as to the location of the exosite.

Our results also provide structural insights into the partial agonism and the biased signaling property of salmeterol, which are attributed to its saligenin ethanolamine group bound in the orthosteric binding pocket. Although the interactions with the receptor in the orthosteric binding pocket are very similar for the full agonist epinephrine and the partial agonist salmeterol, we observe subtle differences in hydrogen bonding interactions. Most notable is the absence of interactions between salmeterol and Asn $293^{6.55}$, which is further supported by molecular dynamics simulations. The meta-hydroxyl of epinephrine forms a hydrogen bond with Asn $293^{6.55}$, which is also hydrogen bonded with Ser $204^{5.43}$. Our mutagenesis studies suggest that this hydrogen bond network may be important for stabilizing TM6 in a conformation necessary for efficient G protein coupling as well as GRK phosphorylation and/or arrestin coupling. Therefore, the less extensive polar interactions between salmeterol and Asn $293^{6.55}$ may contribute to the weaker efficacy of salmeterol in activating Gs and the near absence of β-arrestin recruitment, possibly due to inefficient coupling as a result of reduced GRK phosphorylation[19].

The structure of salmeterol-bound β2AR revealed a smaller outward movement of TM6 compared to the epinephrine-bound β2AR. While this conformation implies a 'partially active' conformation of the receptor, it is likely imposed by the nanobody Nb71 rather than by the partial agonist salmeterol. Previous studies have suggested relatively weak allosteric coupling between the orthosteric site and the cytoplasmic site[31]. Thus, it is difficult to capture the ligand specific conformation of β2AR by protein crystallography. We took spectroscopic approaches using two different reporter systems to interrogate the conformational changes of β2AR

associated with salmeterol, and showed that indeed TM6 did not achieve the same extent of outward motion compared to the full agonist epinephrine. This correlates with previous single molecule investigations of TM6 motion in the β2AR[33], and provides a structural basis for salmeterol's weaker Gs efficacy and possibly ligand bias. Whether this mechanism applies to other GPCRs needs further investigation.

Acknowledgments

This work was supported by National Institutes of Health grants R01NS028471 (B.K.K.), the Canadian Institute for Health Research foundation grant FDN-148431 (M.B.), the American Heart Association Postdoctoral fellowship (17POST33410958) (M.M.) and Predoctoral Fellowship (13PRE17110027) (J.P.M.), a studentship from the FRQ-S (L.P.P.) and the NIH Pharmacological Sciences Training Program (T32GM007767) (J.P.M.). B.K.K. is supported by the Chan Zuckerberg Biohub. M.B. Holds a Canada Research Chair in Signal Transduction and Molecular Pharmacology. The authors thank J. Gullingsrud for assistance with MD software.

Author Contributions

C.Z. and Y.Z. expressed and purified the receptor and nanobody for crystallography studies, collected X-ray diffraction data and solved the crystal structure. M.M. developed the Atto655 reporter system, purified and labeled receptors used in fluorescence studies, collected spectroscopic data, and performed radioactive ligand binding assays. L.P.P. generated mutants of N293 and S204. E.W. and L.P.P. performed Gs activation and β-arrestin2 recruitment BRET

assays under supervision from M.B. J.M. performed octet red experiments under supervision from R.S. J.P.G.L.M.R. performed modeling and sampling of the Atto655 dye on the receptor structures. T.J.M. and R.O.D. performed and analyzed MD simulation studies. R.O.D. and D.E.S. oversaw MD simulations and analysis. E.P. generated the nanobody library and performed the initial selections. J.S. supervised nanobody production. W.I.W. supervised and assisted with the structure refinement. M.M., C.Z. and B.K.K. interpreted data, made figures and wrote the manuscript. B.K.K. provided overall project supervision.

Competing Interests Statement

The BRET-based biosensors used in the present study are licensed to Domain Therapeutics but are freely available from M.B. for non-commercial academic use. M.B. is the chair of the Scientific Advisory Board of Domain Therapeutics. B.K.K. is a co-founder of and consultant for ConfometRx.

References

1. Kenakin, T. Drug efficacy at G protein-coupled receptors. *Annu Rev Pharmacol Toxicol* **42**, 349-79 (2002).
2. Zhu, B.T. Rational design of receptor partial agonists and possible mechanisms of receptor partial activation: a theory. *J Theor Biol* **181**, 273-91 (1996).
3. Cazzola, M. & Donner, C.F. Long-acting beta2 agonists in the management of stable chronic obstructive pulmonary disease. *Drugs* **60**, 307-20 (2000).
4. Baker, J.G., Proudman, R.G. & Hill, S.J. Salmeterol's extreme beta2 selectivity is due to residues in both extracellular loops and transmembrane domains. *Mol Pharmacol* **87**, 103-20 (2015).
5. Ferguson, G.T., Funck-Brentano, C., Fischer, T., Darken, P. & Reisner, C. Cardiovascular safety of salmeterol in COPD. *Chest* **123**, 1817-24 (2003).
6. Twentyman, O.P., Finnerty, J.P., Harris, A., Palmer, J. & Holgate, S.T. Protection against allergen-induced asthma by salmeterol. *Lancet* **336**, 1338-42 (1990).
7. Ball, D.I. et al. Salmeterol, a novel, long-acting beta 2-adrenoceptor agonist: characterization of pharmacological activity in vitro and in vivo. *Br J Pharmacol* **104**, 665-71 (1991).
8. Johnson, M. et al. The pharmacology of salmeterol. *Life Sci* **52**, 2131-43 (1993).
9. Calverley, P.M. et al. Salmeterol and fluticasone propionate and survival in chronic obstructive pulmonary disease. *N Engl J Med* **356**, 775-89 (2007).
10. Wijesinghe, M., Perrin, K., Harwood, M., Weatherall, M. & Beasley, R. The risk of asthma mortality with inhaled long acting beta-agonists. *Postgrad Med J* **84**, 467-72 (2008).
11. Weatherall, M., Wijesinghe, M., Perrin, K., Harwood, M. & Beasley, R. Meta-analysis of the risk of mortality with salmeterol and the effect of concomitant inhaled corticosteroid therapy. *Thorax* **65**, 39-43 (2010).
12. Coleman, R.A., Johnson, M., Nials, A.T. & Vardey, C.J. Exosites: their current status, and their relevance to the duration of action of long-acting beta 2-adrenoceptor agonists. *Trends Pharmacol Sci* **17**, 324-30 (1996).
13. Clark, R.B., Allal, C., Friedman, J., Johnson, M. & Barber, R. Stable activation and desensitization of beta 2-adrenergic receptor stimulation of adenylyl cyclase by salmeterol: evidence for quasi-irreversible binding to an exosite. *Mol Pharmacol* **49**, 182-9 (1996).
14. Green, S.A., Spasoff, A.P., Coleman, R.A., Johnson, M. & Liggett, S.B. Sustained activation of a G protein-coupled receptor via "anchored" agonist binding. Molecular localization of the salmeterol exosite within the 2-adrenergic receptor. *J Biol Chem* **271**, 24029-35 (1996).
15. Isogaya, M. et al. Identification of a key amino acid of the beta2-adrenergic receptor for high affinity binding of salmeterol. *Mol Pharmacol* **54**, 616-22 (1998).
16. Rong, Y. et al. Probing the salmeterol binding site on the beta 2-adrenergic receptor using a novel photoaffinity ligand, [(125)I]iodoazidosalmeterol. *Biochemistry* **38**, 11278-86 (1999).
17. Gimenez, L.E., Baameur, F., Vayttaden, S.J. & Clark, R.B. Salmeterol Efficacy and Bias in the Activation and Kinase-Mediated Desensitization of beta2-Adrenergic Receptors. *Mol Pharmacol* **87**, 954-64 (2015).

18. van der Westhuizen, E.T., Breton, B., Christopoulos, A. & Bouvier, M. Quantification of ligand bias for clinically relevant beta2-adrenergic receptor ligands: implications for drug taxonomy. *Mol Pharmacol* **85**, 492-509 (2014).
19. Tran, T.M. et al. Characterization of agonist stimulation of cAMP-dependent protein kinase and G protein-coupled receptor kinase phosphorylation of the beta2-adrenergic receptor using phosphoserine-specific antibodies. *Mol Pharmacol* **65**, 196-206 (2004).
20. Drake, M.T. et al. beta-arrestin-biased agonism at the beta2-adrenergic receptor. *J Biol Chem* **283**, 5669-76 (2008).
21. Carter, A.A. & Hill, S.J. Characterization of isoprenaline- and salmeterol-stimulated interactions between beta2-adrenoceptors and beta-arrestin 2 using beta-galactosidase complementation in C2C12 cells. *J Pharmacol Exp Ther* **315**, 839-48 (2005).
22. Moore, R.H. et al. Salmeterol stimulation dissociates beta2-adrenergic receptor phosphorylation and internalization. *Am J Respir Cell Mol Biol* **36**, 254-61 (2007).
23. Walker, J.K. & DeFea, K.A. Role for beta-arrestin in mediating paradoxical beta2AR and PAR2 signaling in asthma. *Curr Opin Pharmacol* **16**, 142-7 (2014).
24. Billington, C.K., Penn, R.B. & Hall, I.P. beta2 Agonists. *Handb Exp Pharmacol* **237**, 23-40 (2017).
25. Rasmussen, S.G. et al. Structure of a nanobody-stabilized active state of the beta(2) adrenoceptor. *Nature* **469**, 175-80 (2011).
26. Rasmussen, S.G. et al. Crystal structure of the beta2 adrenergic receptor-Gs protein complex. *Nature* **477**, 549-55 (2011).
27. Rosenbaum, D.M. et al. Structure and function of an irreversible agonist-beta(2) adrenoceptor complex. *Nature* **469**, 236-40 (2011).
28. Warne, T. et al. The structural basis for agonist and partial agonist action on a beta(1)-adrenergic receptor. *Nature* **469**, 241-4 (2011).
29. Ring, A.M. et al. Adrenaline-activated structure of beta2-adrenoceptor stabilized by an engineered nanobody. *Nature* **502**, 575-579 (2013).
30. Nygaard, R. et al. The dynamic process of beta(2)-adrenergic receptor activation. *Cell* **152**, 532-42 (2013).
31. Manglik, A. et al. Structural Insights into the Dynamic Process of β2-Adrenergic Receptor Signaling. *Cell* **161**, 1101-1111 (2015).
32. Sounier, R. et al. Propagation of conformational changes during mu-opioid receptor activation. *Nature* **524**, 375-8 (2015).
33. Gregorio, G.G. et al. Single-molecule analysis of ligand efficacy in β2AR-G-protein activation. *Nature* **547**, 68-73 (2017).
34. Staus, D.P. et al. Regulation of beta2-adrenergic receptor function by conformationally selective single-domain intrabodies. *Mol Pharmacol* **85**, 472-81 (2014).
35. Caffrey, M. Crystallizing membrane proteins for structure determination: use of lipidic mesophases. *Annual review of biophysics* **38**, 29-51 (2009).
36. Baker, J.G. The selectivity of beta-adrenoceptor agonists at human beta1-, beta2- and beta3-adrenoceptors. *Br J Pharmacol* **160**, 1048-61 (2010).
37. Kruse, A.C. et al. Activation and allosteric modulation of a muscarinic acetylcholine receptor. *Nature* **504**, 101-6 (2013).
38. Fronik, P., Gaiser, B.I. & Sejer Pedersen, D. Bitopic Ligands and Metastable Binding Sites: Opportunities for G Protein-Coupled Receptor (GPCR) Medicinal Chemistry. *J Med Chem* **60**, 4126-4134 (2017).

39. Wieland, K., Zuurmond, H.M., Krasel, C., Ijzerman, A.P. & Lohse, M.J. Involvement of Asn-293 in stereospecific agonist recognition and in activation of the beta 2-adrenergic receptor. *Proc Natl Acad Sci U S A* **93**, 9276-81 (1996).
40. Liapakis, G., Chan, W.C., Papadokostaki, M. & Javitch, J.A. Synergistic contributions of the functional groups of epinephrine to its affinity and efficacy at the beta2 adrenergic receptor. *Mol Pharmacol* **65**, 1181-90 (2004).
41. Thomsen, A.R.B. et al. GPCR-G Protein-β-Arrestin Super-Complex Mediates Sustained G Protein Signaling. *Cell* **166**, 907-919 (2016).
42. Namkung, Y. et al. Monitoring G protein-coupled receptor and beta-arrestin trafficking in live cells using enhanced bystander BRET. *Nat Commun* **7**, 12178 (2016).
43. Gregorio, G.G. et al. Single-molecule analysis of ligand efficacy in beta2AR-G-protein activation. *Nature* **547**, 68-73 (2017).
44. Picard, L.-P., Schönegge, A.M., Lohse, M.J. & Bouvier, M. Bioluminescence resonance energy transfer-based biosensors allow monitoring of ligand- and transducer-mediated GPCR conformational changes. *Communications Biology* **1**(2018).
45. Yao, X.J. et al. The effect of ligand efficacy on the formation and stability of a GPCR-G protein complex. *Proc Natl Acad Sci U S A* **106**, 9501-6 (2009).
46. Dawaliby, R. et al. Allosteric regulation of G protein-coupled receptor activity by phospholipids. *Nat Chem Biol* **12**, 35-9 (2016).
47. Schafer, C.T., Fay, J.F., Janz, J.M. & Farrens, D.L. Decay of an active GPCR: Conformational dynamics govern agonist rebinding and persistence of an active, yet empty, receptor state. *Proc Natl Acad Sci U S A* **113**, 11961-11966 (2016).
48. Fay, J.F. & Farrens, D.L. Purification of Functional CB1 and Analysis by Site-Directed Fluorescence Labeling Methods. *Methods Enzymol* **593**, 343-370 (2017).
49. Doose, S., Neuweiler, H. & Sauer, M. A close look at fluorescence quenching of organic dyes by tryptophan. *Chemphyschem* **6**, 2277-85 (2005).
50. Cazzola, M., Calzetta, L. & Matera, M.G. beta(2) -adrenoceptor agonists: current and future direction. *Br J Pharmacol* **163**, 4-17 (2011).

Online Methods

Receptor Constructs

All constructs have an N-terminal Flag tag. The *T4L-β2AR-ΔICL3*, consists of an N-terminal T4 lysozyme fusion to β2AR(29-365) ΔICL3, *i.e.* Δ(235-263) with mutations M96T, M98T and N187E. The *β2AR-PN1* consists of β2(1-24) – TEV – β2(25-365) – 3C – β2(366-413), with "TEV" and "3C" indicating TEV protease and 3C protease cut sites, respectively. Additionally, mutations M96T, M98T, C378A, N187E and C406A were introduced, as previously described51. The *β2AR Δ 6 L230W:L266C* consists of full-length WT receptor with a minimal cysteine background[33] (C77V, C265A, C327S, C341L, C378A, C406A), as well as mutations L230W and L266C and a C-terminal hexahistidine tag.

Expression, purification and labeling of β2AR constructs

Receptor constructs were expressed in *Sf*9 insect cell cultures infected with recombinant baculovirus (BestBac, Expression Systems), and solubilized in *n*-dodecyl-β-d-maltoside (DDM) according to methods described previously[51]. The solubilized receptor was purified through M1 FLAG chromatography followed by alprenolol-sepharose chromatography to remove non-functional receptor[51]. A second M1 FLAG chromatography was applied such that the receptor-bound alprenolol could be removed for unliganded protein or exchanged for salmeterol. For the T4L-β2AR-ΔICL3, after the protein was eluted from the M1 resin, the FLAG epitope tag of T4L-β2AR-Δ-ICL3 was removed by the treatment of tobacco etch virus (TEV) protease (Invitrogen) for 3h at room temperature or overnight at 4°C. When necessary, a 50kDa MWCO

Vivaspin concentrator (GE Healthcare) was used to concentrate the receptor. Theβ2AR constructs used for fluorescence studies were concentrated and flash-frozen in the presence of 20% glycerol at a final concentration of 200μM. Aliquots were then stored at –80°C until use.

Full-length PN1–β2AR was labeled with monobromobimane as previously described[52]. Briefly, FLAG pure receptor (~2μM) was incubated overnight on ice with 100μM TCEP and 20μM monobromobimane (Thermo Fisher Scientific). Subsequently, 5mM cysteine was added to quench the labeling reaction followed by alprenolol-sepharose chromatography as described above. A similar procedure was followed for labeling β2AR Δ 6 L230W:L266C with Atto655-iodoacetamide (Atto-TEC).

G protein expression and purification

Wild-type Gs heterotrimer was expressed and purified as previously described[33]. Following purification, the protein was dialyzed into 20mM HEPES pH 7.5, 100mM NaCl, 0.02%DDM, 100μM TCEP and 20μM GDP, concentrated, and flash-frozen in the presence of 20% glycerol at a final concentration of 200μM. Aliquots were then stored at –80 °C until use.

Preparation of Nb71 and Nb80

The recombinant Nb71 was generated in the same way as Nb80[25]. These two nanobodies were screened from a same library of single-chain nanobody clones after immunizing a llama with purified agonist-bound β2AR reconstituted at high density into phospholipid vesicles. Nb71 was

expressed in *E. coli* and purified by nickel affinity chromatography in a same manner as Nb80[25]. The protein was then further purified by *cation exchange* using a Mono-S column (GE Healthcare), loading the protein at 20mM NaCl in 20mM MES pH 6.0 and eluting with a linear gradient from 50 to 500mM NaCl. In order to minimize severe precipitation of Nb71 over time, the purified protein was stored at a concentration below 5 mg/mL in 20mM Hepes, 1M NaCl.

Crystallization

Salmeterol bound receptor (~40mg/ml) was incubated with a 5.5-fold molar excess of Nb71 (~50mg/mL) for 1 hour on ice. Size exclusion chromatography was then performed to remove free Nb71. The purified complex was concentrated to ~60mg/mL for crystallization using the lipid cubic phase (LCP) method as previously described[35]. The protein complex was reconstituted in monoolein containing 10% cholesterol at a 1:1.5 protein to lipid ratio (w/w). Reconstituted protein-lipid mixture drops of 30 nL were deposited in each well of a 96-well glass sandwich plate (Molecular Dimensions). The drop was then overlaid with 650nL of precipitant and the wells sealed with a glass coverslip. Diffraction-quality crystals were grown at 20°C in 31-34% PEG 400, 100mM HEPES pH 7.5, 1% 1,2,3-heptanetriol following 3 days of incubation at 20°C.

Data collection, structure determination and analysis

Crystals were harvested and frozen in liquid nitrogen directly without using additional cryo-protectant. Diffraction data from 24 different crystals were measured using the GM/CA-CAT

microfocus beam at 23-ID-D (Advanced Photon Source, Argonne National Labs). The data were processed with HKL2000 and the structure solved by molecular replacement using Phaser. Further model rebuilding was performed by using Coot and the structure was refined with Phenix. The validation of the final structural model was performed using Molprobity. The overall MolProbity score is 1.35. For the Ramachandran analysis, 96.8% atoms are in Ramachandran favored regions and 3.2% atoms are in Ramachandran allowed regions. Data processing and refinement statistics are shown in Supplementary Table 2. The structure of the inactive β2AR (PDB ID 2RH1), the β2AR complexed with Nb80 (PDB ID 3P0G), the β2AR complexed with Gs (PDB ID 3SN6), the chain A of sabultamol bound β1AR (PDB ID 2Y04) were used for structural alignments in PYMOL based on Cα only. The secondary structure of β2AR ICL2 was assigned by PYMOL and DSSP.

Reconstitution of β2AR in HDL particles for Octet Red measurements

The β2AR was reconstituted in high-density lipoprotein (HDL) particles using established methods[51]. The scaffold protein ApoA-I used for reconstitution was purified as previously described[51]. Purified ApoA-I was biotinylated for 30 min at room temperature using NHS-PEG4-biotin (Thermo) at a 1:1 molar ratio in a buffer composed of 20 mM HEPES, pH 8.0, 100mM NaCl, 1mM EDTA, 5 mM sodium cholate. Following the labeling reaction, unreacted biotin was quenched by the addition of Tris-HCl, pH 8.0 to a final concentration of 20 mM. Biotinylated protein was separated from free biotin by size exclusion chromatography on Superdex 75 HR 10/30. FLAG-tagged β2AR was incorporated into HDL particles using biotinylated ApoA-I and receptor-containing HDL particles were isolated using M1 anti-FLAG

immunoaffinity chromatography. Nanobody binding to β2AR in biotinylated HDL particles was monitored using the OctetRED biolayer interferometry system (Pall FortéBio) using streptavidin-coated biosensors (Pall 665 FortéBio). Sensors were hydrated for at least 10 min at room temperature in assay buffer (20 mM Tris-HCl pH 7.4, 136 mM NaCl, 2.7 mM KCl, 1 mM EDTA, 0.02% w/v ascorbic acid, 0.05% w/v BSA), then incubated with biotinylated β2AR-HDL (~100 nM) for 10 min at room temperature prior to loading the sensors onto the OctetRED instrument. All steps on the OctetRED were performed at 25 °C with the assay plate shaking at 1,000 rpm. After an initial baseline reading, sensors were dipped into wells containing assay buffer with a saturating concentration of agonist (100μM Epinephrine, 0.1μM BI-167107, or 1μM Salmeterol) and incubated for 20 min to equilibrate β2AR with agonist. The sensors were transferred to wells containing assay buffer plus agonist and nanobody (1, 3.2, 10, 32, 100, or 320 nM) for 5 min to monitor nanobody association. Nanobody dissociation was monitored by then transferring the sensors to wells containing assay buffer plus agonist for 30 min. Nonspecific nanobody binding at each concentration was measured in a parallel experiment in which sensors were loaded with empty HDL. Buffer-only controls were also included in each experiment to correct for baseline drift. Data were first analyzed using Octet Data Analysis 7.0 software (Pall FortéBio) to remove baseline and nonspecific binding, and the processed data were exported to Prism 6 (GraphPad) for curve fitting. All association and dissociation curves were fit using single-phase exponential association or decay.

BRET measurements for Gs activation, β-arrestin recruitment and β2AR conformational change in live cells.

HEK293T cells used for the BRET assays were grown in Dulbecco's modified Eagle's medium (DMEM), supplemented with 10% newborn calf serum (NCS), at 37 °C with 5% CO_2. Cells were detached with trypsin-EDTA and transfected with 2.5 µg of total DNA per 10^6 cells, using linear polyethyleneimine (PEI, Polysciences) as transfecting agent, at a ratio of 3:1 (PEI:DNA). Gs activation was evaluated with Gs-117-RLucII/Gβ1/Gγ1-GFP10[41] and β-arrestin recruitment with CAAX-rGFP/β-arr2-RLucII[42] sensors, in presence of WT 3HA-β2AR or mutant receptors. The conformational changes were detected with the NY-β2AR sensor[53]. Directly after transfection, cells were plated in 96-well white plates (Greiner) at a density of 50,000 cells/well, and incubated for 48 h. After that period, the plates were washed with PBS and assay buffer (Hank's balanced salt solution (HBSS)) was added. Cells were stimulated with the ligands during 5 or 15 min for evaluating, respectively, Gs activation or β-arrestin recruitment and conformational changes. Coelenterazine 400a (2.5 µM) was added 5 min before the reads. BRET was monitored using a TriStar LB942 microplate reader (Berthold) equipped with a 410/80 nm donor filter and a 515/40 nm acceptor filter (for Gs activation and β-arrestin recruitment) or a 485/20 nm donor filter and a 530/25 nm acceptor filter (for receptor conformational changes). BRET ratio was calculated by dividing the acceptor emission by the donor emission. The data were analyzed with Prism (Graphpad) using "dose-response- stimulation log(agonist) vs normalized response- variable slope" with the constraint of sharing the hill slope across all data sets.

Molecular Dynamics Simulations

We simulated the β2-adrenergic receptor bound to the partial agonist salmeterol as well as the full agonist epinephrine. We initiated these simulations from crystal structures of the receptor bound to each of these ligands. Each of the crystal structures we used includes a nanobody that binds to the intracellular side of the receptor and stabilizes an active or intermediate receptor state: Nb71 for salmeterol and Nb6B9 for epinephrine[29].

We performed three simulations of β2AR–salmeterol–Nb71 and three simulations of β2AR–epinephrine–Nb6B9. Each of the crystallized constructs was a β2AR–T4 lysozyme (T4L) fusion protein, with T4L replacing the receptor's N-terminus. T4L was omitted from all simulations, while all other resolved residues were included. The majority of ICL3 was absent in all simulations, because it was deleted from the crystallized construct in β2AR–salmeterol– Nb71 and β2AR–epinephrine–Nb6B9. Because the simulations were performed before the published coordinates had been finalized, they were initiated using coordinates that differed very slightly from the published ones (root mean squared deviation below 0.3 Å, computed over all resolved receptor Cα atoms); these differences were much smaller than the typical motions of the atoms in simulation. In all simulations, a palmitoyl group not resolved but presumed to be present in the crystallized constructs was added to Cys341 using Maestro (Schrödinger LLC, New York, NY).

The β2AR was embedded in a hydrated lipid bilayer in all simulations; all atoms (including those in lipids and water) were represented explicitly. Hydrogen atoms were added to the crystal structures using Maestro, as described previously, and receptor chain termini were capped with neutral groups (acetyl and methylamide). Titratable residues other than Glu122$^{3.41}$ were left in

their dominant protonation state at pH 7.0. Glu122$^{3.41}$, which faces the lipid bilayer, was neutral (protonated) in all simulations.

Prepared protein structures were inserted into an equilibrated bilayer solvated with 0.15 M NaCl, using a previously described protocol54. The bilayer consisted of palmitoyl-oleoyl phosphatidylcholine, with 24% palmitoyl-oleoyl-phosphatidylserine in the inner membrane leaflet. Simulated systems initially measured roughly 71 x 71 x 115 Å^3 and contained approximately 140 lipid molecules, 12,000 water molecules, 32 chloride ions, and 40 sodium ions.

We also performed three simulations of β2AR–salmeterol with the nanobodies removed (but otherwise starting from the same structures as above). Simulation setup was as described above, except that the removal of the nanobody allowed the simulated volume to be somewhat smaller. These simulations initially measured roughly 69 x 69 x 85 Å^3 and contained approximately 120 lipid molecules, 7200 water molecules, 19 chloride ions, and 30 sodium ions.

We used the CHARMM-h force field for proteins. We used the CHARMM36 lipid force field, along with standard CHARMM salt ion parameters and the CHARMM TIP3P model for water. Parameters for palmitoyl-cysteine were as described previously[27,54], and parameters for epinephrine were obtained by adapting previously published parameters for isoproterenol[55]. Parameters for salmeterol were obtained from the ParamChem server. Full parameter sets are available upon request.

Each simulation consisted of a 50-ns equilibration run followed by a longer production run. Systems were equilibrated in the NPT ensemble (310 K, 1 bar, Martyna-Tuckerman-Klein Nosé-Hoover chain coupling scheme using a multigrator, with initial velocities sampled from the Boltzmann distribution and with 5 kcal mol-1 Å-2 harmonic position restraints applied to the protein and ligand atoms, which were tapered off linearly over 50 ns. Production simulations used the same integrator, pressure and temperature, and were initiated from the final snapshot of the corresponding equilibration simulation. All simulations were performed on an Anton 1 computer[56].

All bond lengths to hydrogen atoms were constrained using M-SHAKE. An r-RESPA integrator was used with a time step of 2.5 fs, and long-range electrostatics were computed every 7.5 fs. Long-range electrostatics were computed in reciprocal space with the *u*-series method[57].

Simulation snapshots were saved every 180 ps. For the purposes of evaluating the fraction of time a hydrogen bond was formed in simulation, such a bond was considered to be formed in snapshots in which the relevant non-hydrogen atoms were within 3.0 Å of one another. Because the bound ligands shifted pose during the later parts of certain simulations (possibly as a result of motion of the nanobodies, which are not held in place by crystallographic contacts), we used the first microsecond of each simulation for these analyses. Each error bar was calculated as standard error of the mean across three simulations.

Dye modeling

The structure of the iodoacetamide derivative of the Atto655 dye (Atto-TEC GmbH) was obtained from PubChem (CID 16218785) and optimized using Avogadro and the GAFF force field. The structures of β2AR in the active (PDB ID 3SN6) and inactive conformations (PDB ID 2RH1) were retrieved from the RCSB PDB and mutated (L230W and L266C) using PyMOL. Parameters for the dye molecule attached to a cysteine residue were obtained using PRODRG and manually edited to enforce planarity of the ring system of the dye. The Crystallography and NMR System (CNS) software, version 1.358, was used to attach the dye to L266C and simulate its positions using rigid-body docking and multi-trial simulated annealing, respectively, as done previously by Brunger and co-workers[59]. The entire receptor structure was kept rigid, except for the side-chain atoms of L230W and L266C. Distances between the centers of mass of the tryptophan side-chain atoms and center of mass of the ring system of the dye were calculated for each generated model (300 for each conformation of β2AR).

Fluorescence measurements on purified receptor in detergent solution

Bimane-labeled and Atto-labeled receptors were used at respective concentrations of 0.2μM and 0.1μM in buffer containing 20mM Hepes pH 7.4, 100mM NaCl, 0.02% (w/v) DDM and 0.002% (w/v) cholesterol hemisuccinate. Salmeterol and epinephrine stocks were prepared as 50mM and 100mM solutions in DMSO and added at indicated final concentrations. Ligand concentrations were chosen to achieve saturation of detergent-solubilized receptor. To avoid any non-specific vehicle effects, care was taken to obtain the same final concentration of DMSO in all samples. Where indicated, Gs was added to a final concentration of 2μM. To allow efficient ligand binding and full equilibration, samples were incubated at the final concentrations

used for 1 hour in the dark prior to measurements. Fluorescence data was collected in a quartz cuvette with 500µL of sample using FluorEssence v3.8 software on a Fluorolog instrument (Horiba) in photon counting mode. Bimane fluorescence was measured by excitation at 370nm with excitation and emission bandwidth passes of 4nm, and emission spectra were recorded from 410 to 510 nm in 1nm increments and 1s integration time. Atto fluorescence was measured by excitation at 650nm with excitation and emission bandwidth passes of 5nm, and emission spectra were recorded from 660 to 730 nm in 1nm increments and 1s integration time. Measurements were performed in triplicate.

Radioligand binding assays

Binding curves were obtained by incubating the DDM purified wild-type, bimane- and Atto655-labeled receptors in the presence of M1 FLAG–sepharose and 2 mM Ca^{2+}, under shaking at room temperature for 1.5h. The antagonist [3H]-dihydroalprenolol (DHA) (PerkinElmer) was used to obtain saturation binding curves. Competition binding measurements for salmeterol and epinephrine were performed in a similar way, using DHA at a concentration slightly above Kd, as determined by saturation binding. Non-specific binding was accounted for by measuring in the presence of 10µM cold alprenolol. Beads were harvested using a 48-well Brandell harvester and counted in a LS6000TA scintillator (Beckman) using Cytoscint (MP Biomedical).

Statistical Analysis.

Statistical significance of hydrogen bond duration from MD trajectories (Fig. 5a) was assessed using the one-sided Welch's unequal variances t-test. Statistical significance of the binding affinities (Supplementary Table 1) was assessed using Ordinary One-way ANOVA (Tukey) test at a multiplicity adjusted P value = 0.05. Statistical significance of the fitted mean logKi values (Supplementary Fig. 1) was assessed using a one-way ANOVA Tukey test at a P values of 0.05 (adjusted for multiple comparisons).

Data Availability.

Atomic coordinates and the structure factors for the crystal structure have been deposited with the Protein Data Bank under accession code 6CSY. Other data and results are available upon request.

Methods-only References

51. Dawaliby, R. et al. Allosteric regulation of G protein–coupled receptor activity by phospholipids. *Nature Chemical Biology* **12**, 35-41 (2015).
52. Rosenbaum, D.M. et al. GPCR engineering yields high-resolution structural insights into beta2-adrenergic receptor function. *Science (New York, N.Y.)* **318**, 1266-73 (2007).
53. Picard, L.P., Schonegge, A. M., Lohse, M. J. & Bouvier, M. BRET-based biosensors to monitor ligand- and transducer-mediated GPCR conformational changes. (Communications Biology, 2018).
54. Dror, R.O. et al. Identification of two distinct inactive conformations of the beta2-adrenergic receptor reconciles structural and biochemical observations. *Proc Natl Acad Sci U S A* **106**, 4689-94 (2009).
55. Dror, R.O. et al. Pathway and mechanism of drug binding to G-protein-coupled receptors. *Proceedings of the National Academy of Sciences of the United States of America* **108**, 13118-23 (2011).
56. Shaw, D.E. et al. Millisecond-scale molecular dynamics simulations on Anton. In *Proceedings of the Conference on High Performance Computing Networking, Storage and Analysis* 1-11 (ACM, Portland, Oregon, 2009).

57. Shaw, D.E. et al. Anton 2: Raising the bar for performance and programmability in a special-purpose molecular dynamics supercomputer. *Sc14: International Conference for High Performance Computing, Networking, Storage and Analysis*, 41-53 (2014).
58. Brunger, A.T. Version 1.2 of the Crystallography and NMR system. *Nature Protocols* **2**, 2728 (2007).
59. Choi, U.B. et al. Single-molecule FRET-derived model of the synaptotagmin 1-SNARE fusion complex. *Nat Struct Mol Biol* **17**, 318-24 (2010).

Figure legends

Figure 1: Crystal structure of salmeterol-bound β2AR. a. Chemical structures of β2AR ligands: partial agonists salmeterol and salbutamol; full agonists epinephrine and BI-16707. The respective pharmacophores that bind the orthosteric ligand binding pocket are highlighted in purple, and the aryloxyalkyl tail of salmeterol, which binds the exosite, is highlighted in blue. **b.** Overall ribbon representation of the salmeterol-bound β2AR – Nb71 complex structure. The T4L lysozyme fusion facilitates crystallization, while Nb71 stabilizes the active, salmeterol-bound (orange spheres) β2AR. **c.** Cross-section through the receptor, with the interior in black, highlighting salmeterol (orange spheres) occupying the orthosteric site and the exosite.

Figure 2: Structural features of the β2AR-salmeterol-Nb71 complex. a,b,c. Overlay of inactive carazolol bound receptor (grey), Nb71 and salmeterol bound β2AR (purple) and the BI-167107 bound β2AR - Gs complex (green and pink, respectively). **a.** Side view (inset) and cytoplasmic view of TM6, showing the position of TM6 relative to the helical bundle. The extent of TM6 movement, indicated by black arrows, was measured using the Cα of Glu268 as reference point. **b.** Rearrangement of Pro211$^{5.50}$, Ile121$^{3.40}$ and Phe282$^{6.44}$ and the associated outward movement of the cytoplasmic end of TM6. The inactive structure of β2AR is colored silver. The active structures of β2AR are colored blue (coupled with salmeterol and Nb71), cyan (coupled with epinephrine and 6B9) and green (coupled with BI-167107 and Gs). **c.** Extracellular (top) view of β2AR, with major conformational changes between structures indicated by red arrows and ligands in stick representation.

Figure 3: Salmeterol exosite and receptor subtype-selectivity determinants. a. Side and **b.** top view of β2AR, with stick representation of salmeterol (orange). **c.** Spherical representation of the salmeterol aryloxyalkyl moiety (orange) and the β2AR (blue). **d.** Residues important for interaction and specificity are highlighted in yellow and labeled. Withthe exception of Y308 (indicated by a red arrow), the amino acids that form the orthosteric binding pocket for epinephrine are identical between β1AR and β2AR. **e.** Comparison of the ligand binding sites between β2AR (left panel) bound to salmeterol (orange sticks) and M2R (right panel) bound to the allosteric modulator LY2119620 (green sticks).

Figure 4: **Hydrogen bond interactions in the orthosteric site and re-arrangement of the ligand binding pocket.** Comparison of ligand-mediated hydrogen bonds (black dashed lines) in **a.** epinephrine-bound and **b.** salmeterol-bound β2AR.

Figure 5: **Ligands and specific residues in the orthosteric site modulate hydrogen bonding and signaling outcome. a.** Frequency of hydrogen bonding between Ser203$^{5.42}$ / Asn293$^{6.55}$ and the ligand *m*-OH group, Ser207$^{5.46}$ and the ligand *p*-OH group, and Asn312$^{7.39}$ and the ligand β-OH group in MD simulations of receptor bound to epinephrine or salmeterol. Individual datapoints (black dots) and SEM (error bars) of 3 independent experiments are shown. Statistical significance was assessed using the one-side Welch's unequal variances t-test (p values: Ser203$^{5.42}$=0.00003; Ser207$^{5.46}$=0.08; Asn293$^{6.55}$=0.004; Asn312$^{7.39}$=0.01). The actual statistical significance of the differences (e.g. for Ser207) may be better than computed, as each of the data points is based on a trajectory with thousands of samples. **b,c.** BRET-based assays monitoring β-arrestin2 recruitment and G-protein activation on wild-type and mutant β2AR

constructs. Data represent the mean (symbols) ± SEM (error bars) of 3 independent experiments. Error bars shorter than the height of the symbol are not shown.

Figure 6: Spectroscopic interrogation of ligand-induced changes in TM6 conformation on detergent-solubilized, purified labeled receptor. a,c. Schematic representation of labeled receptor constructs used to probe the outward motion of TM6. The β2AR transmembrane helices 1-5 and 7 are shown as grey cylinders. The blue cylinders represent TM6 in the inactive (light blue) and active (dark blue) conformation, with the labels attached at the intracellular end of TM6 depicted according to their overall structure. The bimane fluorophore (teal) is an environment-sensitive reporter, while the Atto655 dye (pink) is quenched in a distance-dependent way by an engineered tryptophan (L230W, in yellow). **b,d.** Steady-state fluorescence emission spectra of bimane-labeled and Atto655-labeled receptor in the presence of epinephrine or salmeterol. The spectra are normalized relative to unliganded receptor (apo, light blue curve) and show the fluorescence dose-response of receptor up to saturating ligand concentrations, in the absence and presence of G protein. Data is plotted as mean (curves) and standard deviation (error bars) of triplicate measurements.

Supplementary Figure 1. Salmeterol and isoproterenol competition binding on purified β2AR in detergent, in the presence of Nb71 and Nb80. Purified β2AR (1nM) in detergent buffer was incubated for 1h at room temperature in the presence of 5nM [3H]dihydroalprenolol and, when indicated, 2μM Nb71 or Nb80, in the presence of increasing concentrations of salmeterol (left panel) or isoproterenol (right panel). Data points for the competition binding curves are presented as mean values +/- SEM from three independent measurements. The data

were analyzed in Prism (GraphPad) using "Nonlinear Regression – One site – Fit Ki" fitting, with the fitted curve shown in color and 95% confidence intervals plotted as dashed black lines for each fit (top plots). Ki values are reported as means with 95% confidence intervals in square brackets. To assess whether the difference between the calculated logKi values was statistically significant, a one-way ANOVA Tukey test was performed to compare the fitted mean logKi values. As shown in the bottom plots, all differences are statistically significant at P values of 0.05 (adjusted for multiple comparisons), although the 95% confidence intervals clearly indicate that the logKi difference +/- Nb is larger and more significant for Nb80 than for Nb71.

Supplementary Figure 2. Different modes of Nb71 and Nb80 binding to the β2AR. (a) β2AR with Nb71. **(b)** β2AR with Nb80. **(c)** Interactions between β2AR and Nb71. Two residues L101 and L102 in the Nb71 CDR3 insert into a hydrophobic cavity at the cytoplasmic region of β2AR to form extensive hydrophobic interactions with residues I278, Y326, I127, V222, I135 and I72. Additional salt bridge interaction between E268 in β2AR and R35 in Nb71 and cation-π interaction between K270 in β2AR and W99 in Nb71 also contribute to the binding of Nb71.

Supplementary Figure 3. Composite omit electron density map of salmeterol. β2AR is colored blue. Salmeterol is colored orange. The 2*F*o-*F*c composite omit electron density map of salmeterol is shown as purple mesh contoured at 1.2s.

Supplementary Figure 4. Interactions between salmeterol and β2AR. The 2-D representation figure was generated by LigPlot+1. The bonds in the salmeterol molecule are colored purple, while the bonds in the β2AR residues are colored orange. Residues forming

hydrogen-bonding interactions with the ligand and the hydrogen bonds are colored green. Residues and atoms involved in the hydrophobic interactions are colored black and marked with red half-circles. 1. Laskowski, R. A. & Swindells, M. B. LigPlot+: multiple ligand-protein interaction diagrams for drug discovery. *J Chem Inf Model* **51**, 2778-2786, (2011).

Supplementary Figure 5. Important role of the ether oxygen in salmeterol. The ether oxygen at position 16 in salmeterol forms a hydrogen bond with the main chain amine of residue Phe193 (black dashed line). Changing the position of the ether oxygen to positions 14 (salmeterol derivative 1) or position 18 (salmeterol derivative 2) greatly reduces the ligand affinities, and removing this oxygen (salmeterol derivative 3) reduces the affinity even further2. This is most likely due to the loss of the hydrogen bond, since the distance between the main chain amine of Phe193 and the atom at position 14 or 18 in salmeterol (represented by yellow dashed lines) is longer than 3.5A. On the other hand, another long-lasting β2AR agonist vilanterol, which shares a high structural similarity with salmeterol but has one more ether oxygen atom at position 19 that may form an additional hydrogen bond, exhibits higher affinity and longer *in vivo* duration of action compared to salmeterol3. 2 Isogaya, M. *et al.* Identification of a key amino acid of the beta2-adrenergic receptor for high affinity binding of salmeterol. *Mol Pharmacol* **54**, 616-622 (1998). 3 Slack, R. J. *et al.* In vitro pharmacological characterization of vilanterol, a novel long-acting beta2-adrenoceptor agonist with 24-hour duration of action. *J Pharmacol Exp Ther* **344**, 218-230 (2013).

Supplementary Figure 6. Sequence alignment of human β2AR (b2AR) and β1AR (b1AR). The seven transmembrane helices in the human β2AR-salmeterol structure are shown above the

sequences. The residues of β2AR that interact with the head group of salmeterol in the orthosteric-binding pocket are indicated by dark blue boxes, which are highly conserved in β2AR and β1AR. The yellow boxes highlight residues of β2AR in the exosite that interact with the tail of salmeterol, which are far less conserved.

Supplementary Figure 7. (a) Dose-response curves of β2AR full agonist isoproterenol (ISO) and partial agonsits salmeterol (SALM) and salbutamol (SALB) on cell-based BRET measurements between Gai-91-RLuc and nic/myc- β2AR-GFP10. Isoproterenol and salmeterol increased the interaction between Gai-91-RLuc and nic/myc- β2AR-GFP10 in a concentration-dependent manner (pEC50 for isoproterenol = -6.2 ± 0.2) Salbutamol and Salmeterol had no effect in this assay. Data are the mean ± SEM of 3 independent experiments performed in duplicates. **(b)** Dose-response curves of isoproterenol, salmeterol and salbutamol on cell-based BRET measurements between β-arrestin 2-RLucII and rGFPCAAX. Isoproterenol and Salmeterol increased the recruitment of β-arrestin 2-RLucII to the rGFP-CAAX in a dose-dependent manner (pEC50 for isoproterenol= -7.3 ± 0.04; pEC50 for salbutamol= -5.9 ±0.5, n=4). Data are the mean ± SEM of four experiments with repeats in duplicates. **(c)** Dose-response curves of isoproterenol, salbutamol and salmeterol on cell-based BRET measurements between Gαs-117-RLuc and Gγ1-GFP10. 5min stimulation with isoproterenol, salbutamol or salmeterol decreased the BRET signal between Gαs-117-RLucII and Gγ1-GFP10 in a concentration dependent manner (pEC50 for isoproterenol = -8.1 ± 0.3, pEC50 for salbutamol= -6.7 ± 0.5 and for salmeterol = -10 ± 0.4). Data are the mean ± SEM of 3 independent experiments performed in duplicates. Error bars shorter than the height of the symbol are not shown.

Supplementary Figure 8. The β2AR conformational sensor in live cells shows distinct ligand responses. Full and unbiased agonists induce strong conformational changes on the β2AR in live cells, whereas partial and biased agonists do not induce detectable conformation changes, suggesting that the 2 types of ligand stabilize different conformations of the receptor. Data represent the mean ± SEM of 3 independent experiments. NR = not reported.

Supplementary Figure 9. Fluorescent reporters of β2AR activation. (a) Chemical structures of the β2AR-conjugated fluorophores used in spectroscopic studies of receptor activation (left panel), and overlay of carazolol-bound (grey), salmeterol-bound (blue), epinephrine-bound (green) and BI-167107-bound (yellow) β2AR crystal structures (right panel). The side view and cytoplasmic view show the outward TM6 motion upon activation, as indicated by black arrows. The labeling sites for bimane and Atto655 are shown as spheres, colored green and pink, respectively. **(b)** Simulating the ensembles of Atto655 bound to Cys 266 in the inactive (antagonist-bound structure, PDB ID 2RH1) and active (agonist- and Gsbound structure, PDB ID 3SN6) β2AR structures (left panel), yields an average Atto655 -Trp 230 (Dye-Quencher) distance change of about 5 A upon receptor activation (right panel), compatible with the reported threshold quenching distance.

Supplementary Figure 10. Radioligand binding on purified wild-type, bimane-labeled and Atto655-labeled β2AR in detergent. The engineered β2AR constructs labeled with bimane (β2 Bimane) or Atto655 (β2 Atto) show similar ligand binding properties as the wild type β2AR (β2 WT). **(a)** [3H]-dihydroalprenolol (DHA) saturation binding assays, total binding (tot.), non-

specific binding (N.S.). Purified β2AR (1nM) in detergent buffer was incubated for 1h at room temperature in the presence of increasing amounts of DHA. **(b)** Salmeterol and epinephrine competition binding assays. Purified β2AR in detergent buffer (1nM) was incubated for 1h at room temperature in the presence of 5nM DHA and in the presence of increasing concentrations of salmeterol or epinephrine. Data points are presented as mean values ± SD from 3 independent measurements. The data was analyzed in Prism (GraphPad).

Supplementary Figure 11. a) Dose-response of the fluorescence of Atto655-labeled s2AR in detergent, in the presence of epinephrine and salmeterol. The intensity changes at 680nm for the emission spectra presented in **Fig. 5d** are calculated relative to the unliganded response (apo, 100%). The Atto-labeled β2AR shows a dose-dependent increase in Atto655 fluorescence intensity in the presence of epinephrine, indicating a conformational change upon binding sufficient to partly unquench the Atto fluorescence. Little change is observed in the presence of increasing amounts of salmeterol, suggesting that the receptor conformational changes associated with salmeterol binding are not sufficient to substantially alter Atto quenching. Bar graphs represent the mean ± S.D. (error bars) of triplicate measurements (data points shown as black dots). **b)** Emission spectra of Atto655-labeled β2ARD6-L266C with and without the L230W mutation in detergent. The minor fluorescence intensity changes observed on Atto-labeled β2AR with the native Leu230 compared to β2AR with the L230W mutation indicate that the engineered tryptophan is responsible for the observed quenching/unquenching of Atto655 at residues L266C. The spectra are normalized to the respective unliganded data (apo, grey curve). **c)** Atto-β2AR response in the presence of Nb71 and Nb80. Fluorescence emission spectra of Atto655-labeled β2ARΔ6 L230W:L266C in detergent, in the presence of saturating

concentrations of epinephrine or salmeterol, with and without Nb71 or Nb80. For both ligands the Atto response in the presence of Nb80 is much larger than in the presence of Nb71. Nb71 in the presence of epinephrine or salmeterol gives a response similar to epinephrine alone. These data indicate that when both nanobody and ligand are present, the intracellular receptor conformation is mainly imposed by the former and not the latter.

Figure 1

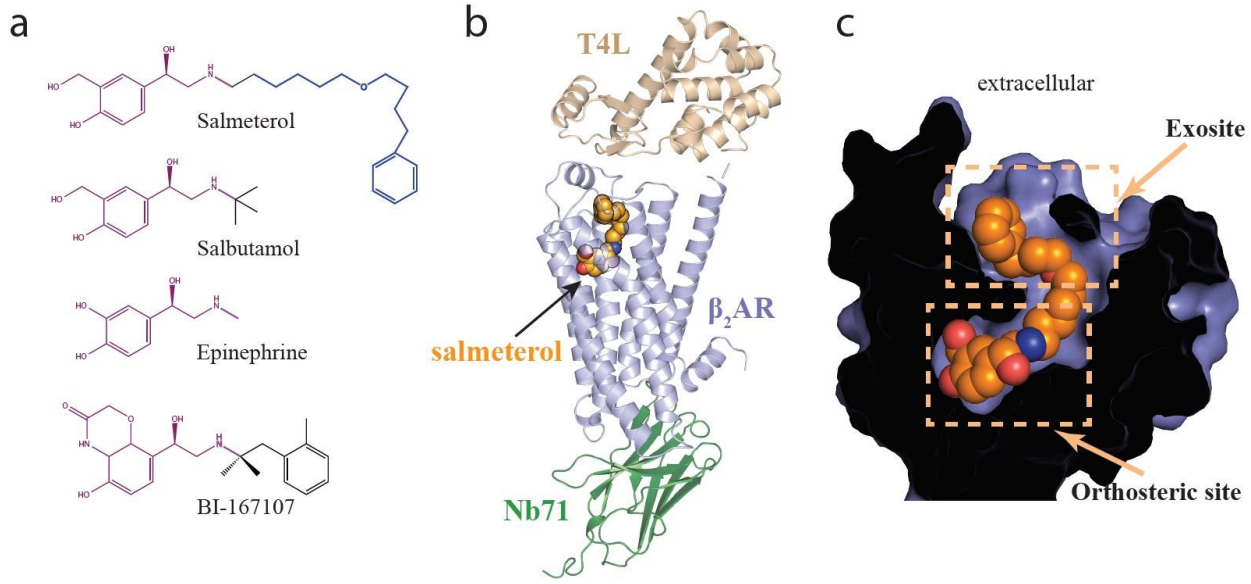
a
Salmeterol
Salbutamol
Epinephrine
BI-167107
b
T4L
salmeterol
β_2AR
Nb71
c
extracellular
Exosite
Orthosteric site

Figure 2

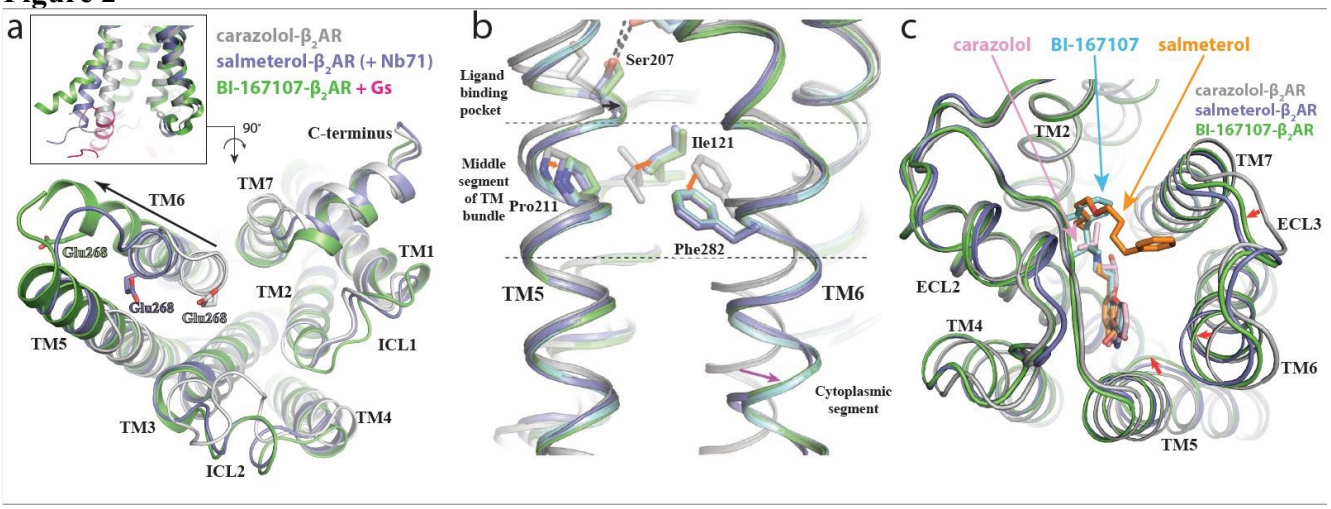
a
carazolol-β2AR
salmeterol-β2AR (+ Nb71)
BI-167107-β2AR + Gs
90°
C-terminus
TM7
TM6
TM1
Glu268
Glu268
Glu268
TM2
TM5
ICL1
TM3
TM4
ICL2
b
Ligand binding pocket
Ser207
Ile121
Middle segment of TM bundle
Pro211
Phe282
TM5
TM6
Cytoplasmic segment
c
carazolol
BI-167107
salmeterol
carazolol-β2AR
salmeterol-β2AR
BI-167107-β2AR
TM2
TM7
ECL3
ECL2
TM4
TM6
TM5

Figure 3

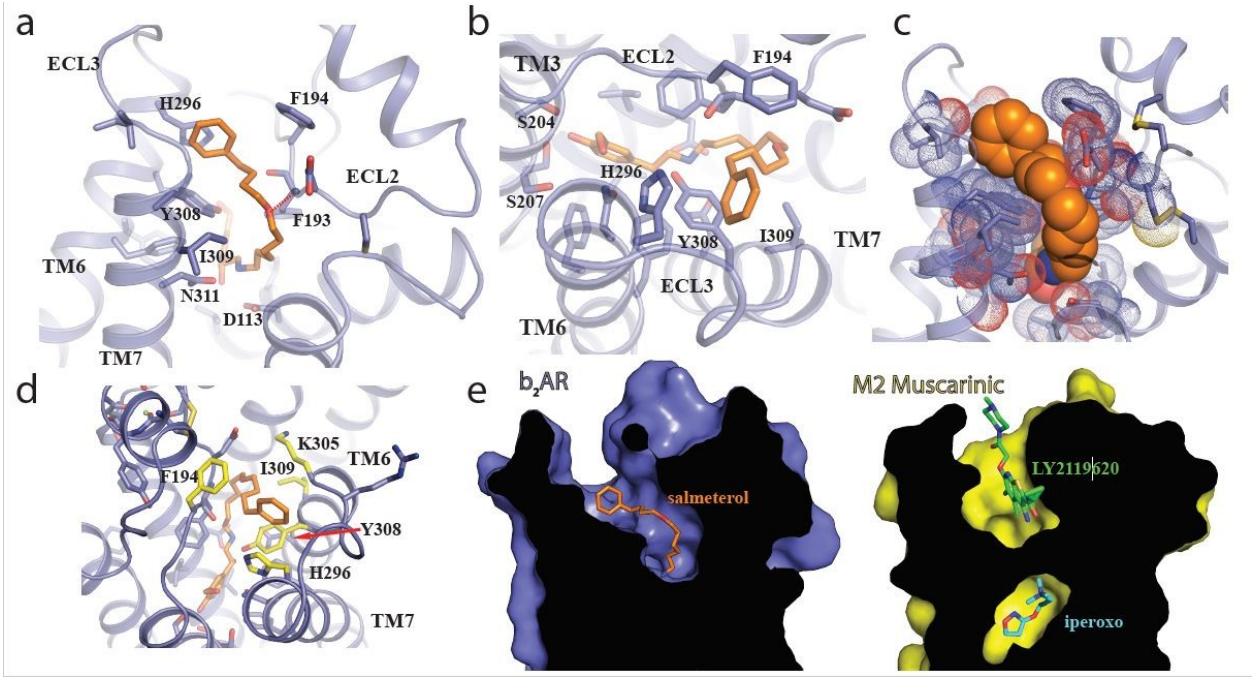
a
ECL3
H296
F194
ECL2
Y308
F193
I309
TM6
N311
D113
TM7
b
TM3
ECL2
F194
S204
H296
S207
Y308
I309
TM7
ECL3
TM6
c
d
K305
TM6
I309
F194
Y308
H296
TM7
e
b2AR
salmeterol
M2 Muscarinic
LY2119620
iperoxo

Figure 4

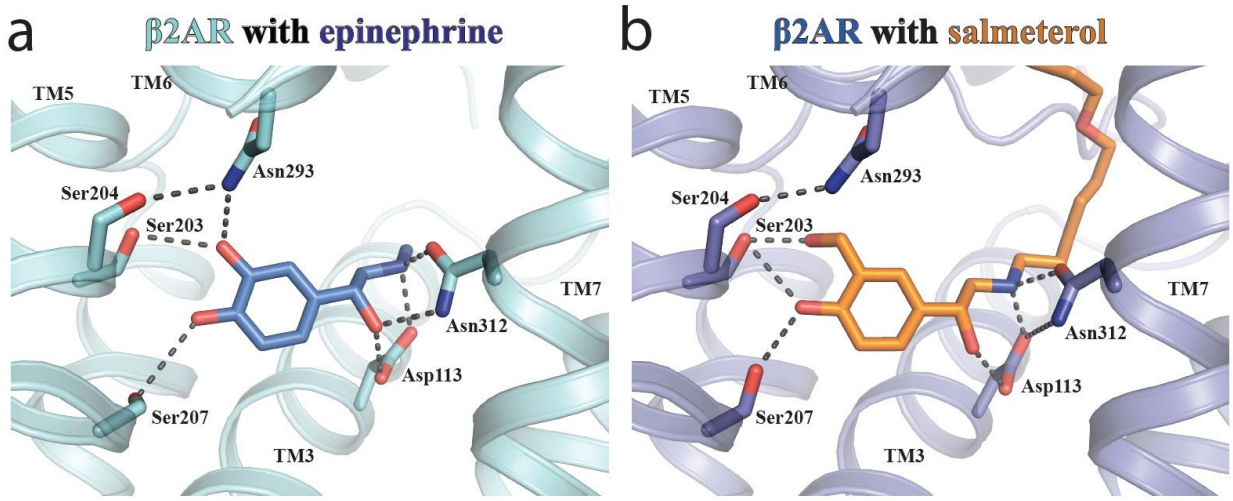
a
β2AR with epinephrine
TM5
TM6
Asn293
Ser204
Ser203
TM7
Asn312
Asp113
Ser207
TM3
b
β2AR with salmeterol
TM5
TM6
Asn293
Ser204
Ser203
TM7
Asn312
Asp113
Ser207
TM3

Figure 5

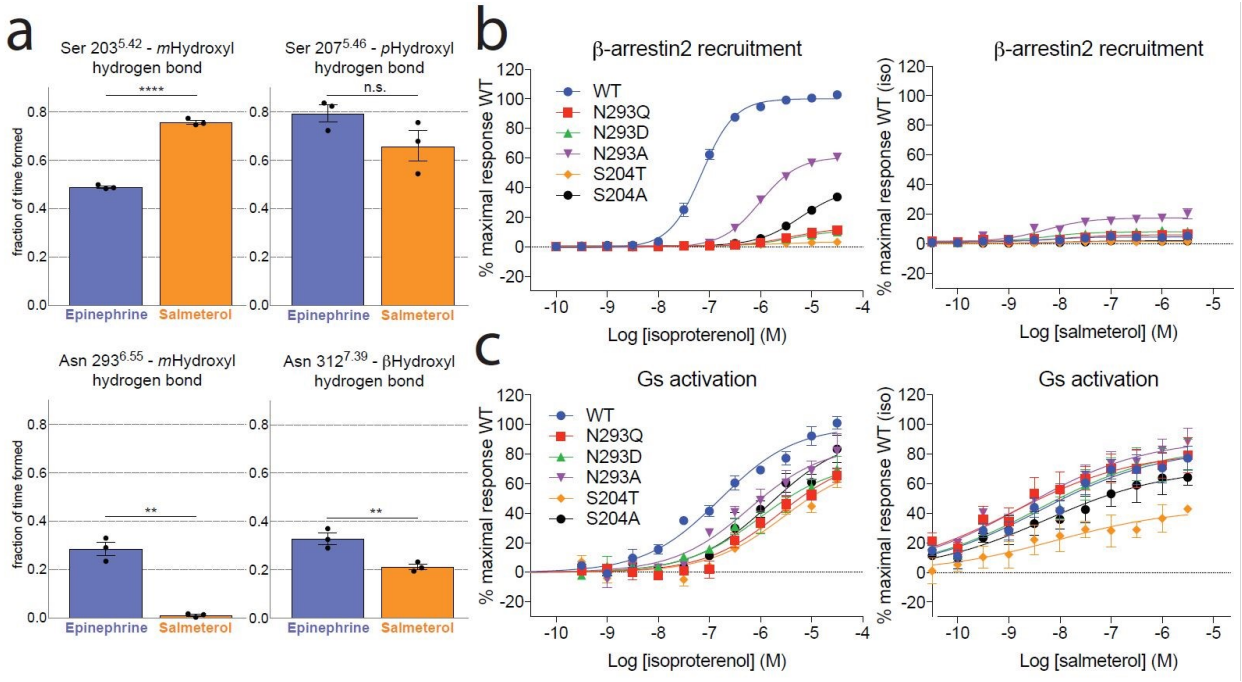
a
Ser 203^5.42 - mHydroxyl hydrogen bond
Ser 207^5.46 - pHydroxyl hydrogen bond
Asn 293^6.55 - mHydroxyl hydrogen bond
Asn 312^7.39 - βHydroxyl hydrogen bond
fraction of time formed
Epinephrine
Salmeterol
****
n.s.
**
b
β-arrestin2 recruitment
% maximal response WT
% maximal response WT (iso)
WT
N293Q
N293D
N293A
S204T
S204A
Log [isoproterenol] (M)
Log [salmeterol] (M)
c
Gs activation

Figure 6

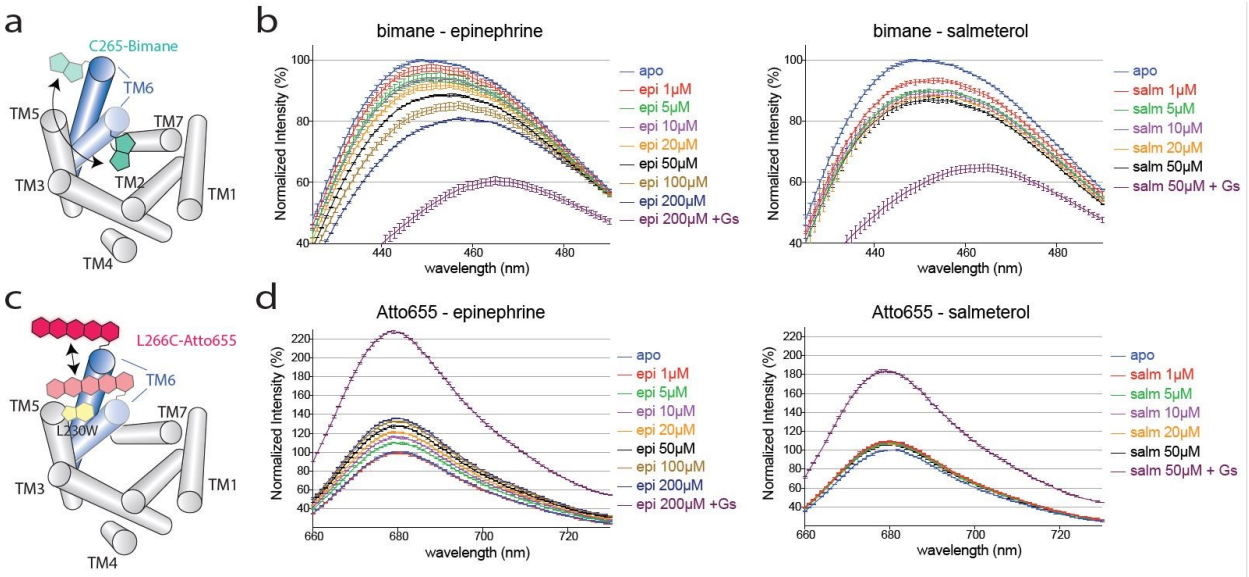
a
C265-Bimane
TM6
TM5
TM7
TM3
TM2
TM1
TM4
b
bimane - epinephrine
Normalized Intensity (%)
wavelength (nm)
apo
epi 1μM
epi 5μM
epi 10μM
epi 20μM
epi 50μM
epi 100μM
epi 200μM
epi 200μM +Gs
bimane - salmeterol
salm 1μM
salm 5μM
salm 10μM
salm 20μM
salm 50μM
salm 50μM + Gs
c
L266C-Atto655
L230W
d
Atto655 - epinephrine
Atto655 - salmeterol

Supplementary Table 1. The affinities of Nb80 and Nb71 for HDL-reconstituted β2AR with different agonists measured by Octet Red.

	Agonist	K_{on} ($M^{-1}s^{-1}$)	K_{off} (s^{-1})	K_d (nM)
Nb80	Epinephrine	$7.2x10^5 \pm 0.1\ x10^5$	$1.6\ x10^{-3} \pm 0.1\ x10^{-3}$	2.2 ± 0.1(n.s.)
	BI-167107	$4.0x10^5 \pm 0.1\ x10^5$	$1.3\ x10^{-3}. \pm 0.1\ x10^{-3}$	3.2 ± 0.3 (n.s.)
	Salmeterol	$1.8x10^5 \pm 0.1x10^5$	$1.6\ x10^{-3} \pm 0.1\ x10^{-3}$	8.8 ± 0.7 (***)
Nb71	Epinephrine	$2.4x10^5 \pm 0.2\ x10^5$	$2.5\ x10^{-3} \pm 0.1\ x10^{-3}$	10 ± 1 (n.s.)
	BI-167107	$3.3x10^5 \pm 0.1\ x10^5$	$2.6\ x10^{-3} \pm 0.3\ x10^{-3}$	8.0 ± 0.9 (n.s.)
	Salmeterol	$2.4x10^5 \pm 0.5\ x10^5$	$2.1\ x10^{-3} \pm 0.1\ x10^{-3}$	8.8 ± 0.5 (n.s.)

The on- and off-rates (Kon and Koff) and the Kd values are listed as mean ± SEM from three independent experiments. Analysis of the binding affinities using Ordinary One-way ANOVA (Tukey) test at a multiplicity adjusted P value = 0.05 indicate that the difference in Nb80 affinities between epinephrine and BI-167107 and the differences in Nb71 affinities between epinephrine, BI-167107 and salmeterol bound b2ar are non-significant (n.s, P values > 0.3), while the difference in Nb80 affinities between epinephrine and salmeterol and BI-167107 and salmeterol are (***), at respective P values of 0.0001 and 0.0003.

Supplementary Table 2: Data collection and refinement statistics (molecular replacement)

	β_2AR-Nb71-Salmeterol* **(PDB code : 6CSY)**
Data collection	
Space group	*C2*
Cell dimensions	
a,b,c (Å)	178.68, 52.59, 125.92
α,β,γ (°)	90,123.86, 90
Resolution(Å)	28.52 – 2.96 (3.07 – 2.96)[a]
R_{merge} (%)[b]	16.7 (52.5)
$< I/\sigma >$	7.5 (1.5)
Completeness (%)	92.6 (75.1)
Redundancy (%)	3.3 (2.0)
Refinement	
Resolution (Å)	28.52 – 2.96 (3.09 – 2.96)
No. Reflections	18742 (1012)
R_{cryst} / R_{free} (%)[c]	20.9 (29.8) / 24.6 (33.2)
Number of atoms	
Protein	4560
Ligand/ion	111
Water	20
Average B factor (Å^2)	
β2AR	47.2
T4L	61.5
Nb71	50.6
Salmeterol	36.4
Water	36.3
R.m.s. deviations	
Bond lenghts (Å)	0.007
Bond angles (°)	0.8

*X-ray diffraction data from 24 LCP crystals was merged to get the final complete data set.
aValues in parentheses are for highest-resolution shell.
b Rmerge = Σ|Ii - Im|/ΣIi, where Ii is the intensity of the measured reflection and Im is the mean
intensity of all symmetry related reflections.
c Rcryst = Σ||Fobs| - |Fcalc||/Σ|Fobs|, where Fobs and Fcalc are observed and calculated structure

factors.
Rfree = ΣT||Fobs| - |Fcalc||/ΣT|Fobs|, where T is a test data set of about 5% of the total reflections
randomly chosen and set aside prior to refinement.

Supplementary Table 3. Emax and pEC50 values for BRET-based βarrestin-2 recruitment and Gs activation assays in cells from Figure 4. NR = not reported

	βarr-2 recruitment (ISO)		**Gs activation (ISO)**		**Gs activation (SALM)**	
	Emax	pEC50	Emax	pEC50	Emax	pEC50
WT	100 ± 1	-7.1 ± 0.1	99 ± 5	-6.8 ± 0.1	84 ± 7	-8.4 ± 0.3
N293Q	13 ± 1	-5.4 ± 0.1	80 ± 9	-5.6 ± 0.2	82 ± 6	-8.9 ± 0.3
N293D	11 ± 2	-5.4 ± 0.2	75 ± 7	-6.0 ± 0.2	85 ± 7	-8.4 ± 0.3
N293A	61 ± 1	-6.0 ± 0.1	86 ± 6	-6.2 ± 0.2	91 ± 6	-8.7 ± 0.3
S204T	4 ± 2	-5.5 ± 0.8	76 ± 10	-5.5 ± 0.3	44 ± 7	-8.1 ± 0.6
S204A	40 ± 4	-5.2 ± 0.1	93 ± 8	-5.8 ± 0.2	71 ± 7	-8.3 ± 0.4

Supplementary figure 1

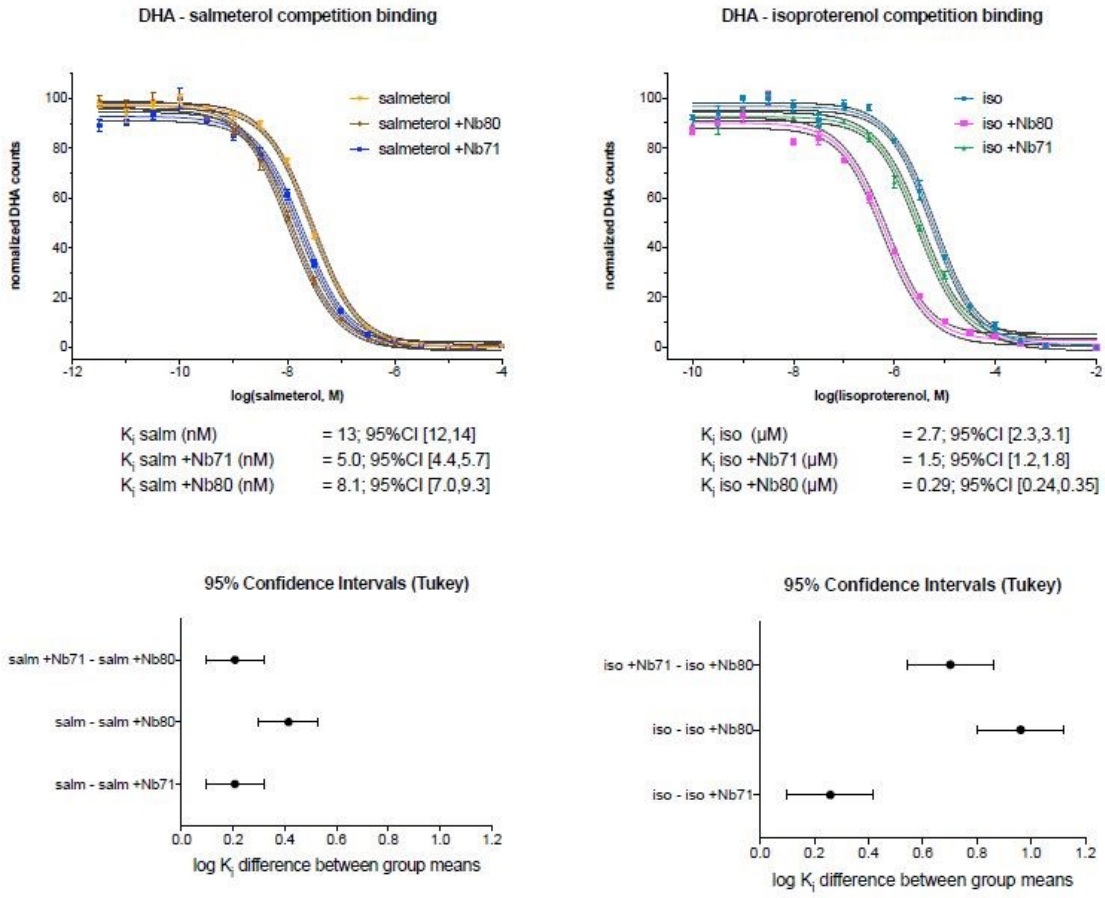

Supplementary figure 2

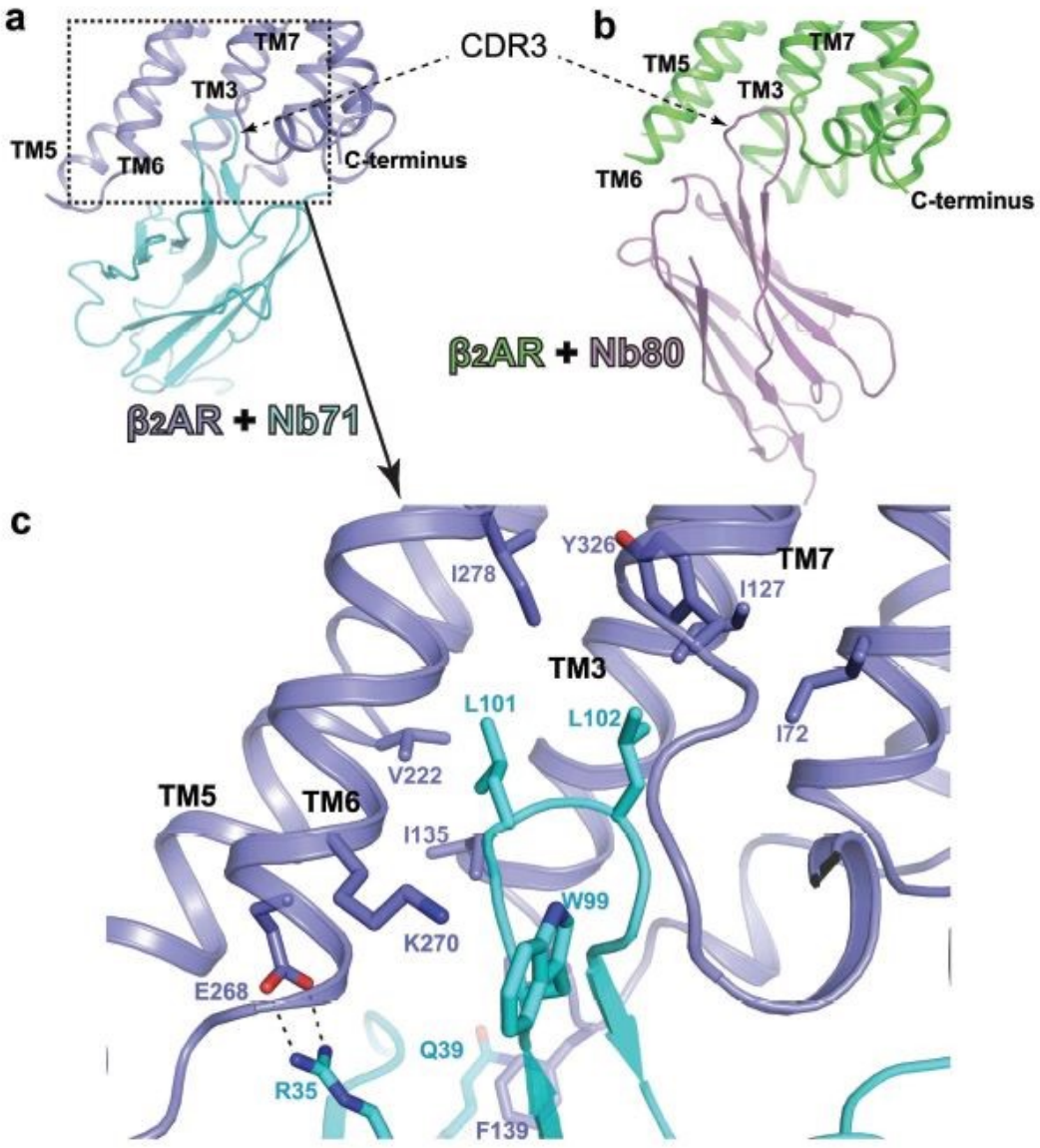

Supplementary figure 3

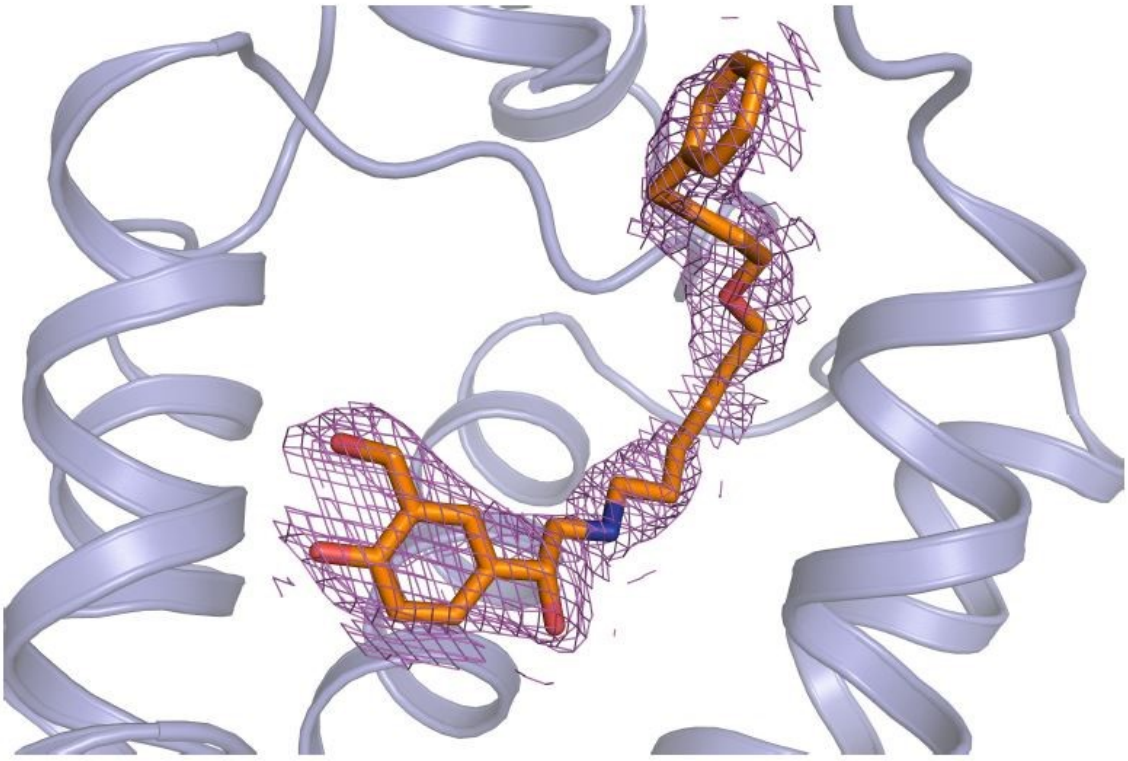

Supplementary figure 4

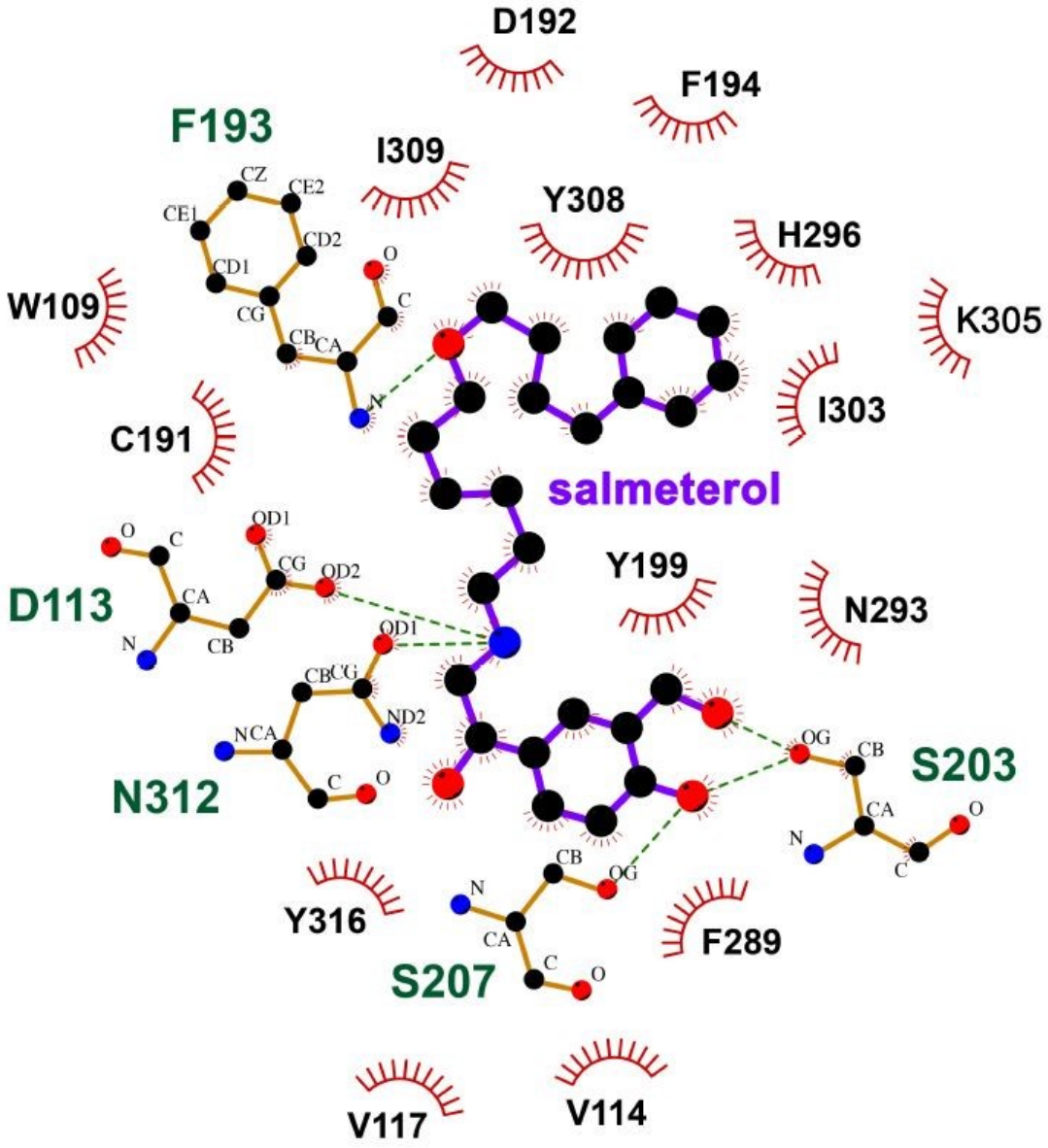

Supplementary figure 5

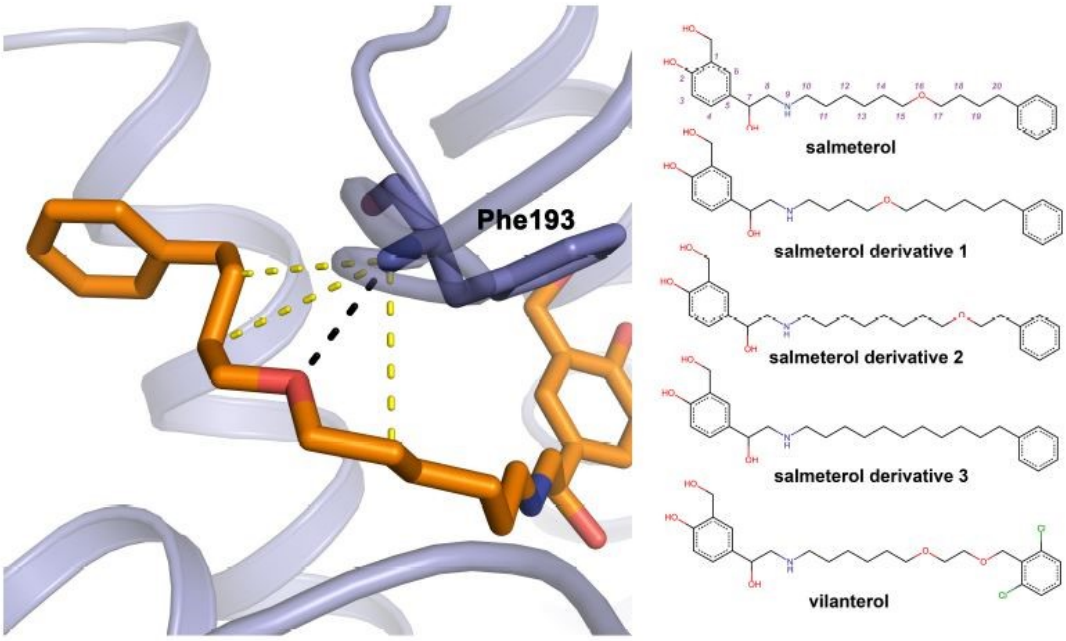

Supplementary figure 6

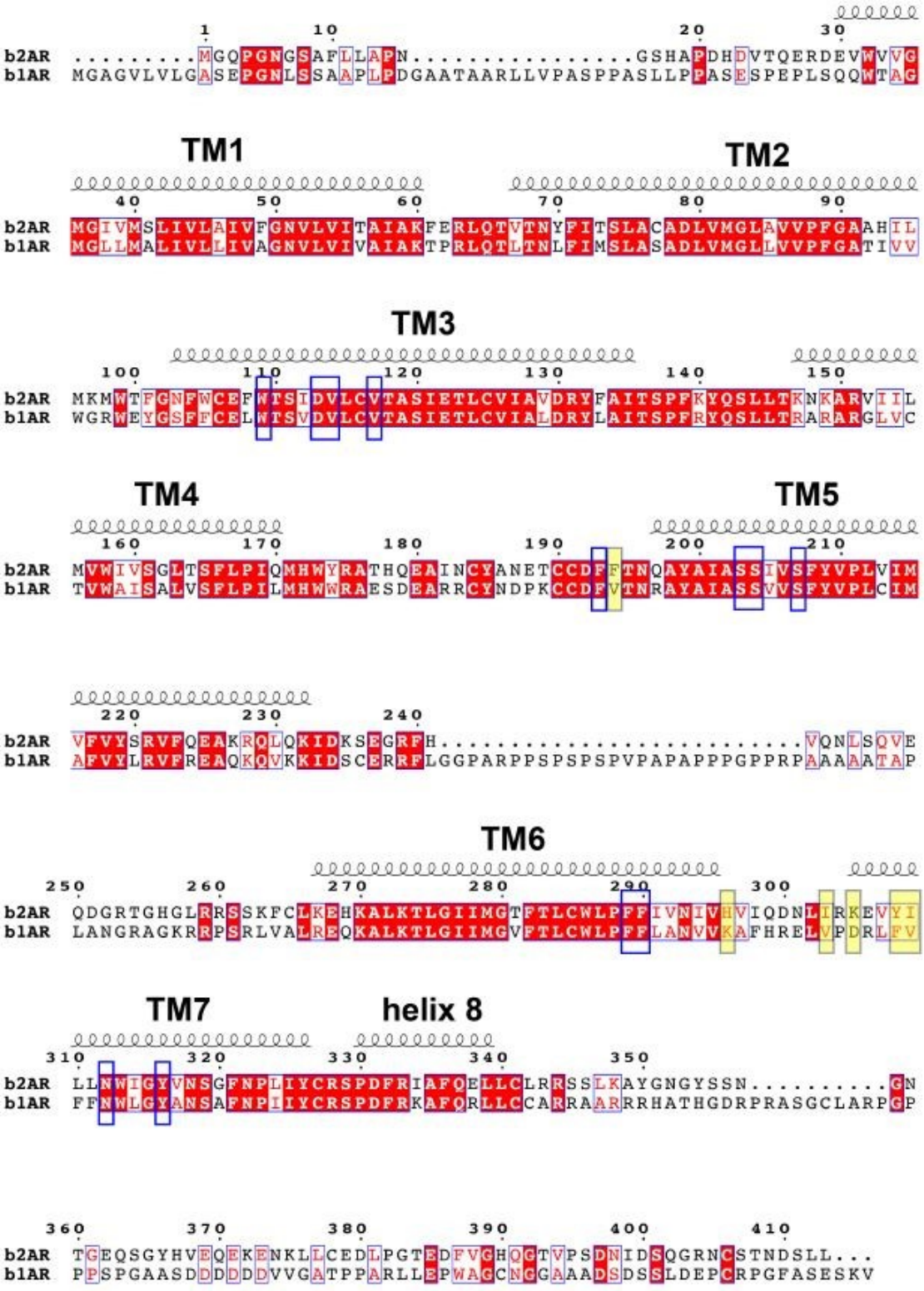

Supplementary figure 7

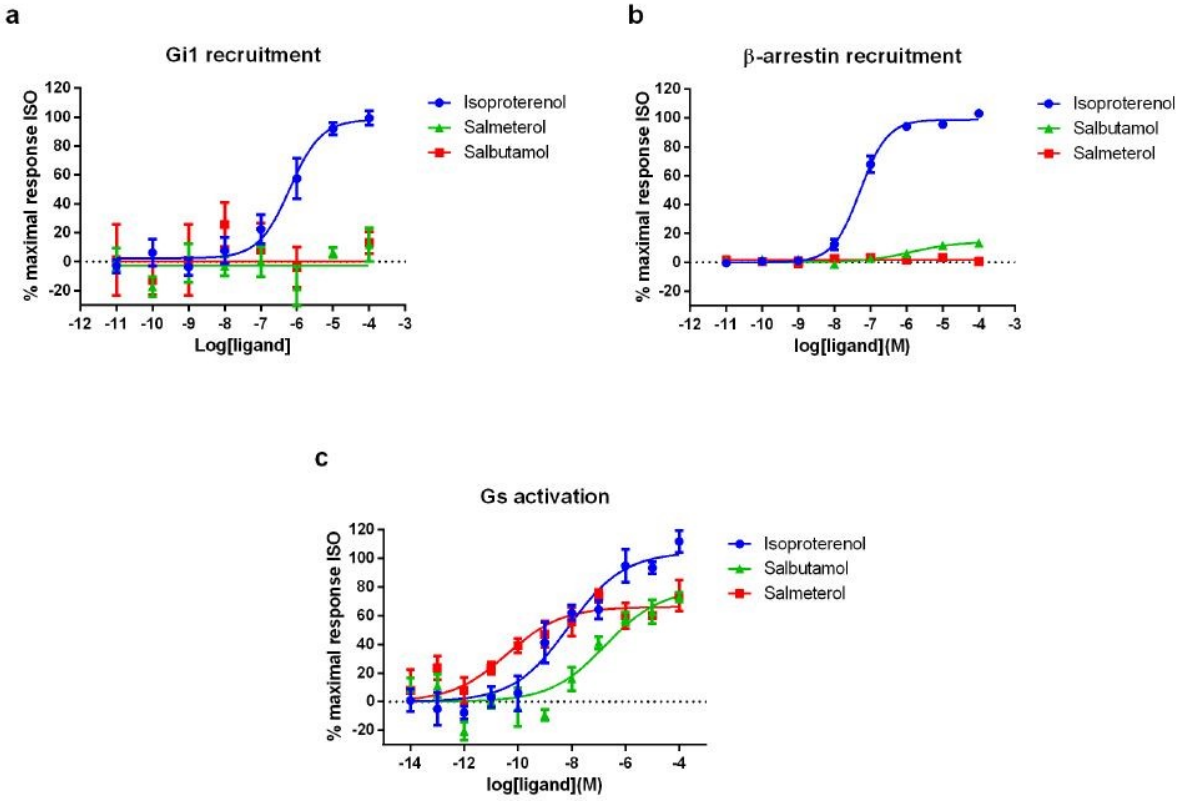

Supplementary figure 8

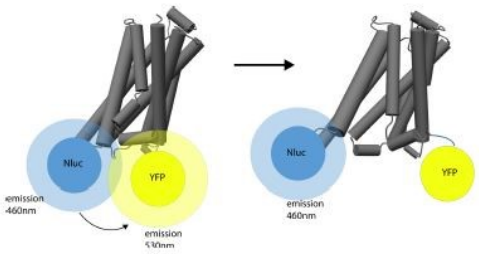

	eMAX	pEC50
ISO	100 ± 4	-7.4 ± 0.1
EPI	110 ± 6	-6.6 ± 0.1
SALB	NR	NR
SALM	NR	NR

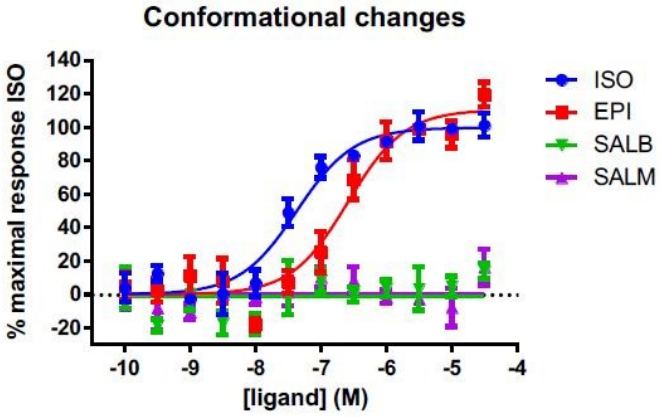

Supplementary figure 9

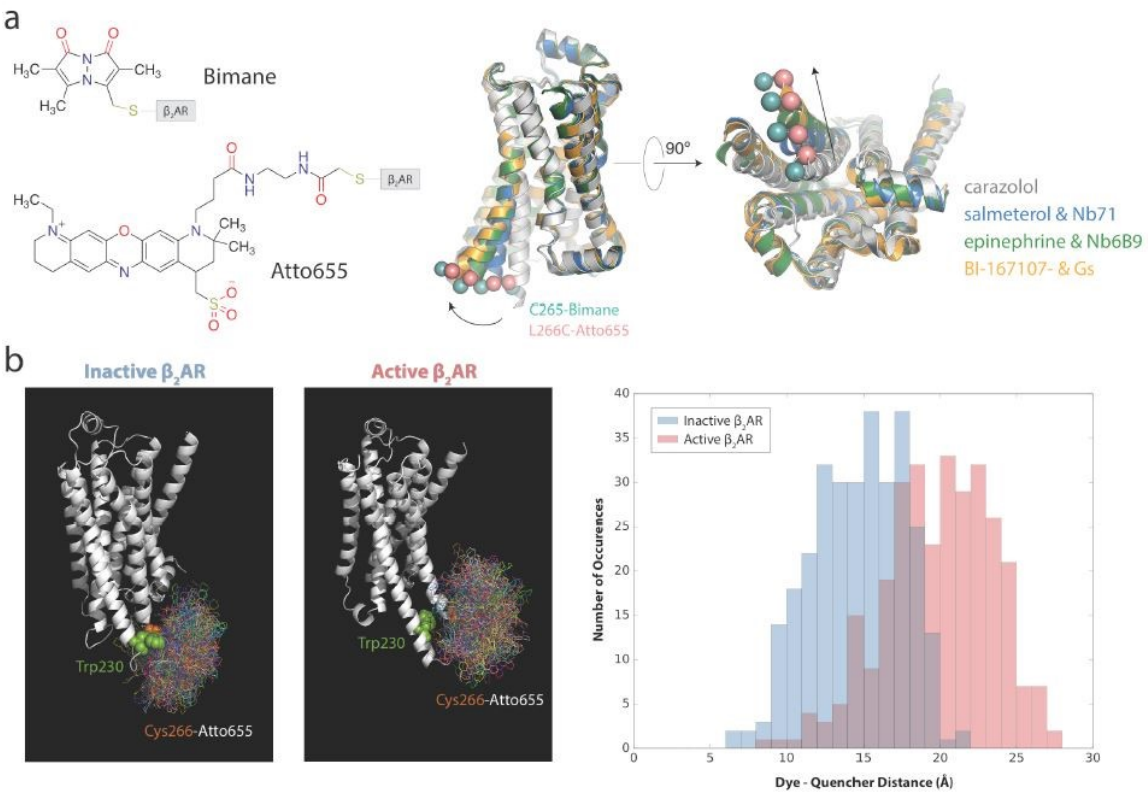

Supplementary figure 10

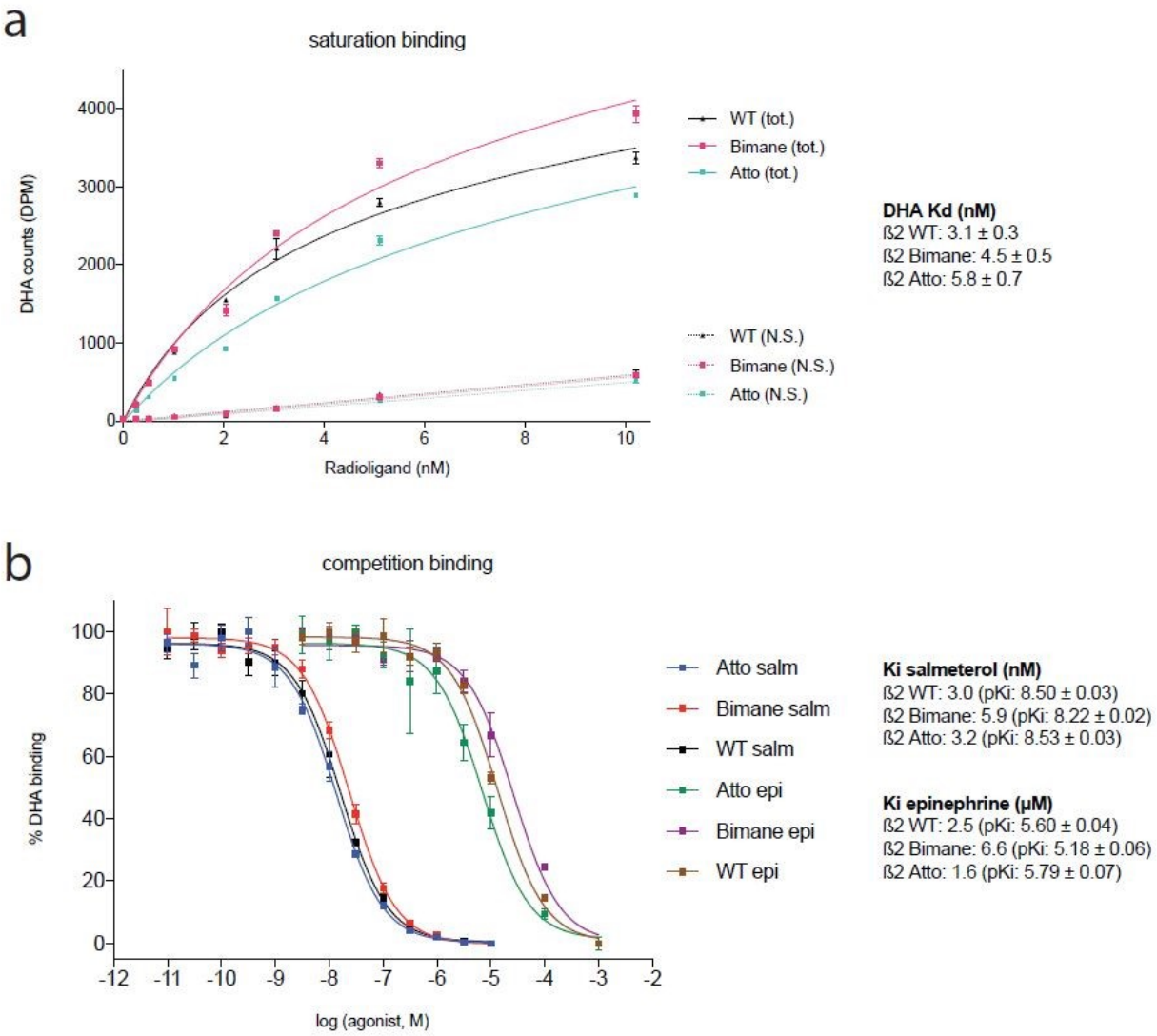

Supplementary figure 11

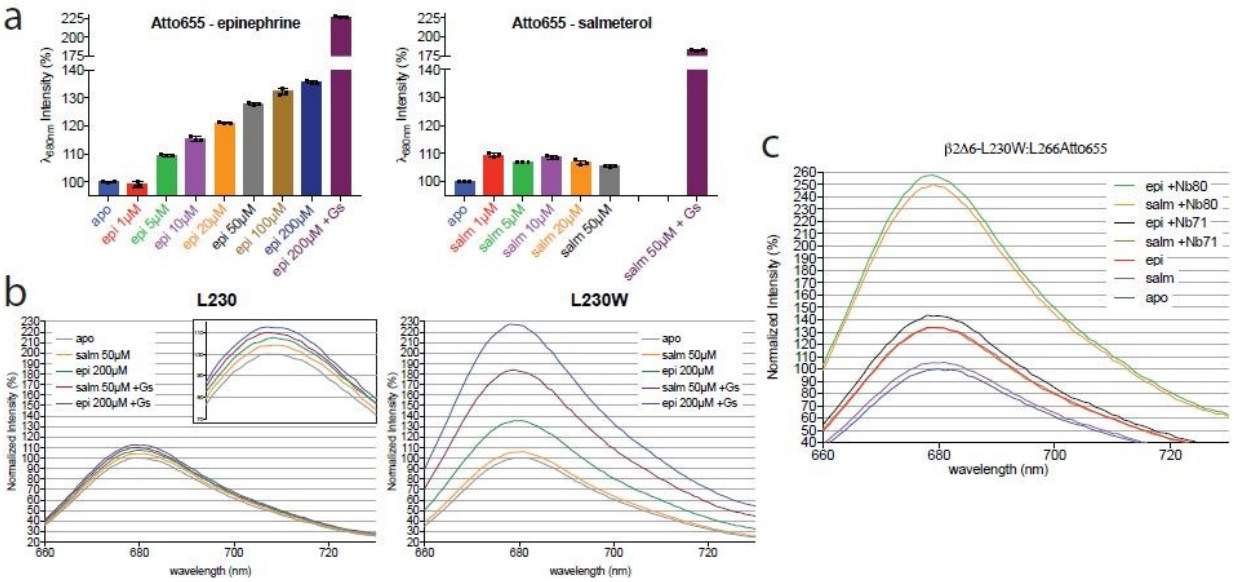

Article 3

Structural insight into β2AR signaling efficacy and bias between Gs and β-arrestin

Louis-Philippe Picard, Anne-Marie Schönegge et Michel Bouvier

Publié dans *ACS Pharmacology and translational science,* le 3 avril 2019

Résumé

Dans les dernières années, il a été démontré que divers ligands d'un récepteur couplé aux protéines G(RCPG) peuvent engager différentes voies de signalisations avec des efficacités distinctes, un concept connu sous le nom de signalisation biaisée. Cependant, les déterminants structuraux menant à ce phénomène demeurent très peu compris. Utilisant le récepteur β2-adrénergique (β2AR) nous avons identifié un résidu ($L124^{3.34}$) liant les motifs PIF et NPxxY et jouant un rôle central dans l'efficacité différentielle entre l'activation de Gs et le recrutement de la β-arrestine pour les ligands biaisés. Étant donné le niveau élevé de conservation de ce résidu, cette étude fournit des explications structurales pour la signalisation biaisée qui peuvent être extrapolées pour d'autres RCPGs

Contributions: j'ai, en collaboration avec mon directeur de thèse, effectué le design de l'étude. J'ai réalisé toutes les expériences ainsi que les analyses des résultats et l'interprété ceux-ci. De plus, j'ai écrit le papier avec l'aide de mon superviseur de thèse.

Structural insight into G protein-coupled receptor signaling efficacy and bias between Gs and β-arrestin

Author's list:

Louis-Philippe Picard[1], Anne-Marie Schonegge[1] and Michel Bouvier[1,*]

[1]Department of Biochemistry and Molecular Medicine, Institute for Research in Immunology and Cancer, Université de Montréal, Montreal, QC, Canada, H3C 3J7.

*Corresponding author: Michel Bouvier, Institute for Research in Immunology and Cancer, Université de Montréal, C.P. 6128 Succursale Centre-Ville, Montréal, Qc. Canada, H3C 3J7. Phone number: (514) 343-6319. Email: michel.bouvier@umontreal.ca

Short title: Structural insight into β2AR biased signaling

Abstract

G protein-coupled receptors (GPCRs) form the largest family of membrane proteins involved in signal transduction. Due to their ability to regulate a wide range of cellular responses and their dysregulation being associated with many diseases, GPCRs remain a key therapeutic target for several clinical indications. In recent years, it has been demonstrated that ligands for a given receptor can engage distinct pathways with different relative efficacies, a concept known as biased signaling or functional selectivity. However, the structural determinants of this phenomenon remain poorly understood. Using the β2-adrenergic receptor as a model, we identified a linker residue ($L124^{3.43}$) between the known PIF and NPxxY structural motifs, that plays a central role in the differential efficacy of biased ligands toward the Gs and β-arrestin pathways. Given the high level of conservation of this linker residue, the study provides structural explanations for biased signaling that can be extrapolated to other GPCRs.

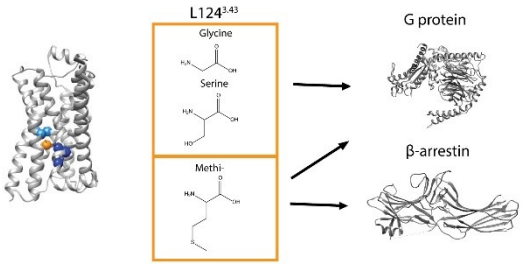

Keywords: G protein-coupled receptors (GPCR), Biased ligands, Bioluminescence Resonance Energy transfer (BRET), Biosensors, β2-adrenergic receptor (β2AR), Mutagenesis, Structural microswitches, Signal transduction.

Abbreviations: BRET: bioluminescence resonance-energy transfer, RET: resonance-energy transfer, GPCR: G protein-coupled receptors, β2AR: β2-adrenergic receptor, ISO: isoproterenol, SALB: salbutamol, SALM: salmeterol, WT: wild-type.

Introduction

G protein-coupled receptors (GPCRs) constitute a family of membrane proteins that initiate signaling cascades in several biological processes. This family has been successfully targeted in several clinical indications. Recently, it has been demonstrated that ligands of a given receptor can preferentially engage some signaling pathways over others, a concept known as biased signaling(1, 2). The emergence of this concept has raised the possibility of identifying ligands that selectively modulate therapeutically relevant pathways while avoiding the ones leading to side effects(3). The ability of different ligands to differentially bias signaling of a given receptor toward distinct pathways is believed to result from the stabilization of distinct conformational ensembles(4-6) that may involve conserved residues forming microswitches(7, 8). Consistent with this notion, distinct dynamic receptor conformations upon binding of different ligands were observed using resonance-energy transfer (RET) biosensors(9-11) , solution-state nuclear magnetic resonance spectroscopy and molecular dynamic simulations(12, 13) .

The β2-adrenergic receptor (β2AR) is a prototypical receptor for which ligands with different propensity to activate different pathways have been identified(14, 15). In particular, salbutamol (SALB) and salmeterol (SALM), which are partial agonists, have been show to preferentially activate the stimulatory G protein, Gs, over promoting the recruitment of β-arrestin(11, 16). Thus, these compounds can be qualified as partial biased agonists. The difference in the binding mode between one of these partial biased agonists, salmeterol, and the full balanced β2AR agonist, epinephrine, has recently been published(16), providing a first level of structural explanation for the different efficacies. However, how these different

binding modalities are propagated from the binding pocket toward the structural elements involved in the engagement of Gs and β-arrestin remains unsolved.

Indeed, although several microswitches such as the toggle switch, PIF/connector, NPxxY and DRY motifs have been reported to be important for receptor activation, their specific roles in biased signaling remain poorly understood. The PIF/connector motif has been suggested to play an important role in connecting the agonist binding pocket to downstream conformational rearrangements required for receptor activation(17). The NPxxY motif for its part has been proposed as a stabilizing element of the active conformation(18). In a previous study, mutations of the residue L124$^{3.43}$ (Ballesteros-Weinstein numbering(19) in superscript) located between the PIF and NPxxY motifs of the β2AR (Figure 1a) resulted in a selective loss of isoproterenol (ISO)-stimulated β-arrestin recruitment(20). To test the hypothesis that this residue could represent a linker between the two microswitches and play a role in signal propagation and bias, we tested the impact of substituting L124 for M, G and S on the activity of both balanced and biased ligands toward Gs activation and β-arrestin recruitment. These substitutions were selected based on evolutionary trace analysis(20) where the conservation of a given amino acid in class A GPCRs through evolution is considered, and suggested that these three substitutions could results in distinct effect on receptor signaling.

Results and discussion

The impacts of L124M/G/S mutations were first assessed on Gs activation using a bioluminescence RET (BRET)-based sensor(21). As shown in Figure1b-c and Table S1, L124G/S substitutions greatly increase the ligand-independent (constitutive) activity of the receptor toward Gs while abolishing the ability of the agonists ISO and SALB to further

activate Gs. This loss in agonist responsiveness does not result from reduced binding, since L124S substitution results in a 100-fold increased affinity for ISO(20). The L124M substitution for its part results in a modest increase of the constitutive activation of the receptor toward Gs (40 ± 5 % for WT to 68 ± 5 % for L124M; Table S1) while maintaining an agonist-promoted response that reaches similar maximal level as the wild-type (WT) receptor (99 ± 8 % for WT and 102 ± 6% for L124M upon ISO stimulation and 90± 6% for WT and 104 ± 8 % for L124M upon SALB stimulation; Figure 1c and Table S1).

A different outcome is observed for β-arrestin recruitment monitored by BRET(22). No constitutive activity to either WT or any of the mutant forms of the receptor was observed. In contrast, the mutations have residue- and ligand-specific impacts on the agonist promoted recruitment. L124G/S abrogate the ISO-promoted β-arrestin recruitment (Figure 1d) whereas L124M resulted in an increased potency for the full and balanced agonists ISO and epinephrine (EPI) (Figure 1d, 2a and Table S2). For the partial and biased agonists, SALB and SALM that only poorly promote β-arrestin recruitment to the WT receptor (Figure 1d and 2a), L124M but not L124G/S led to a gain of function resulting in an increase in β-arrestin recruitment (Figure 1d and 2a). However, the mutation does not confer β-arrestin recruitment to antagonists (alprenolol, labetalol, propranolol and xamoterol) or inverse agonists (metoprolol and timolol) (Figure 2c-b). These results suggest that the L124M mutation enhances the ability of the receptor to transduce agonists signal towards β-arrestin engagement.

To further explore the hypothesis that the effects of the L124 mutations result from a change in signal transduction affecting the equilibrium between conformational ensembles, the impact of the mutations on a previously described sensor (NY-β2AR) able to detect conformational rearrangements of the receptor by monitoring the BRET between probes located in the 3rd cytoplasmic loop and the carboxyl terminal of the receptor(11) was assessed. As shown in Figure. 3a, mutations L124G/S result in a significant decrease in basal NY-β2AR BRET signal, reflecting a switch in the conformational ensemble that favors open conformations associated with active states. This is consistent with the increased constitutive activity of the receptor for Gs (Figure 1c). Furthermore, these mutations abolish the ISO-promoted conformational changes observed for the WT receptor (Figure 3b-c), consistent with the loss of agonist responsiveness for Gs activation (Figure 1c) and β-arrestin recruitment (Figure 1d) thus suggesting that these mutations disrupt the link between the binding pocket and the conformational changes leading to signal transduction. The uncoupling between the binding pocket and signaling is also supported by the lack of effect of the inverse agonist, ICI 118,551 on the constitutive cAMP production promoted by L124G/S mutants (Figure S1). Disruption between the binding pocket and signaling has previously been reported for the adenosine A2a receptor(23). The increase constitutive activity and absence of responsiveness to ligands also indicates a shift of equilibrium of the unbound receptor towards the active states consistent with the increased affinity for ISO observed for the mutant L124S(20). The modest decrease in basal NY-β2AR BRET for the L124M (Figure 3a) is also consistent with the small increase in the receptor constitutive activity for Gs (Figure 1c). However, in contrast with the effects of L124G/S, the L124M mutation does not affect the ISO-promoted conformational changes of the receptor (Figure 3b). In contrast to the full and balanced agonist ISO, the biased and partial

agonist SALB did not promote any detectable conformational rearrangement of NY-β2AR. Mutations L124G/S do not confer any detectable conformational changes upon SALB stimulation. However, the mutation L124M results in a gain of SALB-induced NY-β2AR BRET change (Figure 3c), reflecting the occurrence of conformational changes upon activation. Such activation is consistent with the gain of SALB-promoted β-arrestin recruitment (Figure 1d).

In order to gain structural insight on the role of L124, impacts of the mutations were assessed using *in silico* modeling. For L124G/S, a complete loss of interactions between residue 124 and the PIF motif is observed in the inactive conformation derived from the crystal structures, PDB 2RH1 representing the carazolol bound β2AR (Figure 4). These changes should lead to a reduction of the structural constraints, allowing more flexibility, thus increasing the probability of the receptor to adopt an active conformation, leading to increased constitutive activation of Gs. Furthermore, this loss of interaction between the residue 124 and the PIF motif in the inactive conformation would decrease the stability of the inactive form shifting the equilibrium towards the active states, as suggested by the decrease in BRET level for the NY-β2AR sensor in absence of ligand (Figure 3a). The weakening of the interaction between the PIF and NPxxY microswitches can also explain the loss of response to ligand stimulation observed for L124G/S. The PIF motif has been described to play a crucial role for signal transduction from the binding pocket(24) and the NPxxY for active conformation stabilisation(25). Therefore, disconnecting the two motifs by mutating the newly identified linker residue L124 most likely uncouples ligand binding from signal transduction. In addition to this reduction of structural constraints in the inactive conformation, the mutant L124S could

form a hydrogen bond with Y326 of the NPxxY motif in the active conformation derived from the crystal structure, PDB 4LDE, representing the BI167107 bound β2AR. This additional hydrogen bound could stabilize the active state thus partially explaining the constitutive activity of this mutant for Gs activation. However, the mutant L124G has the same functional effects as L124S, therefore, the main structural explanation for constitutive activity is more likely to be due to a loss of interaction between residue 124 and the PIF motif.

In contrast with L124G/S, L124M mutation places the sulfur atom of the methionine in a position to interact with the π-electrons of the aromatic ring of F282 in the inactive and active conformations, and with the π electrons of the Y326 in the active conformation (Figure 4) providing a more general stabilization of the receptor with a greater increase being seen in the active one. These gains of interactions most likely stabilize active conformation ensembles, as such interactions have been demonstrated to display stabilizing effects on different protein structures(26), thus increasing the efficiency of signal transduction and resulting in a gain of β-arrestin recruitment. This is supported by the gain of SALB-promoted NY-β2AR opening by the L124M mutation. It is noteworthy that ligands biased against β-arrestin, such as SALB and SALM, cannot on their own promote a detectable conformational change of WT NY-β2AR(11). This could indicate that balanced and biased ligands stabilize distinct conformations (Figure 5a) as previously suggested by a single molecule FRET study(9) and by the recently obtained crystal structure of the SALM-β2AR complex(16). Another possibility is that the differences in equilibrium are caused by the difference in overall stability of active conformations, where balanced ligands would stabilize them for a longer time as compared with biased ligands (Figure 5b). The strengthening of the link between the PIF and NPxxY

motifs by the L124M mutation would increase the time spent in active conformations for all agonists, through methionine-aromatic interaction, leading to increased β-arrestin recruitment. Such differences in conformational equilibrium would not affect Gs activation since G protein engagement is faster than β-arrestin recruitment(22, 27). The observation that Gs on its own can promote conformational changes(11) associated with activation and several studies indicating the existence of a pre-coupling between receptors and G proteins(28, 29) would be compatible with the faster activation rate of Gs compared with β-arrestin. For L124G/S mutants, the main effect would be a reduced stabilisation of the inactive states, thus increasing Gs activation at the basal level, while the absence of additional stabilisation by the ligands would prevent β-arrestin recruitment. The difference in the active conformations' haft-life that would be required to engage Gs versus β-arrestin agrees with studies showing that the residency time of the ligand in the binding pocket of the receptor is important for β-arrestin recruitment but does not affect G protein activation(30).

In conclusion, L124$^{3.43}$ plays a major role in receptor activation by interacting with the PIF and NPxxY motifs. Whether the mutations at this position modify the receptor conformation or the equilibrium between active and inactive states remains to be further investigated, but it is clear that this region plays a crucial role in dictating the selective engagement of G protein vs β-arrestin and linking ligand binding to effectors engagement. Given the conservation (73%) of this linker residue among class A GPCRs (GPCRdb.org), we can propose that it represents a key element in signal propagation and biased signalling. This opens the possibility of rationally designing allosteric ligands that would target this region to generate biased ligands.

Methods

Reagents. (-)-Isoproterenol hydrochloride (ISO), (-)-Epinephrine (EPI), (-)-Norepinephrine (NE), Alprenolol hydrochloride (ALP), Labetalol hydrochloride (LAB), (±)-Propranolol hydrochloride (PRO), Metoprolol tartrate (MET), Timolol maleate (TIM) were purchased from Sigma Aldrich. Salbutamol hemisulfate (SALB) and Xamoterol hemifumarate (XAM) were purchased from Tocris Bioscience. Salmeterol xinofolate was purchased from Selleckchem. Coelenterazine 400a (Coel400a) was purchased from NanoLight Technology.

Plasmids. The β-arrestin-RlucII(22), HA-β2AR WT and mutant forms(20), Gαs-117-RlucII(21), Gβ1(31), Gγ1-GFP10(31), β2AR-GFP10(32) and NY-β2AR(11) have been previously described. Point mutations in the NY-β2AR and β2AR-GFP10 were introduced by PCR using QuickChange Site-directed Mutagenesis Kit (Agilent Technologies) following the manufacturer's instructions. All variants were verified by sequencing.

Cell culture and transfection. HEK293T cells were grown in Dulbecco's modified Eagle's medium (DMEM) supplemented with 10% newborn calf serum (NCS) at 37°C with 5% CO_2. For transfection, cells were detached with trypsin, diluted at a density of 500,000 cells/mL and transfected with 2.5 µg of total DNA per 10^6 cells using linear polyethylenimine (PEI, Polysciences) as transfecting agent with a PEI:DNA ratio of 3:1. Directly after transfection, cells were plated in white 96-wells culture plates (Greiner) coated with Poly-L-Ornithine (Sigma-Aldrich) at a density of 50,000 cells per well and incubated for 48 h before experiments. Cells were regularly tested for mycoplasma contamination (PCR Mycoplasma Detection kit, abm).

BRET measurements. 48 h after transfection, cells were washed with PBS and stimulation buffer (Hank's balanced salt solution, HBSS) was added. 10X concentrated ligand was added 5 min (Gs) or 15 min (NY-β2AR and β-arrestin assays) before BRET measurement while Coel400a was added to a final concentration of 2.5 μM, 5 min before reading. BRET was monitored with a TriStar2 LB942 microplate reader (Berthold) equipped with a donor filter of 410/80 nm and an acceptor filter of 515/40 nm (Gs and β-arrestin assays) or a donor filter of 485/20 nm and an acceptor filter of 530/25 nm (NY-β2AR assay). BRET ratios were calculated by dividing the acceptor emission by the donor emission.

Conformational sensor. HEK293T cells were transfected with the conformational biosensor (NY-β2AR)(11). BRET was then monitored as described above. The NY-β2AR consists of a β2AR construct where Nluc was fused to the ICL3 between positions 251 and 252 and YFP at position 369 of a truncated receptor. These positions allow the detection of conformational changes resulting from the TM5 rotation and TM6 outward movement upon receptor activation.

β-arrestin recruitment. HEK293T cells were co-transfected with the BRET-based biosensors β2AR-GFP10 (WT or mutants) and βarr2-RlucII, as described above. BRET was then monitored as described above. After recruitment of β-arrestin to the receptor, the increase proximity between the two proteins leads to an increase in BRET ratio.

Gs activation. HEK293T cells were co-transfected with the β2AR receptor (WT or mutants) along with Gαs-117-RlucII, Gβ1, Gγ1-GFP10 (G protein activation BRET biosensor(21)) and BRET monitored as described above. The dissociation of the Gα and Gβ/Gγ subunits upon G protein activation leads to a decrease in BRET ratio.

Cell surface ELISA. HEK293T cells transfected with the different receptor constructs were washed with PBS, then fixed with 3% PFA diluted in PBS. Fixed cells were washed with WashB solution (0.5% BSA in PBS). The monoclonal anti-HA-HRP (3f10, Roche Diagnostics) was added at a dilution of 1/2,000 and cells were incubated at RT for 1 h. After incubation, cells were washed with WashB solution. HBSS was added in the wells, and 2 min before the reading, ECL (Perkin Elmer) was added. Total luminescence was monitored with a Mithras LB 940 microplate reader (Berthold).

BRET signal analysis. Concentration-response curves were analysed using GraphPad Prism 6 software (version 6, GraphPad Software). The data were normalized to WT curves. The maximal response upon ISO stimulation was used as 100% and the values of unstimulated mock conditions were used as 0%. This normalization allows the detection of changes in constitutive activity, which correspond to the lower asymptotes of the concentration-response curves. Cell surface ELISA was performed as described above to control receptors expression.

Structure prediction and analysis. Protein structure prediction was performed as previously described(20). Briefly, MOE structure-based design package was used. Automated structure preparation protocol Protonate3D was run on both inactive and active receptor templates (2RH1 and 4LDE, respectively), then the mutations were inserted using the Residue Scanning in the Protein Design panel. The conformation of the side chain was determined by a selection from a rotamer library followed by a force field energy minimization-based protocol, using AMBER12EHT force field. Structure predictions were visualized and analysed using chimera visualization system. Interactions between mutated residues and the microswitches have been

determined by a distance inferior to 0.4 Å between the van der Waals radii of the different atoms.

Acknowledgements. This work was supported by grants from the Canadian Institutes for Health Research (CIHR), [MOP11215] and [FDN148431]. L.-P.P. received scholarships from CIHR and the Fonds de la Recherche du Quebec – Santé (FRQ-S). A.M.S. received a post-doctoral fellowship from FRQ-S. M.B. holds a Canada Research Chair in Signal Transduction and Molecular Pharmacology. We are grateful to Dr. Brian Kobilka and Monique Lagacé for their critical reading of the manuscript.

Authors contributions. L.-P.P. A.M.S and M.B. designed the study. L.-P.P. and A.M.S performed the experiments, and the analysis of the data. L.-P.P. and M.B. interpreted the data and wrote the manuscript.

Competing interests. The authors declare no competing interests.

Supporting Information. The supporting information is available free of charge on the ACS Publications website. Supplementary Figure S1 for cAMP production of WT and mutants β2AR and Supplementary Table S1 and S2 reporting efficacies, potencies and errors for Gs activation and β-arrestin recruitment essay.

References

[1] Pupo, A. S., Duarte, D. A., Lima, V., Teixeira, L. B., Parreiras, E. S. L. T., and Costa-Neto, C. M. (2016) Recent updates on GPCR biased agonism, *Pharmacol Res 112*, 49-57.

[2] Rankovic, Z., Brust, T. F., and Bohn, L. M. (2016) Biased agonism: An emerging paradigm in GPCR drug discovery, *Bioorg Med Chem Lett 26*, 241-250.

[3] Kenakin, T. (2012) The potential for selective pharmacological therapies through biased receptor signaling, *BMC Pharmacol Toxicol 13*, 3.

[4] Zocher, M., Fung, J. J., Kobilka, B. K., and Muller, D. J. (2012) Ligand-specific interactions modulate kinetic, energetic, and mechanical properties of the human beta2 adrenergic receptor, *Structure 20*, 1391-1402.

[5] Dror, R. O., Arlow, D. H., Maragakis, P., Mildorf, T. J., Pan, A. C., Xu, H., Borhani, D. W., and Shaw, D. E. (2011) Activation mechanism of the beta2-adrenergic receptor, *Proceedings of the National Academy of Sciences of the United States of America 108*, 18684-18689.

[6] Smith, J. S., Lefkowitz, R. J., and Rajagopal, S. (2018) Biased signalling: from simple switches to allosteric microprocessors, *Nature reviews. Drug discovery 17*, 243-260.

[7] Tehan, B. G., Bortolato, A., Blaney, F. E., Weir, M. P., and Mason, J. S. (2014) Unifying family A GPCR theories of activation, *Pharmacology & therapeutics 143*, 51-60.

[8] Deupi, X., Standfuss, J., and Schertler, G. (2012) Conserved activation pathways in G-protein-coupled receptors, *Biochem Soc Trans 40*, 383-388.

[9] Gregorio, G. G., Masureel, M., Hilger, D., Terry, D. S., Juette, M., Zhao, H., Zhou, Z., Perez-Aguilar, J. M., Hauge, M., Mathiasen, S., Javitch, J. A., Weinstein, H., Kobilka, B. K., and Blanchard, S. C. (2017) Single-molecule analysis of ligand efficacy in beta2AR-G-protein activation, *Nature 547*, 68-73.

[10] Reiner, S., Ambrosio, M., Hoffmann, C., and Lohse, M. J. (2010) Differential signaling of the endogenous agonists at the beta2-adrenergic receptor, *The Journal of biological chemistry 285*, 36188-36198.

[11] Picard, L.-P., Schönegge, A. M., Lohse, M. J., and Bouvier, M. (2018) Bioluminescence resonance energy transfer-based biosensors allow monitoring of ligand- and transducer-mediated GPCR conformational changes, *Communications Biology 1*, 106.

[12] Nygaard, R., Zou, Y., Dror, R. O., Mildorf, T. J., Arlow, D. H., Manglik, A., Pan, A. C., Liu, C. W., Fung, J. J., Bokoch, M. P., Thian, F. S., Kobilka, T. S., Shaw, D. E., Mueller, L., Prosser, R. S., and Kobilka, B. K. (2013) The dynamic process of beta(2)-adrenergic receptor activation, *Cell 152*, 532-542.

[13] Liu, J. J., Horst, R., Katritch, V., Stevens, R. C., and Wuthrich, K. (2012) Biased signaling pathways in beta2-adrenergic receptor characterized by 19F-NMR, *Science 335*, 1106-1110.

[14] Wisler, J. W., DeWire, S. M., Whalen, E. J., Violin, J. D., Drake, M. T., Ahn, S., Shenoy, S. K., and Lefkowitz, R. J. (2007) A unique mechanism of beta-blocker action: carvedilol stimulates beta-arrestin signaling, *Proceedings of the National Academy of Sciences of the United States of America 104*, 16657-16662.

[15] van der Westhuizen, E. T., Breton, B., Christopoulos, A., and Bouvier, M. (2014) Quantification of ligand bias for clinically relevant beta2-adrenergic receptor ligands: implications for drug taxonomy, *Molecular pharmacology 85*, 492-509.

[16] Masureel, M., Zou, Y., Picard, L.-P., van der Westhuizen, E., Mahoney, J. P., Rodrigues, J. P. G. L. M., Mildorf, T. J., Dror, R. O., Shaw, D. E., Bouvier, M., Pardon, E., Steyaert, J., Sunahara, R. K., Weis, W. I., Zhang, C., and Kobilka, B. K. (2018) Structural insights into binding specificity, efficacy and bias of a β2AR partial agonist, *Nature chemical biology 14*, 1059-1066.

[17] Rasmussen, S. G., DeVree, B. T., Zou, Y., Kruse, A. C., Chung, K. Y., Kobilka, T. S., Thian, F. S., Chae, P. S., Pardon, E., Calinski, D., Mathiesen, J. M., Shah, S. T., Lyons, J. A., Caffrey, M., Gellman, S. H., Steyaert, J., Skiniotis, G., Weis, W. I., Sunahara, R. K., and Kobilka, B. K. (2011) Crystal structure of the beta2 adrenergic receptor-Gs protein complex, *Nature 477*, 549-555.

[18] Huang, W., Manglik, A., Venkatakrishnan, A. J., Laeremans, T., Feinberg, E. N., Sanborn, A. L., Kato, H. E., Livingston, K. E., Thorsen, T. S., Kling, R. C., Granier, S., Gmeiner, P., Husbands, S. M., Traynor, J. R., Weis, W. I., Steyaert, J., Dror, R. O., and Kobilka, B. K. (2015) Structural insights into micro-opioid receptor activation, *Nature 524*, 315-321.

[19] Ballesteros, J. A., and Weinstein, H. (1995) [19] Integrated methods for the construction of three-dimensional models and computational probing of structure-function relations in G protein-coupled receptors, *25*, 366-428.

[20] Schonegge, A. M., Gallion, J., Picard, L. P., Wilkins, A. D., Le Gouill, C., Audet, M., Stallaert, W., Lohse, M. J., Kimmel, M., Lichtarge, O., and Bouvier, M. (2017) Evolutionary action and structural basis of the allosteric switch controlling beta2AR functional selectivity, *Nat Commun 8*, 2169.

[21] Thomsen, A. R., Plouffe, B., Cahill, T. J., 3rd, Shukla, A. K., Tarrasch, J. T., Dosey, A. M., Kahsai, A. W., Strachan, R. T., Pani, B., Mahoney, J. P., Huang, L., Breton, B., Heydenreich, F. M., Sunahara, R. K., Skiniotis, G., Bouvier, M., and Lefkowitz, R. J. (2016) GPCR-G Protein-beta-Arrestin Super-Complex Mediates Sustained G Protein Signaling, *Cell 166*, 907-919.

[22] Azzi, M., Charest, P. G., Angers, S., Rousseau, G., Kohout, T., Bouvier, M., and Pineyro, G. (2003) Beta-arrestin-mediated activation of MAPK by inverse agonists reveals distinct active conformations for G protein-coupled receptors, *Proceedings of the National Academy of Sciences of the United States of America 100*, 11406-11411.

[23] Lebon, G., Warne, T., Edwards, P. C., Bennett, K., Langmead, C. J., Leslie, A. G., and Tate, C. G. (2011) Agonist-bound adenosine A2A receptor structures reveal common features of GPCR activation, *Nature 474*, 521-525.

[24] Wacker, D., Wang, C., Katritch, V., Han, G. W., Huang, X. P., Vardy, E., McCorvy, J. D., Jiang, Y., Chu, M., Siu, F. Y., Liu, W., Xu, H. E., Cherezov, V., Roth, B. L., and Stevens, R. C. (2013) Structural features for functional selectivity at serotonin receptors, *Science 340*, 615-619.

[25] Barak, L. S., Menard, L., Ferguson, S. S., Colapietro, A. M., and Caron, M. G. (1995) The conserved seven-transmembrane sequence NP(X)2,3Y of the G-protein-coupled receptor superfamily regulates multiple properties of the beta 2-adrenergic receptor, *Biochemistry 34*, 15407-15414.

[26] Valley, C. C., Cembran, A., Perlmutter, J. D., Lewis, A. K., Labello, N. P., Gao, J., and Sachs, J. N. (2012) The methionine-aromatic motif plays a unique role in stabilizing protein structure, *The Journal of biological chemistry 287*, 34979-34991.

[27] Gales, C., Rebois, R. V., Hogue, M., Trieu, P., Breit, A., Hebert, T. E., and Bouvier, M. (2005) Real-time monitoring of receptor and G-protein interactions in living cells, *Nat Methods 2*, 177-184.

[28] Nobles, M., Benians, A., and Tinker, A. (2005) Heterotrimeric G proteins precouple with G protein-coupled receptors in living cells, *Proceedings of the National Academy of Sciences of the United States of America 102*, 18706-18711.

[29] Cevheroglu, O., Becker, J. M., and Son, C. D. (2017) GPCR-Galpha protein precoupling: Interaction between Ste2p, a yeast GPCR, and Gpa1p, its Galpha protein, is formed before ligand binding via the Ste2p C-terminal domain and the Gpa1p N-terminal domain, *Biochimica et biophysica acta 1859*, 2435-2446.

[30] Wacker, D., Wang, S., McCorvy, J. D., Betz, R. M., Venkatakrishnan, A. J., Levit, A., Lansu, K., Schools, Z. L., Che, T., Nichols, D. E., Shoichet, B. K., Dror, R. O., and Roth, B. L. (2017) Crystal Structure of an LSD-Bound Human Serotonin Receptor, *Cell 168*, 377-389 e312.
[31] Gales, C., Van Durm, J. J., Schaak, S., Pontier, S., Percherancier, Y., Audet, M., Paris, H., and Bouvier, M. (2006) Probing the activation-promoted structural rearrangements in preassembled receptor-G protein complexes, *Nature structural & molecular biology 13*, 778-786.
[32] Mercier, J. F., Salahpour, A., Angers, S., Breit, A., and Bouvier, M. (2002) Quantitative assessment of beta 1- and beta 2-adrenergic receptor homo- and heterodimerization by bioluminescence resonance energy transfer, *The Journal of biological chemistry 277*, 44925-44931.

Figure legends

Figure 1. Functional impacts of L124 mutations on the β2AR. a) Position of the mutated residue (orange) relative to the position of the PIF and NPxxY motifs (light and dark blue) on the β2AR (pdb:2Rh1). b) Cell surface expression of the receptors detected by ELISA. c-d) Concentration-response curves for the WT and mutant forms of β2AR (L124M/G/S) upon ISO and SALB stimulation for Gs activation (c) and β-arrestin recruitment (d) detected using BRET-based sensors. Data are shown as the mean ± SEM of 3-4 independent experiments.

Figure 2. Functional impacts of L124M mutation on β-arrestin recruitment for different ligands. a-c) Concentration-response curves for the WT (left) and L124M (right)-promoted β-arrestin recruitment upon stimulation with agonists (ISO, EPI, NE, SALB, SALM) (a), antagonists (ALP, LAB, PRO, XAM) (b) and inverse agonists (MET, TIM) (c). Data are shown as the mean ± SEM of 3-4 independent experiments.

Figure 3. Conformational impacts of L124 mutations on the β2AR. a) Effect of L124 mutations on the basal BRET level of the NY-β2AR conformational sensor. Statistical analysis was performed using ANOVA (* p-value < 0.05). b-c) Effects of the L124 mutations on ISO- (b) and SALB- (c)-promoted conformational changes of the NY-β2AR sensor. Data are shown as the mean ± SEM of 4 independent experiments.

Figure 4. Modeling of the impacts of L124 mutant forms compared to the WT receptor using the crystal structure for the carazolol-bound inactive β2AR state (PDB: 2RH1) and the BI-167107-β2AR-NB80 active complex (PDB: 4LDE). The PIF motif(P211-I121-F282) is shown

in orange and NPxxY (P323-N322-Y326) motif is shown light blue, while the mutated residue is shown in purple. Black lines represent predicted stabilizing interactions.

Figure 5. Schematic representation of proposed models. a) Different active conformations are stabilized by balanced and full agonists (green) and partial and biased agonists (orange). b) Balanced and biased ligands stabilize similar conformations but for different time lengths as represented by the equilibrium arrow and color intensity.

Figure S1. Effect of the full agonist isoproterenol and inverse agonist ICI 118,551 on cAMP production by the WT and L124G/S β2AR. cAMP was measured using the EPAC-BRET sensor[242]. The results show a clear effect of both agonist and inverse agonist on the WT receptors, while no significant effects are seen on L124G and L124S mutants. Statistical analysis was performed using ANOVA (* p-value < 0.05). Data are shown as mean ± SEM of 3 independent experiments.

Figure 1

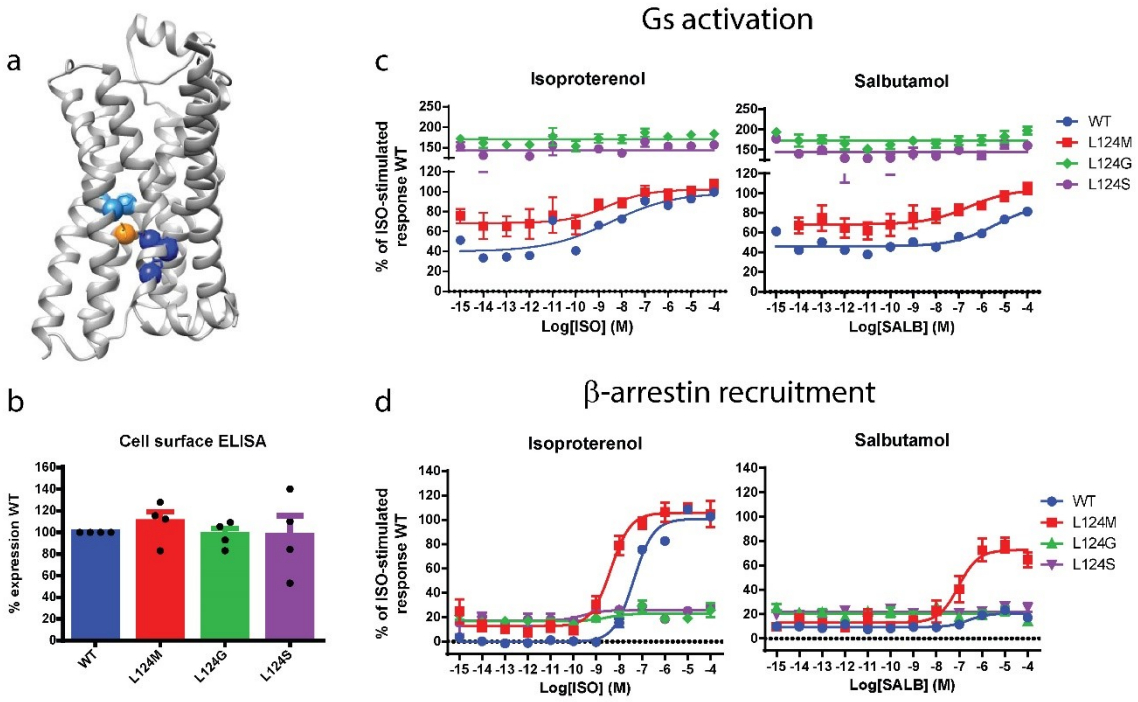
a
b
Cell surface ELISA
% expression WT
WT
L124M
L124G
L124S
c
Gs activation
Isoproterenol
Salbutamol
% of ISO-stimulated response WT
Log[ISO] (M)
Log[SALB] (M)
WT
L124M
L124G
L124S
d
β-arrestin recruitment
Isoproterenol
Salbutamol
% of ISO-stimulated response WT
Log[ISO] (M)
Log[SALB] (M)
WT
L124M
L124G
L124S

Figure 2

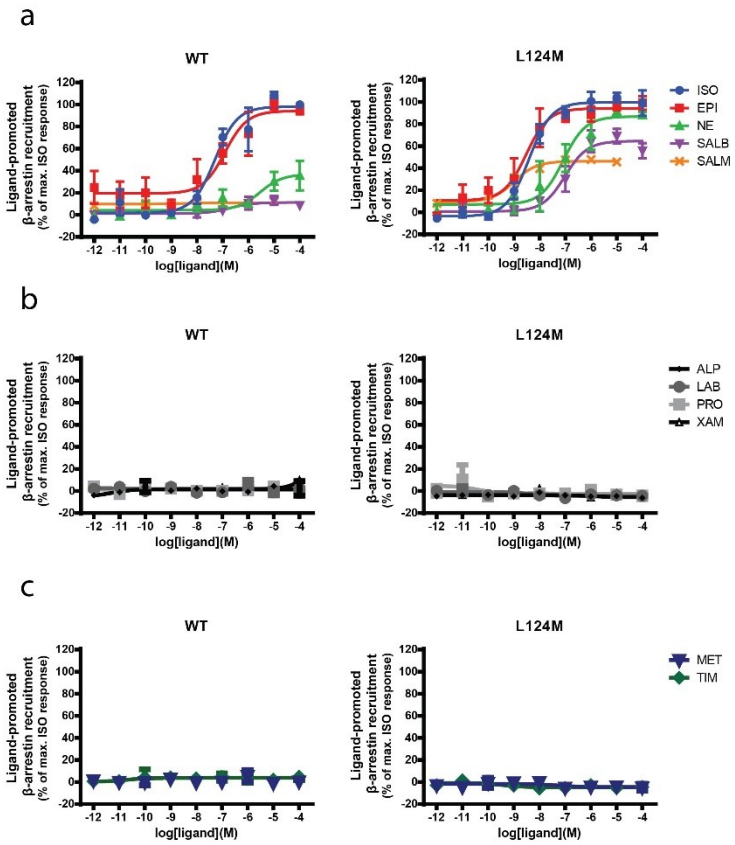
a
WT
L124M
Ligand-promoted β-arrestin recruitment (% of max. ISO response)
log[ligand](M)
ISO
EPI
NE
SALB
SALM
b
WT
L124M
ALP
LAB
PRO
XAM
c
WT
L124M
MET
TIM

Figure 3

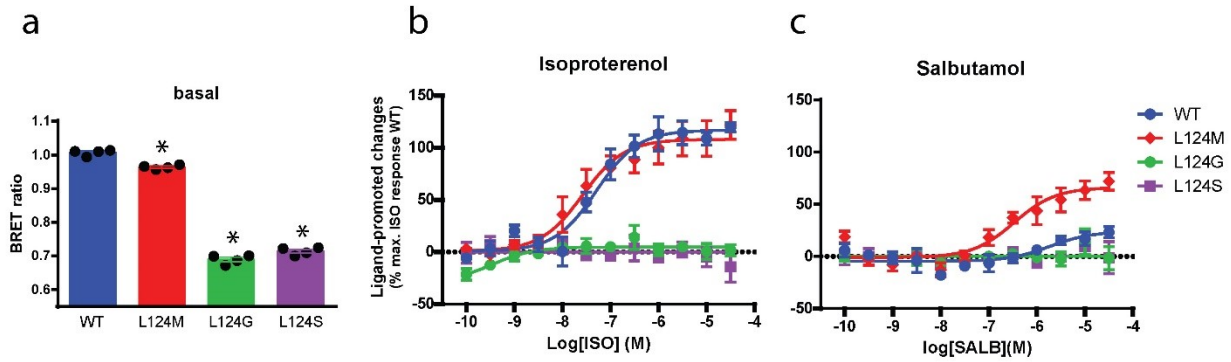
a
basal
BRET ratio
1.1
1.0
0.9
0.8
0.7
0.6
*
*
*
WT
L124M
L124G
L124S
b
Isoproterenol
Ligand-promoted changes (% max. ISO response WT)
150
100
50
0
-50
-10
-9
-8
-7
-6
-5
-4
Log[ISO] (M)
c
Salbutamol
150
100
50
0
-50
-10
-9
-8
-7
-6
-5
-4
log[SALB](M)
WT
L124M
L124G
L124S

Figure 4

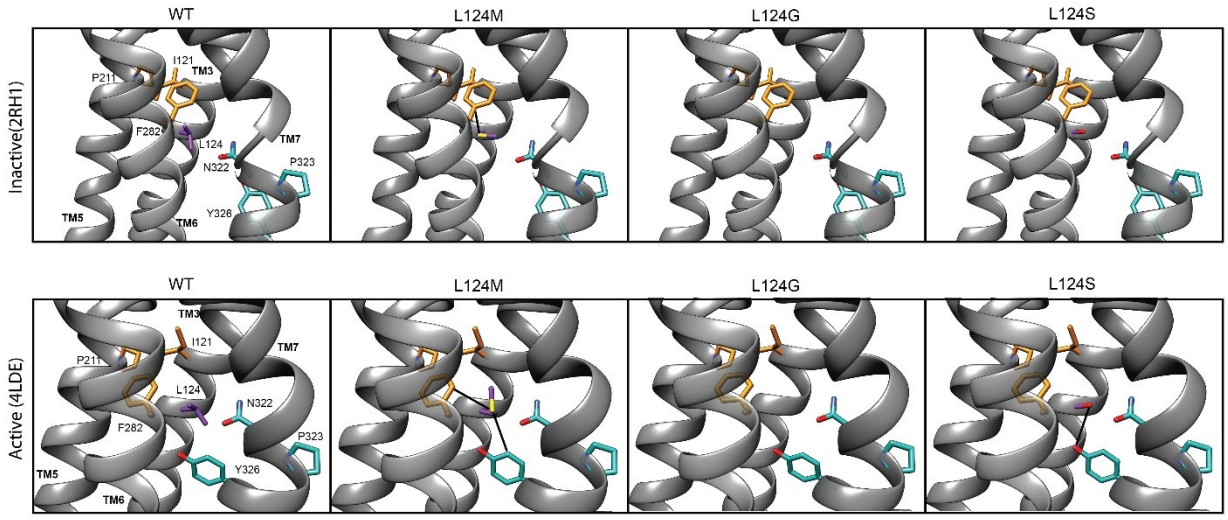
WT
L124M
L124G
L124S
Inactive(2RH1)
I121
TM3
P211
F282
L124
TM7
N322
P323
TM5
Y326
TM6
WT
L124M
L124G
L124S
Active (4LDE)
TM3
I121
TM7
P211
L124
N322
F282
P323
TM5
Y326
TM6

Figure 5

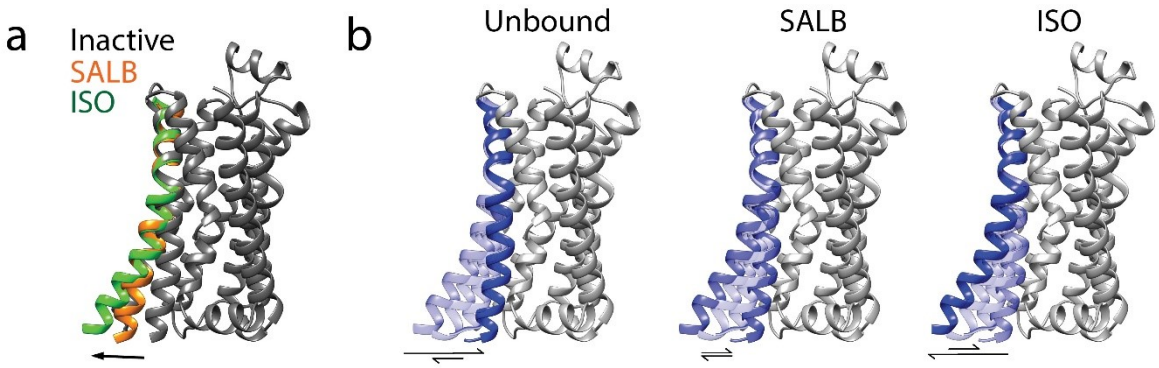

Figure S1

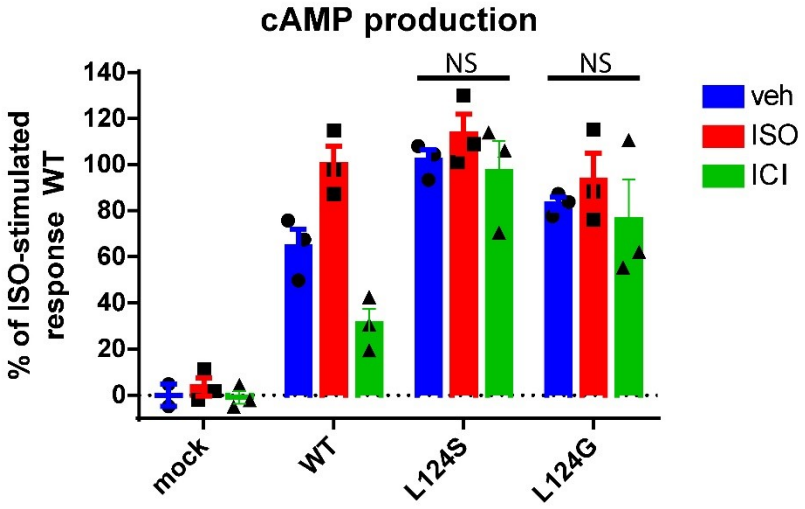
cAMP production
% of ISO-stimulated response WT
140
120
100
80
60
40
20
0
NS
NS
veh
ISO
ICI
mock
WT
L124S
L124G

Table S1. Gs activation of WT and mutant receptors upon isoproterenol and salbutamol stimulations. The data are derived from figure 1c[a].

	Isoproterenol			Salbutamol		
	Constitutive activity	Emax	pEC50	Constitutive activity	Emax	pEC50
WT	40 ± 5	99 ± 8	8.5 ± 0.6	46 ± 2	90 ± 6	5.4 ± 0.7
L124M	68 ± 5	102 ± 6	8.6 ±0.8	68 ± 3	104 ± 8	6.6 ± 0.9
L124G	171 ± 3	NR[b]	NR	174 ± 3	NR	NR
L124S	144 ± 3	NR	NR	144 ± 3	NR	NR

[a]Data represent mean ± SEM of three to four independent experiments expressed as % of the isoproterenol response for the WT β2AR

[b]NR. Stand for no response upon ligand stimulation

Table S2. β-arrestin recruitment by WT and mutant receptors upon isoproterenol and salbutamol stimulations. The data are derived from figure 1d[a].

	Isoproterenol			Salbutamol		
	Constitutive activity	Emax	pEC50	Constitutive activity	Emax	pEC50
WT	0 ± 1	100 ± 2	7.36 ± 0.06	9.3 ± 0.4	20.7 ± 0.8	6.6 ± 0.2
L124M	12 ± 2	106 ± 3	8.3 ±0.1	13 ± 2	73 ± 4	7.0 ± 0.2
L124G	17 ± 1	23 ± 2	8.5 ± 1	20.6 ± 0.9	NR[b]	NR
L124S	17 ± 2	26 ± 2	9.6 ± 1	22.0 ± 0.7	NR	NR

[a]Data represent mean ± SEM of three to four independent experiments expressed as % of the isoproterenol response for the WT β2AR

[b]NR. Stand for no response upon ligand stimulation

Discussion

L'objectif global de ma thèse fut de mieux comprendre les mécanismes moléculaires et structuraux de la sélectivité fonctionnelle du récepteur β2AR. Pour ce faire, j'ai tout d'abord développé un biocapteur de conformation du récepteur à base de BRET qui peut être utilisé directement dans des cellules. Avec ce biocapteur, j'ai pu développer une technique de multiplex avec d'autres biocapteurs à base de BRET possédant un donneur et un accepteur différent, mais aussi déterminer les changements conformationnels provenant de différents ligands ainsi que de différents effecteurs. De plus, à l'aide d'étude de mutagenèse, j'ai pu identifier des points de contact différentiels entre les agonistes non biaisés et biaisés ainsi qu'une région du récepteur qui régule différentiellement l'activation de Gs et le recrutement de la β-arrestine au récepteur. Tous ces résultats pris ensemble ont permis d'émettre de nouvelles hypothèses quant à l'activation du récepteur β2AR ainsi que de corréler celle-ci avec les composantes requises pour les ligands dans le contexte de la signalisation biaisée. Par conséquent, il sera possible d'utiliser les informations mécanistiques révélées dans ma thèse pour le design rationnel de ligand adrénergique avec des profils de sélectivité distincts.

Multiplex BRET

Une avancée technique que j'ai développée durant ma thèse est la possibilité de faire de combiner en parallèle deux essais BRET à partir de la même population de cellules. Pour ce faire, nous avons tiré avantage de la spécificité vis-à-vis des substrats ainsi que de la différence des spectres d'émission entre la Rluc et la Nluc (résultats des articles 1 et 4). En utilisant cette technique, nous avons essayé de corréler les résultats obtenus avec un biocapteur de conformation du récepteur et les voies de signalisation engager par celui-ci. Malheureusement,

les résultats n'ont pas été concluants dans le sens qu'aucune corrélation directe entre les changements de conformation détectés et une voie de signalisation n'a pu être établie. Cependant, les résultats ont pu déterminer que les changements conformationnels détectés par le biocapteur NY-β2AR peuvent intégrer différentes transductions de signal menant à une analyse plus complexe des changements de BRET détecté par le biocapteur de conformation.

L'avantage d'utiliser la spécificité de substrat entre la Nluc et la Rluc pour faire des essais en parallèle avec deux biocapteurs à base de BRET dans la même population de cellule permet probablement de réduire la variation due à différente condition pour des essais complètement indépendants. Cependant, il pourrait y avoir la possibilité d'améliorer la façon dont le multiplex est fait afin de tester simultanément deux essais BRET sur les mêmes cellules. Pour cela, il faudrait prendre avantage des protéines fluorescentes qui ont été modifiées pour avoir un stroke shift plus grand tel la cyOFP ou cyRFP[243,244]. De cette façon, il serait possible de combiner deux biocapteurs ayant le même donneur (Nluc par exemple), mais deux accepteurs différents (YFP et cyRFP par exemple) et ainsi enregistrer la luminescence à trois longueurs d'onde différentes. Une telle stratégie a déjà été utilisée avec la Rluc comme donneur et la eBFP2 et mAmetrine[242]. Cependant, la résolution spectrale en utilisant cette combinaison n'est pas optimale dû à la superposition des spectres d'émission de la Rluc et eBFP2 rendant la séparation spectrale difficile et une contamination élevée du signal de eBFP2 par Rluc.

Différente conformation du récepteur pour le biais.

Les résultats de l'article1 montrent deux modes d'activation du récepteur par les agonistes complets et non biaisés ainsi que les agonistes partiels et biaisés. Tout d'abord, les agonistes non biaisés, l'isoprotérénol (ISO) ainsi que l'épinéphrine (EPI) sont capable d'induire des

changements conformationnels détectables avec le biocapteur NY-β2AR tandis que les agonistes biaisés pour Gs, le salbutamol (SALB) et le salmétérol (SALM), n'engendrent pas de changements conformationnels détectables. Ce résultat suggère que deux ensembles de conformations différents sont stabilisés par ces deux ligands. Ce qui est tout à fait en accord avec les études de FRET en molécules uniques fait sur le récepteur β2AR qui montrent différentes ouvertures entre le TM6 et TM4 du récepteur entre l'EPI et le SALB et SALM[209]. De plus, dans l'article 2, la structure cristalline du complexe entre le récepteur et le SALM montre une différence majeure dans l'ouverture du TM6, point essentiel pour les interactions avec les protéines G ainsi que la boucle finger de la β-arrestin[186,191]. Cette différence d'ouverture pourrait partiellement expliquer le biais des composés SALB et SALM ainsi que leur nature d'agoniste partiel sur Gs. D'ailleurs, les résultats de l'article 1 ont démontré qu'en présence de surexpression de la protéine Gs, l'ISO stabilise des changements conformationnels plus grands. Ce résultat est en accord avec les données montrant un couplage allostérique faible entre le site de liaison du ligand et les changements conformationnels à l'interface cytoplasmique du récepteur[182-184]. De plus, ce résultat renforce le modèle d'activation actuellement accepté de l'activation des protéines G ou le ligand augmente l'oscillation des changements conformationnels, mais ne peut stabiliser la conformation active sans la présence de la protéine G[177]. Par contre, la stimulation par le ligand SALB en présence de Gs surexprimée, diminue le changement de BRET induit par Gs du biocapteur NY-β2AR. Ce résultat laisse suggérer au moins deux conformations capables d'activer la protéine G et différente entre l'agoniste complet ISO et partiel SALB. Ce qui implique que la conformation active menant à l'activation complète et l'activation partielle de Gs sont différentes. Cette hypothèse est en accord avec une étude de RMN sur le récepteur d'adénosine A2A qui a démontré que le peptide de Gs peut se lier à deux

conformations différentes du récepteur, mais a une préférence pour l'une des deux[176]. De plus, dans cette étude il a aussi été démontré que les agonistes complets stabilisent la conformation préférée par le peptide Gs, tandis que les agonistes partiel l'autre conformation capable de lier Gs.

Pour ce qui est de l'effet de l'arrestine sur les changements conformationnels suivant la stimulation à l'ISO, une potentialisation du changement de BRET est observée. Cette potentialisation peut suggérer deux hypothèses. Premièrement, le changement de conformation menant au couplage de l'arrestine est plus prononcé que celui menant à l'activation de la protéine Gs ce qui est peu probable considérant l'absence de différence dans l'ouverture du TM6 entre les structures de la rhodopsine en complexe entre l'arrestine visuelle et le peptide Gt[191]. Une autre hypothèse est que la surexpression de l'arrestine permet de maintenir le récepteur plus longtemps dans la conformation active ce qui mènerait à une plus grande quantité de récepteurs dans la conformation active à l'équilibre. Si l'on considère que les RCPGs sont des systèmes allostériques, la loi de réciprocité voudrait que le couplage à l'arrestine augmente le temps de résidence du ligand. À défaut d'avoir des données sur l'effet de l'arrestine sur le temps de résidence du ligand, des études de radioliaison qui ont démontré que le couplage de l'arrestine au récepteur augmentait l'affinité des agonistes au récepteur [163]. De plus, il a été démontré que le temps de résidence du ligand a un impact sur le recrutement de la β-arrestine[211]. Ces informations semblent appuyer la deuxième hypothèse que la potentialisation des changements de BRET par la surexpression de la β-arrestine provient d'une stabilisation des changements induits par l'ISO.

L'ensemble de ces résultats semble indiquer que les mécanismes structuraux entre l'activation de l'arrestine et Gs sont différents et incluent différents ensembles de conformations du récepteur ainsi que leur temps de résidence. C'est d'ailleurs ce que les résultats de l'article 3 et 5 laissent aussi suggérer en utilisant des ligands non biaisés et biaisés. Dans ces articles, l'impact de la mutagenèse démontre que le mécanisme de transduction de signal est différent entre l'ISO et le SALB et que dans le cas de stimulation à l'ISO différentes régions du récepteur sont responsables pour la stabilisation des formes actives menant à l'activation spécifique de diverses voies de signalisation.

Précouplage des protéines G au récepteur.

Une autre observation intéressante provenant de l'article 1 est le changement de conformation induit par les protéines G en absence de ligand. Ce changement de conformation pourrait être lié à deux phénomènes. Tout d'abord, il serait possible que ce soit lié à l'activité constitutive du récepteur. En augmentant la concentration de protéine G, un couplage au récepteur activé est alors favorisé et par conséquent la stabilisation de l'état actif augmentée. Cette hypothèse est alors appuyée par le résultat montrant que la surexpression de la β-arrestine n'affecte pas la conformation du biocapteur NY-β2AR en absence de ligand et que le récepteur β2AR ne possède pas d'activité constitutive pour le recrutement de la β-arrestine. De plus, le changement de conformation induit par la protéine G est observable à des niveaux endogènes tel que démontré par la différence des niveaux basaux de BRET entre les lignées parentales et déficientes en protéine G suggérant le précouplage de la protéine G au récepteur. Dans le cas de la β-arrestine où la surexpression de cette dernière n'a aucun effet sur l'ensemble de conformation du récepteur, il ne faudrait pas exclure la possibilité qu'une stabilisation de

certains changements conformationnels soit nécessaire pour induire le recrutement de la β-arrestine ce qui pourrait expliquer non seulement l'absence de recrutement constitutif de la β-arrestine, mais aussi le biais.

L'hypothèse alternative à l'activité constitutive pour expliquer le changement de conformation induit par la protéine G en absence de ligand serait la possibilité de préassemblage entre la protéine G lié au GDP et le récepteur inactif. Cette hypothèse pourrait expliquer certains concepts pharmacologiques, mais aussi certains résultats d'études de radioliaison. Tout d'abord, la surexpression de la protéine G permet de générer un site de haute affinité pour la liaison d'un agoniste au récepteur ce qui a mené au développement du modèle ternaire simple[162]. De plus, il a été démontré que l'affinité du carbachol, un agoniste du récepteur M2 muscarinique diminue en augmentant les concentrations de GTP dans les essais de radioliaison[163]. Cette étude suggère que le site de haute affinité est causé par l'interaction entre le récepteur et la protéine G liée au GDP, dans sa conformation inactive.

La possibilité de préassemblage entre la conformation inactive de la protéine G et le récepteur permet de réviser le modèle structural de l'activation de la protéine G par le récepteur. À partir de cette information, il est possible de proposer un modèle où la première étape de l'activation est le couplage entre la protéine G inactive et le récepteur non lié à l'agoniste. Cette interaction pourrait être médié par la conformation ouverte du récepteur tel que suggèrent la titration de Gs au biocapteur NY-β2AR. Cette interaction pourrait se faire via l'hélice α5 et la crevasse du récepteur formé par le déplacement du TM6, mais dans une conformation différente de l'hélice α5, qui ne pénètrerait pas aussi profondément dans la crevasse, mais resterait couplée au bas de celle-ci. Par la suite, la liaison du ligand permettrait d'engager l'hélice α5 dans la crevasse et

induire le changement conformationnel du domaine hélical observé dans la structure cristalline[186]. Ce changement de conformation du domaine hélical ainsi que les autres interactions décrites dans la section couplage au protéine G pourraient alors se produire pour activer la protéine G en favorisant la relâche du GDP et la liaison au GTP. Suivant ce changement de nucléotide, la protéine G se découplerait du récepteur ce qui expliquerait la baisse d'affinité de l'agoniste par une titration de GTP, en favorisant l'activation de la protéine G en absence du ligand et ainsi la découplé du récepteur résultant en la perte du site de haute affinité correspondant au complexe récepteur-protéine G lié au GDP. À l'inverse, pour ce qui est des agonistes inverses ou bien des antagonistes, un changement de BRET correspondant à un désassemblage est observé. Ce qui pourrait correspondre à la stabilisation de la forme inactive du récepteur par ces ligands qui favoriserait le désassemblage du complexe à haute affinité pour les agonistes correspondant au récepteur couplé à la protéine G inactive, lié au GDP, ce qui corroborerait les données de radioliaison montrant une baisse d'affinité pour les agonistes inverses en présence de protéine G surexprimé.

Bien qu'une certaine quantité de donné sont manquantes pour déterminer si le changement de conformation induit par la protéine G provient de la stabilisation de la conformation active du récepteur par la protéine G ou que le précouplage entre la protéine G et le récepteur inactif existe ainsi que de valider le modèle d'activation de la protéine G proposée plus haut, il est possible de prendre avantage de ce phénomène en considérant que le design de biocapteur de conformation est transposable sur d'autre récepteur[245]. Il serait possible de gagner plus d'information sur le couplage de récepteur orphelin, où aucun ligand n'a été identifié, en titrant différentes protéines G sur un biocapteur similaire. Ainsi, les protéines G interagissant avec le

récepteur devraient induire un changement conformationnel détectable par le biocapteur et ainsi permettre d'effectuer le profil de couplage des récepteurs orphelins.

Points de contact important pour le biais

Après avoir déterminé que le biais et l'agonisme partiel proviennent de différents ensembles de conformations stabilisés par les différents ligands, nous avons voulu déterminer quels sont les modes de liaison des différents ligands (résultat de l'article 2). Pour ce faire, nos collaborateurs ont résolu la structure du complexe entre le récepteur β2AR et l'agoniste partiel et biaisé SALM. À partir de cette structure, et sa comparaison avec celle du complexe entre le β2AR et l'EPI, nous avons pu identifier un réseau d'interaction polaire différent entre l'anneau catéchol retrouvé sur les agonistes complets et non biaisés, ISO et EPI, et l'anneau saligène retrouvé sur les agonistes partiel et biaisé SALB et SALM. La différence dans ce réseau d'interaction polaire a d'ailleurs été confirmée par une simulation MD ou la différence majeure provient de la perte de l'interaction entre le résidu $N293^{6.55}$ et l'EPI. Afin d'évaluer les impacts de ce réseau sur la fonctionnalité du récepteur β2AR, le résidu $N293^{6.55}$ et $S204^{5.43}$ ont été mutés. Le résidu $S204^{5.43}$ forme une interaction avec le résidu $N293^{6.55}$ permettant la propagation du réseau d'interaction polaire entre le ligand et le récepteur. L'impact de ces mutations est intéressant, puisqu'ils n'ont pas d'effet suivant la stimulation par l'agoniste partiel et biaisé SALM suggérant une absence d'interaction entre ce ligand et le récepteur. Cependant, les mutations en position $S204^{5.43}$ et $N293^{6.55}$ affectent la capacité du récepteur à activer Gs et à recruter la β-arrestine suivant une stimulation à l'ISO suggérant que ces interactions sont présentes lorsque le ligand possède le pharmacophore catéchol, mais pas lorsque le ligand possède le pharmacophore saligène. De plus, il est intéressant de constater que la capacité du récepteur à activer Gs est réduite de 100%

à 80% de la réponse obtenue avec le récepteur de type sauvage. Puisque cette valeur correspond à la réponse obtenue suite à la stimulation par le SALM, cela renforce l'hypothèse que la différence observée entre ces deux ligands provient du groupement catéchol versus saligène et non du groupement amine de ces molécules.

Afin de confirmer le rôle des groupements catéchol et saligène dans la différence de profil de signalisation suivant la stimulation par ces ligands, la capacité de trois différents ligands, l'ISO, le SALB et le coltérol (COLT), à activer Gs et recruter la β-arrestine a été testée. COLT est un ligand adrénergique intéressant pour tester cette hypothèse, puisqu'il possède le groupement catéchol, mais le même groupement amine que le SALB formant ainsi un hybride entre l'ISO et le SALB. Les résultats démontrent que le COLT possède un profil de signalisation identique à celui de l'ISO (voir figure 23), confirmant ainsi l'importance du réseau d'interaction entre le ligand et le résidu $N293^{6.55}$ pour l'activation complète de Gs et le recrutement de la β-arrestine.

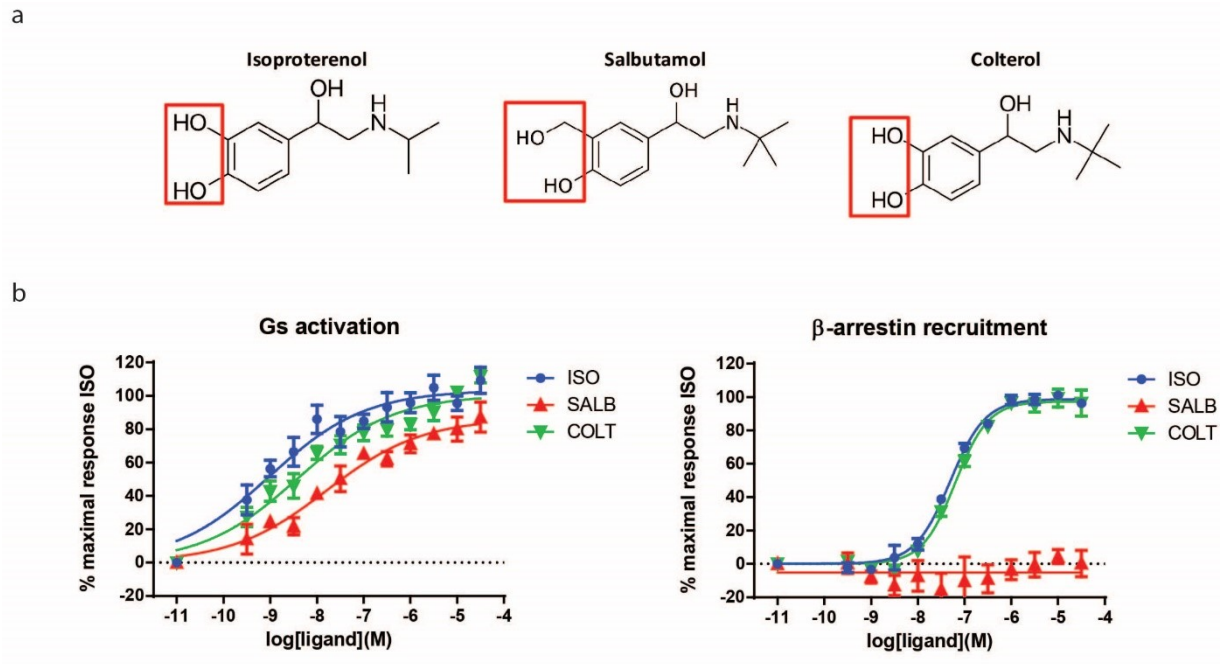

Figure 23. Profil de signalisation de l'isoprotérénol, salbutamol et coltérol. A) structure chimique des composés. Le rectangle rouge représente la différence entre le groupement catéchol et saligène. B) évaluation de la capacité des ligands à activer la protéine Gs et recruter la β-arrestine à l'aide des biocapteurs BRET Gαs-117-RlucUU/Gβ1/Gγ1-GFP10 et β-arr2-RlucII/rGFP-CAAX.

Un mécanisme structural qui expliquerait la différence de signalisation engendrée par ce réseau d'interaction polaire serait une différence de contraction de la poche de liaison du ligand. Les résidus S204$^{5.43}$ et N293$^{6.55}$ sont situés sur les TM5 et TM6 respectivement. Or, une caractéristique commune lors de l'activation des RCPGs est la contraction de la partie extracellulaire de ces deux domaines transmembranaires refermant ainsi la poche de liaison du ligand[246]. Cette contraction pourrait en effet être stabilisée par le réseau d'interaction polaire entre le ligand et le récepteur. Cette contraction permettrait d'induire les changements conformationnels des résidus F$^{6.40}$ et I$^{3.40}$ du motif PIF/connecteur, qui sont liés à l'ouverture du TM6 au niveau cytoplasmique, et ainsi induire l'activation du récepteur. Cette hypothèse n'est malheureusement pas supportée les structures des complexes EPI-β2AR et SALM-β2AR. En

effet, une superposition du motif dans les deux structures est observée. Cependant, il ne faut pas exclure la possibilité que la conformation observée pour le motif PIF/connecteur dans les deux structures cristallines soit due au processus de cristallisation qui force la structure à adopter la conformation la plus stable d'un puits énergétique précis. Par conséquent, il est possible que la structure obtenue dans le complexe SALM-β2AR soit en réalité un intermédiaire et que la différence de transduction de signal à partir de la poche de liaison du ligand passe bel et bien par une différence de contraction de la poche de liaison du ligand et que cela affecte le motif PIF/connecteur. Par contre, cette différence, au lieu d'être causée par une conformation complètement différente, pourrait être causée par une différence sur le temps de stabilisation de la conformation active et que la différence d'ouverture du TM6 représente un état intermédiaire de la cristallisation stabilisé par un nanobody différent que celui utilisé pour le complexe EPI-β2AR. En absence de structure du complexe SALM-β2AR-Gs, il est impossible de conclure que la différence d'ouverture représente une conformation intermédiaire. Cependant, cette hypothèse semble encore une foi corréler avec les données démontrant que le temps de résidence du ligand est important pour sur le recrutement de la β-arrestine[211]. Par conséquent, si un ligand possède une capacité moins grande à stabiliser une conformation active, l'effet serait similaire à un temps de résidence moins long d'un ligand permettant une meilleure stabilisation à partir de la poche de liaison.

Synchronisation des microswitchs pour la transduction de signal

L'hypothèse générée par la différence du mode de liaison ainsi que la différence entre la transduction de signal suivant la stimulation par l'ISO et le SALM laisse suggérer que la façon dont le signal est transmis par les motifs conservés dans le récepteur aussi nommé microswitchs

pourrait mener à une activation différentielle des différentes voies de signalisation d'un récepteur. Afin d'étudier cette question nous avons voulu vérifier l'impact de mutations de résidus conservés dans les RCPGs de classe A dans le contexte de la sélectivité fonctionnelle. Pour ce faire, nous avons pris avantage de mutants identifiés dans l'article 5. Ces mutations affectent spécifiquement certaines voies de signalisation suivant une stimulation à l'ISO, mais leurs impacts suivant une stimulation par des ligands biaisés n'étaient pas encore connus. Une position intéressante pour expliquer la propagation du mécanisme d'activation de la poche de liaison du ligand jusqu'au motif PIF/connecteur est le résidu L124$^{3.43}$ qui est situé entre le motif connecteur et le motif NPxxY. La position de ce résidu ainsi que sa conservation à travers des RCPGs de classe A (73%) suggèrent un rôle potentiel dans l'activation du récepteur via des interactions avec les deux motifs. Afin de tester cette hypothèse, nous avons effectué trois mutations sur ce résidu (L124M, L124G et L124S), puis testé l'impact de ces mutations sur la capacité du récepteur à activer Gs et à recruter la β-arrestine suivant une stimulation par différents ligands (article 3). Les résultats montrent que les substitutions L124G et L124S rendent le récepteur constitutivement actif pour Gs, et non répondant aux agonistes. De plus, le recrutement de la β-arrestine par ces mutants suite à la stimulation par l'ISO est complètement perdu. En contraste, la substitution L124M augmente peu l'activité constitutive du récepteur pour Gs, mais potentialise le recrutement de la β-arrestine suite à la stimulation par l'ISO et l'EPI et un gain de fonction est observé suite à une stimulation par le SALB et SALM. Ces données suggèrent que cette région du récepteur pourrait contrôler la transduction de signal différentiellement pour Gs et β-arrestine. De plus, les résultats avec le biocapteur de conformation NY-β2AR de ces mutants démontrent clairement un changement du BRET basal pour ces mutants en comparaison avec le récepteur de type sauvage corrélant avec l'activité

constitutive de Gs, mais aussi un gain dans les changements conformationnels suivants la stimulation par le SALB corrélant avec le gain de fonction pour le recrutement de la β-arrestine. Ces résultats suggèrent que le mécanisme structural pour l'activation de Gs et le recrutement de la β-arrestine sont différent et relèvent de changements structuraux différents. Afin de mieux comprendre les détails structuraux menant à l'activation différentielle d'une voie de signalisation versus une autre, la modélisation des mutations sur les structures inactives et actives du récepteur a été effectuée. Les résultats montrent que les mutations L124G et L124S induisent une perte d'interactions avec les motifs PIF/connecteur et NPxxY tandis que la mutation L124 provoque un gain d'interactions avec les deux motifs. Ceci suggère que le rôle du résidu L124 est de transmettre le signal du PIF au NPxxY. De cette façon en combinant les résultats de l'article 2 et 3 de la thèse, il est possible de lier le mode de liaison du ligand et son interaction avec le réseau polaire formé par les résidus S204 et N293, la contraction de la poche de liaison du ligand ainsi que le mouvement du motif PIF/connecteur au motif NPxxY expliquant ainsi la différence de transduction de signal entre les agonistes non biaisés et biaisés de la poche de liaison jusqu'au motif NPxxY. Ceci permet aussi de proposer un deuxième mécanisme pour le recrutement de la β-arrestine qui est différent du mécanisme proposé plus haut pour l'activation de Gs.

À partir des résultats de l'article 1,2 et 3, il est possible de conclure que le mécanisme d'activation de l'arrestine est fondamentalement différent de celui de la protéine G. Dans un premier temps, l'absence de précouplage de l'arrestine au récepteur β2AR semble indiquée qu'au contraire de ce qui est observé pour la protéine G, les changements conformationnels requis pour le recrutement de la β-arrestine doivent provenir principalement du ligand et non du de l'arrestine ce qui expliquerait pourquoi un ligand qui n'engage pas de changement significatif

dans le biocapteur NY-β2AR ne permet pas le recrutement de la β-arrestine, mais permet quand même l'activation de la protéine G. Ce qui laisse suggérer que pour avoir le recrutement de la β-arrestine le ligand doit par lui-même stabiliser la conformation active du récepteur durant une période de temps assez long pour permettre le couplage de l'arrestine et que cette stabilisation passerait par la contraction de la poche de liaison du ligand, le motif PIF/connecteur et le motif NPxxY. Si un ligand ne permet pas cette stabilisation pour une période de temps assez long dû à une absence d'interaction permettant la contraction de la poche de liaison par exemple en absence de réseau d'interaction polaire entre le ligand et le récepteur, le recrutement de l'arrestine ne peut se faire. De plus, ce modèle d'activation pour l'arrestine pourrait expliquer pourquoi le temps de résidence du ligand affecte le recrutement de l'arrestine et non l'activation de la protéine G[211] ainsi que l'absence de différence majeure entre la structure de la rhodopsine en complexe avec le peptide Gt et l'arrestine visuelle[191] en plus d'être cohérent avec le modèle de sélection de conformation comme certaines données de spectroscopie RMN suggère[176]. Le modèle de sélection de conformation est analogue au modèle probabiliste, puisque le ligand ne va pas induire de changement de conformation majeur, mais plutôt lier une conformation favorable la stabilisant et ainsi augmentant la durée de vie de cette conformation.

Mécanisme proposé pour le biais de signalisation observé pour le β2AR

Les résultats de cette thèse ainsi que leurs interprétations permettent de proposer des modèles d'activations différents pour les protéines G et l'arrestine. Non seulement, les mécanismes structuraux menant à l'activation d'une ou l'autre des voies de signalisation semblent différent, mais peuvent expliquer le biais d'une manière différente et permettent de proposer un modèle mécanistique pour le biais.

Ce mécanisme proposerait que l'activation de la protéine G se fasse principalement via le précouplage de la protéine G au récepteur via sa conformation inactive liée au GDP. Cette interaction se ferait sans l'engagement de l'hélice α5 dans le récepteur. Suivant la liaison du ligand, le récepteur engagerait l'hélice α5 au cœur de la crevasse formé par l'ouverture du TM6 et mènerait aux changements conformationnels requis pour l'échange du GDP au GTP, incluant le mouvement du domaine hélical. Par conséquent, les changements conformationnels du récepteur menant à l'ouverture du TM6 seraient principalement initiés par la protéine G ce qui expliquerait pourquoi la cristallisation des complexes entre un agoniste et le récepteur en absence d'une protéine stabilisant la conformation active mène à la cristallisation de la structure inactive du récepteur[182]. Un ligand qui permet une meilleure stabilisation de l'ouverture du TM6 permettrait aussi un meilleur couplage avec la protéine G lié au GDP via l'hélice α5 en réduisant les changements conformationnels du récepteur que la protéine G doit initier et par conséquent pourrait expliquer pourquoi la différence d'ouverture du TM6 corrèle avec l'efficacité des ligands[209,245,247,248]. Un ligand qui favoriserait le découplage de la protéine G aurait par conséquent l'effet inverse expliquant ainsi l'agonisme inverse au niveau mécanistique. Par conséquent, les ligands possédant une capacité limitée à stabiliser l'ouverture du TM6 peuvent quand même activer la protéine G, mais avec une efficacité moindre.

Pour ce qui est du recrutement de la β-arrestine, le ligand doit impérativement stabiliser à lui seul l'ouverture du TM6 dû à l'absence de précouplage avec l'arrestine. De plus, cette stabilisation doit être assez longue pour permettre à l'arrestine d'interagir avec le récepteur. Une telle stabilisation impliquerait : une contraction de la poche de liaison du ligand, un changement conformationnel du motif PIF/connecteur qui est transmis au motif NPxxY via le résidu L124. Ce mécanisme expliquerait aussi l'absence de différence majeure de conformation sur les

complexes de la rhodopsine et l'importance de du temps de résidence du ligand[191,211]. Par conséquent, un ligand qui stabilise la conformation inactive du récepteur serait un antagoniste tout comme un ligand qui ne permet pas une stabilisation prolongée de la conformation active. Un agoniste pour cette voie de signalisation doit stabiliser la conformation active du récepteur par lui-même pour une période de temps suffisante. Ce modèle mécanistique pour le biais permet l'ajout de la cinétique des conformations en plus de changements conformationnels différents pour expliquer le biais entre la protéine G et l'arrestine. De plus, ce modèle implique que l'étude des complexes récepteurs-protéine G (dans différentes conformations) ainsi que récepteur-arrestine devrait être étudier plus en détail pour mieux comprendre comment la transduction de signal permet une activation différentielle menant au biais avec une plus grande précision.

Conclusion

En conclusion, cette thèse apporte des informations sur les différences mécanistiques entre l'activation de Gs et le recrutement de la β-arrestine dans le contexte de la sélectivité fonctionnel et l'agonisme partiel sur Gs. Ces informations supplémentaires ont été apportées grâce au développement d'un biocapteur de conformation du récepteur β2AR qui a permis de déterminer que les ligands non biaisés et biaisés n'activent pas le récepteur de la même façon et que dans le cas de l'activation de Gs le précouplage de cette dernière joue un rôle primordial. L'identification d'éléments structuraux importants pour la stabilisation de la forme active du récepteur a aussi été effectuée à l'aide d'étude de mutagenèse et de l'évaluation de leur impact sur la fonction et les changements conformationnels du récepteur. Ces régions permettent de mettre en évidence le lien entre un réseau d'interactions polaires dans la poche de liaison du

ligand et la contraction de celle-ci. Ce qui permettrait la transduction du signal vers le motif PIF/connecteur qui serait transmis vers le motif NPxxY en parti par le résidu L124M. De plus, un modèle pour la sélectivité fonctionnelle du ligand a été proposé où la différence entre l'état de précouplage d'un effecteur influencerait les mécanismes structuraux requis pour son activation. Non seulement ce modèle intègre l'idée de différentes conformations du récepteur, mais aussi le temps de résidence dans ces conformations pour expliquer le biais. Plusieurs recherches seront nécessaires pour affirmer ou infirmer ce modèle. Cependant, il est clair que l'étude des complexes entre le récepteur et les différents effecteurs ainsi que de la cinétique de ceux-ci et du récepteur seul va apporter une meilleure compréhension des détails mécanistique de l'activation des RCPGs. Par conséquent, les travaux présentés dans cette thèse pourraient bénéficier d'étude future en Cryo-EM de différent complexe récepteur protéine G dans différente conformation ainsi que du récepteur et de la β-arrestine. De plus, des études de spectroscopie en RMN pourraient complémenter l'aspect de la cinétique du modèle proposé. Finalement, il serait intéressant d'évaluer les composantes structurales reliées à l'activation de différentes protéines G par le même récepteur.

Reference

1 Audet, M. & Bouvier, M. Insights into signaling from the beta2-adrenergic receptor structure. *Nature chemical biology* **4**, 397-403, doi:10.1038/nchembio.97 (2008).

2 Stoy, H. & Gurevich, V. V. How genetic errors in GPCRs affect their function: Possible therapeutic strategies. *Genes Dis* **2**, 108-132, doi:10.1016/j.gendis.2015.02.005 (2015).

3 Caron, M. G., Srinivasan, Y., Pitha, J., Kociolek, K. & Lefkowitz, R. J. Affinity chromatography of the beta-adrenergic receptor. *The Journal of biological chemistry* **254**, 2923-2927 (1979).

4 Shorr, R. G., Lefkowitz, R. J. & Caron, M. G. Purification of the beta-adrenergic receptor. Identification of the hormone binding subunit. *The Journal of biological chemistry* **256**, 5820-5826 (1981).

5 Benovic, J. L., Shorr, R. G., Caron, M. G. & Lefkowitz, R. J. The mammalian beta 2-adrenergic receptor: purification and characterization. *Biochemistry* **23**, 4510-4518 (1984).

6 Lomasney, J. W. *et al.* Mammalian alpha 1-adrenergic receptor. Purification and characterization of the native receptor ligand binding subunit. *The Journal of biological chemistry* **261**, 7710-7716 (1986).

7 Regan, J. W., Nakata, H., DeMarinis, R. M., Caron, M. G. & Lefkowitz, R. J. Purification and characterization of the human platelet alpha 2-adrenergic receptor. *The Journal of biological chemistry* **261**, 3894-3900 (1986).

8 Dixon, R. A. *et al.* Cloning of the gene and cDNA for mammalian beta-adrenergic receptor and homology with rhodopsin. *Nature* **321**, 75-79, doi:10.1038/321075a0 (1986).

9 Kobilka, B. K. *et al.* Delineation of the intronless nature of the genes for the human and hamster beta 2-adrenergic receptor and their putative promoter regions. *The Journal of biological chemistry* **262**, 7321-7327 (1987).

10 Kobilka, B. K. *et al.* Cloning, sequencing, and expression of the gene coding for the human platelet alpha 2-adrenergic receptor. *Science* **238**, 650-656 (1987).

11 Sunahara, R. K. *et al.* Human dopamine D1 receptor encoded by an intronless gene on chromosome 5. *Nature* **347**, 80-83, doi:10.1038/347080a0 (1990).

12 Bouvier, M. *et al.* Expression of a human cDNA encoding the beta 2-adrenergic receptor in Chinese hamster fibroblasts (CHW): functionality and regulation of the expressed receptors. *Molecular pharmacology* **33**, 133-139 (1988).

13 Kolakowski, L. F., Jr. GCRDb: a G-protein-coupled receptor database. *Receptors Channels* **2**, 1-7 (1994).

14 Munk, C. *et al.* GPCRdb: the G protein-coupled receptor database - an introduction. *Br J Pharmacol* **173**, 2195-2207, doi:10.1111/bph.13509 (2016).

15 Schulte, G. & Wright, S. C. Frizzleds as GPCRs - More Conventional Than We Thought! *Trends in pharmacological sciences* **39**, 828-842, doi:10.1016/j.tips.2018.07.001 (2018).

16 Schioth, H. B. & Fredriksson, R. The GRAFS classification system of G-protein coupled receptors in comparative perspective. *Gen Comp Endocrinol* **142**, 94-101, doi:10.1016/j.ygcen.2004.12.018 (2005).

17 Ross, E. M. & Gilman, A. G. Resolution of Some Components of Adenylate-Cyclase Necessary for Catalytic Activity. *Journal of Biological Chemistry* **252**, 6966-6969 (1977).

18 Ross, E. M., Maguire, M. E., Sturgill, T. W., Biltonen, R. L. & Gilman, A. G. Relationship between the beta-adrenergic receptor and adenylate cyclase. *The Journal of biological chemistry* **252**, 5761-5775 (1977).

19 Tobin, A. B. G-protein-coupled receptor phosphorylation: where, when and by whom. *Brit J Pharmacol* **153**, S167-S176, doi:10.1038/sj.bjp.0707662 (2008).
20 Smith, F. D., Samelson, B. K. & Scott, J. D. Discovery of cellular substrates for protein kinase A using a peptide array screening protocol. *Biochemical Journal* **438**, 103-110, doi:10.1042/Bj20110720 (2011).
21 Cheng, X. D., Ji, Z. Y., Tsalkova, T. & Mei, F. Epac and PKA: a tale of two intracellular cAMP receptors. *Acta Bioch Bioph Sin* **40**, 651-662, doi:10.1111/j.1745-7270.2008.00438.x (2008).
22 Hildebrandt, J. D. *et al.* Stimulation and inhibition of adenylyl cyclases mediated by distinct regulatory proteins. *Nature* **302**, 706-709 (1983).
23 Taussig, R., Iniguez-Lluhi, J. A. & Gilman, A. G. Inhibition of adenylyl cyclase by Gi alpha. *Science* **261**, 218-221 (1993).
24 Ridge, K. D., Abdulaev, N. G., Sousa, M. & Palczewski, K. Phototransduction: crystal clear. *Trends in biochemical sciences* **28**, 479-487, doi:10.1016/S0968-0004(03)00172-5 (2003).
25 Sanematsu, K., Yoshida, R., Shigemura, N. & Ninomiya, Y. Structure, function, and signaling of taste G-protein-coupled receptors. *Curr Pharm Biotechnol* **15**, 951-961 (2014).
26 Kinnamon, S. C. Taste receptor signalling - from tongues to lungs. *Acta Physiol (Oxf)* **204**, 158-168, doi:10.1111/j.1748-1716.2011.02308.x (2012).
27 Morris, A. J. & Scarlata, S. Regulation of effectors by G-protein alpha- and beta gamma-subunits. Recent insights from studies of the phospholipase c-beta isoenzymes. *Biochem Pharmacol* **54**, 429-435 (1997).
28 Siehler, S. Regulation of RhoGEF proteins by G12/13-coupled receptors. *Br J Pharmacol* **158**, 41-49, doi:10.1111/j.1476-5381.2009.00121.x (2009).
29 Suzuki, N., Hajicek, N. & Kozasa, T. Regulation and physiological functions of G12/13-mediated signaling pathways. *Neurosignals* **17**, 55-70, doi:10.1159/000186690 (2009).
30 Downes, G. B. & Gautam, N. The G protein subunit gene families. *Genomics* **62**, 544-552, doi:10.1006/geno.1999.5992 (1999).
31 Neer, E. J. Heterotrimeric G proteins: organizers of transmembrane signals. *Cell* **80**, 249-257 (1995).
32 Yokogawa, M., Osawa, M., Takeuchi, K., Mase, Y. & Shimada, I. NMR analyses of the Gbetagamma binding and conformational rearrangements of the cytoplasmic pore of G protein-activated inwardly rectifying potassium channel 1 (GIRK1). *The Journal of biological chemistry* **286**, 2215-2223, doi:10.1074/jbc.M110.160754 (2011).
33 De Waard, M., Hering, J., Weiss, N. & Feltz, A. How do G proteins directly control neuronal Ca2+ channel function? *Trends in pharmacological sciences* **26**, 427-436, doi:10.1016/j.tips.2005.06.008 (2005).
34 Logothetis, D. E., Kurachi, Y., Galper, J., Neer, E. J. & Clapham, D. E. The beta gamma subunits of GTP-binding proteins activate the muscarinic K+ channel in heart. *Nature* **325**, 321-326, doi:10.1038/325321a0 (1987).
35 Rozengurt, E. Signal transduction pathways in the mitogenic response to G protein-coupled neuropeptide receptor agonists. *J Cell Physiol* **177**, 507-517, doi:10.1002/(SICI)1097-4652(199812)177:4<507::AID-JCP2>3.0.CO;2-K (1998).
36 Maier, U. *et al.* Gbeta 5gamma 2 is a highly selective activator of phospholipid-dependent enzymes. *The Journal of biological chemistry* **275**, 13746-13754 (2000).
37 Diel, S., Klass, K., Wittig, B. & Kleuss, C. Gbetagamma activation site in adenylyl cyclase type II. Adenylyl cyclase type III is inhibited by Gbetagamma. *The Journal of biological chemistry* **281**, 288-294, doi:10.1074/jbc.M511045200 (2006).

38 Gurevich, E. V., Tesmer, J. J., Mushegian, A. & Gurevich, V. V. G protein-coupled receptor kinases: more than just kinases and not only for GPCRs. *Pharmacology & therapeutics* **133**, 40-69, doi:10.1016/j.pharmthera.2011.08.001 (2012).
39 Ferguson, S. S. Evolving concepts in G protein-coupled receptor endocytosis: the role in receptor desensitization and signaling. *Pharmacol Rev* **53**, 1-24 (2001).
40 Perroy, J., Adam, L., Qanbar, R., Chenier, S. & Bouvier, M. Phosphorylation-independent desensitization of GABA(B) receptor by GRK4. *EMBO J* **22**, 3816-3824, doi:10.1093/emboj/cdg383 (2003).
41 Tesmer, V. M., Kawano, T., Shankaranarayanan, A., Kozasa, T. & Tesmer, J. J. Snapshot of activated G proteins at the membrane: the Galphaq-GRK2-Gbetagamma complex. *Science* **310**, 1686-1690, doi:10.1126/science.1118890 (2005).
42 Lohse, M. J., Lefkowitz, R. J., Caron, M. G. & Benovic, J. L. Inhibition of beta-adrenergic receptor kinase prevents rapid homologous desensitization of beta 2-adrenergic receptors. *Proceedings of the National Academy of Sciences of the United States of America* **86**, 3011-3015 (1989).
43 Sallese, M., Mariggio, S., D'Urbano, E., Iacovelli, L. & De Blasi, A. Selective regulation of Gq signaling by G protein-coupled receptor kinase 2: direct interaction of kinase N terminus with activated galphaq. *Molecular pharmacology* **57**, 826-831 (2000).
44 Breton, B., Lagace, M. & Bouvier, M. Combining resonance energy transfer methods reveals a complex between the alpha2A-adrenergic receptor, Galphai1beta1gamma2, and GRK2. *FASEB J* **24**, 4733-4743, doi:10.1096/fj.10-164061 (2010).
45 Inglese, J., Koch, W. J., Caron, M. G. & Lefkowitz, R. J. Isoprenylation in regulation of signal transduction by G-protein-coupled receptor kinases. *Nature* **359**, 147-150, doi:10.1038/359147a0 (1992).
46 Pitcher, J. A., Touhara, K., Payne, E. S. & Lefkowitz, R. J. Pleckstrin homology domain-mediated membrane association and activation of the beta-adrenergic receptor kinase requires coordinate interaction with G beta gamma subunits and lipid. *The Journal of biological chemistry* **270**, 11707-11710 (1995).
47 Pack, T. F., Orlen, M. I., Ray, C., Peterson, S. M. & Caron, M. G. The dopamine D2 receptor can directly recruit and activate GRK2 without G protein activation. *The Journal of biological chemistry* **293**, 6161-6171, doi:10.1074/jbc.RA117.001300 (2018).
48 Premont, R. T. *et al.* Characterization of the G protein-coupled receptor kinase GRK4. Identification of four splice variants. *The Journal of biological chemistry* **271**, 6403-6410 (1996).
49 Stoffel, R. H., Randall, R. R., Premont, R. T., Lefkowitz, R. J. & Inglese, J. Palmitoylation of G protein-coupled receptor kinase, GRK6. Lipid modification diversity in the GRK family. *The Journal of biological chemistry* **269**, 27791-27794 (1994).
50 Premont, R. T., Koch, W. J., Inglese, J. & Lefkowitz, R. J. Identification, purification, and characterization of GRK5, a member of the family of G protein-coupled receptor kinases. *The Journal of biological chemistry* **269**, 6832-6841 (1994).
51 Cong, M. *et al.* Regulation of membrane targeting of the G protein-coupled receptor kinase 2 by protein kinase A and its anchoring protein AKAP79. *The Journal of biological chemistry* **276**, 15192-15199, doi:10.1074/jbc.M009130200 (2001).
52 Elorza, A., Sarnago, S. & Mayor, F., Jr. Agonist-dependent modulation of G protein-coupled receptor kinase 2 by mitogen-activated protein kinases. *Molecular pharmacology* **57**, 778-783 (2000).

53 Paradis, J. S. *et al.* Receptor sequestration in response to beta-arrestin-2 phosphorylation by ERK1/2 governs steady-state levels of GPCR cell-surface expression. *Proceedings of the National Academy of Sciences of the United States of America* **112**, E5160-5168, doi:10.1073/pnas.1508836112 (2015).
54 Pronin, A. N. & Benovic, J. L. Regulation of the G protein-coupled receptor kinase GRK5 by protein kinase C. *The Journal of biological chemistry* **272**, 3806-3812 (1997).
55 Sarnago, S., Elorza, A. & Mayor, F., Jr. Agonist-dependent phosphorylation of the G protein-coupled receptor kinase 2 (GRK2) by Src tyrosine kinase. *The Journal of biological chemistry* **274**, 34411-34416 (1999).
56 Penela, P., Rivas, V., Salcedo, A. & Mayor, F., Jr. G protein-coupled receptor kinase 2 (GRK2) modulation and cell cycle progression. *Proceedings of the National Academy of Sciences of the United States of America* **107**, 1118-1123, doi:10.1073/pnas.0905778107 (2010).
57 Salcedo, A., Mayor, F., Jr. & Penela, P. Mdm2 is involved in the ubiquitination and degradation of G-protein-coupled receptor kinase 2. *EMBO J* **25**, 4752-4762, doi:10.1038/sj.emboj.7601351 (2006).
58 Wilden, U., Hall, S. W. & Kuhn, H. Phosphodiesterase activation by photoexcited rhodopsin is quenched when rhodopsin is phosphorylated and binds the intrinsic 48-kDa protein of rod outer segments. *Proceedings of the National Academy of Sciences of the United States of America* **83**, 1174-1178 (1986).
59 Lohse, M. J., Benovic, J. L., Codina, J., Caron, M. G. & Lefkowitz, R. J. beta-Arrestin: a protein that regulates beta-adrenergic receptor function. *Science* **248**, 1547-1550 (1990).
60 DeWire, S. M., Ahn, S., Lefkowitz, R. J. & Shenoy, S. K. Beta-arrestins and cell signaling. *Annu Rev Physiol* **69**, 483-510, doi:10.1146/annurev.ph.69.013107.100021 (2007).
61 Luttrell, L. M. *et al.* Beta-arrestin-dependent formation of beta2 adrenergic receptor-Src protein kinase complexes. *Science* **283**, 655-661 (1999).
62 DeFea, K. A. *et al.* The proliferative and antiapoptotic effects of substance P are facilitated by formation of a beta -arrestin-dependent scaffolding complex. *Proceedings of the National Academy of Sciences of the United States of America* **97**, 11086-11091, doi:10.1073/pnas.190276697 (2000).
63 Luttrell, L. M. *et al.* Activation and targeting of extracellular signal-regulated kinases by beta-arrestin scaffolds. *Proceedings of the National Academy of Sciences of the United States of America* **98**, 2449-2454, doi:10.1073/pnas.041604898 (2001).
64 Coffa, S., Breitman, M., Spiller, B. W. & Gurevich, V. V. A single mutation in arrestin-2 prevents ERK1/2 activation by reducing c-Raf1 binding. *Biochemistry* **50**, 6951-6958, doi:10.1021/bi200745k (2011).
65 Azzi, M. *et al.* Beta-arrestin-mediated activation of MAPK by inverse agonists reveals distinct active conformations for G protein-coupled receptors. *Proceedings of the National Academy of Sciences of the United States of America* **100**, 11406-11411, doi:10.1073/pnas.1936664100 (2003).
66 McDonald, P. H. *et al.* Beta-arrestin 2: a receptor-regulated MAPK scaffold for the activation of JNK3. *Science* **290**, 1574-1577 (2000).
67 Kruk, J. S., Vasefi, M. S., Liu, H., Heikkila, J. J. & Beazely, M. A. 5-HT(1A) receptors transactivate the platelet-derived growth factor receptor type beta in neuronal cells. *Cellular signalling* **25**, 133-143, doi:10.1016/j.cellsig.2012.09.021 (2013).
68 Maudsley, S. *et al.* The beta(2)-adrenergic receptor mediates extracellular signal-regulated kinase activation via assembly of a multi-receptor complex with the epidermal growth factor receptor. *The Journal of biological chemistry* **275**, 9572-9580 (2000).

69 Oligny-Longpre, G. *et al.* Engagement of beta-arrestin by transactivated insulin-like growth factor receptor is needed for V2 vasopressin receptor-stimulated ERK1/2 activation. *Proceedings of the National Academy of Sciences of the United States of America* **109**, E1028-1037, doi:10.1073/pnas.1112422109 (2012).
70 Buchanan, F. G. *et al.* Role of beta-arrestin 1 in the metastatic progression of colorectal cancer. *Proceedings of the National Academy of Sciences of the United States of America* **103**, 1492-1497, doi:10.1073/pnas.0510562103 (2006).
71 Noma, T. *et al.* Beta-arrestin-mediated beta1-adrenergic receptor transactivation of the EGFR confers cardioprotection. *J Clin Invest* **117**, 2445-2458, doi:10.1172/JCI31901 (2007).
72 Kim, I. M. *et al.* Beta-blockers alprenolol and carvedilol stimulate beta-arrestin-mediated EGFR transactivation. *Proceedings of the National Academy of Sciences of the United States of America* **105**, 14555-14560, doi:10.1073/pnas.0804745105 (2008).
73 Hirota, N. *et al.* Histamine may induce airway remodeling through release of epidermal growth factor receptor ligands from bronchial epithelial cells. *FASEB J* **26**, 1704-1716, doi:10.1096/fj.11-197061 (2012).
74 Prenzel, N. *et al.* EGF receptor transactivation by G-protein-coupled receptors requires metalloproteinase cleavage of proHB-EGF. *Nature* **402**, 884-888, doi:10.1038/47260 (1999).
75 Povsic, T. J., Kohout, T. A. & Lefkowitz, R. J. Beta-arrestin1 mediates insulin-like growth factor 1 (IGF-1) activation of phosphatidylinositol 3-kinase (PI3K) and anti-apoptosis. *The Journal of biological chemistry* **278**, 51334-51339, doi:10.1074/jbc.M309968200 (2003).
76 Lin, F. T., Daaka, Y. & Lefkowitz, R. J. beta-arrestins regulate mitogenic signaling and clathrin-mediated endocytosis of the insulin-like growth factor I receptor. *The Journal of biological chemistry* **273**, 31640-31643 (1998).
77 Lodeiro, M., Theodoropoulou, M., Pardo, M., Casanueva, F. F. & Camina, J. P. c-Src regulates Akt signaling in response to ghrelin via beta-arrestin signaling-independent and -dependent mechanisms. *PLoS One* **4**, e4686, doi:10.1371/journal.pone.0004686 (2009).
78 Goel, R., Phillips-Mason, P. J., Raben, D. M. & Baldassare, J. J. alpha-Thrombin induces rapid and sustained Akt phosphorylation by beta-arrestin1-dependent and -independent mechanisms, and only the sustained Akt phosphorylation is essential for G1 phase progression. *The Journal of biological chemistry* **277**, 18640-18648, doi:10.1074/jbc.M108995200 (2002).
79 Luan, B. *et al.* Deficiency of a beta-arrestin-2 signal complex contributes to insulin resistance. *Nature* **457**, 1146-1149, doi:10.1038/nature07617 (2009).
80 Christensen, G. L. *et al.* Quantitative phosphoproteomics dissection of seven-transmembrane receptor signaling using full and biased agonists. *Mol Cell Proteomics* **9**, 1540-1553, doi:10.1074/mcp.M900550-MCP200 (2010).
81 Beaulieu, J. M. *et al.* An Akt/beta-arrestin 2/PP2A signaling complex mediates dopaminergic neurotransmission and behavior. *Cell* **122**, 261-273, doi:10.1016/j.cell.2005.05.012 (2005).
82 Lima-Fernandes, E. *et al.* Distinct functional outputs of PTEN signalling are controlled by dynamic association with beta-arrestins. *EMBO J* **30**, 2557-2568, doi:10.1038/emboj.2011.178 (2011).
83 Simonin, A. & Fuster, D. Nedd4-1 and beta-arrestin-1 are key regulators of Na+/H+ exchanger 1 ubiquitylation, endocytosis, and function. *The Journal of biological chemistry* **285**, 38293-38303, doi:10.1074/jbc.M110.115089 (2010).
84 Szabo, E. Z., Numata, M., Lukashova, V., Iannuzzi, P. & Orlowski, J. beta-Arrestins bind and decrease cell-surface abundance of the Na+/H+ exchanger NHE5 isoform. *Proceedings of the*

National Academy of Sciences of the United States of America **102**, 2790-2795, doi:10.1073/pnas.0407444102 (2005).

85 Lipsky, R. *et al.* beta-Adrenergic receptor activation induces internalization of cardiac Cav1.2 channel complexes through a beta-arrestin 1-mediated pathway. *The Journal of biological chemistry* **283**, 17221-17226, doi:10.1074/jbc.C800061200 (2008).

86 Shukla, A. K. *et al.* Arresting a transient receptor potential (TRP) channel: beta-arrestin 1 mediates ubiquitination and functional down-regulation of TRPV4. *The Journal of biological chemistry* **285**, 30115-30125, doi:10.1074/jbc.M110.141549 (2010).

87 Busillo, J. M. *et al.* Site-specific phosphorylation of CXCR4 is dynamically regulated by multiple kinases and results in differential modulation of CXCR4 signaling. *The Journal of biological chemistry* **285**, 7805-7817, doi:10.1074/jbc.M109.091173 (2010).

88 Kara, E. *et al.* A phosphorylation cluster of five serine and threonine residues in the C-terminus of the follicle-stimulating hormone receptor is important for desensitization but not for beta-arrestin-mediated ERK activation. *Mol Endocrinol* **20**, 3014-3026, doi:10.1210/me.2006-0098 (2006).

89 Liu, Q., Dewi, D. A., Liu, W., Bee, M. S. & Schonbrunn, A. Distinct phosphorylation sites in the SST2A somatostatin receptor control internalization, desensitization, and arrestin binding. *Molecular pharmacology* **73**, 292-304, doi:10.1124/mol.107.038570 (2008).

90 Jones, B. W. & Hinkle, P. M. Arrestin binds to different phosphorylated regions of the thyrotropin-releasing hormone receptor with distinct functional consequences. *Molecular pharmacology* **74**, 195-202, doi:10.1124/mol.108.045948 (2008).

91 Zidar, D. A., Violin, J. D., Whalen, E. J. & Lefkowitz, R. J. Selective engagement of G protein coupled receptor kinases (GRKs) encodes distinct functions of biased ligands. *Proceedings of the National Academy of Sciences of the United States of America* **106**, 9649-9654, doi:10.1073/pnas.0904361106 (2009).

92 Kim, J. *et al.* Functional antagonism of different G protein-coupled receptor kinases for beta-arrestin-mediated angiotensin II receptor signaling. *Proceedings of the National Academy of Sciences of the United States of America* **102**, 1442-1447, doi:10.1073/pnas.0409532102 (2005).

93 Ren, X. R. *et al.* Different G protein-coupled receptor kinases govern G protein and beta-arrestin-mediated signaling of V2 vasopressin receptor. *Proceedings of the National Academy of Sciences of the United States of America* **102**, 1448-1453, doi:10.1073/pnas.0409534102 (2005).

94 Nobles, K. N. *et al.* Distinct phosphorylation sites on the beta(2)-adrenergic receptor establish a barcode that encodes differential functions of beta-arrestin. *Sci Signal* **4**, ra51, doi:10.1126/scisignal.2001707 (2011).

95 Pitcher, J., Lohse, M. J., Codina, J., Caron, M. G. & Lefkowitz, R. J. Desensitization of the isolated beta 2-adrenergic receptor by beta-adrenergic receptor kinase, cAMP-dependent protein kinase, and protein kinase C occurs via distinct molecular mechanisms. *Biochemistry* **31**, 3193-3197 (1992).

96 Magalhaes, A. C., Dunn, H. & Ferguson, S. S. Regulation of GPCR activity, trafficking and localization by GPCR-interacting proteins. *Br J Pharmacol* **165**, 1717-1736, doi:10.1111/j.1476-5381.2011.01552.x (2012).

97 Lohse, M. J. *et al.* Receptor-specific desensitization with purified proteins. Kinase dependence and receptor specificity of beta-arrestin and arrestin in the beta 2-adrenergic receptor and rhodopsin systems. *The Journal of biological chemistry* **267**, 8558-8564 (1992).

98 Nelson, C. D. *et al.* Targeting of diacylglycerol degradation to M1 muscarinic receptors by beta-arrestins. *Science* **315**, 663-666, doi:10.1126/science.1134562 (2007).
99 Perry, S. J. *et al.* Targeting of cyclic AMP degradation to beta 2-adrenergic receptors by beta-arrestins. *Science* **298**, 834-836, doi:10.1126/science.1074683 (2002).
100 Bouvier, M. *et al.* Two distinct pathways for cAMP-mediated down-regulation of the beta 2-adrenergic receptor. Phosphorylation of the receptor and regulation of its mRNA level. *The Journal of biological chemistry* **264**, 16786-16792 (1989).
101 Freedman, N. J. & Lefkowitz, R. J. Desensitization of G protein-coupled receptors. *Recent Prog Horm Res* **51**, 319-351; discussion 352-313 (1996).
102 Sunahara, R. K., Dessauer, C. W. & Gilman, A. G. Complexity and diversity of mammalian adenylyl cyclases. *Annual review of pharmacology and toxicology* **36**, 461-480, doi:10.1146/annurev.pa.36.040196.002333 (1996).
103 Daaka, Y., Luttrell, L. M. & Lefkowitz, R. J. Switching of the coupling of the beta2-adrenergic receptor to different G proteins by protein kinase A. *Nature* **390**, 88-91, doi:10.1038/36362 (1997).
104 Martin, N. P., Whalen, E. J., Zamah, M. A., Pierce, K. L. & Lefkowitz, R. J. PKA-mediated phosphorylation of the beta1-adrenergic receptor promotes Gs/Gi switching. *Cellular signalling* **16**, 1397-1403, doi:10.1016/j.cellsig.2004.05.002 (2004).
105 Dhami, G. K. *et al.* G Protein-coupled receptor kinase 2 regulator of G protein signaling homology domain binds to both metabotropic glutamate receptor 1a and Galphaq to attenuate signaling. *The Journal of biological chemistry* **279**, 16614-16620, doi:10.1074/jbc.M314090200 (2004).
106 Dicker, F., Quitterer, U., Winstel, R., Honold, K. & Lohse, M. J. Phosphorylation-independent inhibition of parathyroid hormone receptor signaling by G protein-coupled receptor kinases. *Proceedings of the National Academy of Sciences of the United States of America* **96**, 5476-5481 (1999).
107 Reiter, E. *et al.* Kinase-inactive G-protein-coupled receptor kinases are able to attenuate follicle-stimulating hormone-induced signaling. *Biochem Biophys Res Commun* **282**, 71-78, doi:10.1006/bbrc.2001.4534 (2001).
108 Lembo, P. M., Ghahremani, M. H. & Albert, P. R. Receptor selectivity of the cloned opossum G protein-coupled receptor kinase 2 (GRK2) in intact opossum kidney cells: role in desensitization of endogenous alpha2C-adrenergic but not serotonin 1B receptors. *Mol Endocrinol* **13**, 138-147, doi:10.1210/mend.13.1.0217 (1999).
109 Sethakorn, N., Yau, D. M. & Dulin, N. O. Non-canonical functions of RGS proteins. *Cellular signalling* **22**, 1274-1281, doi:10.1016/j.cellsig.2010.03.016 (2010).
110 Sjogren, B. & Neubig, R. R. Thinking outside of the "RGS box": new approaches to therapeutic targeting of regulators of G protein signaling. *Molecular pharmacology* **78**, 550-557, doi:10.1124/mol.110.065219 (2010).
111 Bernstein, L. S. *et al.* RGS2 binds directly and selectively to the M1 muscarinic acetylcholine receptor third intracellular loop to modulate Gq/11alpha signaling. *The Journal of biological chemistry* **279**, 21248-21256, doi:10.1074/jbc.M312407200 (2004).
112 Hague, C. *et al.* Selective inhibition of alpha1A-adrenergic receptor signaling by RGS2 association with the receptor third intracellular loop. *The Journal of biological chemistry* **280**, 27289-27295, doi:10.1074/jbc.M502365200 (2005).
113 Lefkowitz, R. J. & Shenoy, S. K. Transduction of receptor signals by beta-arrestins. *Science* **308**, 512-517, doi:10.1126/science.1109237 (2005).

114 Hamdan, F. F. *et al.* Unraveling G protein-coupled receptor endocytosis pathways using real-time monitoring of agonist-promoted interaction between beta-arrestins and AP-2. *The Journal of biological chemistry* **282**, 29089-29100, doi:10.1074/jbc.M700577200 (2007).
115 Goodman, O. B., Jr. *et al.* Beta-arrestin acts as a clathrin adaptor in endocytosis of the beta2-adrenergic receptor. *Nature* **383**, 447-450, doi:10.1038/383447a0 (1996).
116 Laporte, S. A. *et al.* The beta2-adrenergic receptor/betaarrestin complex recruits the clathrin adaptor AP-2 during endocytosis. *Proceedings of the National Academy of Sciences of the United States of America* **96**, 3712-3717 (1999).
117 Laporte, S. A., Oakley, R. H., Holt, J. A., Barak, L. S. & Caron, M. G. The interaction of beta-arrestin with the AP-2 adaptor is required for the clustering of beta 2-adrenergic receptor into clathrin-coated pits. *The Journal of biological chemistry* **275**, 23120-23126, doi:10.1074/jbc.M002581200 (2000).
118 Rapoport, I. *et al.* Regulatory interactions in the recognition of endocytic sorting signals by AP-2 complexes. *EMBO J* **16**, 2240-2250, doi:10.1093/emboj/16.9.2240 (1997).
119 Diviani, D., Lattion, A. L., Abuin, L., Staub, O. & Cotecchia, S. The adaptor complex 2 directly interacts with the alpha 1b-adrenergic receptor and plays a role in receptor endocytosis. *The Journal of biological chemistry* **278**, 19331-19340, doi:10.1074/jbc.M302110200 (2003).
120 Zerial, M. & McBride, H. Rab proteins as membrane organizers. *Nat Rev Mol Cell Biol* **2**, 107-117, doi:10.1038/35052055 (2001).
121 Seachrist, J. L. *et al.* Rab5 association with the angiotensin II type 1A receptor promotes Rab5 GTP binding and vesicular fusion. *The Journal of biological chemistry* **277**, 679-685, doi:10.1074/jbc.M109022200 (2002).
122 Premont, R. T. *et al.* beta2-Adrenergic receptor regulation by GIT1, a G protein-coupled receptor kinase-associated ADP ribosylation factor GTPase-activating protein. *Proceedings of the National Academy of Sciences of the United States of America* **95**, 14082-14087 (1998).
123 Claing, A. *et al.* beta-Arrestin-mediated ADP-ribosylation factor 6 activation and beta 2-adrenergic receptor endocytosis. *The Journal of biological chemistry* **276**, 42509-42513, doi:10.1074/jbc.M108399200 (2001).
124 Gines, S. *et al.* Involvement of caveolin in ligand-induced recruitment and internalization of A(1) adenosine receptor and adenosine deaminase in an epithelial cell line. *Molecular pharmacology* **59**, 1314-1323 (2001).
125 Rapacciuolo, A. *et al.* Protein kinase A and G protein-coupled receptor kinase phosphorylation mediates beta-1 adrenergic receptor endocytosis through different pathways. *The Journal of biological chemistry* **278**, 35403-35411, doi:10.1074/jbc.M305675200 (2003).
126 Kong, M. M. *et al.* Regulation of D1 dopamine receptor trafficking and signaling by caveolin-1. *Molecular pharmacology* **72**, 1157-1170, doi:10.1124/mol.107.034769 (2007).
127 Shmuel, M., Nodel-Berner, E., Hyman, T., Rouvinski, A. & Altschuler, Y. Caveolin 2 regulates endocytosis and trafficking of the M1 muscarinic receptor in MDCK epithelial cells. *Mol Biol Cell* **18**, 1570-1585, doi:10.1091/mbc.e06-07-0618 (2007).
128 Kovtun, O., Tillu, V. A., Ariotti, N., Parton, R. G. & Collins, B. M. Cavin family proteins and the assembly of caveolae. *J Cell Sci* **128**, 1269-1278, doi:10.1242/jcs.167866 (2015).
129 Raposo, G. *et al.* Internalization of beta-adrenergic receptor in A431 cells involves non-coated vesicles. *Eur J Cell Biol* **50**, 340-352 (1989).
130 Chun, M., Liyanage, U. K., Lisanti, M. P. & Lodish, H. F. Signal transduction of a G protein-coupled receptor in caveolae: colocalization of endothelin and its receptor with caveolin. *Proceedings of the National Academy of Sciences of the United States of America* **91**, 11728-11732 (1994).

131 Zhang, J., Ferguson, S. S., Barak, L. S., Menard, L. & Caron, M. G. Dynamin and beta-arrestin reveal distinct mechanisms for G protein-coupled receptor internalization. *The Journal of biological chemistry* **271**, 18302-18305 (1996).
132 Freedman, N. J. *et al.* Phosphorylation and desensitization of human endothelin A and B receptors. Evidence for G protein-coupled receptor kinase specificity. *The Journal of biological chemistry* **272**, 17734-17743 (1997).
133 Werbonat, Y., Kleutges, N., Jakobs, K. H. & van Koppen, C. J. Essential role of dynamin in internalization of M2 muscarinic acetylcholine and angiotensin AT1A receptors. *The Journal of biological chemistry* **275**, 21969-21974, doi:10.1074/jbc.M001736200 (2000).
134 Roseberry, A. G. & Hosey, M. M. Internalization of the M2 muscarinic acetylcholine receptor proceeds through an atypical pathway in HEK293 cells that is independent of clathrin and caveolae. *J Cell Sci* **114**, 739-746 (2001).
135 Delaney, K. A., Murph, M. M., Brown, L. M. & Radhakrishna, H. Transfer of M2 muscarinic acetylcholine receptors to clathrin-derived early endosomes following clathrin-independent endocytosis. *The Journal of biological chemistry* **277**, 33439-33446, doi:10.1074/jbc.M205293200 (2002).
136 Krueger, K. M., Daaka, Y., Pitcher, J. A. & Lefkowitz, R. J. The role of sequestration in G protein-coupled receptor resensitization. Regulation of beta2-adrenergic receptor dephosphorylation by vesicular acidification. *The Journal of biological chemistry* **272**, 5-8 (1997).
137 Shih, M., Lin, F., Scott, J. D., Wang, H. Y. & Malbon, C. C. Dynamic complexes of beta2-adrenergic receptors with protein kinases and phosphatases and the role of gravin. *The Journal of biological chemistry* **274**, 1588-1595 (1999).
138 Lin, F., Wang, H. & Malbon, C. C. Gravin-mediated formation of signaling complexes in beta 2-adrenergic receptor desensitization and resensitization. *The Journal of biological chemistry* **275**, 19025-19034 (2000).
139 Oakley, R. H., Laporte, S. A., Holt, J. A., Caron, M. G. & Barak, L. S. Differential affinities of visual arrestin, beta arrestin1, and beta arrestin2 for G protein-coupled receptors delineate two major classes of receptors. *The Journal of biological chemistry* **275**, 17201-17210, doi:10.1074/jbc.M910348199 (2000).
140 Oakley, R. H., Laporte, S. A., Holt, J. A., Barak, L. S. & Caron, M. G. Molecular determinants underlying the formation of stable intracellular G protein-coupled receptor-beta-arrestin complexes after receptor endocytosis*. *The Journal of biological chemistry* **276**, 19452-19460, doi:10.1074/jbc.M101450200 (2001).
141 Wang, Y., Zhou, Y., Szabo, K., Haft, C. R. & Trejo, J. Down-regulation of protease-activated receptor-1 is regulated by sorting nexin 1. *Mol Biol Cell* **13**, 1965-1976, doi:10.1091/mbc.e01-11-0131 (2002).
142 Gullapalli, A., Wolfe, B. L., Griffin, C. T., Magnuson, T. & Trejo, J. An essential role for SNX1 in lysosomal sorting of protease-activated receptor-1: evidence for retromer-, Hrs-, and Tsg101-independent functions of sorting nexins. *Mol Biol Cell* **17**, 1228-1238, doi:10.1091/mbc.e05-09-0899 (2006).
143 Vines, C. M. *et al.* N-formyl peptide receptors internalize but do not recycle in the absence of arrestins. *The Journal of biological chemistry* **278**, 41581-41584, doi:10.1074/jbc.C300291200 (2003).
144 Krilov, L., Nguyen, A., Miyazaki, T., Unson, C. G. & Bouscarel, B. Glucagon receptor recycling: role of carboxyl terminus, beta-arrestins, and cytoskeleton. *Am J Physiol Cell Physiol* **295**, C1230-1237, doi:10.1152/ajpcell.00240.2008 (2008).

145 Mahabaleshwar, H., Tarbashevich, K., Nowak, M., Brand, M. & Raz, E. beta-arrestin control of late endosomal sorting facilitates decoy receptor function and chemokine gradient formation. *Development* **139**, 2897-2902, doi:10.1242/dev.080408 (2012).
146 Hamelin, E., Theriault, C., Laroche, G. & Parent, J. L. The intracellular trafficking of the G protein-coupled receptor TPbeta depends on a direct interaction with Rab11. *The Journal of biological chemistry* **280**, 36195-36205, doi:10.1074/jbc.M503438200 (2005).
147 Wikstrom, K. *et al.* Recycling of the human prostacyclin receptor is regulated through a direct interaction with Rab11a GTPase. *Cellular signalling* **20**, 2332-2346, doi:10.1016/j.cellsig.2008.09.003 (2008).
148 Parent, A., Hamelin, E., Germain, P. & Parent, J. L. Rab11 regulates the recycling of the beta2-adrenergic receptor through a direct interaction. *Biochem J* **418**, 163-172, doi:10.1042/BJ20080867 (2009).
149 Esseltine, J. L., Dale, L. B. & Ferguson, S. S. Rab GTPases bind at a common site within the angiotensin II type I receptor carboxyl-terminal tail: evidence that Rab4 regulates receptor phosphorylation, desensitization, and resensitization. *Molecular pharmacology* **79**, 175-184, doi:10.1124/mol.110.068379 (2011).
150 Ren, M. *et al.* Hydrolysis of GTP on rab11 is required for the direct delivery of transferrin from the pericentriolar recycling compartment to the cell surface but not from sorting endosomes. *Proceedings of the National Academy of Sciences of the United States of America* **95**, 6187-6192 (1998).
151 Seachrist, J. L., Anborgh, P. H. & Ferguson, S. S. beta 2-adrenergic receptor internalization, endosomal sorting, and plasma membrane recycling are regulated by rab GTPases. *The Journal of biological chemistry* **275**, 27221-27228, doi:10.1074/jbc.M003657200 (2000).
152 Innamorati, G., Le Gouill, C., Balamotis, M. & Birnbaumer, M. The long and the short cycle. Alternative intracellular routes for trafficking of G-protein-coupled receptors. *The Journal of biological chemistry* **276**, 13096-13103, doi:10.1074/jbc.M009780200 (2001).
153 Meresse, S., Gorvel, J. P. & Chavrier, P. The rab7 GTPase resides on a vesicular compartment connected to lysosomes. *J Cell Sci* **108 (Pt 11)**, 3349-3358 (1995).
154 Clark, A. J. The reaction between acetyl choline and muscle cells. *J Physiol* **61**, 530-546 (1926).
155 Stephenson, R. P. A modification of receptor theory. *Br J Pharmacol Chemother* **11**, 379-393 (1956).
156 Black, J. W. & Leff, P. Operational models of pharmacological agonism. *Proc R Soc Lond B Biol Sci* **220**, 141-162 (1983).
157 Kenakin, T. Principles: receptor theory in pharmacology. *Trends in pharmacological sciences* **25**, 186-192, doi:10.1016/j.tips.2004.02.012 (2004).
158 Del Castillo, J. & Katz, B. Interaction at end-plate receptors between different choline derivatives. *Proc R Soc Lond B Biol Sci* **146**, 369-381 (1957).
159 Karlin, A. On the application of "a plausible model" of allosteric proteins to the receptor for acetylcholine. *J Theor Biol* **16**, 306-320 (1967).
160 Leff, P. The two-state model of receptor activation. *Trends in pharmacological sciences* **16**, 89-97 (1995).
161 Limbird, L. E. & Lefkowitz, R. J. Agonist-induced increase in apparent beta-adrenergic receptor size. *Proceedings of the National Academy of Sciences of the United States of America* **75**, 228-232 (1978).
162 De Lean, A., Stadel, J. M. & Lefkowitz, R. J. A ternary complex model explains the agonist-specific binding properties of the adenylate cyclase-coupled beta-adrenergic receptor. *The Journal of biological chemistry* **255**, 7108-7117 (1980).

163 Gurevich, V. V., Pals-Rylaarsdam, R., Benovic, J. L., Hosey, M. M. & Onorato, J. J. Agonist-receptor-arrestin, an alternative ternary complex with high agonist affinity. *The Journal of biological chemistry* **272**, 28849-28852 (1997).
164 Samama, P., Cotecchia, S., Costa, T. & Lefkowitz, R. J. A mutation-induced activated state of the beta 2-adrenergic receptor. Extending the ternary complex model. *The Journal of biological chemistry* **268**, 4625-4636 (1993).
165 Costa, T. & Herz, A. Antagonists with negative intrinsic activity at delta opioid receptors coupled to GTP-binding proteins. *Proceedings of the National Academy of Sciences of the United States of America* **86**, 7321-7325 (1989).
166 Chidiac, P., Hebert, T. E., Valiquette, M., Dennis, M. & Bouvier, M. Inverse agonist activity of beta-adrenergic antagonists. *Molecular pharmacology* **45**, 490-499 (1994).
167 Weiss, J. M., Morgan, P. H., Lutz, M. W. & Kenakin, T. P. The cubic ternary complex receptor-occupancy model. III. resurrecting efficacy. *J Theor Biol* **181**, 381-397, doi:10.1006/jtbi.1996.0139 (1996).
168 Galandrin, S., Oligny-Longpre, G. & Bouvier, M. The evasive nature of drug efficacy: implications for drug discovery. *Trends in pharmacological sciences* **28**, 423-430, doi:10.1016/j.tips.2007.06.005 (2007).
169 van der Westhuizen, E. T., Breton, B., Christopoulos, A. & Bouvier, M. Quantification of ligand bias for clinically relevant beta2-adrenergic receptor ligands: implications for drug taxonomy. *Molecular pharmacology* **85**, 492-509, doi:10.1124/mol.113.088880 (2014).
170 Kenakin, T. & Christopoulos, A. Measurements of ligand bias and functional affinity. *Nature reviews. Drug discovery* **12**, 483, doi:10.1038/nrd3954-c2 (2013).
171 Kenakin, T. & Christopoulos, A. Signalling bias in new drug discovery: detection, quantification and therapeutic impact. *Nature reviews. Drug discovery* **12**, 205-216, doi:10.1038/nrd3954 (2013).
172 Liu, J. J., Horst, R., Katritch, V., Stevens, R. C. & Wuthrich, K. Biased signaling pathways in beta2-adrenergic receptor characterized by 19F-NMR. *Science* **335**, 1106-1110, doi:10.1126/science.1215802 (2012).
173 Zocher, M., Fung, J. J., Kobilka, B. K. & Muller, D. J. Ligand-specific interactions modulate kinetic, energetic, and mechanical properties of the human beta2 adrenergic receptor. *Structure* **20**, 1391-1402, doi:10.1016/j.str.2012.05.010 (2012).
174 Nygaard, R. *et al.* The dynamic process of beta(2)-adrenergic receptor activation. *Cell* **152**, 532-542, doi:10.1016/j.cell.2013.01.008 (2013).
175 Christopoulos, A. & Kenakin, T. G protein-coupled receptor allosterism and complexing. *Pharmacol Rev* **54**, 323-374 (2002).
176 Ye, L., Van Eps, N., Zimmer, M., Ernst, O. P. & Prosser, R. S. Activation of the A2A adenosine G-protein-coupled receptor by conformational selection. *Nature* **533**, 265-268, doi:10.1038/nature17668 (2016).
177 Manglik, A. *et al.* Structural Insights into the Dynamic Process of beta2-Adrenergic Receptor Signaling. *Cell* **161**, 1101-1111, doi:10.1016/j.cell.2015.04.043 (2015).
178 Kenakin, T. The potential for selective pharmacological therapies through biased receptor signaling. *BMC Pharmacol Toxicol* **13**, 3, doi:10.1186/2050-6511-13-3 (2012).
179 Latorraca, N. R., Venkatakrishnan, A. J. & Dror, R. O. GPCR Dynamics: Structures in Motion. *Chem Rev* **117**, 139-155, doi:10.1021/acs.chemrev.6b00177 (2017).
180 Wacker, D., Stevens, R. C. & Roth, B. L. How Ligands Illuminate GPCR Molecular Pharmacology. *Cell* **170**, 414-427, doi:10.1016/j.cell.2017.07.009 (2017).

181 Ghanouni, P., Steenhuis, J. J., Farrens, D. L. & Kobilka, B. K. Agonist-induced conformational changes in the G-protein-coupling domain of the beta 2 adrenergic receptor. *Proceedings of the National Academy of Sciences of the United States of America* **98**, 5997-6002, doi:10.1073/pnas.101126198 (2001).
182 Rosenbaum, D. M. *et al.* Structure and function of an irreversible agonist-beta(2) adrenoceptor complex. *Nature* **469**, 236-240, doi:10.1038/nature09665 (2011).
183 Dror, R. O. *et al.* Activation mechanism of the beta2-adrenergic receptor. *Proceedings of the National Academy of Sciences of the United States of America* **108**, 18684-18689, doi:10.1073/pnas.1110499108 (2011).
184 Dror, R. O. *et al.* Pathway and mechanism of drug binding to G-protein-coupled receptors. *Proceedings of the National Academy of Sciences of the United States of America* **108**, 13118-13123, doi:10.1073/pnas.1104614108 (2011).
185 Okude, J. *et al.* Identification of a Conformational Equilibrium That Determines the Efficacy and Functional Selectivity of the mu-Opioid Receptor. *Angew Chem Int Ed Engl* **54**, 15771-15776, doi:10.1002/anie.201508794 (2015).
186 Rasmussen, S. G. *et al.* Crystal structure of the beta2 adrenergic receptor-Gs protein complex. *Nature* **477**, 549-555, doi:10.1038/nature10361 (2011).
187 Liang, Y. L. *et al.* Phase-plate cryo-EM structure of a class B GPCR-G-protein complex. *Nature* **546**, 118-123, doi:10.1038/nature22327 (2017).
188 Zhang, Y. *et al.* Cryo-EM structure of the activated GLP-1 receptor in complex with a G protein. *Nature* **546**, 248-253, doi:10.1038/nature22394 (2017).
189 Carpenter, B., Nehme, R., Warne, T., Leslie, A. G. & Tate, C. G. Structure of the adenosine A(2A) receptor bound to an engineered G protein. *Nature* **536**, 104-107, doi:10.1038/nature18966 (2016).
190 Scheerer, P. *et al.* Crystal structure of opsin in its G-protein-interacting conformation. *Nature* **455**, 497-502, doi:10.1038/nature07330 (2008).
191 Kang, Y. *et al.* Crystal structure of rhodopsin bound to arrestin by femtosecond X-ray laser. *Nature* **523**, 561-567, doi:10.1038/nature14656 (2015).
192 Manglik, A., Kobilka, B. K. & Steyaert, J. Nanobodies to Study G Protein-Coupled Receptor Structure and Function. *Annual review of pharmacology and toxicology* **57**, 19-37, doi:10.1146/annurev-pharmtox-010716-104710 (2017).
193 Ballesteros, J. A. & Weinstein, H. [19] Integrated methods for the construction of three-dimensional models and computational probing of structure-function relations in G protein-coupled receptors. **25**, 366-428, doi:10.1016/s1043-9471(05)80049-7 (1995).
194 Janz, J. M. & Farrens, D. L. Rhodopsin activation exposes a key hydrophobic binding site for the transducin alpha-subunit C terminus. *The Journal of biological chemistry* **279**, 29767-29773, doi:10.1074/jbc.M402567200 (2004).
195 Audet, M. & Bouvier, M. Restructuring G-protein- coupled receptor activation. *Cell* **151**, 14-23, doi:10.1016/j.cell.2012.09.003 (2012).
196 Deupi, X., Standfuss, J. & Schertler, G. Conserved activation pathways in G-protein-coupled receptors. *Biochem Soc Trans* **40**, 383-388, doi:10.1042/BST20120001 (2012).
197 Tehan, B. G., Bortolato, A., Blaney, F. E., Weir, M. P. & Mason, J. S. Unifying family A GPCR theories of activation. *Pharmacology & therapeutics* **143**, 51-60, doi:10.1016/j.pharmthera.2014.02.004 (2014).
198 Goncalves, J. A. *et al.* Highly conserved tyrosine stabilizes the active state of rhodopsin. *Proceedings of the National Academy of Sciences of the United States of America* **107**, 19861-19866, doi:10.1073/pnas.1009405107 (2010).

199 Rasmussen, S. G. *et al.* Structure of a nanobody-stabilized active state of the beta(2) adrenoceptor. *Nature* **469**, 175-180, doi:10.1038/nature09648 (2011).
200 Huang, W. *et al.* Structural insights into micro-opioid receptor activation. *Nature* **524**, 315-321, doi:10.1038/nature14886 (2015).
201 Kruse, A. C. *et al.* Activation and allosteric modulation of a muscarinic acetylcholine receptor. *Nature* **504**, 101-106, doi:10.1038/nature12735 (2013).
202 Hua, T. *et al.* Crystal structures of agonist-bound human cannabinoid receptor CB1. *Nature* **547**, 468-471, doi:10.1038/nature23272 (2017).
203 Pert, C. B., Pasternak, G. & Snyder, S. H. Opiate agonists and antagonists discriminated by receptor binding in brain. *Science* **182**, 1359-1361 (1973).
204 Ye, L. *et al.* Mechanistic insights into allosteric regulation of the A2A adenosine G protein-coupled receptor by physiological cations. *Nat Commun* **9**, 1372, doi:10.1038/s41467-018-03314-9 (2018).
205 Katritch, V. *et al.* Allosteric sodium in class A GPCR signaling. *Trends in biochemical sciences* **39**, 233-244, doi:10.1016/j.tibs.2014.03.002 (2014).
206 Rose, A. S. *et al.* Position of transmembrane helix 6 determines receptor G protein coupling specificity. *Journal of the American Chemical Society* **136**, 11244-11247, doi:10.1021/ja5055109 (2014).
207 Koehl, A. *et al.* Structure of the micro-opioid receptor-Gi protein complex. *Nature* **558**, 547-552, doi:10.1038/s41586-018-0219-7 (2018).
208 Draper-Joyce, C. J. *et al.* Structure of the adenosine-bound human adenosine A1 receptor-Gi complex. *Nature* **558**, 559-563, doi:10.1038/s41586-018-0236-6 (2018).
209 Gregorio, G. G. *et al.* Single-molecule analysis of ligand efficacy in beta2AR-G-protein activation. *Nature* **547**, 68-73, doi:10.1038/nature22354 (2017).
210 Masureel, M. *et al.* Structural insights into binding specificity, efficacy and bias of a β2AR partial agonist. *Nature chemical biology* **14**, 1059-1066, doi:10.1038/s41589-018-0145-x (2018).
211 Wacker, D. *et al.* Crystal Structure of an LSD-Bound Human Serotonin Receptor. *Cell* **168**, 377-389 e312, doi:10.1016/j.cell.2016.12.033 (2017).
212 Oldham, W. M. & Hamm, H. E. Structural basis of function in heterotrimeric G proteins. *Q Rev Biophys* **39**, 117-166, doi:10.1017/S0033583506004306 (2006).
213 Wall, M. A. *et al.* The structure of the G protein heterotrimer Gi alpha 1 beta 1 gamma 2. *Cell* **83**, 1047-1058 (1995).
214 Schmidt, C. J., Thomas, T. C., Levine, M. A. & Neer, E. J. Specificity of G protein beta and gamma subunit interactions. *The Journal of biological chemistry* **267**, 13807-13810 (1992).
215 Lambright, D. G. *et al.* The 2.0 A crystal structure of a heterotrimeric G protein. *Nature* **379**, 311-319, doi:10.1038/379311a0 (1996).
216 Noel, J. P., Hamm, H. E. & Sigler, P. B. The 2.2 A crystal structure of transducin-alpha complexed with GTP gamma S. *Nature* **366**, 654-663, doi:10.1038/366654a0 (1993).
217 Van Eps, N. *et al.* Interaction of a G protein with an activated receptor opens the interdomain interface in the alpha subunit. *Proceedings of the National Academy of Sciences of the United States of America* **108**, 9420-9424, doi:10.1073/pnas.1105810108 (2011).
218 Ceruso, M. A., Periole, X. & Weinstein, H. Molecular dynamics simulations of transducin: interdomain and front to back communication in activation and nucleotide exchange. *J Mol Biol* **338**, 469-481, doi:10.1016/j.jmb.2004.02.064 (2004).
219 Dror, R. O. *et al.* SIGNAL TRANSDUCTION. Structural basis for nucleotide exchange in heterotrimeric G proteins. *Science* **348**, 1361-1365, doi:10.1126/science.aaa5264 (2015).

220 Westfield, G. H. *et al.* Structural flexibility of the G alpha s alpha-helical domain in the beta2-adrenoceptor Gs complex. *Proceedings of the National Academy of Sciences of the United States of America* **108**, 16086-16091, doi:10.1073/pnas.1113645108 (2011).
221 Markby, D. W., Onrust, R. & Bourne, H. R. Separate GTP binding and GTPase activating domains of a G alpha subunit. *Science* **262**, 1895-1901 (1993).
222 Aris, L. *et al.* Structural requirements for the stabilization of metarhodopsin II by the C terminus of the alpha subunit of transducin. *The Journal of biological chemistry* **276**, 2333-2339, doi:10.1074/jbc.M002533200 (2001).
223 Schwindinger, W. F., Miric, A., Zimmerman, D. & Levine, M. A. A novel Gs alpha mutant in a patient with Albright hereditary osteodystrophy uncouples cell surface receptors from adenylyl cyclase. *The Journal of biological chemistry* **269**, 25387-25391 (1994).
224 Sullivan, K. A. *et al.* Identification of receptor contact site involved in receptor-G protein coupling. *Nature* **330**, 758-760, doi:10.1038/330758a0 (1987).
225 Oldham, W. M., Van Eps, N., Preininger, A. M., Hubbell, W. L. & Hamm, H. E. Mechanism of the receptor-catalyzed activation of heterotrimeric G proteins. *Nature structural & molecular biology* **13**, 772-777, doi:10.1038/nsmb1129 (2006).
226 Herrmann, R., Heck, M., Henklein, P., Hofmann, K. P. & Ernst, O. P. Signal transfer from GPCRs to G proteins: role of the G alpha N-terminal region in rhodopsin-transducin coupling. *The Journal of biological chemistry* **281**, 30234-30241, doi:10.1074/jbc.M600797200 (2006).
227 Chung, K. Y. *et al.* Conformational changes in the G protein Gs induced by the beta2 adrenergic receptor. *Nature* **477**, 611-615, doi:10.1038/nature10488 (2011).
228 Posner, B. A., Mixon, M. B., Wall, M. A., Sprang, S. R. & Gilman, A. G. The A326S mutant of Gialpha1 as an approximation of the receptor-bound state. *The Journal of biological chemistry* **273**, 21752-21758 (1998).
229 Thomas, T. C., Schmidt, C. J. & Neer, E. J. G-protein alpha o subunit: mutation of conserved cysteines identifies a subunit contact surface and alters GDP affinity. *Proceedings of the National Academy of Sciences of the United States of America* **90**, 10295-10299 (1993).
230 Franke, R. R., Konig, B., Sakmar, T. P., Khorana, H. G. & Hofmann, K. P. Rhodopsin mutants that bind but fail to activate transducin. *Science* **250**, 123-125 (1990).
231 Muradov, K. G. & Artemyev, N. O. Coupling between the N- and C-terminal domains influences transducin-alpha intrinsic GDP/GTP exchange. *Biochemistry* **39**, 3937-3942 (2000).
232 Ostermaier, M. K., Peterhans, C., Jaussi, R., Deupi, X. & Standfuss, J. Functional map of arrestin-1 at single amino acid resolution. *Proceedings of the National Academy of Sciences of the United States of America* **111**, 1825-1830, doi:10.1073/pnas.1319402111 (2014).
233 Lally, C. C., Bauer, B., Selent, J. & Sommer, M. E. C-edge loops of arrestin function as a membrane anchor. *Nat Commun* **8**, 14258, doi:10.1038/ncomms14258 (2017).
234 Scheerer, P. & Sommer, M. E. Structural mechanism of arrestin activation. *Curr Opin Struct Biol* **45**, 160-169, doi:10.1016/j.sbi.2017.05.001 (2017).
235 Gimenez, L. E., Vishnivetskiy, S. A., Baameur, F. & Gurevich, V. V. Manipulation of very few receptor discriminator residues greatly enhances receptor specificity of non-visual arrestins. *The Journal of biological chemistry* **287**, 29495-29505, doi:10.1074/jbc.M112.366674 (2012).
236 Peterson, S. M. *et al.* Elucidation of G-protein and beta-arrestin functional selectivity at the dopamine D2 receptor. *Proceedings of the National Academy of Sciences of the United States of America* **112**, 7097-7102, doi:10.1073/pnas.1502742112 (2015).
237 Prokop, S. *et al.* Differential manipulation of arrestin-3 binding to basal and agonist-activated G protein-coupled receptors. *Cellular signalling* **36**, 98-107, doi:10.1016/j.cellsig.2017.04.021 (2017).

238 Cerione, R. A. *et al.* The mammalian beta 2-adrenergic receptor: reconstitution of functional interactions between pure receptor and pure stimulatory nucleotide binding protein of the adenylate cyclase system. *Biochemistry* **23**, 4519-4525 (1984).
239 Yatani, A., Tajima, Y. & Green, S. A. Coupling of beta-adrenergic receptors to cardiac L-type Ca2+ channels: preferential coupling of the beta1 versus beta2 receptor subtype and evidence for PKA-independent activation of the channel. *Cellular signalling* **11**, 337-342 (1999).
240 Hall, R. A. *et al.* The beta2-adrenergic receptor interacts with the Na+/H+-exchanger regulatory factor to control Na+/H+ exchange. *Nature* **392**, 626-630, doi:10.1038/33458 (1998).
241 Shukla, A. K., Singh, G. & Ghosh, E. Emerging structural insights into biased GPCR signaling. *Trends in biochemical sciences* **39**, 594-602, doi:10.1016/j.tibs.2014.10.001 (2014).
242 Breton, B. *et al.* Multiplexing of multicolor bioluminescence resonance energy transfer. *Biophysical journal* **99**, 4037-4046, doi:10.1016/j.bpj.2010.10.025 (2010).
243 Chu, J. *et al.* A bright cyan-excitable orange fluorescent protein facilitates dual-emission microscopy and enhances bioluminescence imaging in vivo. *Nat Biotechnol* **34**, 760-767, doi:10.1038/nbt.3550 (2016).
244 Laviv, T. *et al.* Simultaneous dual-color fluorescence lifetime imaging with novel red-shifted fluorescent proteins. *Nat Methods* **13**, 989-992, doi:10.1038/nmeth.4046 (2016).
245 Schihada, H. *et al.* A universal bioluminescence resonance energy transfer sensor design enables high-sensitivity screening of GPCR activation dynamics. *Communications Biology* (2018).
246 Manglik, A. & Kruse, A. C. Structural Basis for G Protein-Coupled Receptor Activation. *Biochemistry* **56**, 5628-5634, doi:10.1021/acs.biochem.7b00747 (2017).
247 Reiner, S., Ambrosio, M., Hoffmann, C. & Lohse, M. J. Differential signaling of the endogenous agonists at the beta2-adrenergic receptor. *The Journal of biological chemistry* **285**, 36188-36198, doi:10.1074/jbc.M110.175604 (2010).
248 Picard, L.-P., Schönegge, A. M., Lohse, M. J. & Bouvier, M. Bioluminescence resonance energy transfer-based biosensors allow monitoring of ligand- and transducer-mediated GPCR conformational changes. *Communications Biology* **1**, 106, doi:10.1038/s42003-018-0101-z (2018).

Annexes

Article 4

Bioluminescence Resonance Energy Transfer (BRET)-based Imaging of Protein-Protein Interactions in Living Cells

Hiroyuki Kobayashi[1], Louis-Philippe Picard[1], Anne-Marie Schönegge[1], Michel Bouvier[1*]

Accepté dans *Nature Protocol,* le 8 janvier 2019

Contributions. J'ai contribué au niveau technique pour ce papier en testant les caractéristiques de l'enzyme Nluc que j'ai utilisé par la suite pour le multiplex dans l'article 1 de ma thèse.

Bioluminescence Resonance Energy Transfer (BRET)-based Imaging of Protein-Protein Interactions in Living Cells

Hiroyuki Kobayashi[1], **Louis-Philippe Picard[1]**, Anne-Marie Schönegge[1], Michel Bouvier[1*]

[1] Institute for Research in Immunology and Cancer (IRIC), Université de Montréal, Montreal

* Corresponding author: michel.bouvier@umontreal.ca. Institute for Research in Immunology and Cancer (IRIC), Department of Biochemistry and Molecular Medicine, Université de Montréal, Montréal, Québec H3T 1J4 CANADA. Telephone number: +1-514-343-6319

KEYWORDS microscopy, imaging, luminescence, , bioluminescence resonance energy transfer, BRET, electron multiplying charge-coupled device, EMCCD, photon-counting, protein-protein interactions, G proteins, G protein-coupled receptor, βarrestin,

EDITORIAL SUMMARY This protocol describes the experimental design and procedures for bioluminescence resonance energy transfer (BRET) imaging. The authors discuss choices of energy donors and acceptors, luminescent substrates, microscope setup and optimal cameras.

TWEET A new protocol describing the experimental design and procedures for bioluminescence resonance energy transfer imaging.

COVER TEASER Bioluminescence resonance energy transfer Imaging

Up to three primary research articles where the protocol has been used and/or developed:

1. Namkung, Y. et al. Monitoring G protein-coupled receptor and β-arrestin trafficking in live cells using enhanced bystander BRET. Nat. Commun. 7, 12178 (2016).

2. Beautrait, A. et al. A new inhibitor of the β-arrestin/AP2 endocytic complex reveals interplay between GPCR internalization and signalling. Nat. Commun. 8, (2017).

ABSTRACT

Bioluminescence resonance energy transfer (BRET) is a transfer of energy between a luminescence donor and a fluorescence acceptor. Because BRET occurs when the distance between the donor and acceptor is less than 10 nm, and its efficiency is inversely proportional to the 6^{th} power of distance, it has gained popularity as a proximity-based assay to monitor protein-protein interactions and conformational rearrangements in live cells. In such assays, one protein of interest is fused to a bioluminescent energy donor (*luciferases from Renilla Reniformis* or *Oplophorus Gracilirostris*) while the other protein is fused to a fluorescent energy acceptor (such as green or yellow fluorescent protein). Because BRET donor does not require an external light source, it does not lead to phototoxicity or autofluorescence. It therefore represents an interesting alternative to fluorescence-based imaging such as FRET. However, the low signal output of BRET energy donors has limited the spatio-temporal resolution of BRET imaging. Here, we describe how recent improvements in the detection devices and BRET probes can be used to drastically improve the resolution of BRET imaging, thus widening the field of BRET imaging applications. The protocol described herein involves three main stages. First, cell preparation and transfection requires 3 days, including cell culture time. Second, image acquisition takes 10-120 min per sample, after an initial 60 min for microscope setup. Finally, image analysis typically takes 1-2 hours. The choices of energy donor, acceptor, luminescent substrates, cameras, microscope setup as well as acquisition modes to be used for different applications are also discussed.

INTRODUCTION

Protein trafficking and interactions with different partners are at the core of most physiological responses. Monitoring these processes in real time in living cells provides important information about the spatio-temporal regulation of multiple cell functions. In recent years, the use of fluorescence and luminescence tools have led to major breakthroughs in our understanding of cellular dynamics, by allowing to monitor movement and interaction of proteins. Among the approaches used, resonance energy transfer (RET) has gained in popularity.

RET is a natural phenomenon occurring between two photoactive molecules[1]. It corresponds to the transfer of energy from a donor to an acceptor molecule through a non-radiative resonance process occurring through dipole-dipole coupling that happens only at permissive distance and proper orientation. The transfer of energy results in the excitation of the acceptor that then emits light at a specific wavelength. Two type of RET phenomenon have been largely used to monitor biological processes: they are fluorescence resonance energy transfer (FRET)[2,3] and bioluminescence resonance energy transfer (BRET)[4,5], using fluorescent and luminescent donor, respectively. For most RET pairs, efficient transfer can occur only if the distance between the donor and the acceptor is less than 10 nm and the efficiency of transfer decreases as a function of the sixth power of the distance between them. The average size of a protein being ≅ 5 nm, changes in RET between donors and acceptors fused to proteins of interest reflect changes in the distance between the tagged proteins, which are consistent with the occurrence of macromolecular rearrangements. As a result, RET assays have been widely used to characterize protein-protein interactions and conformational changes within proteins or protein complexes.

BRET has been extensively used to investigate GPCR dynamics and signaling activity. For instance, BRET-based assays have been used to study receptor multimerization[4,6,7], coupling to and activation of G protein[8,9], trafficking[10], engagement and activation of accessory proteins such as βarrestins[11–15] and receptor activity-modifying proteins (RAMPs)[16] as well as post-translational modifications such as ubiquitination[17]. More recently, BRET has also been used for ligand binding assays using fluorophore-conjugated ligands and receptor-fused to an energy donor[18,19]. In most cases, the BRET signal was quantified by spectrometric measures using luminometers equipped with monochromator or filters separating the donor and acceptor emissions. Classically, BRET is quantified by dividing the light signal of the acceptor by the luminescence emitted by the donor. Although useful, such spectrometric studies cannot provide information about the subcellular localization of the processes monitored. Although it has been difficult to image BRET signals with high spatial resolution because of the low light output of luciferase (the energy luminescent donor), recent enzymatic improvement[20] of *Renilla* luciferase (Rluc)-based BRET donor and the development of new luciferases, such as NanoLuc (Nluc)[21], improved signal strength drastically, allowing the development of BRET imaging approaches, including imaging of protein-protein interactions in culture cells[22–27] and even in living animals using red-shifted BRET probes[28,29] that overcome tissue absorption. In this protocol, we present the procedures for BRET-based microscopic visualization of protein-protein interactions and trafficking that combines recent improvements in ultra-low light detectors, new generations of BRET probes as well as new approaches such as enhanced bystander BRET (ebBRET)[26,27]. G proteincoupled receptor (GPCR) activation and trafficking are used as an example of the biological systems that can be studied using such high-resolution BRET microscopy imaging.

The protocol provides in a single manuscript all the information needed to select the best BRET pairs and detection systems for different applications and presents the advantages and inconvenients of the different approaches. In addition, the step-by-step procedure allows investigators to easily perform BRET imaging experiments.

The major components of BRET imaging microscopy system are illustrated in Figure 1. The system used in the present protocol is composed of an inverted microscope connected to an electron multiplying charge-coupled device (EMCCD) camera through a regular port equipped with a motorized filter wheel. The motorized system allows rapid switching between filter-on (GFP emission) or filter-off (corresponding to the entire light emitted that is used as a measure of the donor emission). Since BRET is a luminescence-based assay, it does not require external illumination, but a light source for bright-field or epi-fluorescence is required for focusing purposes. Luminescence is produced by the direct application of the luciferase substrate to the cells.

Comparison with other methods

Unlike most other protein-protein interaction assays such as co-immunoprecipitation, pull-down, protein ligation assay[30] or crosslinking assay, RET-based assays can directly monitor protein-protein interactions in living cells. This non-invasive characteristic of the RET assay is particularly useful when the properties of the interacting proteins can be changed by their extraction or purification, or when the influence of the cellular environment is being studied. Another assay that allows detection of protein-protein interaction in living cells is protein complementation assay (PCA)[31]. PCA imaging is based on the reconstitution of a reporter protein (typically fluorescent proteins or luminescent enzymes) from its split fragments fused

to the proteins of interest. Therefore, the PCA signal can be detected only when two PCA fragments reconstitute the functional reporter as a consequence of the interaction of the fusion proteins. Although this assay can provide robust signals, the background signal can be relatively high due to the propensity of some of the fragments to self-associate. In addition, the dynamics of the interactions can also be affected by the complementation process itself, since reconstitution of the reporter protein can stabilize the complex. Unlike RET-assays that allow the quantitative monitoring of each of the partners (by monitoring luminescence and fluorescence independently), this is not possible for PCA since no information can be directly obtained on the quantity and distribution of the non-interacting fragments. Despite these limitations, PCA remains a useful assay. In particular, modifications of the interacting fragments to reduce their affinity for one another have been used to considerably reduce the possible artefact linked to the self association of the fragments[32]. Also, PCA using either split firefly luciferase[33], Rluc[34], Nluc (NanoBit)[35] or split fluorescent proteins[36] has been combined with BRET to monitor the formation of up to four multiprotein complex[37–39].

Many RET-based microscopic imaging methods have been developed to monitor biological processes in the specific subcellular compartments where they occur. One of the major challenges of RET imaging is separating weak energy transfer signals from background. For that reason, FRET has been favored over BRET for imaging purposes because the level of signal resulting from the excitation (by light) of a fluorescent donor is greater than that from the bioluminescent donors used for BRET. However, the strong external illumination in FRET assays also increases the background autofluorescence signal that can be limiting the signal resolution of FRET imaging. Off-peak excitation of the acceptor by the donor excitation light source is also a source of contamination that is dependent on the amount of acceptor, which is

why acceptor photobleaching or fluorescence life time-FRET imaging are often used. The strong FRET illumination also causes phototoxicity and photobleaching, making long time-lapse measurement difficult. In contrast, BRET does not require an external light mediated excitation of the donor since the energy emitted results from a bioluminescent reaction involving the oxidation of a substrate. It follows that no autofluorescence occurs, yielding a good signal to noise ratio. However, the low light intensity characteristic of BRET assays requires much more sensitive system for signal detection (see Limitations section below).

Limitations

Most of the BRET imaging limitations are related to the ability to collect sufficient light to obtain high resolution images. This limitation depends on the brightness of the partners, the energy transfer efficiency for the sensor pair used and the kinetics of the phenomenon studied. It follows that BRET probes expressed at low levels are more difficult to image. Longer acquisition times can be used to mitigate to some extent this limitation. However, longer acquisition time limit the ability to image real time dynamics because (1) the time required to generate a sufficiently high quality image may be longer than the time-scale of the phenomenon that is being investigated or (2) because the time required is longer than the life-time of the luminescent signal. The low intensity of light may also make it more difficult to obtain valid quantification of the BRET changes observed. This is partly true when the signal of interest is close to the shot noise (the statistical random fluctuation of the photon counts). To mitigate these limitations, selection of the brightest BRET partners and substrates as well as the use of efficient optics and sensitive detectors is of primary importance. In the examples shown in this Protocol, the minimum acquisition time to obtain images for both total luminescence and energy acceptor

channels is 25 seconds. It follows that real-time kinetic analyses are limited to phenomena occurring in time-scale longer than 25 seconds. Although this allows the quantitative assessment of phenomena such as receptor endocytosis[40] or βarrestin recruitment[41], it does not permit the real-time analysis of G protein activation[42] for example.

One of the advantages of BRET imaging over spectrometric (plate reader) BRET measurement is the possibility to assess the subcellular origin of the signal. However, the subcellular resolution remains moderate and does not allow to easily distinguish between discrete subcellular organelles. One of the problems leading to lack of resolution is the extent of time needed to detect sufficient signal. Indeed, cellular movements occurring during the acquisition period will lead to blurred image and could even have an impact on the accuracy of the BRET values calculated for a specific pixel. To limit this effect, we recommend never exceeding an acquisition time of 10 seconds (100 X 100 msec frames) for each wavelength + 5 seconds for processing so that the measurements of the two wave lengths are performed within a time interval during which relatively small changes of shape or cell movement occurred. For measurements that require longer acquisition times because of the low intensity of the signals, we recommend performing several rounds (up to 10) of 25 sec measurements (10 sec for each wavelength + 5 sec processing) and the integration of each of the images that are not significantly affected by cell movement or cell shape changes. This allows increased accuracy of BRET measurements at a specific location.

Experimental design

Energy donors and acceptors The most frequently used BRET donor is Rluc, an oxidase isolated from the bioluminescent sea pansy, *Renilla reniformis*. In the original BRET assays,

the native Rluc was used[4,5]. However, Rluc mutants such as Rluc8 (A55T, C124A, S130A, K136R, A143M, M185V, M253L, S287L)[20] or RlucII (A55T, C124A, M185V)[43,44] have improved enzymatic activity, providing greater brightness and making them donors of choice for BRET imaging. More recently, another luciferase from the sea shrimp, *Oplophorus gracilirostris,* known as Nluc[21] has also emerged as a good choice for some BRET applications (see additional BRET donors section below).

The fluorophores used as BRET acceptors usually belong to the family of green fluorescent proteins (GFP), originating either from *Aequorea victoria* or *Renilla reniformis*. The best fluorophores are selected based on their excitation and emission spectra (depending on the donor/substrate used) as well as their quantum yield and Stokes' shift[45]. The BRET signal can have different characteristics depending on the nature of luciferases used as donors, the luciferase substrates, as well as the acceptor selected. Different combinations with their advantages and limitations are described in the following sections.

BRET1 assays Rluc catalyzes the oxidation of its native substrate, coelenterazine (CTZ), into coelenteramide, and the relaxation of coelenteramide to the ground state produces luminescence with an emission peak at around 480 nm[46]. GFP variants having an overlapping excitation wavelength with this emission spectrum, such as eYFP (excitation: 514 nm) or Venus-GFP (excitation: 515 nm)[47], can be used as BRET acceptors for the Rluc-CTZ donor couple and are used in so called BRET1 assays. A synthetic coelenterazine analog, coelenterazine h (CTZh, 2-deoxy coelenterazine), is also often used as substrate for BRET1 assays, showing similar results as CTZ.

BRET1 was the first BRET assay format developed for protein-protein interaction analyses[4,5]. Because the wavelength profile of BRET1 is similar to that of the frequently used CFP and YFP FRET pairs, devices and constructs already available made it easy to perform BRET1 experiments. However, a major drawback of BRET1 is the poor signal separation between the donor and acceptor emission wave lengths, resulting in a sub-optimal signal to noise ratio. As shown in Figure 2a, the donor and acceptor emission spectra for BRET1 pairs have a large overlap because the spectral width of Rluc-CTZh luminescence (≈ 85 nm) is much larger than the Stokes' shift of EYFP (≈ 15 nm). It follows that the acceptor signal is not well resolved from the contaminating donor signal, making it difficult to quantify especially when the efficiency of transfer is low.

BRET2 assays BRET2 was developed with the objective of increasing the separation between the donor and acceptor emission spectrum so to improve signal to background ratio[14]. BRET2 uses synthetic coelenterazine analogs, such as coelenterazine 400A (CTZ400A, also known as DeepBlueC or bisdeoxy-coelenterazine) or Me-O-e-CTZ (also known as prolume purple), which emit blue-shifted luminescence peaking at around 400nm when oxidized by Rluc[20]. The emission of these substrates has narrower spectral width than the substrates used for BRET1 (~50nm vs 85nm, Fig. 2b). BRET2 acceptors include *Aequorea Victoria* GFP mutants, such as GFP10[48] or GFP2[14], that have much larger Stokes' shift than YFP (~ 90nm vs 15nm) and can be efficiently excited with blueshifted luminescence. As a result, BRET2 provides greater signal separation than BRET1, resulting in a greater dynamic window (see "Anticipated Results"). However, the luminescence signal of BRET2 tends to be weaker than BRET1 due to the low light output of blue-shifted substrates, and may be more difficult to monitor depending of the detection systems used. Figure 3 illustrates the difference in luminescence emitted with the

substrates used for BRET1 and BRET2. The BRET1 substrate, CTZh generates luminescence signals that are 3-17 times brighter than the 3 blue-shifted CTZ analogs tested (Fig. 3a). Among the blue-shifted substrates, Me-O-e-CTZ and Me-O-CTZ-O-Me (also known as prolume purple II) are brighter than CTZ400A, which was the original substrate described for BRET2[14]. Another limitation of BRET2 is that all blue-shifted substrate show much faster signal decay (half-life ≈ 12 min) when compared to CTZh (half-life ≈ 22 min) (Fig. 3b). This difference in the half-life of luminescence can be easily appreciated in luminescence images taken from cells expressing RlucII-tagged βarrestin2. Indeed, the luminescence following CTZh addition is easily detectable for more than 30 min while the image obtained with Me-O-e-CTZ as the substrate decayed rapidly and was barely detectable after 10 minutes (Fig. 3c).

Additional BRET acceptors The GFP from *Renilla reniformis* (rGFP), can be used as a BRET acceptor that also allows a good separation between donor and acceptor emission. It also results in a larger BRET signal due to a better transfer efficiency between Rluc and rGFP[49] than between Rluc and GFPs from other species. Indeed, the fact that the two proteins co-evolved in the same species resulted in an optimal dipoles orientation for transfer in the Rluc-rGFP dimer[50]. The very efficient transfer can easily be seen when comparing BRET images obtained for the Rluc-rGFP vs Rluc- GFP10 fusion constructs (Fig. 4a, two last rows). However, the fact that rGFP spontaneously interacts with Rluc limits the use of this energy acceptor to study protein-protein interactions. Yet, this propensity of Rluc and rGFP pair to interact with one another (albeit with low affinity) can be used to increase the signal originating from random collisions known as bystander BRET. This property has recently been used to monitor the localization of protein in specific subcellular domains[26]. For instance, such enhanced bystander BRET (ebBRET) can readily detect the translocation of Rluc-fused proteins to a specific subcellular

domain or organelle harboring rGFP targeted to these sites with specific subcellular localization motifs. In such cases, Rluc spontaneously interact with rGFP, enabling efficient BRET energy transfer only if Rluc and rGFP are in the same sub-cellular compartment (see Anticipated Results).

Additional BRET donors In addition to *Renilla* luciferase, luciferases from different animal species, firefly *Photinus pyralis*[51], copepod *Gaussia princeps*[52], and deep-sea shrimp *Oplophorus gracilirostris*[18], have also been used in BRET applications. As reported by several groups[24,25], the *Oplophorus* luciferase is especially interesting for BRET imaging because engineered luciferases based on the *Oplophorus* enzyme such as eKAZ[53] and Nluc[21] show greater light output than Rluc and their catalytic subunits (19 kDa) are smaller than that of Rluc (34 kDa)[54]. The enzymatic activity of Nluc[21], similarly to Rluc[55,56], is more stable than firefly luciferase under different environmental conditions such as temperature, pH and salt concentration. These advantageous characteristics of Nluc lead to developments of novel Nluc-based applications such as ligand binding assays using Nluc complementation[57] or BRET with fluorophore-conjugated ligands[58]. Although Oplophorus luciferases can use coelenterazine analogs as substrates[46,53], it should be noted that the emission wavelength and light intensity obtained for various analogs are different from those obtained with Rluc (Fig. 5). For instance, Rluc substrates such as Me-O-e-CTZ and Me-O-CTZ-O-Me do not show luminescence with Nluc, whereas another Rluc substrate CTZ400A, as well as the Nluc substrate furimazine, generated brighter signals with 5.2 and 3.4 times greater light output than CTZh when using Nluc (Fig. 5a). Interestingly, CTZ400A, which emits light at 400 nm with Rluc (blue-shifted compared to CTZh), does not show such blue-shifted spectrum with Nluc, and the peak emission is observed at 460 nm, similarly to what is observed with other coelenterazine analogs such as

CTZh and Furimazine (Fig. 5b). This means that CTZ400A represent the brightest and cheapest alternative for Nluc-based assay. However, the luminescence decay for furimazine is slower than that of CTZ400A when using Nluc, a property that could make it a better alternative for long real time imaging. An advantage of Nluc for BRET imaging is the much slower decay of the luminescent signal when compared to Rluc for all substrates tested (compare Fig. 3b and Fig. 5c), allowing the possibility of longer acquisition time to monitor kinetics of biological processes (Fig. 5d). This characteristic has been taken advantage of in recent studies monitoring ligand binding kinetics using BRET-based assays with Nluc[57,58] as well as for real-time BRET imaging of processes occurring over time scale going from minutes to an hour[25]. However, Nluc cannot be used for ebBRET experiments and thus Rluc still represent an advantageous alternative energy donor that is useful for some applications. It should also be noted that many biosensors using Rluc have already been developed and validated and can be readily used for BRET imaging. Novel Nluc-based sensors will certainly be developed but will require rigorous validation before they become available for imaging.

How to select BRET donor and acceptor The choice of the donor-acceptor pairs to use for BRET imaging largely depends on the specific process being imaged. Whether or not real-time imaging is sought, the time scale of imaging needed and the availability of already validated biosensors are all parameters that will influence the choice of BRET pairs.

For many applications, Rluc can be used as the donor in BRET1 (substrate: CTZh; acceptor: Venus) or BRET2 (substrate: CTZ400A or Me-O-e-CTZ; acceptor: GFP10 or GFP2) configurations. If the expression level of the protein fused to the energy donor is low, BRET1 using Venus as the acceptor should be preferred to GFP10 or GFP2 since it provides higher light

output. However, if sufficient luminescence can be detected using blue shifted substrates for Rluc (CTZ400A or Me-O-e-CTZ), GFP2 or GFP10 could be better acceptor choices since BRET2 provides a greater dynamic window. In case where the luminescence signal generated by Rluc with any substrate is too low, Nluc should be the preferred choice using either Aequorea victoria YFP variants[25], or the newly characterized *Discosoma* coral variants, cyan-excitable orange fluorescent protein (CyOFP) and cyan-excitable red fluorescent protein (CyRFP) with furimazine or CTZ400A as substrates. These fluorescent protein variants have excitation peak similar to that of Venus (≈500nm) but have a larger Stokes' shift than Venus, yielding a greater separation between donor and acceptor emission, thus opening possibilities of developing new generations of BRET imaging sensors[59,60]. Figure 5d illustrates the use of Nluc to image the dissociation of Gαq-Nluc from CyRFP-Gγ1 upon sustained stimulation with the angiotensin-II type-1 receptor (AT1R) agonist angiotensin II for 20 minutes. BRET-based ligandbinding assays using Nluc and red-shifted fluorophore BODIPY 630/650 also took advantage of such larger Stokes' shift[18]. Although Nluc can clearly be advantageous for many applications, the existence of many validated sensors based on Rluc also makes that energy donor an appealing choice in many cases, as long as the expression levels are sufficient.

For real-time imaging applications, although Rluc-based BRET1, BRET2 or Nluc-based BRET can all be used, the time-scale of the process to image will determine the best choice. The imaging time being limited by the intensity and the half-life of the luminescence emission, Nluc-based BRET using either furimazine or CTZ400A would be the preferred energy donor because of its brightness and the long emission half-life (≈30 min), allowing imaging for a few hours. The next best choice would be BRET 1 which provides ≈10 times less light than Nluc but 3 times more than BRET2 with a half-life of ≈22 min, limiting the imaging to ≈ 1 hour . Finally,

BRET2 can also be used but the lower light output and the shorter half-time of the signal (≈12 min) greatly limits the imaging time that cannot be perform for more than ≈ 20 min.

Although fluorescent proteins have been used more frequently as BRET energy acceptor, chemical fluorophores can also be used successfully for imaging[19,61]. Generally speaking, the spectrometric properties of chemical fluorophores are superior to fluorescent proteins and good acceptors could be found for all BRET donors. However, the conjugation methods of the fluorophore to the protein of choice need to be developed and optimized for each sensor.

To monitor protein translocation, ebBRET using Rluc as the donor, rGFP as the acceptor and Me-Oe- CTZ as the substrate, is the superior choice. Both the excellent signal to noise ratio and greater efficiency of transfer (due to the direct association of Rluc and rGFP, Fig. 4a) allow to very robustly monitor protein trafficking (see anticipated results) that cannot be readily image using either BRET1, BRET2 or Nluc-based BRET.

Distinguishing signal from noise The above sections describe a number of novel donor-acceptor pairs with improved properties that allow their use for spatio-temporally resolved BRET imaging in various conditions. Still, one of the main limitations of BRET imaging remains the low level of the light output that makes it difficult to distinguish it from noise. The main source of the noise for such lowlevel signals originates from the statistical random fluctuation of the photon counts that is known as 'shot noise'. When considering only the 'shot noise', the signal-to-noise ratio (SNR) increases as the square root of the incoming photon number. If follows that to increase the SNR of BRET images by 2 folds, the amount of light emitted need to be increased by 4 folds. Accordingly, BRET imaging experiment should be designed to maximize the signal output while maintaining all other sources of noise to a

minimum. The different sections of the protocol present technical and experimental procedures aiming at obtaining the best possible spatio-temporal resolution by limiting background noise, increasing light output of the luciferase (see sections on donor and substrates above), improving the separation between donor and acceptor signals (see section on acceptors above), optimizing the light transmission of microscope optics, and finally increasing the sensitivity of the detector. These latter aspects are discussed below.

Microscope setup There are several bioluminescence imaging systems currently available on the market. These include the Olympus LV200 or Atto Cellgraph. These systems are designed to minimize the contamination by external light during measurements, thus increasing signal to noise ratio. When combined with adequate objective lenses and sensitive cameras, these systems can offer excellent performance. However, most wide-field microscope setup equipped with highly sensitive camera should be amenable to perform BRET microscopy with limited modifications. Although the images collected for this report were obtained using a regular inverted microscope, more sophisticated microscopes equipped for PALM, STORM, total internal reflection fluorescence (TIRF), or calcium imaging should also be suitable for BRET microscopy.

In order to minimize the contaminating lights (background noise), the imaging equipment should be placed in a dark room, and the system should be further shielded from stray light by inserting the microscope in a dark box covering the microscope body. All openings of the dark box should be covered by dark seals hermetic to light. All the light from the equipment within the dark box should be turned off or masked and the use of light-emitting devices in the dark room should be minimal. All illumination sources (pilot lamps and indicators) in the dark room

should be masked except for a maximally dimmed computer screen needed for monitoring the image during the acquisition. To verify the influence of external light, acquisition obtained in the absence of sample with the camera shutter closed should be compared to those obtained when the shutter is open. When comparing mean signal intensity between these two acquisitions, differences of 1 photon/pixel/minute or less should be targeted using non-amplified camera or EMCCD in photon counting mode.

The microscope should be equipped with objective lenses having high light-collecting capacity. The image brightness is known to be influenced by three objective lens parameters: transmission (TR), numerical aperture (NA) and magnification (M), and determined by the following formula.

$$(\text{Image Brightness}) \propto \text{TR} \times \frac{(NA)^2}{(M)^2}$$

Therefore, they are the most important parameters to consider in selecting objective lens for BRET imaging. Optimal lens magnification (M) is dependent on the surface area of detector used. We usually combine 60x or 100x lens with 13mm x 13mm detector. It should be noted that sample brightness using 100x lens is approximately 30% of that obtained with a 60x lens. Objective lens should be oil immersion or water immersion having the highest available NA. Most high-quality objective lenses have high light transmission (TR) properties across the entire visible light spectrum. However, some lenses may have lower transmission in BRET2 assays, which emits violet light that is at the lower edge of the visible spectrum. However, this limitation can be partly solved using lens specifically designed for fluorescence measurement since they tends to have higher transmission in UV-violet range. The 100x objective lens that we are using for BRET imaging (CFI Apocrimat TIRF, Nikon) has a TR that drops from 82% at 510 nm to

48% at 400 nm. The relative transmission efficacy of the lenses can vary significantly between lens types and should be evaluated to select the best ones for the BRET pairs used as a function of the wavelength to be monitored.

Detector Due to the low signal, BRET imaging requires very sensitive cameras. The detection sensitivity of the cameras is mainly determined by two parameters: 1) the quantum efficiency (QE) and 2) the pixel size of the detector. In many scientific cameras, the peak QE at 500-600 nm is very high (80-90%), but drops rapidly to 10-60% in the UV-violet range, greatly compromising the detection sensitivity and thus the quality of the images when using short wavelength donor or acceptor. This is of particular concern for BRET2 assays, which requires imaging of 400 nm violet signals originating from the luminescent donor. Therefore, the spectral response of the camera should be examined very carefully to select its QE characteristics as a function of the type of BRET imaging assays considered. The pixel size is the surface area of a single pixel on the sensor unit. Depending on the camera, it may range from 5 µm x 5 µm to 24 µm x 24 µm. The larger surface area has more chances to catch photon, and improve signal captured per pixel. Cameras having binning functions can bundle several pixels and treat the signal as if it was originating from one single pixel. Although larger pixels allow the detection of lower signals, making the camera more sensitive, it results in lower resolution image. The choice of a given pixel size is therefore always a compromise between sensitivity and resolution. We usually use 170 µm2 (13 µm x 13 µm) or 680 μm^2 (26 µm x 26 µm, 2 x 2 binning of 13 µm x 13 µm) pixel surface area using EMCCD or CCD camera, respectively. Ideally, the size of the detector chip used should be around 13 mm x 13 mm (1024 x 1024 pixels of 13 µm x 13 µm pixels). This is based on the standard field of view (FOV) of microscope (18 mm). Depending

on the combination of microscope system and objective lens, larger detector chips might be used without overfilling the FOV.

The typical signal detected in BRET imaging is a couple of photon per pixel per second (1-10 e- /pixel/sec) in our system. In order to limit the impact of the 'shot noise' at a reasonably low level (< 10dB), we usually adjust exposure time so that the area of interest from the image correspond to at least 100 photons captured per pixel. In addition to 'shot noise', another type of noise reducing image quality is known as 'thermal noise' or 'dark current' and correspond to the random signal generated by thermal electrons produced by the camera itself. To reduce the thermal noise, the camera should be equipped with a cooling unit. In deep-cooled (typically below -60°C) cameras, thermal noise is usually less than 0.01 e-/pixel/sec and it is small enough for good BRET imaging. For the images presented in this report, we used either thermo-electric cooling (Pixis camera) or liquid-nitrogen cooling (NuVu camera).

The final distinguishing factor between cameras is the 'readout noise', which originates from the signal processing of the camera circuit. EMCCD cameras are getting increasingly popular for low-light imaging because they have a lower 'readout noise' relative to the signal. This is achieved by amplifying the photoelectron signals with high gain. However, the multiplication process of EMCCD also amplify other sources of noise[62], it is therefore recommended to use EMCCD camera in photon counting mode[63] in order to mitigate this negative effect of the high-gain amplification. Using a photon counting strategy is also useful to minimize the impact of the cosmic rays on the image. Indeed, because the photon counting image is generated as an integration of many (500-1,000) binary images with very short exposure, the high-energy signal from the cosmic ray is treated as a single photon entry and therefore is diluted in the entire

integrated image. Table 1 shows the comparison of the total noise level between CCD and EMCCD used in photon counting mode or conventional mode. When the signal is strong enough, the noise level is similar between the two types of camera independently of the detection mode because it reflects mainly the 'shot noise'. In contrast, when the signal is very low, EMCCD in photon counting mode shows much lower noise level than CCD or EMCCD in conventional mode. As a result, EMCCD in photon counting mode has a lower detection limit. This probably reflects the stochastic noise known as excess noise factor[62]. Photon counting is ,indeed, known to be an effective way to reduce such noises in low light condition[63]. Another advantage of EMCCD photon counting mode over conventional EM mode, results from the lower detrimental influence of baseline signal drift that are sometime observed as a function of imaging time since the threshold used for photon counting is significantly higher than the baseline signal.

EMCCD is also preferable to CCD when short exposure times are required as in the case of real time imaging. This is well illustrated in Figure 6a, where a weak luminescent signal could be detected for exposure times as short as 0.1 to 0.2 sec using an EMCCD camera but could not be detected with exposure time smaller than 0.5 to 1.0 sec with a CCD. Yet when signal is of sufficient intensity, good quality images can be obtained with both CCD and EMCCD. Indeed, Figure 6b shows that the BRET between the G protein subunits Gαq-RlucII and GFP10-Gγ1 expressed at the cell surface of HEK293 cells could be readily imaged with both cameras.

Based on these observations, we recommend EMCCD camera with photon counting mode as the preferred detector system for BRET imaging. However, it should be noted that photon counting narrows the linear range of quantification. Therefore, when the number of photons per

pixel is more than 0.5 per image, counting become inaccurate compared with other methods[63]. Therefore, exposure time should be adjusted in order to avoid signal saturation.

MATERIALS

BIOLOGICAL MATERIALS

● Cells of interest. In this example we use HEK293T cultured human embryonic kidney cells (American Type Cell Culture Collection (ATCC), cat. no. CRL-3216). The use of this protocol is not limited to HEK293T cells and any other cell types that can express sufficient levels of luciferase- and GFP-fused constructs can be used. **CAUTION** The cell lines used in your research should be regularly checked to ensure they are authentic and are not infected with mycoplasma.

REAGENTS

CRITICAL Although the suppliers used for all listed reagents are provided, alternatives exist in most cases. None of the reagents are harmful as long as they are handled according to general laboratory practice.

● Dulbecco's modified eagle medium (DMEM) (Wisent Inc., cat. no. 319-015-CL)
● Fetal bovine serum (Wisent Inc., cat. no. 080150)
● Penicillin streptomycin mixture (Wisent Inc., cat. no. 450-201-EL)
● Trypsin EDTA mixture (Wisent Inc., cat. no. 325-542-EL)
● Dulbecco's phosphate buffered saline (DPBS) (Wisent Inc., cat. no. 211-410-XK)
● Xtreme GENE9 transfection reagent (Roche diagnostics, cat.no. 0636578700)
● Sodium chloride (Laboratoire MAT, cat. no. SR-0091)
● Potassium chloride (SIGMA, cat. no. P-9541)

● Potassium dihydrogen phosphate (SIGMA, cat. no. P5379)

● Sodium dihydrogen phosphate (SIGMA, cat. no. S0751)

● Calcium chloride (SIGMA, cat. no. C7902)

● Magnesium chloride (Laboratoire MAT, cat. no. MR-0103)

● HEPES (Sigma, cat. no. H4034)

● Anhydrous Ethanol (Greenfield Speciality Alcohols, cat. no. P016EAAN)

● Molecular Sieves 4Å (SIGMA, cat. no. M2635)

Luciferase substrates

CRITICAL Luciferase substrates (CTZh, CTZ400a, Me-O-e-CTZ, Me-O-CTZ-O-Me and furimazine from Nano-Glo kit) are light sensitive and unstable in aqueous solutions. Solutions should be prepared as described in Reagent Setup section.

● Coelenterazine h (CTZh, NanoLight Technology, cat. no. 301)

● Coelenterazine 400a (CTZ400a, NanoLight Technology, cat. no. 340)

● Methoxy e-CTZ (Me-O-e-CTZ and Prolume Purple) (NanoLight Technology, cat. no. 369)

● Methoxy CTZ-Methoxy (Me-O-CTZ-O-Me, Prolume Purple II) (NanoLight Technology, cat. no. 367)

● NanoFuel Solvent (NanoLight Technology, cat. no. 399)

● Nano-Glo Luciferase assay kit (Promega, cat. no. N1110)

EQUIPMENT

Cell culture

● 75 cm2 cell culture flasks (Falcon, cat. no. 353136)

● 35 mm glass bottom poly-d-lysine-coated culture dishes (Mattek Corp., cat. no. P35GC-1.5-14-C)

● 15 ml centrifuge tubes (Falcon, cat. no. 352096)

● 50 ml centrifuge tubes (Falcon, cat. no. 352070)

● 1.5 ml microcentrifuge tubes

● Cell incubator (37°C, 5 % (vol/vol) CO2)

● Biological safety cabinet

● Refrigerator (4°C and -20°C)

BRET imaging

● Inverted microscope (Nikon Eclipse Ti-U)

● EMCCD camera (NöVö Cameras, EM N2)

● Objective lens (Nikon CFI Apochromat TIRF 60x Oil NA 1.49)

● Objective lens (Nikon CFI Apochromat TIRF 100x Oil NA 1.49)

● Cooled CCD camera (Princeton Instruments, Pixis 1024B)

● Optical filter changer (Sutter instruments, Lambda 10-2). **CRITICAL** The motorized filter wheel of Lambda filter changer has an infra-red LED inside the filter wheel for filter turret positioning, and this can be a possible source of light contamination. Lambda filter changer can be modified by the manufacturer to allow turning off the LED during measurement. Alternatively, you can install an infrared blocking filter in front of the camera.

● Optical filters (550/80 nm for BRET1, 480 nm longpass for BRET2, 550 nm longpass for Nluc with CyOFP or CyRFP) 25mm diameter.

● Motorized focus controller (Prior, Proscan)

● Microscope epi-fluorescence illumination (470 nm LED, Thorlabs, M470L3)

● Digital I/O interface (National Instruments, USB-6501)

● Metamorph 7.8 data acquisition software (Molecular Devices). **CRITICAL** In our experiments, all microscope hardwares are controlled using MetaMorph version 7.8, but other instrument control softwares (such as LabVIEW, MATLAB or LabWindows) can be equally used. **CRITICAL** The image analyses presented were performed using MetaMorph version 7.8. However, most of the analysis software that support color-mapping and image arithmetic processing (such as imageJ or MATLAB) can be used.

● Computer system: Windows 7. The system should be equipped with enough PCI card slots, USB ports and serial ports depending on the devices connected to the microscope.

REAGENT SETUP

Cell culture. In the example described in this Protocol (HEK293T cells), the cell culture medium is Dulbecco's Modified Eagle Medium supplemented with 10 % (vol/vol) fetal bovine serum, 100 units/ml penicillin and 100 μg/ml streptomycin. Cell culture medium can be stored at 4°C for up to 4 weeks, not exceeding expiration date of the medium. Maintain HEK293 cells

at 37°C in 5 % (vol/vol) CO_2. Based on a doubling time of approximately 20 hrs, cells should be split in 1:10 to 1:20 (vol:vol) twice a week using a trypsin/EDTA solution to detach the cells.

Modified Hank's balanced salt solution (HBSS). Prepare the following solution from a 10x concentrated stock: 137.9 mM NaCl, 5.33 mM KCl, 0.44 mM KH2PO4, 0.33 mM Na2HPO4. The 10x stock solution can be stored at room temperature (21±2°C) for up to 12 months. Freshly prepare 1x solution and add 1 mM CaCl2, 1 mM MgCl2 and 10 mM HEPES pH 7.4 on the day of experiment.

Substrate (Coelenterazine) solution. Dissolve CTZh and CTZ400A in anhydrous ethanol to generate 1 mM stock solutions. The Ethanol used to dilute the coelenterazines should be completely anhydrous by adding 4Å molecular sieves. Dissolve Me-O-e-CTZ and Me-O-CTZ-O-Me in NanoFuel solvent to generate 2 mM stock solutions. Dilute Furimazine from the Nano-Glo Luciferase assay kit (Promega) with the buffer provided with the kit. All substrate solutions should be stored desiccated, in the dark at -20°C for up to 1 month. Prepare the diluted working concentrations immediately before use.

EQUIPMENT SETUP

Detectors. We recommend EMCCD camera using photon counting acquisition mode. However other types of deep-cooling camera can also be used (see the subsection 'Detectors' in the Experimental design section above).

Culture ware. We are using poly-d-lysine-coated culture dishes for BRET imaging. This is because the attachment of HEK293 cells on glass is weak and cells can detach from the culture surface during washing or treatment steps. Other surface treatments can be used if they provide sufficient cell attachment. The thickness and material of the culture surface should be

compatible with the specification of the objective lens used. Usually, objectives are designed to be used with a cover glass of 0.17mm thickness, and we recommend to use #1.5 thickness (0.16-0.19 mm) glass bottom culture ware. We use commercially available pre-coated culture ware. Alternatively, culture dishes can be coated in the laboratory using cell culture grade 0.1 mg/ml poly-d-lysine solution. In that case, the bottom of the dishes should be covered with 1 ml of poly-d-lysine solution for at least 1 hour, and wash twice with 2 ml of distilled water just before use.

Optical filters. Adequate filter pairs for the BRET donor and acceptor need to be installed in a filter wheel that allows rapid exchange between filters (see section Equipment for a description). The filters to be installed vary according to the BRET configuration used. Filters typically used for BRET1, BRET2, and Nluc-BRET assays are listed in the Equipment section. Because BRET can be calculated by dividing the signal detected in the acceptor channel by the total luminescence, the donor filter position can be left empty.

Microscope Hardware Connection. The imaging device (EMCCD camera or cooled-CCD camera) requires a fast connection, such as Camera Link, GigE Vision or USB2/3. However, because BRET/luminescence microscopy requires a long exposure time, other devices (ex: filter wheels, focus controller, illumination, etc.) do not require very precise timing, and can be controlled through conventional serial ports or TTL outputs. In our setup, the EMCCD camera is connected to the computer with a Camera Link frame grabber board supplied by the camera manufacturer. A cooled- CCD camera is connected via USB2. Optical filter changer and motorized focus controller is connected using serial port. Epi-fluorescence and bright field

illuminations are controlled through TTLswitch or power relays accepting TTL inputs to prevent accidental activation during luminescence measurements.

PROCEDURE

Cell Preparation. TIMING: 30 min seeding cells + 24 h incubation + 1 h for transfection + 48 h incubation

1| Three days before imaging, seed 1x105-3x105 HEK293T cells into 35 mm poly-d-lysine coated glass bottom culture dishes (see Equipment Setup) in 2 ml fresh medium. Incubate the cells at 37°C in 5 % (vol/vol) CO_2 for 24 hours.

2| Two days before imaging, transfect cells with the Luc-tagged BRET donor and GFP-tagged BRET acceptor. For each dish, dilute 3 µl of X-treme GENE 9 DNA transfection reagent with 100 µl of FBSfree culture medium and mix with a total of 1µg of DNA in an eppendorf tube. Vortex and add dropwise to the cells. Incubate the cells at 37°C in 5 % (vol/vol) CO_2 for 48 hours.

CRITICAL STEP: The ratio of expression between BRET donor and acceptor can critically affect the BRET signal level. See Box 1 for guidance on how to determine the adequate donor/acceptor ratio.

3| (Optional) | If the aim is to test the effect of pre-treatment with a drug of interest, add the drug or the vehicle (used as control) into the well of the glass-bottom culture dish and incubate the cells at 37°C in the cell culture incubator for the time of the treatment (see Anticipated Results).

CRITICAL STEP Some drugs may have physicochemical properties (ex: pH, ionic strength, color, red-ox activity, etc…) that may interfere with the luciferase signal, either by affecting the enzyme activity or by having optical properties that affect the readings (ex: quenching, autofluorescence, etc). In order to control for these potentially artefactual effects, the impact of

the drug treatment is tested on the signal from the luciferase expressed alone and/or on a control fusion protein linking the energy donor to the acceptor. If the drug treatment significantly affect either the luminescence signal or the BRET signal from the control fusion protein, such treatment should be avoided.

BRET image acquisition using an EMCCD camera. TIMING 1 h for setup + 10-120 min/dish (depending on the experimental design) for acquisition

4| Turn on the microscope system and launch the image acquisition software. Set the cooling temperature of the camera.

CAUTION We are using a liquid-nitrogen cooled camera. If such a cooling system is used, the ventilation of the microscope room should be verified before starting to fill the liquid-nitrogen tank. Most of the deep-cooling cameras on the market are equipped with Peltier (thermoelectric) cooler.

5| After the camera temperature has reached -85°C, set the EM-gain. We usually use a calibrated EM-gain of 3,000.

CRITICAL STEP Monitor the camera temperature and wait until the sensor unit is fully cooled-down and stabilized. The reading should be performed at a camera temperature that minimize dark noise caused by thermally generated electrons. For our camera, -85°C was selected.

CRITICAL STEP The 3,000 EM-gain value is used for our camera (NüVü EM N2). If a different EMCCD camera is used in photon counting mode, the EM-gain should be set to the

maximal value for the specific camera used. For intensified CCD or EMCCD in conventional acquisition mode, the amplification gain should be determined to maximize SNR.

6| Obtain a dark image: Turn off all microscope illuminations and room lightings. Close microscope dark box. Set the EMCCD camera to photon counting mode. Send a command to filter changer and remove the filter in front of the camera. In order to confirm that there is no external light contaminating the image, set the exposure time to 0.1 sec and repeat 100-200 successive photon counting measurements without filters. Integrate all photon counts for each pixel and generate one image without mounting samples. All pixel values should be close to zero and show only uniform white noise.

CRITICAL STEP Make sure to turn off all illuminations before activating the camera. Exposing EMCCD to excessive light can damage the imaging unit.

CRITICAL STEP To acquire image in non-photon counting mode, either using a cooled-CCD camera or the EMCCD camera, the same procedure can be used, but because of the lower sensitivity of the camera, longer exposure times are required to get images with sufficient signal to noise ratio and resolution. Also, because the dynamic range in non-photon counting mode is wider, there is no need to obtain multiple frames of the same images and therefore integration of multiple images is not required. In that case, we are setting total exposure time so that the signal strength of the area of interest is at least 5-10 times higher than the noise level rms of a blank image having the identical exposure time. This critical step also applies to steps 10-13.

?TROUBLESHOOTING

7| After confirming that the camera stopped recording, turn on the room lightings and bring out one culture dish (from Step 2) from the cell incubator. Remove the cell culture medium, wash

the cells once with 1 ml HBSS and remove the HBSS without drying the cells. For long time-course experiments, phenol red-free culture medium can be used instead of HBSS in order to minimize morphological and physiological changes. However, it should be noted that we obtain weaker signal strength and higher background in culture medium vs. HBSS, most likely due to some form of quenching and spontaneous oxidation of substrates.

8| Open the dark box and mount the dish on the microscope. Focus on a field of cells using bright field or epi-fluorescence illumination.

9| Add 500 µl of HBSS containing the adequate amount of luciferase substrate. We typically use 10-20 µM of CTZh for BRET1 and 10-20 µM of Me-O-e-CTZ for BRET2 and enhanced bystander BRET measurements. We use 10-20 µM of CTZ400a for the Nluc and CyOFP/CyRFP BRET pair.

10| Set up focus (image preview): Turn off all microscope illuminations and room lightings. Close the dark box. Set image exposure time at 0.1 sec and obtain 5 frames without filter. Generate an image by integrating the photon counts from the 5 frames. Continuously generate images and based on these coarse images, move the microscope stage and focus on cells of interest (i.e.: luminescent cells). Stop recording when focusing is finished.

CRITICAL STEP This step describes our default setting for EMCCD camera in photon counting mode. For other types of camera, simply start live imaging with adequate exposure time according to the sensitivity of the camera. Typically, non-amplifying camera requires 5-10 sec exposure to obtain luminescence images.

CRITICAL STEP Make sure to turn off all illuminations before activating the camera. Exposing EMCCD camera to excessive light can damage the signal multiplier.

11| Generate the BRET image: Set the exposure time to 0.1 sec. Obtain 100 photon counting frames without filter and generate the total (donor and acceptor) luminescence image. Then send a command to filter changer to insert the acceptor filter (corresponding to acceptor emission bandwidth, 480 nm longpass in the case of BRET2, see section Equipment for a complete list. Wait until the filter wheel stops moving (~0.1s, depending on wheel model and position of filters). Obtain another 100 frames and generate the acceptor luminescence image, and remove the acceptor filter again using the filter changer. The acquisition of the two images takes approximately 25 sec. Repeat acquisition of the two images (100 photon counting frames at a time) until the total photon counts of the pixels in the region of interest reach approximately 100 counts. Typically, 10 cycles (1,000 frames each for total and acceptor) of acquisition will be required to obtain high quality images.

CRITICAL STEP In order to maximize the number of photons collected to optimize the image quality, we recommend not using filters during the first (donor) measurement and calculating BRET as a ratio between acceptor emission and total luminescence. However, BRET can also be calculated as a ratio between acceptor emission and donor emission using a filter corresponding to donor wavelength during the first measurement.

CRITICAL STEP This step is describing our default setting for EMCCD camera in photon counting mode. For other types of camera, capture single image with adequate exposure time according to the sensitivity of the camera.

CRITICAL STEP The linearity of the measurement can be affected if any given pixel is saturated (ie: if one pixel is excited by more than one photon). To avoid such inaccurate photon

counting, we recommend to select exposure times that lead to the detection of any given pixel less than in 50 frames out of 100 frames[63].

Optional: Time-lapse recording. TIMING depending on the experimental design

12| To assess the dynamics of the process being imaged, perform time-lapse imaging by repeating step 11 several times.

CRITICAL STEP Although the light signal originating form luciferase decays over time, the BRET values will still be valid because it is a ratiometric measurement. However, a minimal luminescence signal is required to maintain image quality. The minimum signal strength required for proper image analysis may differ for different subcellular compartments but generally need to be between 25-100 counts/pixel over 1,000 frames. Since different substrate/luminescent enzyme pairs have different brightness and time decays (see Figs. 3 and 7), the time of continued imaging will vary according to the BRET configuration used.

13| (Optional) When the aim is to monitor the real-time effect of drug treatments, add the drug of interest after 5 minutes of time-lapse imaging, manually adding the drug in an additional 500µl of HBSS and continuing imaging for 15 to 30 minutes (see Anticipated Results).

Image Analysis. TIMING 1-2 h

14| Launch the image analysis software and open the total luminescence images for all acquired frames. Select the image of interest and integrate the photon counts for each pixel using the arithmetic/addition function of Metamorph. Open time-matching acceptor images and integrate the photon counts for each pixel using the same arithmetic/addition function. Save as integrated total (A) and acceptor (B) images, respectively.

15| Calculate the BRET ratio for each pixel. In the case of Metamorph, use the arithmetic/divide function with the following formula:

(Ratiometric image (C)) = (Acceptor count image (B)) * 1,000 / (Total count image (A)).

For other software, divide signal level of (B) with (A) and multiply with 1,000 for all corresponding pixels. The multiplication factor of 1,000 is used because most image analysis software (including Metamorph) cannot handle values lower than 1 that result from the division.

CRITICAL STEP Note that the pixel values calculated here are affected by the difference in the camera sensitivity (quantum efficiency) and optical transparency between the two channels (total vs acceptor). Because microscopy systems (cameras and lenses) usually have lower sensitivity for BRET2 donor luminescence (400 nm) compared with longer wavelengths, the pixel value may not reflect the real ratio of the number of photons released. It follows that the calculated BRET values will be different from those obtained using spectrometric systems with PMTs. Yet, as long as the measurements do not fall outside of the linearity range of the camera, the image BRET values are proportional to the real transfer and thus can be quantitatively compared to one another.

CRITICAL STEP To obtain good quality BRET image that can be reliably quantified, we calculate BRET as the ratio of the light emitted in the acceptor channel divided by the total luminescence detected instead of the ratio of light emitted in the acceptor channel over that in the donor channel that is generally used in spectrometric BRET measurements. The reason for using the total luminescence as the denominator of the ratio is because, in ebBRET in particular, the transfer of energy is extremely efficient, yielding to important decreases in the light emitted in the donor channel, rendering the donor signal more susceptible to noise factors. In addition

the reduced donor signal left after transfer can be too low for proper imaging, decreasing the sensitivity of the assay and increasing the variability. In contrast, using the total luminescence signal as the denominator provides reliable ratiometric values, which robustness is not affected by the extent of transfer.

16| Attribute a heat map to the ratiometric image (C). For the analysis with Metamorph, set LUT mode to pseudocolor and adjust the color scale so that all interesting regions are within the range of the pseudocolor rainbow hue, without saturation. Typically, we attribute 0 to purple (lowest signal) and 800 to red (highest signal). For time-lapse experiments, apply the heat map having the same signal range to all frames. Convert the image to RGB image (24bit/pixel TIFF) and save as the raw BRET image (D).

17| Open the total luminescence image (A). Scale the image so that the image grayscale covers the entire image using the 0.5% brightest pixels as white and the 0.5% darkest pixels as black. Convert the image to 8 bit/pixel monochrome TIFF and save as signal strength image (E)

18| Correct the raw BRET image (D) as a function of signal strength image (E) for each pixel. Because 24bit/pixel TIFF has 8bit depth for red, green and blue channels, calculation in Metamorph is as follows. (raw BRET (D)) * (signal strength (E)) / 256 For other software, multiply each pixel value of R, G, B plane of image (D) with the value of corresponding pixel from image (E) and divide by 256. The resulting image shows the BRET signal level of each pixel.

19 (optional) If quantification of BRET signal originating from different cell compartments is required, a mask corresponding to the region of interest need to be prepared, total photon counts

from donor and acceptor within each of the region of interest should be integrated and BRET calculated as presented in Supplementary data 1.

TROUBLESHOOTING

Step 6: Background signal and contaminating light

If the camera does not have the function to subtract pixel bias (resulting from the variability of the individual detector sensitivity in the camera detector array) automatically, a 'bias image' also known as 'bias frame' need to be generated manually under no illumination condition. Prepare the bias image using the following procedure:

- Close the camera shutter.

- Set the exposure time to zero or a very small value. Obtain 5-10 images.

- Generate the bias image by calculating medians of each pixel using all captured images.

The bias image should be subtracted from all following images. In order to remove the influence of sporadic high-energy artifacts (e.g. cosmic rays), the bias image should be generated using the

medians and not the average of each pixel for the 5-10 images obtained.

If the source of contaminating signal remains after the bias subtraction, this can have a number of causes:

- Light contamination: Block the light source causing the contamination. The motorized microscope components using infrared LEDs to adjust the position of the moving parts may also cause interference. Turning off the infrared LEDs when not in use or use a filter to block the light.

- Elevated camera dark current: Check if the cooling system of the CCD is working correctly and adjust appropriately.

- Cosmic rays: They classically cause bright dots or lines showing up randomly on the image. It is not practical to shield the cosmic rays because they have very high energy. Photon counting measurement with EMCCD compared to traditional imaging mode drastically decreases the contribution of cosmic rays. When using non-photon counting mode for image acquisition, the best way to remove the influence of cosmic rays is to capture 5-10 images and to generate the final image by calculating the medians values and not the average for each pixel.

- Auto-oxidation of substrates: Coelenterazines are unstable in aqueous solutions and emit light by auto-oxidization. The auto-oxidation of substrate is observed as a uniform increase of the background signal. The increase is relatively low when balanced-salt solution is used as the assay medium. However, it might be problematic for other assay media, such as serum containing medium.

TIMING

Steps 1-2, cell preparation: 30 min seeding cells + 24 h incubation + 1 h for transfection + 48 h incubation

Steps 3-10, Microscope, camera and sample setup: 1 h

Steps 11-13, Image acquisition: 10-120 min/dish depending on the experimental design

Steps 14-19, image analysis: 1-2 h.

ANTICIPATED RESULTS

Examples of BRET images that can be expected are provided in Figures 4-7 .A comparison of BRETimage intensity obtained in three different BRET modes (BRET1, BRET2 and ebBRET) is presented in Figure 4. The data were obtained with constructs genetically fusing the energy donor to the acceptor, providing excellent controls to test the imaging systems. Although ebBRET provides the brightest images, it cannot be used to monitor specific interactions between protein partners since it takes advantage of the self assembly between Rluc and rGFP when they are present in the same compartment and could promote interactions between proteins that do not interact with one another normally. Thus, it is mainly suitable to monitor translocation between compartments.

When comparing BRET1 and BRET2, although weaker luminescence is emitted in BRET2, the better separation of the acceptor and donor signals clearly increase the dynamic window of the BRET signal, allowing better imaging when compare to BRET1. This is illustrated in Figure 4a that shows images of total luminescence emitted (left panels), the light emitted by the acceptor (middle panels) and the calculated BRET signal (right panels) for cells expressing the donor alone (βarrestin2-RlucII, row 1 and 3) or a fusion between RlucII and either Venus (BRET1; row 2) or GFP2 (BRET2; row 4) upon addition of CTZh (row 1 and 2) or Me-O-e-CTZ (row 3 and 4). As can be readily observed, a much greater background BRET signal is observed in BRET1 in the absence of acceptor (Fig. 4a, top row, right image and Fig. 4b, BRET1 donor only). This results from the overlap between the wide emission spectrum of Rluc and the emission of Venus, yielding a greater contamination of the donor emission signal in the acceptor channel (Fig. 4a, top row, middle image). A much lower background BRET is observed in BRET2. Since similar maximal BRET signals are observed for BRET1 and BRET2 (Fig. 4b, donor + acceptor), the lower background results in a much greater dynamic BRET window

(maximal/background signals) for BRET2 (6.5 fold in BRET2 vs 1.7 in BRET1) (Fig. 4b). It follows that, although BRET1 generates brighter and longer lasting signals that can be useful for imaging proteins expressed at low levels for extended periods of time, the dynamic window offered by BRET2 allows better separation between background and specific signals (Fig. 4c), making it a better choice for imaging when the process studied leads to small differences in BRET signals. Also shown in Fig.4, is the fact that the BRET dynamic window observed for ebBRET is larger than both BRET2 and BRET1 due to the high transfer efficiency observed for this donor/acceptor pair, making it the best choice to monitor protein translocation (see below).

Wide range of biological processes can be imaged by different BRET modalities. For example, we used BRET2 to monitor the activation of a heterotrimeric G protein (Gαqβ1γ1) by AT1R (Fig. 7a). The separation between Gα and Gβγ can be detected by measuring the decrease in BRET signal between the Gαq tagged with RlucII, and Gγ tagged with GFP10 following the activation of the receptor by angiotensin. This type of approach can be used to monitor the dynamic regulation of any proteinprotein interaction. Both BRET increase and BRET decrease can be monitored, depending on the effect of a particular stimulus on the interaction. In Figure 7b, we illustrate the use of ebBRET to image the subcellular redistribution of AT1R and the regulatory protein βarrestin following activation with the AT1R agonist, angiotensin-II. The translocation of βarrestin to the plasma membrane upon receptor activation is visualized by monitoring the BRET between βarrestin2-RlucII and rGFP tagged with a CAAX box from KRas (rGFP-CAAX)[64] that targets it to the plasma membrane (Fig. 5b, top panels). The ensuing agonist-promoted endocytosis of the receptor that occurs can also be detected by imaging ebBRET between AT1R-RlucII and rGFP targeted to either the plasma membrane (rGFPCAAX) or the early endosomes using the early endosome localization motif, FYVE from

endofin[65] (Fig. 7b, middle and bottom panels, respectively). The use of rGFP selectively targeted to distinct subcellular organelles allows monitoring the localization of a Rluc-tagged protein in these specific organelle. Here, examples for plasma membrane and endosome are provided, but similar experiments can be done for other compartments such as endoplasmic reticulum, Golgi, nucleus, mitochondria, etc.…

The comparison between control and angiotensin-stimulated conditions for βarrestin translocation (Fig. 7b, top panel) was done using the same cell population by taking images before and after treatment. This is made possible because the recruitment of βarrestin to the plasma membrane is relatively rapid following agonist treatment and thus can be monitored in real time before the luminescence signal decays to levels that compromise image quality. However, in the case of the receptor endocytosis (Fig 7b, middle and bottom panels), the control and angiotensin conditions needed to be imaged in different cell populations because the luminescence signal decayed to levels incompatible with quality imaging before reliable endocytosis can be observed. It is important to note that statistically significant differences can be obtained between control and stimulated conditions, both when assessing the phenomenon in the same cell or in different sets of cells (supplementary Fig 1).

Quantification of BRET signals in different subcellular compartments can also be achieved. This is illustrated in Figure 8 that image the dissociation of Gαq-Rluc from GFP10-Gγ1 upon stimulation of AT1R. For this purpose, bright cells from the field of view are manually segmented (panel a, cell mask) and the BRET determined for each cell by dividing the light signal emitted in the acceptor channel over the total light detected. The individual BRET values for each cell is then averaged and the values obtained under basal and receptor stimulated

conditions are compared. As shown in Figure 8b, receptor stimulation leads to a statistically significant reduction in BRET. Next, the quantification is performed on a subcellular domain by dividing each cell area into a peripheral and a central region (panel a, central 50% and peripheral 50%) so to isolate the signal largely originating from the plasma membrane. Figure 8c illustrates the distribution of pixel-by-pixel BRET levels for the population of cells in the field of view expressed as histograms for both untreated and angiotensinstimulated conditions. As can be seen, receptor activation leads to a reduction of the frequency of high BRET pixels. When considering only the signal coming from the periphery, receptor stimulation leads to a statistically significant reduction of the BRET signal (histogram in panel Fig. 8d), indicating that the receptor-promoted dissociation of Gαq-Rluc from GFP10-Gγ1 occurring at the cell surface can be detected and quantified. The raw image data, the cell masks and the MATLAB script used for this quantification are available as Supplementary Data 1.

DATA AVAILABILITY

The authors declare that all data supporting the findings in this study are available from the corresponding author upon request.

AUTHOR CONTRIBUTIONS

M.B. and H.K. conceptualized the method, designed the experiments and wrote the manuscript. H.K. assembled the imaging system, performed the imaging experiments and analyzed the images. AM. S. and L-P.P. designed and generated constructs for BRET microscopy. L-P.P. performed the comparison between the spectrometric characteristics of the different luciferase constructs and participated to the writing of the manuscript.

ACKNOWLEDGMENTS

This work was supported by a Foundation grant from the Canadian Institutes for Health Research (CIHR) [FDN148431] to MB. L.-P.P. received scholarships from CIHR and the Fonds de la Recherche du Quebec – Santé (FRQ-S). A.M.S. received a post-doctoral fellowship from FRQ-S. M.B. holds a Canada Research Chair in Signal Transduction and Molecular Pharmacology. Authors are grateful for the Canadian Space Agency (CSA) loaning the EMCCD camera for BRET imaging, and NüVü Cameras for the technical assistance and developing the camera driver for the Metamorph software. The authors are grateful to Dr. Monique Lagace for her critical reading of the manuscript.

COMPETING INTERESTS

The authors declare no competing financial interests

REFERENCES

1. Förster, T. Zwischenmolekulare Energiewanderung und Fluoreszenz. *Ann. Phys.* **437,** 55– 75 (1948).
2. Jares-Erijman, E. A. & Jovin, T. M. FRET imaging. *Nat. Biotechnol.* **21,** 1387–1395 (2003).
3. Berney, C. & Danuser, G. FRET or No FRET: A Quantitative Comparison. *Biophys. J.* **84,** 3992–4010 (2003).
4. Angers, S. *et al.* Detection of beta 2-adrenergic receptor dimerization in living cells using bioluminescence resonance energy transfer (BRET). *Proc. Natl. Acad. Sci. U. S. A.* **97,** 3684–3689 (2000).
5. Xu, Y., Piston, D. W. & Johnson, C. H. A bioluminescence resonance energy transfer (BRET) system: application to interacting circadian clock proteins. *Proc. Natl. Acad. Sci. U. S. A.* **96,** 151–156 (1999).
6. Ayoub, M. A. *et al.* Monitoring of ligand-independent dimerization and ligand-induced conformational changes of melatonin receptors in living cells by bioluminescence resonance energy transfer. *J. Biol. Chem.* **277,** 21522–8 (2002).
7. Mercier, J.-F., Salahpour, A., Angers, S., Breit, A. & Bouvier, M. Quantitative assessment of beta 1- and beta 2-adrenergic receptor homo- and heterodimerization by bioluminescence resonance energy transfer. *J. Biol. Chem.* **277,** 44925–31 (2002).
8. Galés, C. *et al.* Real-time monitoring of receptor and G-protein interactions in living cells. *Nat. Methods* **2,** 177–84 (2005).

9. Galés, C. *et al.* Probing the activation-promoted structural rearrangements in preassembled receptor-G protein complexes. *Nat. Struct. Mol. Biol.* **13,** 778–786 (2006).

10. Kobayashi, H., Ogawa, K., Yao, R., Lichtarge, O. & Bouvier, M. Functional rescue of betaadrenoceptor dimerization and trafficking by pharmacological chaperones. *Traffic* **10,** 1019– 1033 (2009).

11. Hamdan, F. F., Audet, M., Garneau, P., Pelletier, J. & Bouvier, M. High-throughput screening of G protein-coupled receptor antagonists using a bioluminescence resonance energy transfer 1-based beta-arrestin2 recruitment assay. *J. Biomol. Screen.* **10,** 463–75 (2005).

12. Charest, P. G. & Bouvier, M. Palmitoylation of the V2 vasopressin receptor carboxyl tail enhances beta-arrestin recruitment leading to efficient receptor endocytosis and ERK1/2 activation. *J. Biol. Chem.* **278,** 41541–51 (2003).

13. Terrillon, S., Barberis, C. & Bouvier, M. Heterodimerization of V1a and V2 vasopressin receptors determines the interaction with beta-arrestin and their trafficking patterns. *Proc. Natl. Acad. Sci. U. S. A.* **101,** 1548–53 (2004).

14. Bertrand, L. *et al.* The BRET2/arrestin assay in stable recombinant cells: a platform to screen for compounds that interact with G protein-coupled receptors (GPCRS). *J. Recept. Signal Transduct. Res.* **22,** 533–41 (2002).

15. Azzi, M. *et al.* Beta-Arrestin-mediated activation of MAPK by inverse agonists reveals distinct active conformations for G protein-coupled receptors. *Proc. Natl. Acad. Sci.* **100,** 11406–11411 (2003).

16. Héroux, M., Breton, B., Hogue, M. & Bouvier, M. Assembly and signaling of CRLR and RAMP1 complexes assessed by BRET. *Biochemistry* **46,** 7022–33 (2007).

17. Perroy, J., Pontier, S., Charest, P. G., Aubry, M. & Bouvier, M. Real-time monitoring of ubiquitination in living cells by BRET. *Nat. Methods* **1,** 203–208 (2004).

18. Stoddart, L. A. *et al.* Application of BRET to monitor ligand binding to GPCRs. *Nat. Methods* **12,** 661–3 (2015).

19. Stoddart, L. A., Kilpatrick, L. E. & Hill, S. J. NanoBRET Approaches to Study Ligand Binding to GPCRs and RTKs. *Trends Pharmacol. Sci.* **39,** 136–147 (2018).

20. Loening, A. M., Fenn, T. D., Wu, A. M. & Gambhir, S. S. Consensus guided mutagenesis of Renilla luciferase yields enhanced stability and light output. *Protein Eng. Des. Sel.* **19,** 391– 400 (2006).

21. Hall, M. P. *et al.* Engineered luciferase reporter from a deep sea shrimp utilizing a novel imidazopyrazinone substrate. *ACS Chem. Biol.* **7,** 1848–57 (2012).

22. Xu, X. *et al.* Imaging protein interactions with bioluminescence resonance energy transfer (BRET) in plant and mammalian cells and tissues. *Proc. Natl. Acad. Sci. U. S. A.* **104,** 10264–9 (2007).

23. Coulon, V. *et al.* Subcellular imaging of dynamic protein interactions by bioluminescence resonance energy transfer. *Biophys. J.* **94,** 1001–9 (2008).

24. Kim, J. & Grailhe, R. Nanoluciferase signal brightness using furimazine substrates opens bioluminescence resonance energy transfer to widefield microscopy. *Cytometry. A* **89,** 742– 6 (2016).

25. Goyet, E., Bouquier, N., Ollendorff, V. & Perroy, J. Fast and high resolution single-cell BRET imaging. *Sci. Rep.* **6,** 28231 (2016).

26. Namkung, Y. *et al.* Monitoring G protein-coupled receptor and β-arrestin trafficking in live cells using enhanced bystander BRET. *Nat. Commun.* **7,** 12178 (2016).

27. Beautrait, A. *et al.* A new inhibitor of the β-arrestin/AP2 endocytic complex reveals interplay between GPCR internalization and signalling. *Nat. Commun.* **8,** (2017).

28. De, A., Ray, P., Loening, A. M. & Gambhir, S. S. BRET3: a red-shifted bioluminescence resonance energy transfer (BRET)-based integrated platform for imaging protein-protein interactions from single live cells and living animals. *FASEB J.* **23,** 2702–9 (2009).

29. Yeh, H.-W. *et al.* Red-shifted luciferase-luciferin pairs for enhanced bioluminescence imaging. *Nat. Methods* **14,** 971–974 (2017).

30. Fredriksson, S. *et al.* Protein detection using proximity-dependent DNA ligation assays. *Nat. Biotechnol.* **20,** 473–477 (2002).

31. Kerppola, T. K. Visualization of molecular interactions by fluorescence complementation. *Nat. Rev. Mol. Cell Biol.* **7,** 449–456 (2006).

32. Pelletier, J. N., Campbell-Valois, F. X. & Michnick, S. W. Oligomerization domain-directed reassembly of active dihydrofolate reductase from rationally designed fragments. *Proc. Natl. Acad. Sci. U. S. A.* **95,** 12141–6 (1998).

33. Ozawa, T., Kaihara, A., Sato, M., Tachihara, K. & Umezawa, Y. Split luciferase as an optical probe for detecting protein - Protein interactions in mammalian cells based on protein splicing. *Anal. Chem.* **73,** 2516–2521 (2001).

34. Paulmurugant, R. & Gambhir, S. S. Monitoring protein-protein interactions using split synthetic renilla luciferase protein-fragment-assisted complementation. *Anal. Chem.* **75,** 1584–1589 (2003).

35. Dixon, A. S. *et al.* NanoLuc Complementation Reporter Optimized for Accurate Measurement of Protein Interactions in Cells. *ACS Chem. Biol.* **11,** 400–408 (2016).

36. Kerppola, T. K. Design and implementation of bimolecular fluorescence complementation (BiFC) assays for the visualization of protein interactions in living cells. *Nat. Protoc.* **1,** 1278– 86 (2006).

37. Rebois, R. V. *et al.* Combining protein complementation assays with resonance energy transfer to detect multipartner protein complexes in living cells. *Methods* **45,** 214–218 (2008).

38. Héroux, M., Hogue, M., Lemieux, S. & Bouvier, M. Functional calcitonin gene-related peptide receptors are formed by the asymmetric assembly of a calcitonin receptor-like receptor homo-oligomer and a monomer of receptor activity-modifying protein-1. *J. Biol. Chem.* **282,** 31610–20 (2007).

39. Armando, S. *et al.* The chemokine CXC4 and CC2 receptors form homo- and heterooligomers that can engage their signaling G-protein effectors and βarrestin. *FASEB J.* **28,** 4509–4523 (2014).

40. Fichter, K. M., Flajolet, M., Greengard, P. & Vu, T. Q. Kinetics of G-protein-coupled receptor endosomal trafficking pathways revealed by single quantum dots. *Proc. Natl. Acad. Sci. U. S. A.* **107,** 18658–63 (2010).

41. Ahn, S., Shenoy, S. K., Wei, H. & Lefkowitz, R. J. Differential Kinetic and Spatial Patterns of β-Arrestin and G Protein-mediated ERK Activation by the Angiotensin II Receptor. *J. Biol. Chem.* **279,** 35518–35525 (2004).

42. Lohse, M. J., Maiellaro, I. & Calebiro, D. Kinetics and mechanism of G protein-coupled receptor activation. *Curr. Opin. Cell Biol.* **27,** 87–93 (2014).

43. Breton, B. *et al.* Multiplexing of multicolor bioluminescence resonance energy transfer. *Biophys. J.* **99,** 4037–46 (2010).

44. Leduc, M. *et al.* Functional selectivity of natural and synthetic prostaglandin EP4 receptor ligands. *J. Pharmacol. Exp. Ther.* **331,** 297–307 (2009).

45. Rodriguez, E. A. *et al.* The Growing and Glowing Toolbox of Fluorescent and Photoactive Proteins. *Trends Biochem. Sci.* **42,** 111–129 (2017).

46. Inouye, S. & Shimomura, O. The use of Renilla luciferase, Oplophorus luciferase, and apoaequorin as bioluminescent reporter protein in the presence of coelenterazine analogues as substrate. *Biochem. Biophys. Res. Commun.* **233,** 349–353 (1997).

47. Nagai, T. *et al.* A variant of yellow fluorescent protein with fast and efficient maturation for cell-biological applications. *Nat. Biotechnol.* **20,** 87–90 (2002).

48. Pfleger, K. D. G. & Eidne, K. A. Illuminating insights into protein-protein interactions using bioluminescence resonance energy transfer (BRET). *Nat. Methods* **3,** 165–174 (2006).

49. Molinari, P., Casella, I. & Costa, T. Functional complementation of high-efficiency resonance energy transfer: a new tool for the study of protein binding interactions in living cells. *Biochem. J.* **409,** 251–61 (2008).

50. Wampler, J. E., Hori, K., Lee, J. W. & Cormier, M. J. Structured Bioluminescence. Two Emitters during both the in Vitro and the in Vivo Bioluminescence of the Sea Pansy, Renilla. *Biochemistry* **10,** 2903–2909 (1971).

51. Yamakawa, Y., Ueda, H., Kitayama, A. & Nagamune, T. Rapid homogeneous immunoassay of peptides based on bioluminescence resonance energy transfer from firefly luciferase. *J. Biosci. Bioeng.* **93,** 537–42 (2002).

52. Li, F. *et al.* Buffer enhanced bioluminescence resonance energy transfer sensor based on Gaussia luciferase for in vitro detection of protease. *Anal. Chim. Acta* **724,** 104–10 (2012).

53. Inouye, S., Sato, J., Sahara-Miura, Y., Yoshida, S. & Hosoya, T. Luminescence enhancement of the catalytic 19kDa protein (KAZ) of Oplophorus luciferase by three amino acid substitutions. *Biochem. Biophys. Res. Commun.* **445,** 157–162 (2014).

54. Inouye, S., Watanabe, K., Nakamura, H. & Shimomura, O. Secretional luciferase of the luminous shrimp Oplophorus gracilirostris: cDNA cloning of a novel imidazopyrazinone luciferase. *FEBS Lett.* **481,** 19–25 (2000).

55. Czupryna, J. & Tsourkas, A. Firefly Luciferase and Rluc8 Exhibit Differential Sensitivity to Oxidative Stress in Apoptotic Cells. *PLoS One* **6,** e20073 (2011).

56. Shigehisa, M. *et al.* Stabilization of luciferase from Renilla reniformis using random mutations. *Protein Eng. Des. Sel.* **30,** 7–13 (2017).

57. Hu, M.-J. *et al.* Development of a novel ligand binding assay for relaxin family peptide receptor 3 and 4 using NanoLuc complementation. *Amino Acids* **50,** 1111–1119 (2018).

58. Stoddart, L. A. *et al.* Development of novel fluorescent histamine H1-receptor antagonists to study ligand-binding kinetics in living cells. *Sci. Rep.* **8,** 1572 (2018).

59. Chu, J. *et al.* A bright cyan-excitable orange fluorescent protein facilitates dual-emission microscopy and enhances bioluminescence imaging in vivo. *Nat. Biotechnol.* **34,** 760–767 (2016).

60. Laviv, T. *et al.* Simultaneous dual-color fluorescence lifetime imaging with novel red-shifted fluorescent proteins. *Nat. Methods* **13,** 989–992 (2016).

61. Machleidt, T. *et al.* NanoBRET—A Novel BRET Platform for the Analysis of Protein–Protein Interactions. *ACS Chem. Biol.* **10,** 1797–1804 (2015).

62. Robbins, M. S. & Hadwen, B. J. The Noise Performance of Electron Multiplying Charge- Coupled Devices. *IEEE Trans. Electron Devices* **50,** 1227–1232 (2003).

63. Basden, A. G., Haniff, C. A. & Mackay, C. D. Photon counting strategies with low-light-level CCDs. *Mon. Not. R. Astron. Soc.* **345,** 985–991 (2003).

64. Zacharias, D. A., Violin, J. D., Newton, A. C. & Tsien, R. Y. Partitioning of lipid-modified monomeric GFPs into membrane microdomains of live cells. *Science* **296,** 913–6 (2002).

65. Schink, K. O., Raiborg, C. & Stenmark, H. Phosphatidylinositol 3-phosphate, a lipid that regulates membrane dynamics, protein sorting and cell signalling. *BioEssays* **35,** 900–12 (2013).

FIGURE LEGENDS

Figure 1 | Overview of the setup for BRET microscopy. Microscope elements needed for image acquisition. From right to left: substrate and cell to generate the light, objective with magnification, filter wheel to select the wavelength needed and the high sensitivity/low background camera to capture the image. In the example pictures, HEK293 cells were transfected with V2 vasopressin receptor, βarrestin2-RlucII and rGFP-CAAX. Images are obtained before (no BRET) or 10 min after (BRET) the addition of vasopressin receptor ligand (100 nM Arginine vasopressin) without filter (Total luminescence) or acceptor filter (LP480). The substrate was 10 μM Me-O-eCTZ. Scale bars = 20 μm.

Figure 2 | Comparison of spectral characteristics of BRET assay constructs. (a) The emission spectrum of the donor luminescence and acceptor fluorescence for BRET1. The solid curve is showing BRET1 donor (RlucII + CTZh) luminescence reaching a maximum at 512 nm (bandwidth of 85 nm), and the dashed curve is the BRET1 acceptor (Venus) fluorescence reaching a maximum at 532 nm (20 nm longer than donor maximum). (b) The emission spectrum of donor luminescence and acceptor fluorescence for BRET2. The solid curve is the BRET2 donor (RlucII + Me-O-eCTZ) luminescence reaching a maximum at 417 nm (bandwidth of 50 nm), and the dashed curve is the BRET2 acceptor (GFP2) fluorescence reaching a maximum at 506 nm (89 nm longer than donor maximum). All spectrum measurements were performed in white 96-well plate containing HEK293 cells transiently expressing RlucII, along with either Venus or GFP2 for BRET1 or BRET2, respectively, using a microplate luminescence/fluorescence reader (Synergy Neo2).

Figure 3 | Comparison of RlucII luminescence with different substrates. (a) Comparison of the luminescence intensity 5 min after the addition of substrates. The values on the top of each

bars represent the mean ±SEM (n=3) of the percentage of the CTZh signal intensity (b) Time-dependent decay of luminescence signal for different substrates. Data are the mean ±SEM of 3 independent experiments. In Figure 3a and 3b, luminescence measurements were performed using the Synergy Neo2 microplate reader on HEK293 cells transiently expressing RlucII and re-suspended in 96-well plate with a 1 μM final concentration of substrates. (c) Comparison of the signal decay of CTZh and Me-O-e-CTZ in luminescence imaging. HEK293 cells were transfected with βarrestin2-RlucII and total luminescence image was continuously obtained with an exposure time of 10 seconds. Images at 0, 2, 3, 10, 20 and 30 min are shown. The substrates were added at 10 μM final concentration. The grayscale levels of each pictures are corresponding to 0-30 photons (CTZh), and 0-10 photons (Me-O-eCTZ), respectively. Scale bars = 40 μm. RLU = relative luminescence unit from microplate reader.

Figure 4 | Comparison of BRET dynamic range between BRET1, BRET2 and ebBRET images. (a) BRET1, BRET2 and ebBRET images: HEK293 cells were transfected with fusion proteins encoding Venus-RlucII for BRET1, GFP2-RlucII for BRET2, rGFP-RlucII for ebBRET, and βarrestin2-RlucII as a control. In the FP-RlucII fusion proteins, a linker of 19 amino acid was used to connect either GFP2, YFP or rGFP to RlucII. In each image, BRET levels (the ratio of the acceptor photon count to the total photon count) are expressed as a heat-map color code (lowest being black and purple, and highest being red and white) as shown in the bottom right corner of the panel. Scale bars = 20 μm. (b) Comparison of BRET levels between images from panel a: BRET levels are calculated as the ratio between the luminescence from BRET acceptor and total Luminescence signal from all pixels showing more than 50 photon counts. The distribution of BRET levels was expressed as a histogram. The bin width of the histogram being 0.05 arbitrary BRET values and plotted against relative frequency for each

bin. The values in the figure represent dynamic BRET windows (BRET from donor + acceptor constructs / BRET from donor construct only) calculated using the mean values of each of the distributions. (c) Emission spectrums for donor alone vs donor + acceptor conditions: Photon counts corresponding to the donor emission leaking into acceptor spectrum and true donor emission for BRET1, BRET2 and ebBRET. The equation used to calculate BRET levels was described at the bottom of panel a.

Figure 5 | Comparison of Nluc luminescence with different substrates. HEK293 cells were transiently transfected with Nluc and total luminescence was measured after the addition of 1 µM substrate (final concentration) using a Synergy Neo2 (panels a-c) (a) Comparison of the luminescence intensity 5min after addition of substrates to the cells. The values on the top of each bars represent the mean ±SEM (n=3) of the percentage of the CTZh signal intensity. (b) Luminescence spectrum of different Nluc substrates. (c) Time-dependent decay of luminescence signal of different substrates the data represent the mean ±SEM (n=3). (d) BRET imaging of the interaction between Gαq-Nluc, Gβ1 and CyRFP-Gγ1. HEK293 cells were transiently transfected with Gαq-Nluc (Nluc is inserted at the position 118 of Gαq), Gβ1 and CyRFP-Gγ1, and BRET images were obtained after the addition of 10 µM CTZ400A and treatment with 100nM angiotensin II (AT1R agonist) for 20 min. The BRET levels are expressed using a heat-map as described in Figure 4a. The pixel brightness represents total photon counts of each pixel.

Figure 6 | Comparison between cooled-CCD and EMCCD camera. (a) Comparison of luminescence image of cells expressing βarrestin-RlucII using cooled CCD and EM-CCD cameras. Each image frame is illustrated as a monochrome gradation calibrated between 5% and 95% of maximal signal intensity. Scale bars = 20 µm. (b) BRET2 images using cooled CCD and

EM-CCD cameras. HEK293 cells were transfected with AT1R, Gαq-RlucII, Gβ1 and GFP10-Gγ1. BRET level was expressed as a heat-map color code as described in Figure 4a. The pixel brightness represents total photon counts of each pixel. Note: Bottom three pictures in Figure 6b are derived from the same field of cells as Figure 7a, but taken at different time point and including more cells. Scale bars = 40 μm.

Figure 7 | Examples of BRET imaging in GPCR signaling. (a) BRET2 imaging. Dissociation of G-protein α subunit from βγ complex upon GPCR activaton. HEK293 cells were transfected with AT1R, Gαq-RlucII (RlucII is inserted at the position 118 of Gαq), Gβ1 and GFP10-Gγ1. 10 μM of Me-O-eCTZ was added and BRET2 images were obtained before and after treatment with 100 nM of angiotensin II (AT1R agonist) for 5 min. (b) ebBRET imaging. Recruitment of βarrestin to the plasma membrane and GPCR endocytosis. HEK293 cells were transfected with AT1R, βarrestin2- RlucII and rGFP-CAAX (top panel), with AT1R-RlucII and rGFP-CAAX (middle panel), or with AT1R-RlucII and rGFP-FYVE (bottom panel). In rGFP-CAAX construct, rGPF was linked with CAAX box (GKKKKKKSKTKCVIM) using a 14 amino acids linker (GSAGTMASNNTASG). In rGFP-FYVE construct, rGFP was linked with FYVE domain using a 11 amino acids linker (GSGGSGSGGLE). 10 μM final concentration of Me-O-eCTZ was added, and ebBRET images were obtained before (control) and after treatment with 100 nM of angiotensin II for either 15 min (top panel) or 60 min (middle and bottom panel). In each image, BRET level was expressed as a heat-map color code as described in Figure 4a. The pixel brightness represents total photon counts of each pixel. Scale bars = 20 μm.

Figure 8 | Example of Image Quantification. (a) Image segmentation. Images used for analysis come from the experiment presented in Figure 5a before (top left column) and after

(bottom left column) the treatment with angiotensin II. 13 cells showing high luminescence signals (more than 30~50 photons/pixel) were segmented manually (second column). Each cell area was divided into central (third column) and peripheral (fourth column) regions. These two regions have equal surface areas. BRET level was expressed using a heat-map as described in Figure 4a. (b) Quantification of BRET level. BRET level of each cell before and after the stimulation was calculated from the sums of photon counts in each cell region according to the formula shown in Figure 4. The bars represents the mean±SEM in the presence or absence of angiotensin II. P value was calculated by paired t-test (two tails), n=13. (c) The distribution of BRET levels was expressed as a histogram (left) for central and peripheral regions of cells. The bin width of the histogram being 0.02 arbitrary BRET values and plotted against relative frequency for each bin. The difference of BRET level berween peripheral and central region was quantified using the same calculation with panel b. (d) The bars represents the mean±SEM of the BRET values calculated from peripheral regions of the cells in the presence or absence of angiotensin II. P value was calculated by paired t-test (two tails), n=13.

Table 1: Comparison of the noise level between cooled CCD and EMCCD camera. Each row represents image noise level in typical measurement conditions. Each images are exposed for 1 min, and signal statistics are calculated from 100 x 100 = 10,000 pixels cropped from the area having uniform illumination and not affected by the objective lens halo. Cooled CCD camera

	Cooled CCD camera Pixis 1024, Princeton instruments		EMCCD camera EM N2, Nuvu cameras (photon counting gain 3,000)		EMCCD camera EM N2, Nuvu cameras (conventional gain 500)	
	Average counts (e^-)	Noise level (rms)	Average counts (e^-)	Noise level (rms)	Average counts (e^-)	Noise level (rms)
Shutter Closed	N/A	6.90	N/A	1.07	N/A	295.82
Low Signal	1.27	5.18	0.63	1.34	8.91	166.06
High Signal	154.42	13.73	146.34	11.42	5060.35	641.58

Shutter Closed: camera dark current when closing the camera shutter before CCD.

Low Signal: signal level close to the dark area of a typical luminescence imaging picture capturing the system noise by exposing long time without luminescent sample while opening the camera shutter.

High Signal: signal level close to bright area of luminescence imaging picture obtained by introducing stray light so that the background signal is close to the typical input level from bright pixels of BRET measurement.

Box 1: Determination of donor vs acceptor ratio.

When monitoring intermolecular BRET (for instance when monitoring protein-protein interactions or translocation of a protein from a compartment to another), the expression levels of the donor and acceptor affect the BRET signal. The ideal donor/acceptor ratio is depending on the apparent affinity between the donor- and acceptor-fused components and of the experimental design considered. To determine the best donor/acceptor ratio for a given experimental setting, we are using the following procedure.

Procedure

CRITICAL Although this determination can be performed in imaging mode, it is easier and faster to do it by spectrophotometry using PMT-based plate readers7. The ratios determined this way are generally a good indication of the ratios that should be used for BRET-imaging.

1. Express the donor- and the acceptor-fused components individually into the target cells of interest.

2. Determine the range of the DNA amount for which the luminescence and the fluorescence signals are quantifiable while not affecting the viability or morphology of the cells. Also, make sure that the subcellular distribution of the tagged proteins is not affected by the expression levels.

3. Using the lowest amount of DNA yielding a detectable signal for the donor-fused component, perform an acceptor titration experiment by co-transfecting increasing amount of the acceptorfused component (within the range determined in step 2).

CRITICAL STEP This is important in order to avoid excessive overexpression that could lead to spurious interactions. If possible, it is good practice to quantify the BRET probes expression levels to confirm that it remains close to physiological conditions. BRET signal will increase as a function of the ratio between the acceptor and the donor until the donor is saturated by the acceptor.

4. Depending on the experimental design (monitoring a phenomenon that should lead to an increase or decrease in BRET) select the ratio that will provide the largest BRET change window.

- END OF BOX 1 –

Figure1

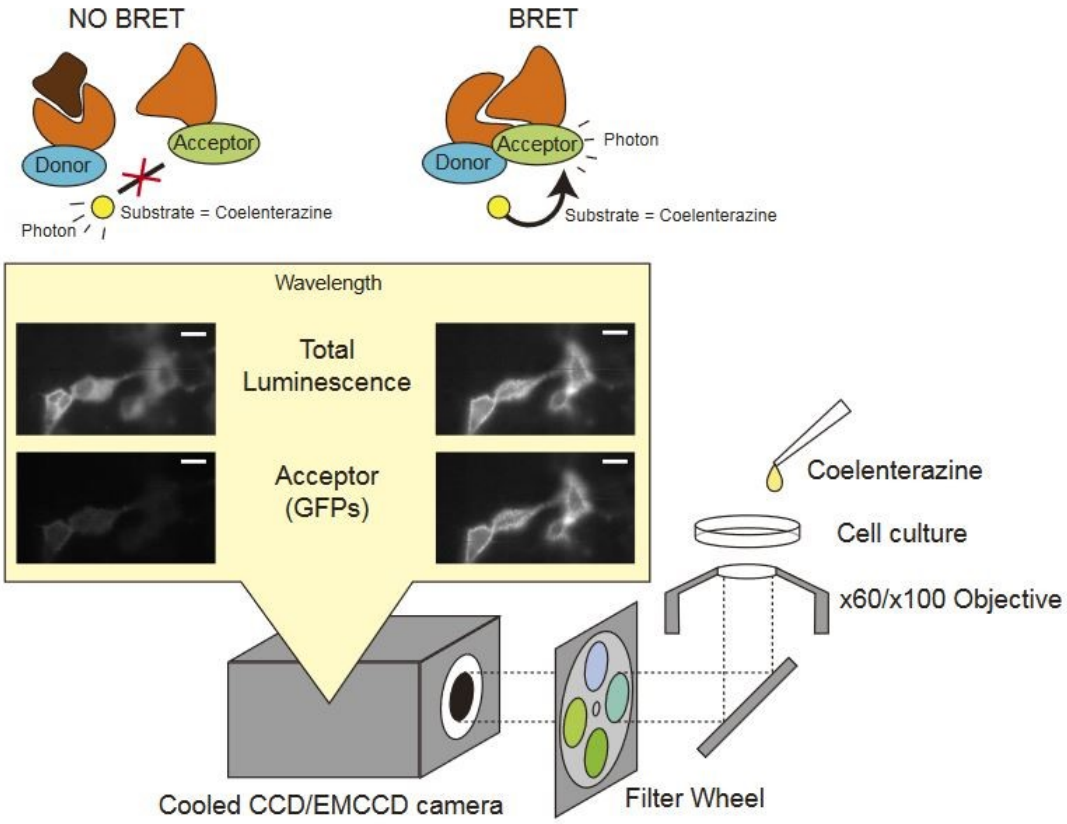
NO BRET
BRET
Acceptor
Donor
Photon
Substrate = Coelenterazine
Acceptor
Donor
Photon
Substrate = Coelenterazine
Wavelength
Total
Luminescence
Acceptor
(GFPs)
Coelenterazine
Cell culture
x60/x100 Objective
Cooled CCD/EMCCD camera
Filter Wheel

Figure2

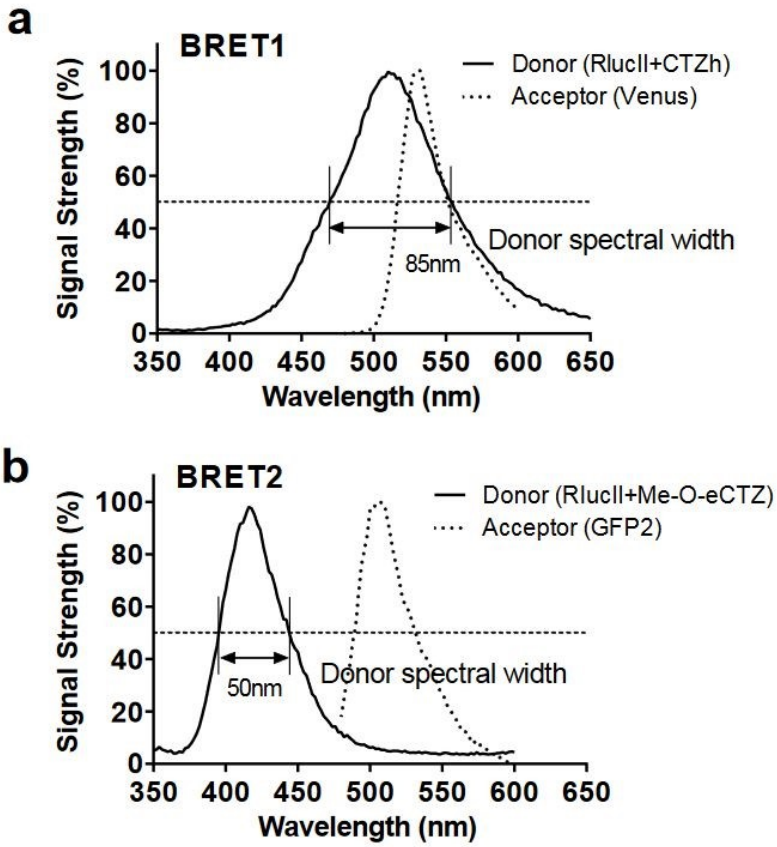
a
BRET1
Donor (RlucII+CTZh)
Acceptor (Venus)
Signal Strength (%)
100
80
60
40
20
0
350 400 450 500 550 600 650
Wavelength (nm)
85nm
Donor spectral width
b
BRET2
Donor (RlucII+Me-O-eCTZ)
Acceptor (GFP2)
Signal Strength (%)
100
80
60
40
20
0
350 400 450 500 550 600 650
Wavelength (nm)
50nm
Donor spectral width

Figure 3

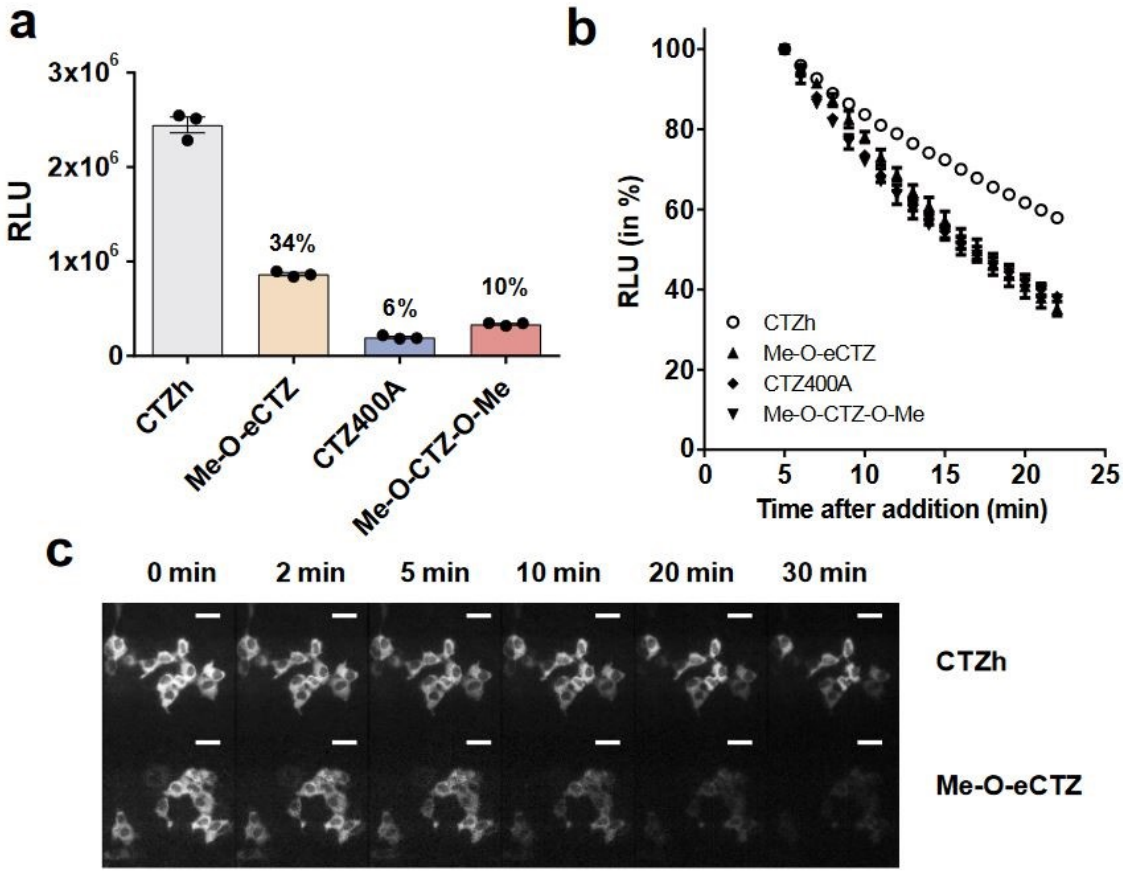
a
3x10^6
2x10^6
1x10^6
0
RLU
34%
6%
10%
CTZh
Me-O-eCTZ
CTZ400A
Me-O-CTZ-O-Me
b
100
80
60
40
20
0
RLU (in %)
CTZh
Me-O-eCTZ
CTZ400A
Me-O-CTZ-O-Me
0
5
10
15
20
25
Time after addition (min)
c
0 min
2 min
5 min
10 min
20 min
30 min
CTZh
Me-O-eCTZ

Figure 4

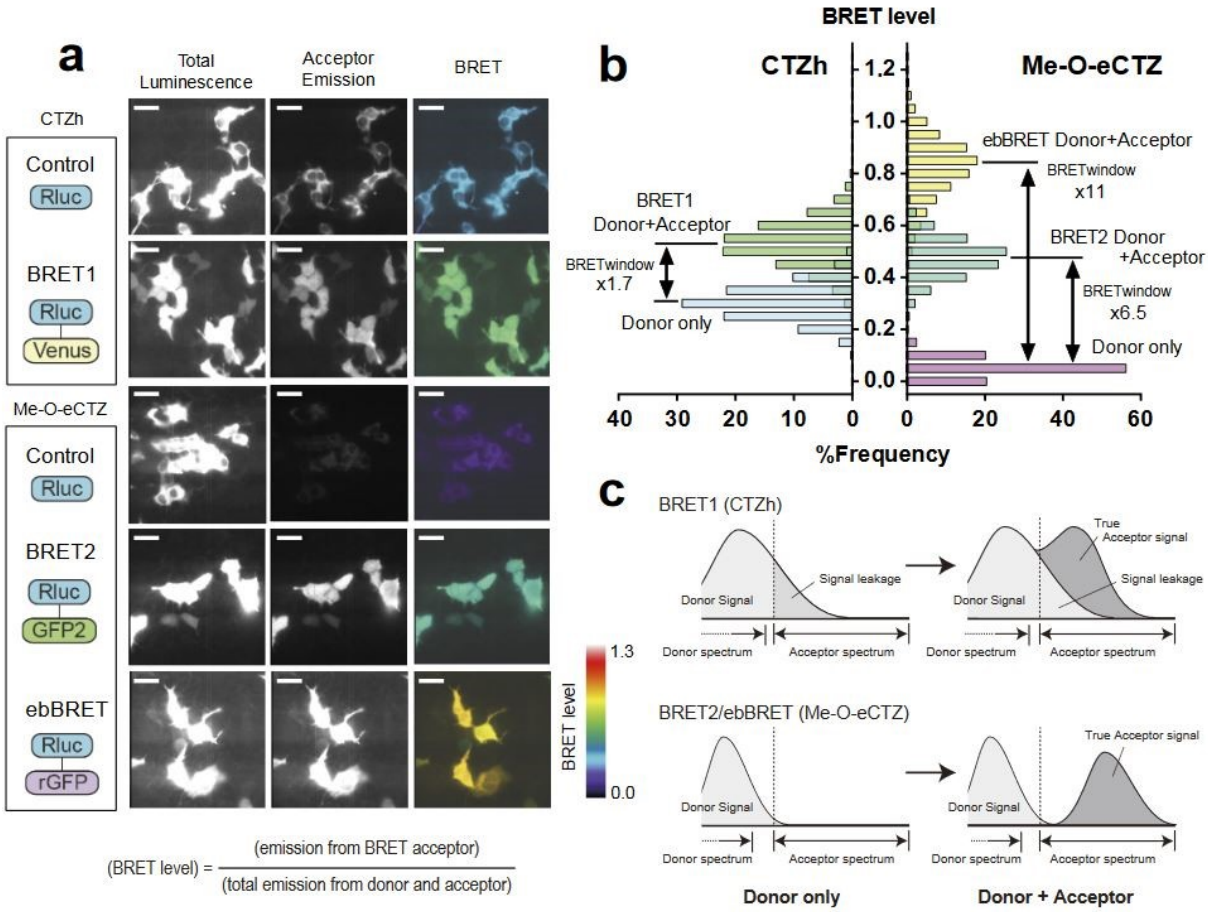
a
Total Luminescence
Acceptor Emission
BRET
CTZh
Control
Rluc
BRET1
Rluc
Venus
Me-O-eCTZ
Control
Rluc
BRET2
Rluc
GFP2
ebBRET
Rluc
rGFP
(BRET level) = (emission from BRET acceptor) / (total emission from donor and acceptor)
b
BRET level
CTZh
Me-O-eCTZ
ebBRET Donor+Acceptor
BRETwindow x11
BRET1 Donor+Acceptor
BRETwindow x1.7
BRET2 Donor +Acceptor
BRETwindow x6.5
Donor only
Donor only
%Frequency
c
BRET1 (CTZh)
Donor Signal
Signal leakage
True Acceptor signal
Donor spectrum
Acceptor spectrum
BRET level
1.3
0.0
BRET2/ebBRET (Me-O-eCTZ)
Donor only
Donor + Acceptor

Figure 5

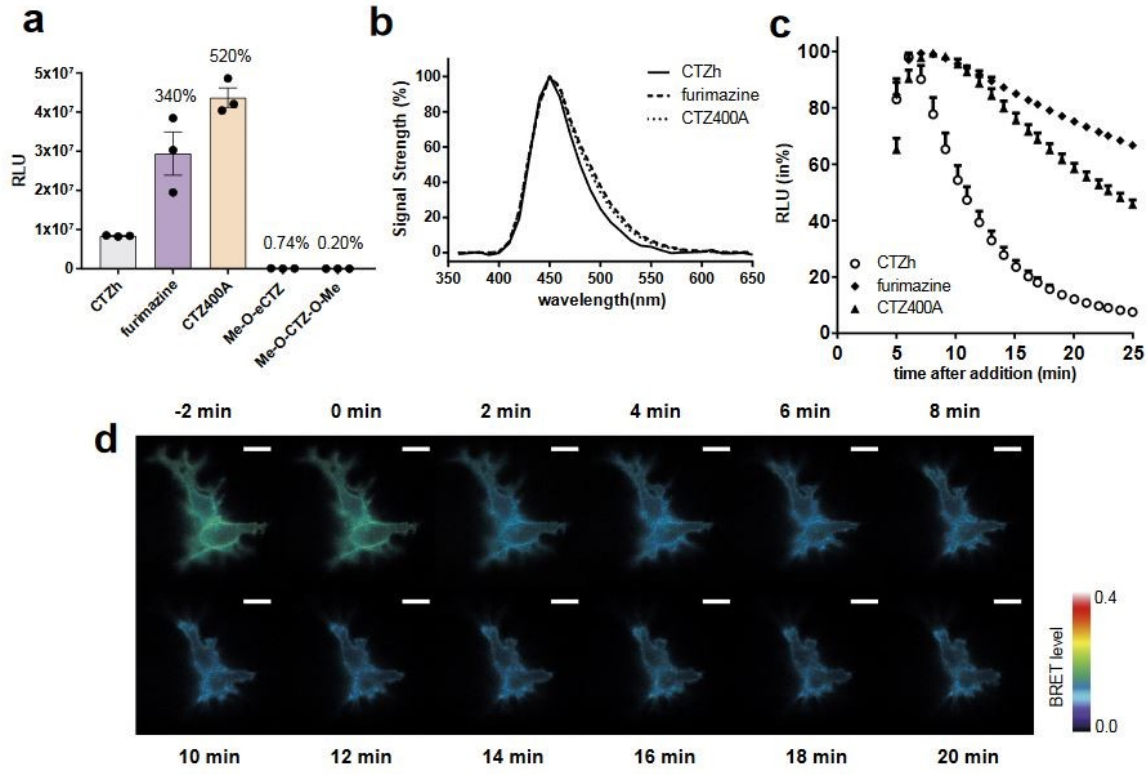
a
RLU
5x10⁷
4x10⁷
3x10⁷
2x10⁷
1x10⁷
0
340%
520%
0.74%
0.20%
CTZh
furimazine
CTZ400A
Me-O-eCTZ
Me-O-CTZ-O-Me
b
Signal Strength (%)
wavelength(nm)
CTZh
furimazine
CTZ400A
c
RLU (in%)
time after addition (min)
CTZh
furimazine
CTZ400A
d
-2 min
0 min
2 min
4 min
6 min
8 min
10 min
12 min
14 min
16 min
18 min
20 min
BRET level
0.4
0.0

Figure 6

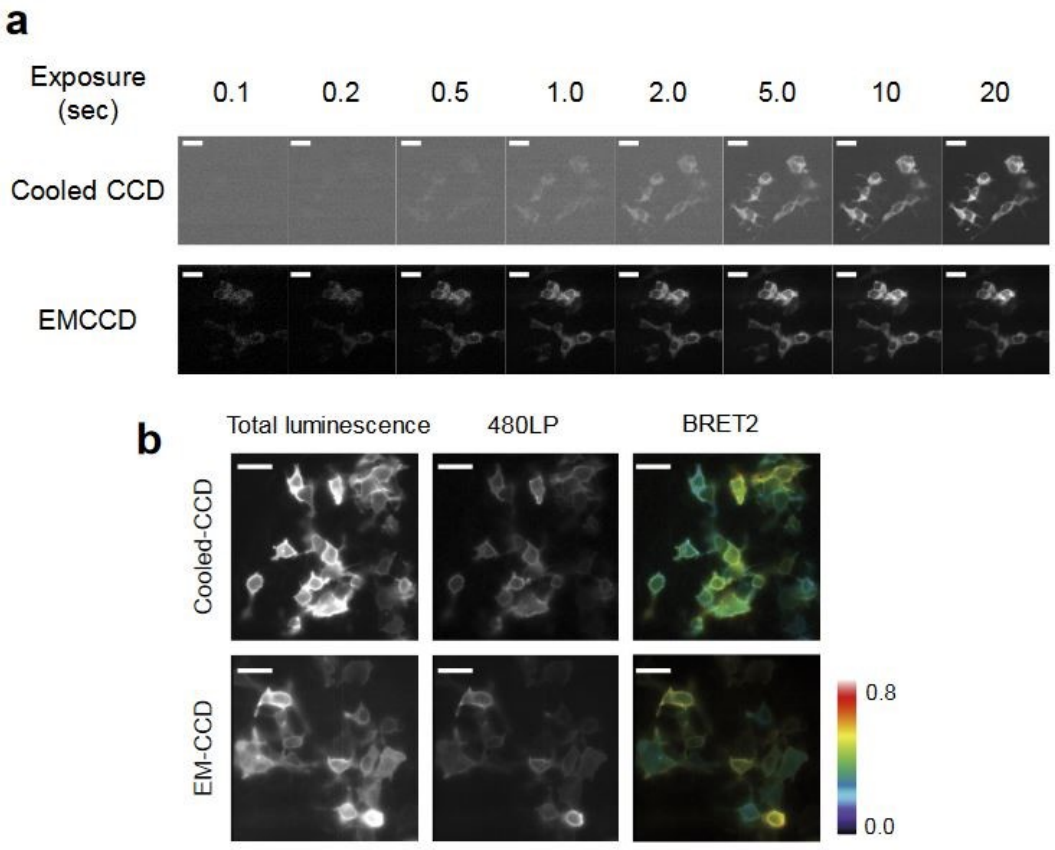
a
Exposure (sec)
0.1
0.2
0.5
1.0
2.0
5.0
10
20
Cooled CCD
EMCCD
b
Total luminescence
480LP
BRET2
Cooled-CCD
EM-CCD
0.8
0.0

Figure 7

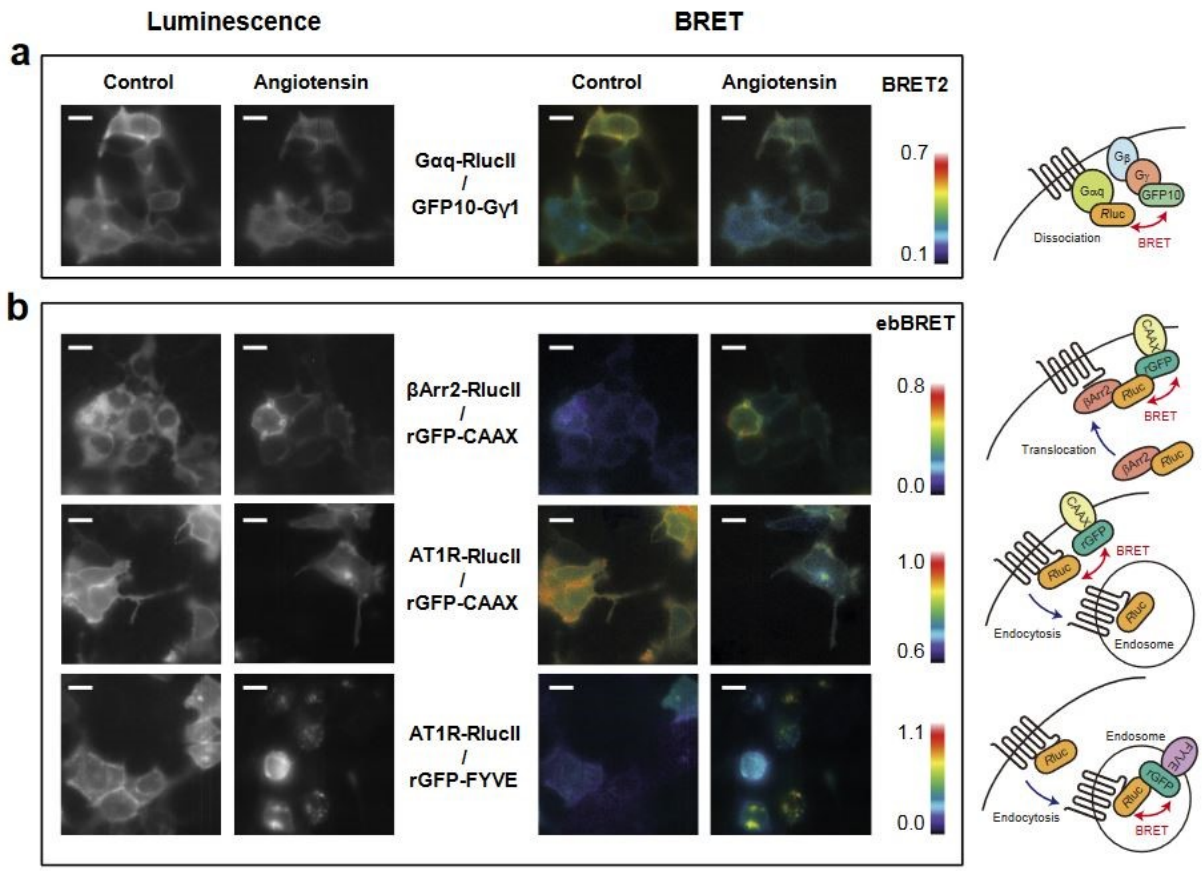
Luminescence
BRET
a
Control
Angiotensin
Control
Angiotensin
BRET2
Gαq-RlucII / GFP10-Gγ1
0.7
0.1
Gβ
Gγ
Gαq
GFP10
Rluc
Dissociation
BRET
b
ebBRET
βArr2-RlucII / rGFP-CAAX
0.8
0.0
CAAX
rGFP
βArr2
Rluc
BRET
Translocation
AT1R-RlucII / rGFP-CAAX
1.0
0.6
Endocytosis
Endosome
AT1R-RlucII / rGFP-FYVE
1.1
0.0
FYVE

Figure 8

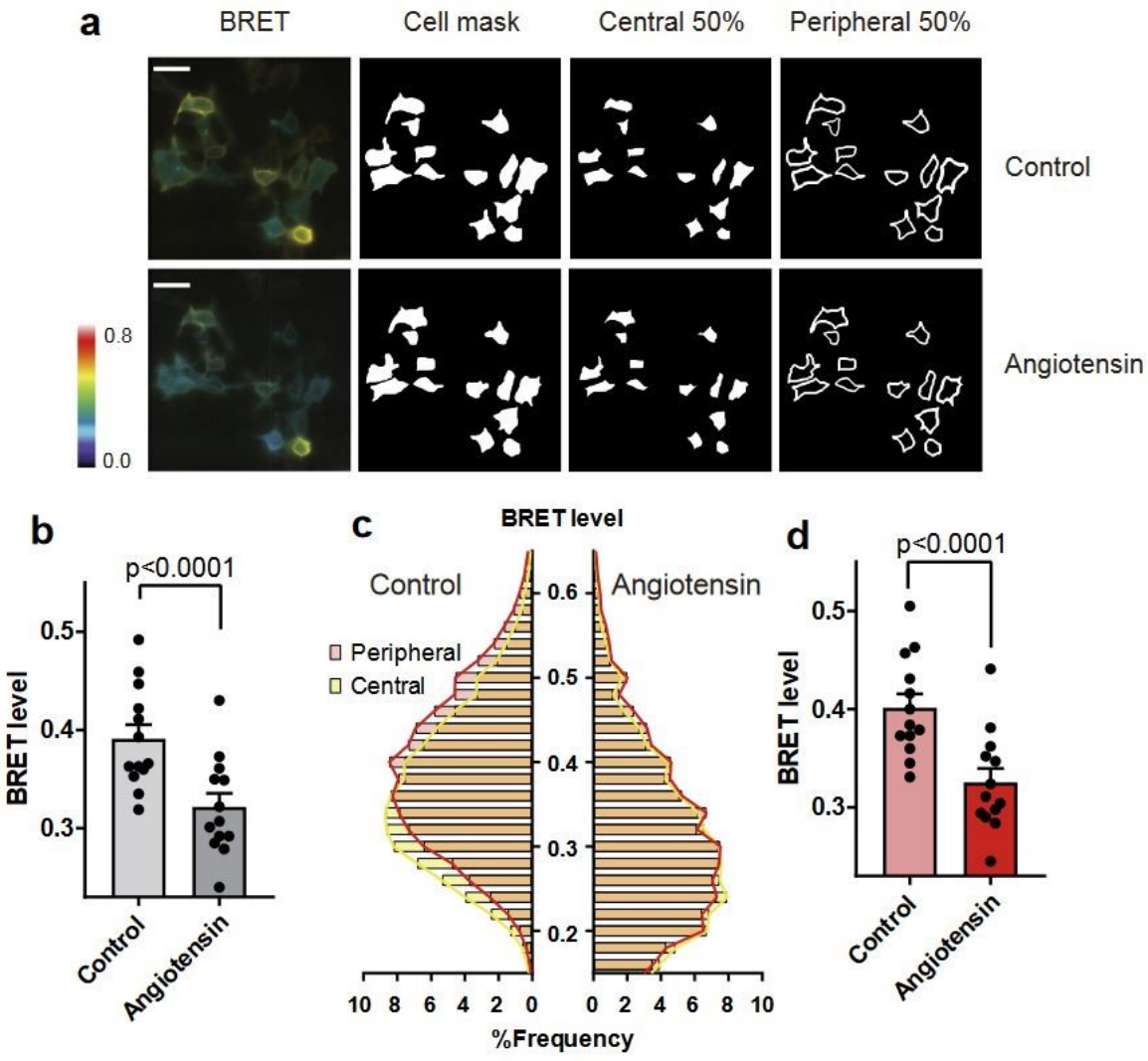
a
BRET
Cell mask
Central 50%
Peripheral 50%
Control
Angiotensin
0.8
0.0
b
p<0.0001
BRET level
0.5
0.4
0.3
Control
Angiotensin
c
BRET level
Control
Angiotensin
Peripheral
Central
0.6
0.5
0.4
0.3
0.2
10 8 6 4 2 0
0 2 4 6 8 10
%Frequency
d
p<0.0001
BRET level
0.5
0.4
0.3
Control
Angiotensin

Supplementary material

- **Supplementary Figure 1:** Examples of Image quantification.
- **Supplementary Data 1:** Raw image data, the cell masks and the MATLAB script.

Article 5

Evolutionary Action and structural basis of the allosteric switch controlling β2AR functional selectivity

Anne-Marie Schönegge1, Jonathan Gallion2, **Louis-Philippe Picard1**, Angela D. Wilkins3, Christian Le Gouill1, Martin Audet1, Wayne Stallaert1, Martin J. Lohse4, Marek Kimmel5, Olivier Lichtarge2,3 and Michel Bouvier

Publié dans *Nature Communication,* le 18 décembre 2017

Contributions. J'ai contribué au niveau technique pour ce papier en transposant certaines mutations du β2AR sur le V2R. J'ai aussi effectué quelques expériences de liaison sur les mutants du β2AR. Finalement, j'ai participé aux révisions du manuscrit et aidé dans l'écriture de manuscrit suite aux révisions.

Evolutionary Action and structural basis of the allosteric switch controlling β2AR functional selectivity

Anne-Marie Schönegge1, Jonathan Gallion2, Louis-Philippe Picard1, Angela D. Wilkins3, Christian Le Gouill1, Martin Audet1, Wayne Stallaert1, Martin J. Lohse4, Marek Kimmel5, Olivier Lichtarge2,3 and Michel Bouvier

1 Department of Biochemistry, Institute for Research in Immunology and Cancer, Université de Montreal, QC, Canada
2Department of Structural and Computational Biology and Molecular Biophysics, Baylor College of Medicine, Houston, TX, USA
3 Department of Molecular and Human Genetics, Baylor College of Medicine, Houston, TX, USA
4 Institute of Pharmacology and Toxicology, Würzburg, Germany and Max Delbrück Center for
Molecular Medicine, Berlin, Germany.
5Departments of Statistics and Bioengineering, Rice University, Houston, TX, USA

Correspondence: M.B. (e-mail: michel.bouvier@umontreal.ca).

Abstract

Functional selectivity of G protein coupled receptors is believed to originate from ligand-specific conformations that activate only subsets of signalling effectors. In this study, to identify molecular motifs playing important roles in transducing ligand binding into distinct signaling responses, we combined *in silico* evolutionary lineage analysis and structure-guided site directed mutagenesis with large-scale functional signaling characterization and non-negative matrix factorization clustering of signaling profiles. Clustering based on the signaling profiles of 28 variants of the β2–adrenergic receptor reveals three clearly distinct phenotypical clusters, showing selective impairments of either the Gi or βarrestin/endocytosis pathways with no effect on Gs activation. Robustness of the results is confirmed using simulation-based error propagation. The structural changes resulting from functionally biasing mutations centered around the DRY-, NPxxY- and PIF-motif, selectively linking these micro-switches to unique signaling profiles. Our data identify different receptor regions that are important for the stabilization of distinct conformations underlying functional selectivity.

Introduction

G protein-coupled receptors (GPCR) form the largest family of receptors involved in cellular signaling. Diverse external stimuli such as hormones, neurotransmitters, metabolites, ions, and fatty acids are translated into a cellular response via GPCR activation. The wide range of GPCR-regulated cellular responses and disease associations with GPCR-dysregulation make this system a prime target for drug discovery and development. In recent years, it has become evident that a single GPCR can couple not only to one but to several different G protein subtypes leading

to complex signaling profiles1,2. In addition, G protein-independent signaling of GPCRs has been reported; primarily through βarrestins, which are also part of the desensitization/endocytosis machinery3,4. It follows that individual GPCRs have greater repertoires of cognate downstream signaling partners than originally anticipated, making their signaling more akin to a network than to a linear cascade. Furthermore, ligands have been identified that bind to the same GPCR but activate distinct and specific subsets of potential signaling pathways 5-9. This phenomenon, called ligand-biased signaling or functional selectivity, has important implication for drug discovery as it paves the way for the identification of ligands that selectively target signaling pathways with therapeutic relevance while sparing pathways that could underlie undesirable effects. Currently, however, the possibility to rationally design compounds with intended signaling profiles is limited by the poorly understood molecular and structural determinants of functional selectivity.

Translating extracellular ligand binding to intracellular signaling relies on numerous small structural rearrangements of receptors, and functional selectivity is believed to result from differences in these rearrangements. Structural changes accompanying GPCR activation include an elongation and rotation of TM5, an outward movement of TM6 and an inward movement of TM710-13. It is thought that these conformational changes are mediated by a conserved network of non-covalent contacts and that these allosteric rearrangements define activation pathways14-17. Such activation pathways include small groups of structurally neighboring amino acids within the seven-helical transmembrane domain common to GPCR that are called microswitches. These include the DRY motif (D1303.49, R1313.50, Y1323.51), the toggle switch (W2866.48), the NPxxY motif (N3227.49, P3237.50, Y3267.53)18-20 and the

PIF/connector motif (P2115.50, I1213.40, F2826.44)13,21. However, in recent years, molecular dynamic simulations and structural studies of GPCRs in solution have shown that GPCR conformations are very dynamic and ligand-dependent22-26. These observations suggest that different ensembles of receptor conformations might engage different effectors and thereby induce functional selectivity.

Mutations in GPCRs, including both synthetic and naturally occurring ones associated to diseases, have been shown to selectively alter subsets of the signaling repertoire27-29. Such mutagenesis-directed functional selectivity has even been introduced in M3 muscarinic-based designer receptors exclusively activated by designer drug (DREADD), resulting in a receptor that could engage βarrestin but could no longer activate Gq in response to the designer drug CNO30. However, connections between structural perturbation and signaling bias are still poorly understood. The available 3D structures of the β2-adrenergic receptor (β2AR) in both active and inactive states10,11,21 provide initial descriptions of receptor activation, which in combination with site directed mutagenesis, could inform us on the structure-function basis of functional selectivity. The impact of mutations depends on the sensitivity of the site that is mutated and on the magnitude of the mutational substitution31. The effect of both is captured by Evolutionary Action (EA), an equation that models the sensitivity by the Evolutionary Trace (ET) method32, and the substitution magnitude using amino acid transition log-odds31. In theory, EA quantifies the evolutionary effect of genotype variations on functional responses. In practice, and spanning molecular, clinical, and population genetic observations, mutations with low EA value are mostly neutral when tested experimentally, those with high EA value drastically affect protein function, and those in between modulate function31,33-35. This

approach generalizes prior observations that ET identifies functionally important (i.e. sensitive sequence) positions31,36-40. In GPCRs, mutations specifically targeted to the most evolutionary sensitive positions rewired ligand specificity of the D2 dopamine receptor by single and multiple site mutations37,41 and separated G-protein activation from βarrestin signaling by a triple-site mutation28,42. By considering the substitution magnitude in addition to site sensitivity, EA can now quantify the effect of specific mutations more precisely, suggesting that we may select a mutation's site and substitution to finely-tune the expected perturbation up or down.

Here we used ET and a visual examination of the β2AR 3D structures to identify residues that could underlie the specific conformational rearrangements involved in the engagement of distinct signaling effectors, thereby determining the structural basis of β2AR functional selectivity. For the nine chosen residues, we utilized EA to select mutations intended to differentially perturb function, resulting in 28 single-site mutations. Their signaling profiles in response to isoproterenol (ISO) were characterized via cell-based assays on five different signaling pathways. Based solely on these experimental assays, non-negative matrix factorization followed by K-means clustering groups the mutations into three different phenotypical clusters, which are not only defined by common signaling signatures but also demonstrate shared conformational alterations, and evolutionary action scores. These observations point to multiple motifs in determining signaling specificity toward the different pathways engaged by the β2AR, thus providing insights in the molecular determinants of functional selectivity.

Results

Choice of mutations

Amino acids to be mutated were first selected by determining the ET values of all transmembrane domain β2AR residues using the previously described ET method43. Given that intramolecular water molecules are known to play a key role in regulating protein activity44-46, we considered ET values, as well as their distances to the water molecules involved in hydrogen bond networks within the receptor structure to identify the residues to be mutated (**Fig. 1, Supplementary Table 1**). In addition, we intentionally selected residues away from the ligand binding pocket (except V86) to avoid interference with ligand binding. Accordingly, the 5 residues (A782.49, V862.57, L1243.43, I1273.46 and I2786.40 – Ballesteros-Weinstein numbering47 is given in superscript) with the highest ET ranking that are located close to intra-protein water molecules and, for 4 of them, distant from the ligand binding pocket were selected. In order to assess the differential effects of mutation with a range of impacts on these residues47, we selected substitutions with a wide range of EA scores from low (<30), to moderate (30-70), to high impact (>70, **Supplementary Table 1**).

In addition to the ET-based selection, visual inspection of the crystal structures of inactive and active β2AR lead us to also consider a cluster of positively charged amino acids (K2736.35, R3287.55 and R3338.51 (**Fig. 1, Supplementary Table 1**) pointing outwards of the helix-bundle. The unusual orientations of these residues that could be involved in helix 8 positioning prompted us to substitute them to amino acids with distinct physicochemical properties (A→L, K→R or R→K). Finally, A2716.33 a residue pointing towards the G-protein binding pocket was substituted to a bulky residue (W) or threonine (T) to assess their ability to interfere with G protein selective coupling.

Signaling Profiles of β2AR variants

In order to examine the effect of the mutations on the signaling profile of the β2AR, we analyzed G protein-dependent and independent signaling pathways. We monitored basal and isoproterenol (ISO) -induced Gs-activation, Gi-activation and βarrestin-engagement as well as their downstream events (cAMP-production and endocytosis; **Fig. 2a**). The responses obtained for each pathway with WT receptor are illustrated in **Supplementary Fig. 1a**. Concentration response curves were generated and normalized to WT β2AR for each pathway and β2AR variant. Representative examples for mutations leading to signaling signatures that are either similar to WT receptor or altered for constitutive and/or agonist-stimulated activity of specific pathways are shown in **Figure 2b**. The entire data set for the 28 mutations is given in **Supplementary Fig. 2**. From these curves, five signaling parameters were determined by curve fitting for each pathway (**Supplementary Fig. 1b,c**). These parameters are basal, lSO-induced and maximal activity as well as pEC50 and logT/KA; except for βarrestin-engagement and endocytosis, where no basal activity can be determined. Hence, the signaling profile of each receptor variant is composed of 23 parameters (see **Supplementary Table 2-6**).

Mutations within TM regions of GPCRs might influence the stability of the receptor and thus the surface expression level. Therefore, we closely monitored the cell surface expression of WT and each β2AR variant in each experiment by cell surface ELISA (**Fig. 3a**). About half of the introduced mutations reduced the expression by approximately 50%. Since we were unable to increase the cell surface levels of these mutated receptors, we used incremental amounts of WT β2AR to generate standard curves reflecting a span of expression levels encompassing the expression levels of all mutants for all signaling parameters determined (**Supplementary Fig**

3). Hence, we were able to compare the signaling parameters of receptor variants to interpolated parameters of WT β2AR at the same expression level using normalized difference (see **Fig. 3b** and **methods** for details).

Clustering of β2AR variants based on their signaling profiles

As shown in **Figure 2b** and **Supplementary Fig. 2**, the mutations in the β2AR lead to a large variety of changes in the signaling profiles. To identify commonalities among the signaling profiles, we used non-negative matrix factorization (nnmf)48,49 and k-means clustering to partition the mutations into the fewest groups within which the assay profiles were most alike and between which they were most distinct (**Fig. 4a,b**, **Supplementary Fig. 4** and **Supplementary Table 7**).

The signaling profile of the largest cluster (V86I/A, L124M, I127V, A271T, K273R/A/L, I278V/L, R328K/H, R333L), cluster 1, displays only minor changes compared to WT β2AR. In contrast to cluster 1, cluster 2 (A271W, R328A/L, R333A) differs significantly from WT β2AR. Whereas Gs signaling and cAMP production were not appreciably affected, and βarrestin engagement and endocytosis were only slightly reduced, the constitutive activity toward Gi activation was considerably increased. The change in constitutive activity was accompanied by a complete loss of ISO-stimulated activity. This lack of responsiveness did not result from a loss of binding ability of the ligand since ISO-binding affinity was not affected (**Supplementary Table 8**) and the agonist potency towards the other pathways was not affected. Similarly, it did not result from a saturation of the assay since higher activity levels could be detected for other β2AR variants (ex: I278V; A271T, **Supplementary Fig. 2**). Similar to cluster 2, variants of

cluster 3 (A78V/N/W, V86Y/D, L124S/G, I127N/G, I278Q/S) also showed increased constitutive Gi activation and loss of ISO-responsiveness. The increase in basal activity was even more dramatic than that observed in cluster 2, as it reached levels that were higher than the maximal ISO-stimulated response observed for WT receptor. In addition, the ISO-stimulated βarrestin engagement and endocytosis of cluster 3 variants were dramatically reduced and their constitutive activity toward Gs activation was increased.

Evolutionary Action predicts the impact of mutations on phenotype. Ideally, if clusters 1, 2 and 3 accurately distinguish three phenotypes, we expect that EA scores should vary much less within each cluster than between them. Indeed, compared to a random distribution, EA scores are significantly closer within each group than between any two of them (*p*-value=1.34x10-05). As expected, cluster 1 is comprised of low, cluster 2 of medium, and cluster 3 of high EA scores. The correlation between EA scores and phenotypic mutational impact can be quantified by calculating the overall phenotypic effect of each mutation compared to wild type signaling, leading to *R2* value of 0.74 (R=0.86, **Fig. 4 c**).

Structural Analysis of mutated β2AR

We used *in silico* mutagenesis and energy minimization to predict the structural changes induced by the mutations. For this purpose, the changes in the neighborhood of each mutation (residues entering and exiting a 4.5 Å radius around the mutation site) were predicted using the Molecular Operating Environment structure-based design package50. The affected residues were then grouped according to the phenotypical clustering of the mutations, and mapped on the inactive and active X-ray structures of the β2AR (**Fig. 5a**). The positions of the residues predicted to be

affected for each of the individual mutations are illustrated for both the inactive (**Supplementary Fig. 5**) and active (**Supplementary Fig. 6**) receptor conformations.

The perturbations promoted by mutations of cluster 1 were dispersed throughout the receptor for both the inactive and the active structure without any appearance of structural grouping. The average number of residues affected by each mutation was smaller in cluster 1 than either cluster 2 or 3 (**Fig. 5b**), consistent with the modest functional consequences observed for these mutations. The affected residues by the cluster 2 mutations grouped in the lower third of the receptor's TM domain, whereas cluster 3 mutations and resulting perturbations were mainly found around the middle of the receptor's TM domain.

The activation process of GPCRs is conveyed by conformational rearrangements of key residues in microswitches. Hence, we investigated whether the predicted clustered changes in cluster 2 and 3 neighbor known microswitches (PIF-motif/connector, DRY-motif, NPxxY-motif, Toggle switch). For cluster 2, the majority of the changes centered around the G protein binding site, which is flanked by the DRY and NPxxY motifs. The alterations in cluster 3 occur both around the PIF-motif as well as the NPxxY-motif (**Fig. 6**).

The prediction of structural changes is consistent with the phenotypic clustering since mutations in the different clusters resulted in distinct structural perturbations. Receptor variants in cluster 2 that displayed increased constitutive Gi activity and loss of ISO-induced Gi activation are characterized mainly by changes around the G protein binding site (DRY/NPxxY). For cluster 3 variants, which showed increased basal activity for both G-proteins and also lost ISO

promoted Gi-activation and βarrestin-engagement, mutations were predicted to affect the PIF and toggle switches in addition to the NPxxY, consistent with a greater functional impact.

These observations suggest that different regions of the receptor may be important for the stabilization of different receptor conformations causing preferential signaling through various effectors.

Discussion

GPCR signaling is pleiotropic, and while the basis of GPCR functional selectivity is not fully characterized, perturbations to the structural conformation have been implicated in biased signaling13,24,25,39,51. To better characterize the structure-function relationship in GPCR signaling bias, we combined complementary approaches including: computational predictions via Evolutionary Trace and Evolutionary Action analyses, experimental receptor signaling profiling via BRET-based biosensors and molecular modeling. First, ET and EA were combined to select and tune the intensity of mutational perturbations at sequence positions that are themselves predicted to be more or less functionally sensitive. Second, in order to disentangle the heterogeneous signaling outputs typical of GPCR signaling, we utilized BRET biosensors to characterize the diversity of these pathways. Third, computational comparison, through nnmf and clustering analyses, grouped the complexity of each mutation's response profile into a simpler and robust classification of the mutation's global effect on the entirety of receptor signaling profile rather than being limited to a specific pathway-based analysis. Taken together, these steps therefore form a comprehensive computational and experimental pipeline to predict, test and validate mutationally induced receptor bias allowing targeted site-specific mutagenesis

and reengineering of receptor function. While we have demonstrated this approach within the β2AR, all the methodologies used were designed for application in any protein and therefore represent a high throughput methodology to interrogate structure-function relationships.

In this study, we demonstrated the pipeline's efficacy to characterize perturbations to the β2AR signaling profile using 28 single-site mutations at nine different structural positions important to receptor function. These 28 mutations clustered into three different major phenotypic outcomes: i) minimal perturbation compared to WT signaling, ii) increased basal activity for Gi activation together with loss of ligand-induced Gi activation and iii) increased basal activity for G-protein activation and loss of both ligand-induced Gi and βarrestin responses. Noticeably only a few mutations affected agonist-stimulated Gs activity so that it did not contribute to the clustering (**Supplementary Fig. 4**).

Strikingly, we note a highly significant trend between predicted impact by EA and actual phenotypic perturbation (**Fig. 4c**), as previously shown in a retrospective analysis31. Evolutionary Action is a first principle equation for evolution. It uses calculus, the mathematical language for the study of variations, to formally link genotype variations, or mutations, to their effect on phenotype or functional readouts. Our results show that even in a multi-functional system as complex as GPCRs, the EA score accurately quantifies the impact of coding mutations on the loss of downstream signaling. EA predictions are validated both on the broad scale, capturing the overall phenotypic change and correlating with the cluster assignments, and on the small scale, as individual mutations at the same structural position result in different signaling biases depending on the severity of the mutation. This trend is exemplified by V86I (EA score of 26), V86A (53), V86Y (73) and V86D (90) (**Supplementary Fig. 4**) where we see

a gradual increase in experimental signaling perturbation as a function of increasing EA scores, substantiating the notion that different receptor conformations engage different effector proteins. We do however note that mutations within cluster 1 deviate from the linear correlation, with some EA predictions being higher than their measured phenotypic response. This is most likely due to the fact that the lower impact of these mutations cannot be detected experimentally by the assays used. We can speculate that either the assays were not sufficiently sensitive to detect the signaling impact or that these mutations affect a signaling pathway that was not assessed in the present study.

Mutations predicted to have a low impact all caused minimal modulation of β2AR signaling and clustered together in cluster 1. The weakness of this biological perturbation is consistent with the relatively minor structural alterations to the β2AR structure inferred from structural modeling. Thus, a native-like structural conformation exhibits wild type-like signaling.

Medium impact mutations in cluster 2, as expected, show moderate signaling changes correlating to structural perturbations mainly affecting the Gi pathway, both in the basal and the ISO-induced activity. In agreement with previous findings on EA, these mid-range mutations (EA around 50) only perturb specific aspects of protein function rather than have a universally deleterious effect. Interestingly, the predicted structural changes for these mutations are centered around the active conformation of the G-protein binding site, including the NPxxY- and DRY-motif. While the R1313.50 of the DRY-motif has been implicated in direct binding of the G protein11,14, the shape of the G-protein binding pocket itself also plays a role in G-protein binding and potentially in G-protein selectivity. Recently, it has been suggested that the position of TM6 determines G-protein specificity. A smaller G-protein binding pocket would favor Gi-

binding due to its slimmer C-terminus, whereas a larger G-protein binding pocket favors Gs-binding52. Given their impact around both the DRY-motif and the G-protein binding pocket, the predicted alterations induced by the mutations in cluster 2 might allow TM6 an easier transition towards the Gi-active state thereby explaining increased basal activity. Furthermore, the fact that no increase in Gi-activation can be induced by ISO indicates that the fraction of receptors in active state is ligand-independent, suggesting a mutation-induced receptor conformation that is uncoupled from the "normal" allosteric regulation of the Gi pathway during receptor activation.

High impact mutations in cluster 3 share a signaling bias against agonist-promoted Gi- and βarrestin-signaling and an increased basal Gs and Gi-activity. Cluster 3 mutations are predicted to promote similar alterations in the active state G-protein binding site (albeit more centered around the NPxxY than the DRY motif) as cluster 2, which likely contributes to the increased basal activity and reduced ISO-induced activity towards Gi-activation. However, the drastically increased constitutive Gi and Gs activity and loss of agonist-promoted βarrestin engagement suggest other causes. Across all mutations in cluster 3 we note a significantly altered structural conformations around the PIF- and NPxxY-motifs, which are not present in clusters 1 or 2. Structural rearrangements in the PIF-motif during activation have been described for various receptors (β2AR10,23, 5HT13, μOR46). So far, these rearrangements have been loosely associated with G-protein signaling13, however no in depth functional analysis on this motif has been performed. The NPxxY-motif in TM7 was shown to be important for normal receptor function, including G-protein signaling and receptor internalization53,54. Furthermore, the conformation of TM7 was linked to βarrestin-engagement13,24,55. Our results are in agreement

with these analyses and implicate both the PIF- and NPxxY-motifs in disruption of receptor signaling, constitutively active G-protein activation, and the elimination of βarrestin signaling.

Within cluster 3, some mutations exclusively affect the NPxxY-motif while others only affect the conformation of the PIF-motif (**Supplementary Fig. 5,6**), yet all mutations within this cluster have a conserved phenotype in regards to the Gi- and βarrestin-pathway. These data suggest that alterations in either motif are sufficient to cause the observed biased signaling profile. Given the nature of the PIF-motif to transduce signal from the ligand binding event through the TM region, we cannot exclude NPxxY involvement in mutations that only affect the PIF-motif. It is possible that the alterations of the PIF-motif result in an identical phenotype to alterations directly to the NPxxY-motif due to a coupling of PIF to the NPxxY-motif. An alternative explanation is that disruptions to the PIF-motif cause phenotypic alterations independent of the NPxxY-motif, indicating that different receptor conformations might have the same signaling output. Another possibility is that the PIF- and the NPxxY-motifs act in parallel and that both rearrangements are needed for some of the signaling activity. Hence, alterations to either one of these two microswitches could result in the same functional outcome. Regardless, our data, in agreement with prior research, implicates both the PIF domain and the NPxxY-motif in receptor activation and signaling through Gi and βarrestin. Additionally, these data suggest a novel function of the PIF-motif in modulating the activation of βarrestin signaling in concert with the NPxxY-motif.

These results highlight the power of EA to inform future mutagenesis and receptor engineering by quantifying the expected impact a mutation has on protein function. Designed mutations can therefore potentially be fine-tuned to the desired impact, thereby reducing time spent on random

mutagenesis to achieve a desired function. This is illustrated by the fact that when transfering three substitutions (I to V, L or Q) at position I6.40 from the β2AR (I278) to the vasopressin type 2 receptor (V2R) (I276), we found that, as was the case for the β2AR, the I276V/L variants had no or modest effects on either Gs activation, cAMP production or βarrestin recruitment whereas I276Q considerably and selectively affected βarrestin recruitment (**Supplementary Fig. 7**).

The approach followed in the present study has obvious implications for a possible understanding of the structural determinants of ligand-biased signaling. Further studies assessing the effects of mutations selectively affecting Gi or βarrestin engagement on the activity of βarrestin- or G protein-biased ligands should shed new light on the specific and/or local conformational rearrangements required to engage specific signaling effectors. Structural studies have already highlighted that ligands with distinct functional selectivity profiles result in distinct receptor conformation26,56,57. Based on NMR signals, Liu et al.24 reported that β-arrestin biased ligands predominantly impact the conformational states of TM7. Interestingly, mutations selectively affecting βarrestin engagement (cluster 3) are predicted to have more impact on residues close to the PIF and NPXXY than the DRY motif. Assessing how these mutations may affect the movement of TM7 upon binding of balanced and biased ligands will be of considerable interest.

In summary, we have developed a comprehensive methodology capable of guiding site directed mutagenesis studies and protein reengineering by coupling *in silico* evolutionary lineage analysis with biological characterization and collaborative filtering clustering techniques. Using this approach, we demonstrate a strong correlation between our computational predictions

stemming from evolutionary history, the actual biological perturbations and structural determinants thereof. Additionally, evolutionary action enables the design of mutations at the same position, which vary gradually in functional effect and magnitude, in effect tuning them like a turn of a rheostat. Even though our designed mutations did not occur directly within the functional motifs, the resulting structural changes altered key functional microswitches, further demonstrating the power of this approach to arrive at non-obvious solutions to signaling perturbation. Through this validation, we have gained a better understanding of the molecular determinants of biased GPCR conformations, a crucial first step for the development of biased ligands that activate only beneficial pathways thereby reducing pharmacological side effects and predicting how clinically relevant mutations result in altered cellular signaling leading to disease progression.

Methods

Reagents. (-)-isoproterenol hydrochloride (ISO) was purchased from Sigma Aldrich (St. Louis, MO, USA). Coelenterazine 400a was purchased from NanoLightTM Technology (Pinetop, AZ, USA). All cell culture reagents were bought from Wisent (Wisent, St-Bruno, QC, Canada).

Plasmids.Single site-mutations in the β2AR and V2R were introduced via PCR with QuickChange™ Site-directed Mutagenesis Kit (Agilent Technologies, Santa Clare, CA, USA) following the manufacturer's instructions. All β2AR variants were verified by sequencing. Receptor constructs contained an Ha tag at their N-terminus, as previously described58,59, to facilitate the quantification of cell surface expression by ELISA. For creating a unimolecular biosensor for monitoring βarrestin recruitment, GFP10 coding sequence (cds) without stop

codon was PCR-amplified with a forward primer encoding the plasma-membrane targeting sequence from the Lyn Kinase and a small linker (MGCIKSKGKDSLSNA), RlucII cds without stop codon was PCR-amplified and both fragments assembled in pCDNA 3.1 Zeo(+) using In-Fusion (Clontech Laboratories, Mountain View, CA, USA), creating pCDNA3.1 Zeo(+) Lyn-GFP10-RlucII. The cds of a structurally disorganized 300 residues-long linker, previously described (Dis300LNK)60, was subcloned in between GFP10 and RlucII, creating pCDNA3.1 Zeo(+) Lyn-GFP10-Dis300LNK-RlucII. The cds of βarrestin2 was PCR-amplified using forward primers encoding a small flexible linker (GSGSAGTA) and inserted at the C-terminus of RlucII, creating pCDNA3.1 Zeo(+)βarr2 trans constructs.

Cells, cell culture and transfections. BCM3 is a clone of the HEK293T cell line in which BRET-based biosensors have been developed in Dr Bouvier's laboratory and was used for all the BRET and ELISA experiments. Cells were regularly tested for mycoplasma contamination (PCR Mycoplasma Detection kit, abm, BC, Canada) and only mycoplasma-negative cells were used for the assays. HEK293T cells were grown at 37°C with 5% CO2 in Dulbecco's modified Eagle's medium (DMEM) supplemented with 10% fetal bovine serum. HEK293T cells were transiently transfected (500 000 cells per well) in 6 well plates with biosensors for bioluminescence resonance energy transfer (BRET) assays and ELISA with X-treme GENE 9 DNA Transfection Reagent (Transfection Reagent: DNA ratio: 3:1; Roche Diagnostics, Indianapolis, IN, USA). Cells were re-plated (50 000 cells per well) 24 h post-transfection into white 96 well Culture Plates (Greiner Bio-One GmbH, Frickenhausen, Germany) coated with poly-L-ornithine. The day of the experiment, cells were washed twice with stimulation buffer (Modified Hank's Balances Salt Solution (HBSS): 137 mM NaCl, 5.4 mM KCl, 0.25 mM

Na2HPO4, 0.44 mM KH2PO4, 1.8 mM CaCl2, 0.8 mM MgSO4, 4.2 mM NaHCO3, 0.2% (w/v) D-glucose, pH 7.4). The activity of each signaling pathway was measured in living cells using BRET-based assays described below. Optimal times of measurement following agonist stimulation were determined from time-course experiments carried out for each assay for the WT receptor. Times for which maximal responses was achieved and stable for a given assay were selected and were 5min, 15 and 30 min for G protein activity, βarrestin recruitment and cAMP production assays, respectively. The ELISA-based endocytosis assay was carried out 60 min following agonist stimulation.

Gs- and Gi-activation assay. HEK293T cells were co-transfected with varying amounts of WT or β2AR variants (250 ng per well) and a three-component G protein activation biosensor composed of Gα-RlucII (Gαs-67-RlucII (5 ng per well)61 for Gs-activation or Gαi2-99-RlucII (1 ng per well)62 for Gi-activation), Gβ1 (100 ng per well) and GFP10-Gγ1 (25 ng per well) as described above. Coelenterazine 400a, diluted in stimulation buffer (final: 2.5 µM) was added to the wells for 6 min, then ISO, diluted in stimulation buffer, was added at the indicated concentrations to the wells for 5 min. Plates were read on the Mithras LB 940 (Berthold Technologies, Bad Wildbad, Germany), for 1 sec per well, with filters set at 410±70 nm (RlucII) and 515±20 nm (GFP10) and BRET ratios were calculated as GFP10 divided by RlucII. Upon formation of the Gα-RlucII:Gβ1:GFP10-Gγ1 hetero-trimer, a significant BRET signal is detected resulting from the proximity between Gα-RlucII and GFP10-Gγ1. Upon activation of Gα, the separation between the Gα and Gβγ subunits leads to a decrease in BRET61.

cAMP production assay. HEK293T cells were co-transfected with varying amounts of WT or β2AR variants (200 ng per well) and BRET-cAMP biosensor (GFP10-mutEPAC1-RlucII; 1 ng

per well)63. Cells were washed twice with stimulation buffer (Modified HBSS: mentioned above). The indicated concentrations of ISO, diluted in stimulation buffer, were added to the wells for 30 min, then coelenterazine 400a, diluted in stimulation buffer (final: 2.5 μM) was added to the wells for 5 min. Plates were read on the Mithras LB 940, as described above. Upon binding of cAMP, EPAC undergoes a conformational change leading to a significant decrease in the observed BRET signal.

βarrestin2-recruitment. HEK293T cells were co-transfected with varying amounts of WT or β2AR variants (250 ng per well) and the BRET-βarrestin2-recruitment biosensor (βarr2 trans constructs, 2 ng per well). The indicated concentrations of ISO, diluted in stimulation buffer, were added to the wells for 15 min, then coelenterazine 400a, diluted in stimulation buffer (final: 2.5 μM) was added to the wells for 5 min. Plates were read on the Mithras LB 940, as described above. Upon recruitment of βarrestin2 to the receptor, a significant increase in BRET signal is observed resulting from the increased proximity between RlucII and GFP10 upon translocation of the βarrestin to the stimulated receptor.

Endocytosis. HEK293T cells were transfected with WT or β2AR variants (50 ng per well) as described above. The indicated concentrations of ISO, diluted in stimulation buffer, were added to the wells for 60 min, then a cell surface ELISA was performed. In short, cells were fixed with 3% paraformaldehyde for 10 min. Cells were washed three times in washing buffer (modified HBSS (see above) + 0.5% BSA), then cells were incubated for 60 min with anti-HA-peroxidase antibody (12013819001, Roche Diagnostics, Indianapolis, IN, USA)(1:1000 in washing buffer). Cells were washed three times in washing buffer. ECL (1:1 ratio; Perkin Elmer, Waltham-MA,

USA) was added to the wells and plates were read on the Mithras LB 940, for 1 sec per well, with no filters.

Cell surface expression. In order to monitor cell surface expression of WT or variants β2AR transfected cells used for BRET or endocytosis assays, cell surface ELISA was performed on cells re-plated 24 h post-transfection, as for endocytosis experiments but without ISO stimulation.

Analysis of concentration response curves. In order to correct for β2AR-unspecific response, the value of cells only transfected with the biosensor (no receptor added) was subtracted from the experimental value. For each repeat of the assays, data was normalized as percentage of WT β2AR maximal ISO-stimulated response (**Supplementary Fig. 1b,c**). Signaling parameters basal activity, maximal activity, ISO-induced activity and pEC50 were determined by fitting the concentration response curve to equation (1):

$$E = basal + \frac{max - basal}{1 + 10^{(logEC50 - [A]) * \mathbf{n}}} \qquad (1)$$

, where E is the effect of the ligand, *[A]* is the concentration of the ligand, *max* is the maximal response, *basal* is the non-stimulated response, n is the slope of the transducer function that links occupancy to response. The signaling parameter logT/KA was determined by fitting the concentration response curve to the equation (2):

$$E = basal + \frac{max - basal}{1 + \left(\frac{\frac{10^{[A]}}{10^{logK_A}} + 1}{\frac{10^{logR}}{10^{[A]}}} \right)^{\mathbf{n}}} \qquad (2)$$

, where E is the effect of the ligand, *[A]* is the concentration of the ligand, *max* is the maximal response, *basal* is the non-stimulated response, *logKA* denote the logarithmic functional equilibrium dissociation constant of the ligand, n is the slope of the transducer function that links occupancy to response, *logR* is the logarithm of the "transduction coefficient", T/KA, where *T* is an index of the coupling efficiency of the agonist. For detail see64,65 In equation (1) and (2), n was fixed to the determined value for WT β2AR and *basal* was not fixed. In equation (2) *max* was shared for all data sets. Values of n for WT β2AR used in the fitting are given in **Supplementary Fig. 1**.

Correction for Cell Surface Expression. For each assay, a concentration response curve for WT β2AR using 5% to 150% of DNA-amount were prepared and the cell surface expression was measured. The signaling parameters (basal activity, maximal activity, ISO-induced activity, pEC50 and logT/KA) were determined and their correlation to the expression level was calculated (**Fig. 3b**). If R2 was higher than 0.3, a linear correlation was presumed and a "theoretical WT value" with the surface expression level of each mutant was calculated using the determined equation. If R2 was lower than 0.3, the average of all values was used as "theoretical WT-value". In order to compare the signaling parameters of β2AR variants to WT β2AR, equation (3) was used:

$$\Delta_{\mathrm{norm}} = \frac{\mathrm{mut} - \mathrm{WT}_{\mathrm{theoretical}}}{\mathrm{mut} + \mathrm{WT}_{\mathrm{theoretical}}} \qquad (3)$$

, where *Δnorm* is the normalized difference, *mut* denotes the value of the β2AR variant and *WTtheoretica*l corresponds to the interpolated value obtained from the WT receptor titration curves obtained for each pathway (**Supplementary Fig. 3, Fig. 3**). This normalization, which

yields values between -1 and +1 (WT being 0 by definition) was done in order to allow direct visual comparison between the parameters without having different scales. *Δnorm* is then plotted for each parameter as the radius of the radial graph.

Evolutionary Trace Analysis. To identify functional residues, ET takes a set of homologues as input. Due to the variation in the GPCR loop regions, we focused solely on the transmembrane domains, a total of 195 residues. The multiple sequence alignment of the transmembrane region was made up of 2512 Class A GPCRs, excluding olfactory receptors, and constructed as previously described37. The sequences were gathered from the GPCRdb database (http://gpcrdb.org/) and included sequences from mammals, amphibians, reptiles, fish, birds, echinoderms, and protostomes. To select key functional amino acids, the ET results were projected on to the protein structure for β2AR (pdb: 2RH1). Targets were chosen based on their ET-scores, their distance to the ligand and to the intramolecular waters.

Evolutionary Action Scores. Evolutionary action represents a first principle equation describing the fundamental basis for evolution by providing an evaluable equation (4) connecting the changes in genotype to their phenotypic effect:

$$d\varphi = \nabla f \, d\gamma \qquad (4)$$

Formally the change in phenotype ($d\varphi$) is equal to the evolutionary fitness gradient at that position ($d\gamma$), calculated by ET, multiplied by the magnitude of the substitution made, calculated by the log odds of the substitution (∇f)31, which is dependent on the ET score of that position and any available secondary structural information. A unique set of log odds is therefore

calculated for every permutation of ET score bins (e.g. EA=1-10 or EA=10-20) with the available secondary structure information (e.g. helix, beta-sheet or coil). When structure is not available, a purely sequence-based EA score is used.

Robustness of the clustering method. In order to establish robustness of the clusters, we propagated random experimental error through the clustering procedure. To accomplish this, we generated 1000 matrices (28 mutation x 29 phenotypes, 5 pathways x 6 parameters (basal, max, ligand induced, EC50, logT/Ka, with no basal for barr) by randomly sampling, for each phenotype data point, a single value from the normal distribution with the mean and standard deviation estimated from the mutation replicates. Each point was then normalized using the normalized difference detailed above. We then performed the clustering method, detailed below, independently on each of the 1000 sampled matrices. Finally, we quantified how frequently each mutation clustered together in each of these 1000 runs, which resulted in a clustering frequency matrix (28 mutations x 28 mutations). To obtain final cluster assignments and create the similarity dendrogram, the frequency matrix was converted to a distance matrix using Pearson's Correlation as a measure of similarity with final cluster designation assigned via hierarchical clustering.

For each independent run using a corresponding sampled matrix, we utilized multiple iterations of non-negative matrix factorization (nnmf)48,49 to cluster β2AR variants based on their signaling signature and their expression. Prior to factorization, values were normalized within each column (assay phenotype measurement) on a scale of 0-1 using equation (5)

$$normalization = \frac{mut - min}{max - min} \quad (5)$$

,where *mut* denotes the value of the β2AR variant and *max* and *min* represent the maximal and minimal values for each column. This normalization was necessary to prevent differences in phenotype scale from biasing the feature reduction step. The resulting mutant x phenotype was deconstructed into its basis vectors [W,H] (where W has the dimensions 28 mutations by k, and H has the dimension k by 28 signaling parameters and expression levels) using the multiplicative algorithm of nnmf with 500 replicates. Cluster assignment was performed using k means on the W basis vector where k equaled the number of features used by nnmf. This methodology was then repeated 100 times to measure how frequently any two mutations clustered together, resulting in a mutation by mutation frequency matrix with each value being the frequency that two mutants co-clustered (**Supplementary Table 7**). This frequency provides a similarity measure between any two mutants. Cluster assignment for each of the 1000 sampled matrices was conducted independently using the Pearson's Correlation method. This cluster assignment for each sampled matrix was then used for the final clustering frequency matrix, detailed above.

We performed this analysis with k=2 up to k=7 to identify the optimal number of clusters to accurately describe the data. The intermediate frequency matrix enabled a measure to quantify clustering robustness. Specifically, cluster assignments with frequencies equal to 0% and 100% indicate very robust and distinct assignments as mutations do not jump around between multiple clusters.

EA score clustering.For each k, we performed 10,000 random simulations permuting the EA scores for all mutations and measuring the variation between EA score in each cluster, where variation= EAi-EAj for all combinations of EA scores within that cluster. All of these values were appended into an array and compared to the phenotypic clusters using a Kolmogorov-

Smirnov test. This process was repeated 10,000 times and the average P-value was used to determine significance.

Structure Prediction and Analysis.Protein structure prediction of the mutated receptors was performed using the Molecular Operating Environment (MOE) structure based design package50. First for both active and inactive receptor templates (2RH1 and 4LDE), the automated structure preparation protocol Protonate3D66 was run. Protonate3D calculates the optimal protonation states, including titration, rotamer and 'flips' using a large-scale combinatorial search. Using Residue Scanning in the Protein Design panel, the intended mutations were inserted. The selection of side chain conformations is made from a rich rotamer library followed by a refinement protocol based on force field energy minimization. For this purpose, the AMBER12EHT force field was used. Structural predictions were then visualized using the chimera visualization system67. Residues within 4.5Å of the mutations sites were identified via chimera both in WT and mutated receptors. By comparing these environments, changes in their amino acid composition (both entering and existing amino acids within this 4.5Å radius) were detected. Additionally, it was analyzed with chimera which of these changes appeared within 4.5Å of known microswitches. Detected changes were back projected on the 3D structure and highlighted as indicated in the figure legends.

Data Analysis. Data analysis was performed using Microsoft Excel (Microsoft, Redmond, WA, USA), GraphPad Prism (versions 6, GraphPad Software, La Jolla, CA, USA) MATLAB and Statistics Toolbox Release 2014b (The MathWorks, Inc. Natick, MA, USA), and NumPy and SciPy packages68.

BRET-based binding assay. Nluc (Promega, Madison, WI, USA) was inserted N-terminally into WT β2AR using the Gibson Assembly Kit (NEB, Ipswich, MA, USA) according to manufacturer's instruction. Both domains were joined by an 8 amino acid Gly-Ser-linker. In order to improve expression, the reported export signal69 was added to the construct. The signaling and binding properties of the construct were verified (**Supplementary Fig. 8**). Single site-mutations in the β2AR were introduced as described above. HEK293T cells were transfected with Nluc-β2AR WT or variants (100 ng per well) as described above. Cells were re-plated (50 000 cells per well) 24 h post-transfection into white 96 well cellGrade™ Plates (Brand GmbH und Co KG, Wertheim, Germany) coated with poly-Lornithine. Cells were washed twice with stimulation buffer (Modified HBSS: mentioned above). 100nM (S)-propranololol-green (labelled with BODIPY-FL; CellAura, Winscombe, UK) and increasing concentrations of ISO, diluted in stimulation buffer, were added to the wells for 30 min, then coelenterazine 400a, diluted in stimulation buffer (final: 0.1 μM) was added to the wells directly before reading. Plates were read on the GloMax® 96 Microplate Luminometer (Promega, Madison, WI, USA), for 0.5 sec per well, with filters set at 465±25 nm (Nluc) and 530 longpass (BODIPY-FL). BRET ratios were calculated as BODIPY-FL divided by Nluc. Upon binding of the fluorescent ligand to the Nluc-tagged receptor, a significant BRET signal is detected. The non-labeled ligand displaces the fluorescent ligand leading to a decrease in the BRET signal. The binding affinity of ISO was determined from the IC50s of the ISO-promoted decrease in propranolol-green binding for each variant.

Data availability. The authors declare that all data supporting the findings in this study are presented within the article and its Supplementary Information files, and are available from the corresponding author upon request.

References

1. Galandrin, S., Oligny-Longpre, G. & Bouvier, M. The evasive nature of drug efficacy: implications for drug discovery. *Trends Pharmacol Sci* **28**, 423-30 (2007).
2. Liu, Y. et al. Biased signalling: the instinctive skill of the cell in the selection of appropriate signalling pathways. *Biochem J* **470**, 155-67 (2015).
3. Moore, C.A., Milano, S.K. & Benovic, J.L. Regulation of receptor trafficking by GRKs and arrestins. *Annu Rev Physiol* **69**, 451-82 (2007).
4. Shukla, A.K., Xiao, K. & Lefkowitz, R.J. Emerging paradigms of beta-arrestin-dependent seven transmembrane receptor signaling. *Trends Biochem Sci* **36**, 457-69 (2011).
5. Azzi, M. et al. Beta-arrestin-mediated activation of MAPK by inverse agonists reveals distinct active conformations for G protein-coupled receptors. *Proc Natl Acad Sci U S A* **100**, 11406-11 (2003).
6. Galandrin, S. et al. Conformational rearrangements and signaling cascades involved in ligand-biased mitogen-activated protein kinase signaling through the beta1-adrenergic receptor. *Mol Pharmacol* **74**, 162-72 (2008).
7. Pupo, A.S. et al. Recent updates on GPCR biased agonism. *Pharmacol Res* **112**, 49-57 (2016).
8. Rankovic, Z., Brust, T.F. & Bohn, L.M. Biased agonism: An emerging paradigm in GPCR drug discovery. *Bioorg Med Chem Lett* **26**, 241-50 (2016).
9. Shukla, A.K., Singh, G. & Ghosh, E. Emerging structural insights into biased GPCR signaling. *Trends Biochem Sci* **39**, 594-602 (2014).
10. Rasmussen, S.G. et al. Structure of a nanobody-stabilized active state of the beta(2) adrenoceptor. *Nature* **469**, 175-80 (2011).
11. Rasmussen, S.G. et al. Crystal structure of the beta2 adrenergic receptor-Gs protein complex. *Nature* **477**, 549-55 (2011).
12. Rosenbaum, D.M. et al. GPCR engineering yields high-resolution structural insights into beta2-adrenergic receptor function. *Science* **318**, 1266-73 (2007).
13. Wacker, D. et al. Structural features for functional selectivity at serotonin receptors. *Science* **340**, 615-9 (2013).
14. Flock, T. et al. Universal allosteric mechanism for Galpha activation by GPCRs. *Nature* **524**, 173-179 (2015).
15. Venkatakrishnan, A.J. et al. Diverse activation pathways in class A GPCRs converge near the G-protein-coupling region. *Nature* **536**, 484-7 (2016).
16. Venkatakrishnan, A.J. et al. Molecular signatures of G-protein-coupled receptors. *Nature* **494**, 185-94 (2013).

17. Wolf, S. & Grunewald, S. Sequence, structure and ligand binding evolution of rhodopsin like G protein-coupled receptors: a crystal structure-based phylogenetic analysis. *PLoS One* **10**, e0123533 (2015).
18 Audet, M. & Bouvier, M. Restructuring G-protein- coupled receptor activation. *Cell* **151**, 14-23 (2012).
19. Tehan, B.G., Bortolato, A., Blaney, F.E., Weir, M.P. & Mason, J.S. Unifying family A GPCR theories of activation. *Pharmacol Ther* **143**, 51-60 (2014).
20. Deupi, X., Standfuss, J. & Schertler, G. Conserved activation pathways in G-protein coupled receptors. *Biochem Soc Trans* **40**, 383-8 (2012).
21. Rasmussen, S.G. et al. Crystal structure of the human beta2 adrenergic G-protein coupled receptor. *Nature* **450**, 383-7 (2007).
22. Bhattacharya, S., Hall, S.E., Li, H. & Vaidehi, N. Ligand-stabilized conformational states of human beta(2) adrenergic receptor: insight into G-protein-coupled receptor activation. *Biophys J* **94**, 2027-42 (2008).
23. Dror, R.O. et al. Activation mechanism of the beta2-adrenergic receptor. *Proc Natl Acad Sci U S A* **108**, 18684-9 (2011).
24. Liu, J.J., Horst, R., Katritch, V., Stevens, R.C. & Wuthrich, K. Biased signaling pathways in beta2-adrenergic receptor characterized by 19F-NMR. *Science* **335**, 1106-10 (2012).
25. Zocher, M., Fung, J.J., Kobilka, B.K. & Muller, D.J. Ligand-specific interactions modulate kinetic, energetic, and mechanical properties of the human beta2 adrenergic receptor. *Structure* **20**, 1391-402 (2012).
26. Manglik, A. et al. Structural Insights into the Dynamic Process of beta2-Adrenergic Receptor Signaling. *Cell* **161**, 1101-11 (2015).
27. Sbai, O. et al. Biased signaling through G-protein-coupled PROKR2 receptors harboring missense mutations. *FASEB J* **28**, 3734-44 (2014).
28. Peterson, S.M. et al. Elucidation of G-protein and beta-arrestin functional selectivity at the dopamine D2 receptor. *Proc Natl Acad Sci U S A* **112**, 7097-102 (2015).
29. Valentin-Hansen, L., Frimurer, T.M., Mokrosinski, J., Holliday, N.D. & Schwartz, T.W. Biased Gs Versus Gq Proteins and beta-Arrestin Signaling in the NK1 Receptor Determined by Interactions in the Water Hydrogen Bond Network. *J Biol Chem* **290**, 24495-508 (2015).
30. Nakajima, K. & Wess, J. Design and functional characterization of a novel, arrestin-biased designer G protein-coupled receptor. *Mol Pharmacol* **82**, 575-82 (2012).
31. Katsonis, P. & Lichtarge, O. A formal perturbation equation between genotype and phenotype determines the Evolutionary Action of protein-coding variations on fitness. *Genome Res* **24**, 2050-8 (2014).
32. Lichtarge, O., Bourne, H.R. & Cohen, F.E. An evolutionary trace method defines binding surfaces common to protein families. *J Mol Biol* **257**, 342-58 (1996).
33. Neskey, D.M. et al. Evolutionary Action Score of TP53 Identifies High-Risk Mutations Associated with Decreased Survival and Increased Distant Metastases in Head and Neck Cancer. *Cancer Res* **75**, 1527-36 (2015).
34. Osman, A.A. et al. Wee-1 kinase inhibition overcomes cisplatin resistance associated with high-risk TP53 mutations in head and neck cancer through mitotic arrest followed by senescence. *Mol Cancer Ther* **14**, 608-19 (2015).

35. Osman, A.A. et al. Evolutionary Action Score of TP53 Coding Variants Is Predictive of Platinum Response in Head and Neck Cancer Patients. *Cancer Res* **75**, 1205-15 (2015).
36. Erdin, S., Ward, R.M., Venner, E. & Lichtarge, O. Evolutionary trace annotation of protein function in the structural proteome. *J Mol Biol* **396**, 1451-73 (2010).
37. Rodriguez, G.J., Yao, R., Lichtarge, O. & Wensel, T.G. Evolution-guided discovery and recoding of allosteric pathway specificity determinants in psychoactive bioamine receptors. *Proc Natl Acad Sci U S A* **107**, 7787-92 (2010).
38. Wilkins, A.D., Bachman, B.J., Erdin, S. & Lichtarge, O. The use of evolutionary patterns in protein annotation. *Curr Opin Struct Biol* **22**, 316-25 (2012).
39. Wilkins, A.D. et al. Accounting for epistatic interactions improves the functional analysis of protein structures. *Bioinformatics* **29**, 2714-21 (2013).
40. Kang, H.J., Wilkins, A.D., Lichtarge, O. & Wensel, T.G. Determinants of endogenous ligand specificity divergence among metabotropic glutamate receptors. *J Biol Chem* **290**, 2870-8 (2015).
41. Sung, Y.M., Wilkins, A.D., Rodriguez, G.J., Wensel, T.G. & Lichtarge, O. Intramolecular allosteric communication in dopamine D2 receptor revealed by evolutionary amino acid covariation. *Proc Natl Acad Sci U S A* **113**, 3539-44 (2016).
42. Shenoy, S.K. et al. beta-arrestin-dependent, G protein-independent ERK1/2 activation by the beta2 adrenergic receptor. *J Biol Chem* **281**, 1261-73 (2006).
43. Mihalek, I., Res, I. & Lichtarge, O. A family of evolution-entropy hybrid methods for ranking protein residues by importance. *J Mol Biol* **336**, 1265-82 (2004).
44. Pardo, L., Deupi, X., Dolker, N., Lopez-Rodriguez, M.L. & Campillo, M. The role of internal water molecules in the structure and function of the rhodopsin family of G protein-coupled receptors. *Chembiochem* **8**, 19-24 (2007).
45. Nygaard, R., Valentin-Hansen, L., Mokrosinski, J., Frimurer, T.M. & Schwartz, T.W. Conserved water-mediated hydrogen bond network between TM-I, -II, -VI, and -VII in 7TM receptor activation. *J Biol Chem* **285**, 19625-36 (2010).
46. Huang, W. et al. Structural insights into micro-opioid receptor activation. *Nature* **524**, 315- 21 (2015).
47. Ballesteros, J. & Weinstein, H. Integrated methods for the construction of three dimensional models and computational probing of structure-function relations in G-protein coupled receptors. *Methods Neurosci* **25**, 366–428 (1995).
48. Kim, H. & Park, H. Sparse non-negative matrix factorizations via alternating non negativity-constrained least squares for microarray data analysis. *Bioinformatics* **23**, 1495- 502 (2007).
49. Lee, D.D. & Seung, H.S. Learning the parts of objects by non-negative matrix factorization. *Nature* **401**, 788-91 (1999).
50. Chemical Computing Group Inc. Molecular Operating Environment (MOE). *1010 Sherbooke St. West, Suite #910, Montreal, QC, Canada, H3A 2R7* (2015).
51. Isogai, S. et al. Backbone NMR reveals allosteric signal transduction networks in the beta1-adrenergic receptor. *Nature* **530**, 237-41 (2016).
52. Rose, A.S. et al. Position of transmembrane helix 6 determines receptor G protein coupling specificity. *J Am Chem Soc* **136**, 11244-7 (2014).
53. Barak, L.S., Menard, L., Ferguson, S.S., Colapietro, A.M. & Caron, M.G. The conserved seven-transmembrane sequence NP(X)2,3Y of the G-protein-coupled

receptor superfamily regulates multiple properties of the beta 2-adrenergic receptor. *Biochemistry* **34**, 15407-14 (1995).
54. Prioleau, C., Visiers, I., Ebersole, B.J., Weinstein, H. & Sealfon, S.C. Conserved helix 7 tyrosine acts as a multistate conformational switch in the 5HT2C receptor. Identification of a novel "locked-on" phenotype and double revertant mutations. *J Biol Chem* **277**, 36577- 84 (2002).
55. Kang, Y. et al. Crystal structure of rhodopsin bound to arrestin by femtosecond X-ray laser. *Nature* **523**, 561-7 (2015).
56. Bokoch, M.P. et al. Ligand-specific regulation of the extracellular surface of a G-protein coupled receptor. *Nature* **463**, 108-12 (2010).
57. Nygaard, R. et al. The dynamic process of beta(2)-adrenergic receptor activation. *Cell* **152**, 532-42 (2013).
58. Lavoie, C. et al. Beta 1/beta 2-adrenergic receptor heterodimerization regulates beta 2-adrenergic receptor internalization and ERK signaling efficacy. *J Biol Chem* **277**, 35402-10 (2002).
59**.** Oakley, R.H., Laporte, S.A., Holt, J.A., Barak, L.S & Caron, M.G. Association of beta arrestin with G protein-coupled receptors during clathrin-mediated endocytosis dictates the profile of receptor resensitization. *J Biol Chem* **274**, 32248-57 (1999).
60. Devost, D. et al. Cellular and subcellular context determine outputs from signaling biosensors. *Methods Cell Biol* **132**, 319-37 (2016).
61. Gales, C. et al. Real-time monitoring of receptor and G-protein interactions in living cells. *Nat Methods* **2**, 177-84 (2005).
62. Quoyer, J. et al. Pepducin targeting the C-X-C chemokine receptor type 4 acts as a biased agonist favoring activation of the inhibitory G protein. *Proc Natl Acad Sci U S A* **110**, E5088-97 (2013).
63. Breton, B. et al. Multiplexing of multicolor bioluminescence resonance energy transfer. *Biophys J* **99**, 4037-46 (2010).
64. Kenakin, T. & Christopoulos, A. Signalling bias in new drug discovery: detection, quantification and therapeutic impact. *Nat Rev Drug Discov* **12**, 205-16 (2013).
65. van der Westhuizen, E.T., Breton, B., Christopoulos, A. & Bouvier, M. Quantification of ligand bias for clinically relevant beta2-adrenergic receptor ligands: implications for drug taxonomy. *Mol Pharmacol* **85**, 492-509 (2014).
66. Labute, P. Protonate3D: assignment of ionization states and hydrogen coordinates to macromolecular structures. *Proteins* **75**, 187-205 (2009).
67. Pettersen, E.F. et al. UCSF Chimera--a visualization system for exploratory research and analysis. *J Comput Chem* **25**, 1605-12 (2004).
68. van der Walt, S., Colbert , S.C. & Varoquaux, G. The NumPy Array: A Structure for Efficient Numerical Computation. *Comput Sci Eng* **13**, 22-30 (2011).
69. Guan, X.M., Kobilka, T.S. & Kobilka, B.K. Enhancement of membrane insertion and function in a type IIIb membrane protein following introduction of a cleavable signal peptide. *J Biol Chem* **267**, 21995-8 (1992).

Acknowledgements. This work was supported, in part, by grants from the Canadian Institutes for Health Research (CIHR) [MOP 11215] to MB and [MOP 102630] to MB and OL and from the National Institute of Health (NIH) subaward [1R01AI110007-01A1] to MB. AMS was supported by post-doctoral research fellowships from the Fonds de la Recherche du Quebec - Santé (FRQ-S). L-PP was supported by a CIHR and a FRQS studentship while MA held studentship from CIHR and the Heart and Stroke Foundation of Canada. WS was supported by the Vanier Canada Graduate Scholarship from the CIHR. MB holds the Canada Research Chair in Signal Transduction and Molecular Pharmacology

Author contributions

A.M.S., O.L. M.L. and M.B. designed the study. A.M.S. performed most of the experimentation (Gs- and Gi- activation assay, cAMP production assay, βarrestin2-recruitment, Endocytosis, Cell surface expression, BRET-based binding assay) as well as the analysis of the data (concentration response curves, correction for Cell Surface Expression, Structure Prediction and Analysis, and Data Analysis). J.G. and A.D.W. performed the Evolutionary Trace Analysis, Evolutionary Action Scores, Clustering and EA score clustering. C.L.G. designed and constructed the pCDNA3.1 Zeo(+)βarr2 trans constructs biosensor. L.-P.P. made the V2R mutants, and performed the experimentation and the data analysis for V2R, as well as did some the binding assays on the β2AR mutants. M.A. and W.S. helped design the study and the mutants to use as well as created part of the mutant receptors. M.K. helped perform the statistical analysis of the data. O.L. designed, supervised and interpreted all Evolutionary Trace Analysis, Evolutionary Action Scores and EA score clustering performed in his lab. A.M.S. and M.B. wrote the manuscript, with the assistance of J.G., A.D.W., L.-P.P., ML and O.L.

Competing financial interests Statement. The authors declare that they have no competing financial interest

Figure Legends

Figure 1 | Location of mutated residues in the β2AR. (a) 3D representation of WT β2AR structure (pdb: 2RH1). Mutated residues are shown as orange spheres. Residues part of microswitches are shown in stick representation and are colored in dark grey. Blue ellipses denote the ligand binding and the effector binding regions. **(b)** Snakeplot of β2AR depicting the location of mutated residues (colored in orange). Residues part of known microswitches are colored in light grey.

Figure 2 | Signaling of the β2AR. (a) Simplified schematic of β2AR signaling pathways monitored in this study. **(b)** Concentration response curves of the five monitored pathways for WT and three variants of β2AR to exemplify original data. K273A is representative of mutations that yielded a signalling profile similar to WT whereas I127N exemplifies mutations increasing the constitutive activity of Gi that abrogate its ISO-stimulation and reducing most of βarrestin engagement and endocytosis whereas R328A exemplifies mutations in which Gi constitutive activity is increased and ISO stimulation is abrogated but βarrestin and endocytosis are maintained. For each concentration response curve, the β2AR-unspecific response (value of cells only transfected with the biosensor (no receptor added)) was set to 0% and the maximal ISO-stimulated response of WT β2AR to 100%. The non-stimulated condition (veh) represents the basal activity in each monitored pathway. Data for all β2AR variants is given in Supplementary Fig. 2. For details, see Methods.

Figure 3 | Normalizing to cell surface expression. (a) surface expression as % of WT for WT and β2AR variants. The standard curve of WT β2AR was performed by increasing the transfected DNA-amount and controlling surface expression-level. Data shown are the average ±s.e.m. of at least 3 independent experiments performed in duplicate. **(b)** Standard curves for all measures of WT β2AR were generated in order to compensate for variations in expression level. If there is a linear correlation between expression and measure, an interpolated value for wild type is used for comparison. Otherwise the variant is compared to an average WT-value. For details see Methods.

Figure 4 | Clustering and Signaling Profiles of β2AR variants. (a) Clustering by NNMF/K means method based on the signaling parameters. The clusters one to three are color coded. The EA-score for each mutation is given in brackets. n/a: not available. **(b)** Radial graphs of the signaling profile for each cluster. Each cluster is displayed by overlaying the receptor variant profiles. The data is shown as normalized difference (mut-WT divided by mut+WT). WT is shown in red as reference. Each mutant receptor is in blue, resulting in darker areas when overlayed. The signaling profiles of all receptor variants are given in Supplementary Fig. 3. **(c)** Correlation of EA with magnitude of phenotypic change by addition of the magnitude of change in each parameter of the signaling profile.

Figure 5 | Structural changes induced by mutations in the β2AR. (a) Predicted changes within 4.5Å of the mutated position of β2AR shown by cluster for the inactive conformation (pdb: 2RH1, top) and the active conformation (pdb: 4LDE, bottom). Residues are colored by cluster (mutated residues – black, cluster 1 – green, cluster 2 – orange, cluster 3 – blue) and

depicted as spheres. **(b)** Number of affected residues in the inactive (left) and active (right) conformation normalized by cluster size.

Figure 6 | Influence on microswitches. Predicted changes in the environment of four microswitches (toggle-W2866.48, PIF-P2115.50,I1213.40,F2826.44, NPxxY-N3227.49,P3237.50,Y3267.53,L752.46,D792.50, DRY-D1303.49,R1313.50,Y1323.51,E2686.30) in **(a)** the inactive (pdb: 2RH1) and **(b)** the active conformation (pdb: 4LDE). The predicted changes are colored by cluster (cluster 1 – green, cluster 2 – orange, cluster 3 – blue) and depicted as spheres. Residues of the microswitches and known interaction partners are colored yellow, shown in stick representation and labeled in the upper most row of (a) and (b).

Supplementary Figure 1 | β_2AR data analysis. (**a**) Raw data of concentration response curves of β_2AR for the five monitored pathways were determined with log(agonist) vs response -- Variable slope (four parameters) in Prism. Fitted values for the Hill slope were also used when fitting the β_2AR variants and are given here. Data shown are representatives of at least 3 independent experiments performed in duplicate. Data analysis (**b**) for BRET-based assays and (**c**) ELISA-based assay. For details see Methods.

Supplementary Figure 2 | Experimental results. Concentration response curves for five monitored pathways of 28 β_2AR variants. Data shown are the average ±s.e.m. of at least 3 independent

experiments performed in duplicate.

Supplementary Figure 3 | Correction for the variation in cell surface expression level. In order to correct for the difference in cell surface expression of the different β_2AR variants, concentration response

curves for WT β_2AR using 5% to 150% of DNA-amount used for the variants were generated for each assay (Gs-activation, Gi activation, cAMP production, βarrestin recruitment and endocytosis) and cell surface expression measured (**Fig. 3a**). The signaling parameters (basal, maximal and lSO-induced activity, pEC_{50} and $logT/K_A$) were then determined for each % of WT β_2AR DNA for each assay and their correlation to expression level calculated (**Fig. 3b**).

Supplementary Figure 4 | Radial graphs of signaling signature for each mutant. **(a)** cluster 1, **(b)** cluster 2 and **(c)** cluster 3. Signaling signature for four V86-mutations with increasing EA score are highlighted by red squares. The low EA-score mutation (V86I) slightly increases basal G-protein activation and slightly reduces ISO-stimulated Gsactivation and βarrestin2-engagement. The medium low EA-score mutation (V86A) increases basal G-protein activity, as well as maximal and ISO-induced Gi activation. ISO-stimulated Gs-activation and βarrestin2-engagement are slightly reduced. The medium high EA-score mutation (V86Y) increases basal G-protein activation and Gi maximal activity. Additionally, a decrease in ISO-stimulated Gs-activation and no response to ISO in Gi activation, βarrestin2-engagement and endocytosis are observed. The high EA-score mutation (V86D) shows a similar phenotype to V86Y, but slightly more pronounced. Data is shown as normalized difference (mut-WT/mut+WT). WT is shown in red as reference and each receptor variant is shown in blue.

Supplementary Figure 5 | Predicted changes within 4.5 Å of each mutated position on the inactive conformation. (**a**) cluster 1, (**b**) cluster 2 and (**c**) cluster 3 are mapped on the inactive conformation (pdb: 2RH1).

Supplementary Figure 6 | Predicted changes within 4.5 Å of each mutated position on the active conformation. (**a**) cluster 1, (**b**) cluster 2 and (**c**) cluster 3 are mapped on the active conformation (pdb: 4LDE).

Supplementary Figure 7 | Transferability of mutations from β2AR to V2R. Concentration response curves for (**a**) Gs activation, (**b**) cAMP production and (**c**) βarrestin recruitment of $I_{6.40}$ position in β2AR and V2R. Mutants are shown in red and an equivalent concentration of WT receptor in blue. Data show that the mutation is transferable from the β2AR to the V2R with similar effects. I276V/L doesn't or slightly affect Gαs activation, cAMP production and βarrestin recruitment whereas the I276Q variant affects βarrestin recruitment without affecting the two other pathways. Data shown are the average ±s.e.m. of at least 3 independent experiments performed in duplicate.

Supplementary Figure 8 | BRET-based binding assay. (**a**) Principle of BRET-based binding assay. (**b**) Schematic representation of receptor constructs. The receptor was modified at the N-terminus as indicated. (**c**) ISO-induced cAMP-production is not changed in Nluc-β2AR. (**d**) The Kd of the radioligand CpG12177 to Nluc-β2AR is slightly increased. (**e**) Total and non-specific binding of (S)-Propranolol-green was determined by saturation experiments. (**f**) For several β2AR ligands the pK_i can be determined in competition with 100nM (S)-Propranolol-green and fitting with "One-site - Fit Ki" for competition binding in Prism. All data shown are representatives of at least 2 independent experiments performed in duplicate.

Figure 1

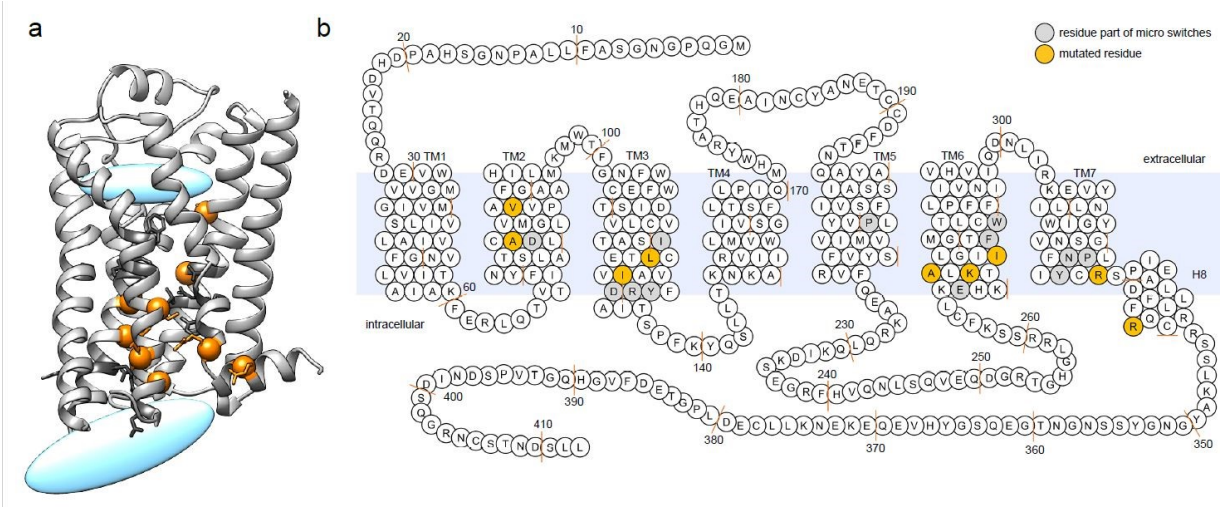
a
b
residue part of micro switches
mutated residue
extracellular
intracellular
TM1
TM2
TM3
TM4
TM5
TM6
TM7
H8

c

Figure 2

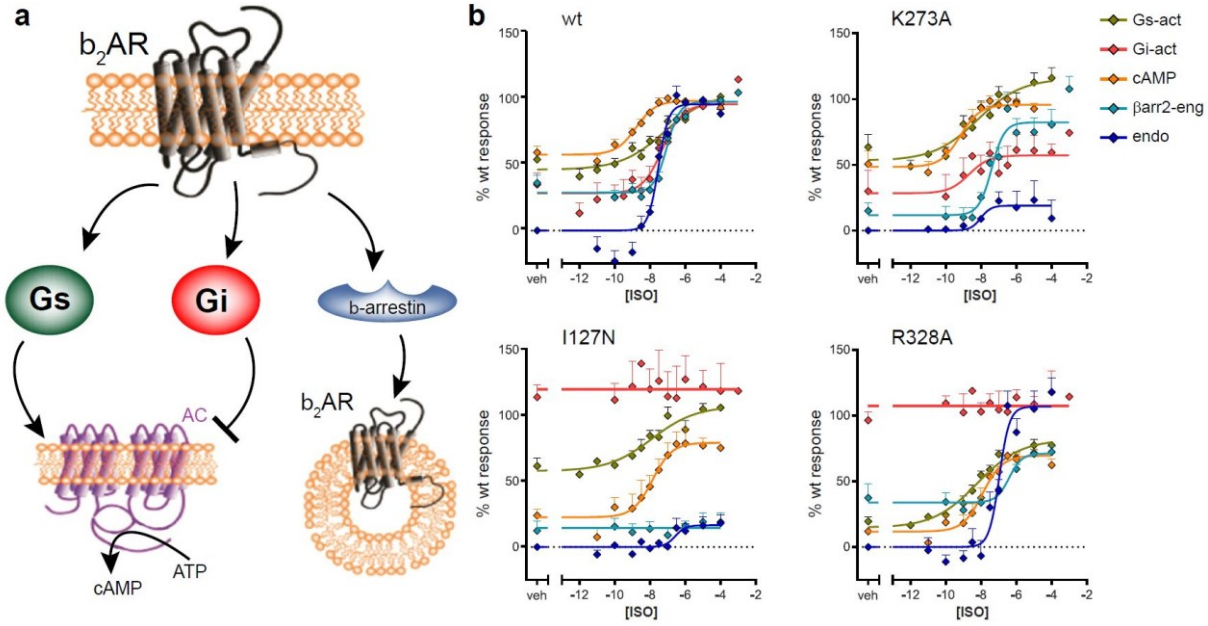
a
b2AR
Gs
Gi
b-arrestin
AC
ATP
cAMP
b2AR
b
wt
K273A
I127N
R328A
% wt response
[ISO]
veh
Gs-act
Gi-act
cAMP
βarr2-eng
endo

Figure3

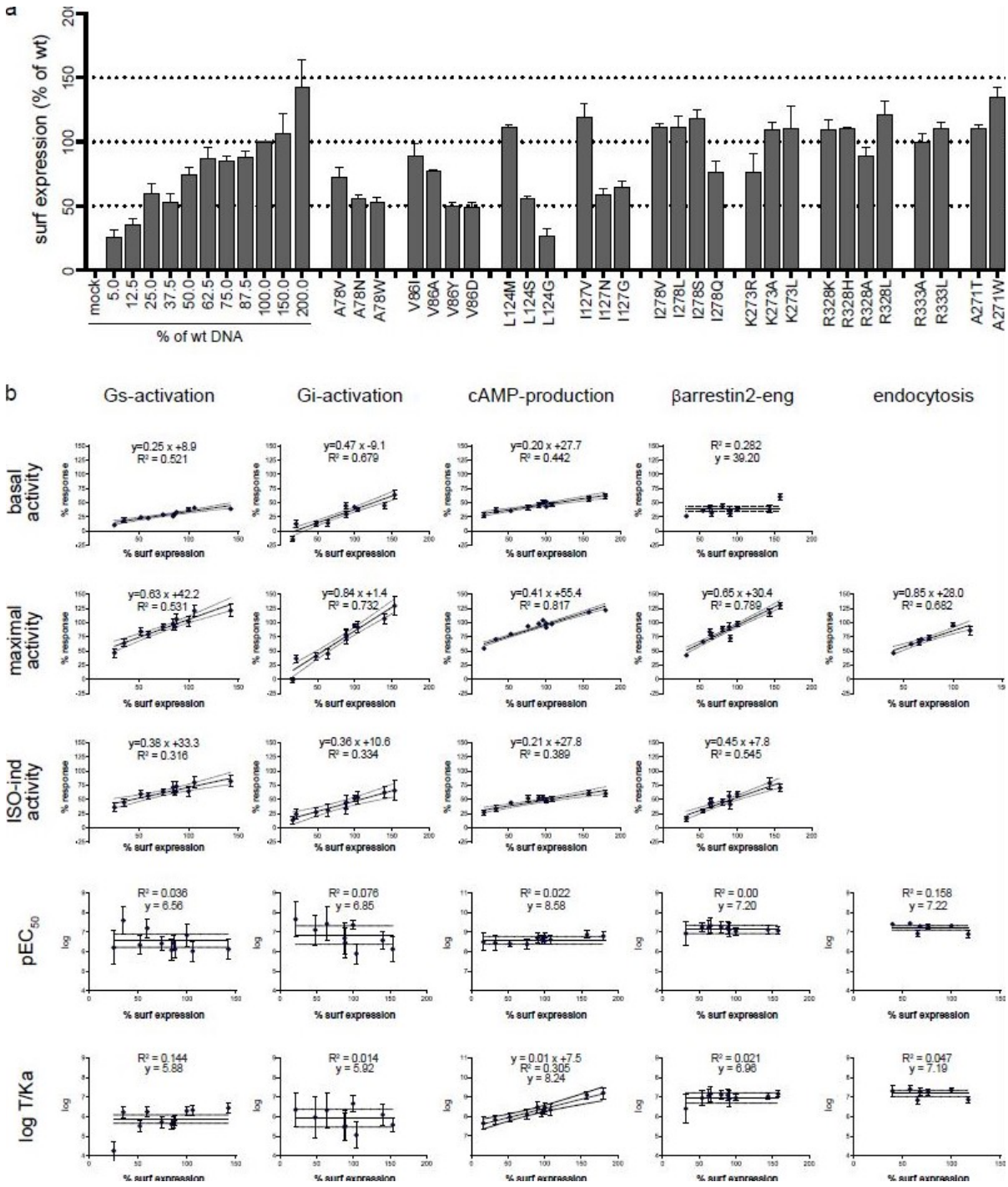
a
surf expression (% of wt)
0
50
100
150
200
mock
5.0
12.5
25.0
37.5
50.0
62.5
75.0
87.5
100.0
150.0
200.0
% of wt DNA
A78V
A78N
A78W
V86I
V86A
V86Y
V86D
L124M
L124S
L124G
I127V
I127N
I127G
I278V
I278L
I278S
I278Q
K273R
K273A
K273L
R328K
R328H
R328A
R328L
R333A
R333L
A271T
A271W
b
Gs-activation
Gi-activation
cAMP-production
βarrestin2-eng
endocytosis
basal activity
maximal activity
ISO-ind activity
pEC50
log T/Ka
% response
% surf expression
y=0.25 x +8.9
R² = 0.521
y=0.47 x -9.1
R² = 0.679
y=0.20 x +27.7
R² = 0.442
R² = 0.282
y = 39.20
y=0.63 x +42.2
R² = 0.531
y=0.84 x +1.4
R² = 0.732
y=0.41 x +55.4
R² = 0.817
y=0.65 x +30.4
R² = 0.789
y=0.85 x +28.0
R² = 0.682
y=0.38 x +33.3
R² = 0.316
y=0.36 x +10.6
R² = 0.334
y=0.21 x +27.8
R² = 0.389
y=0.45 x +7.8
R² = 0.545
R² = 0.036
y = 6.56
R² = 0.076
y = 6.85
R² = 0.022
y = 8.58
R² = 0.00
y = 7.20
R² = 0.158
y = 7.22
R² = 0.144
y = 5.88
R² = 0.014
y = 5.92
y = 0.01 x +7.5
R² = 0.305
y = 8.24
R² = 0.021
y = 6.96
R² = 0.047
y = 7.19

Figure4

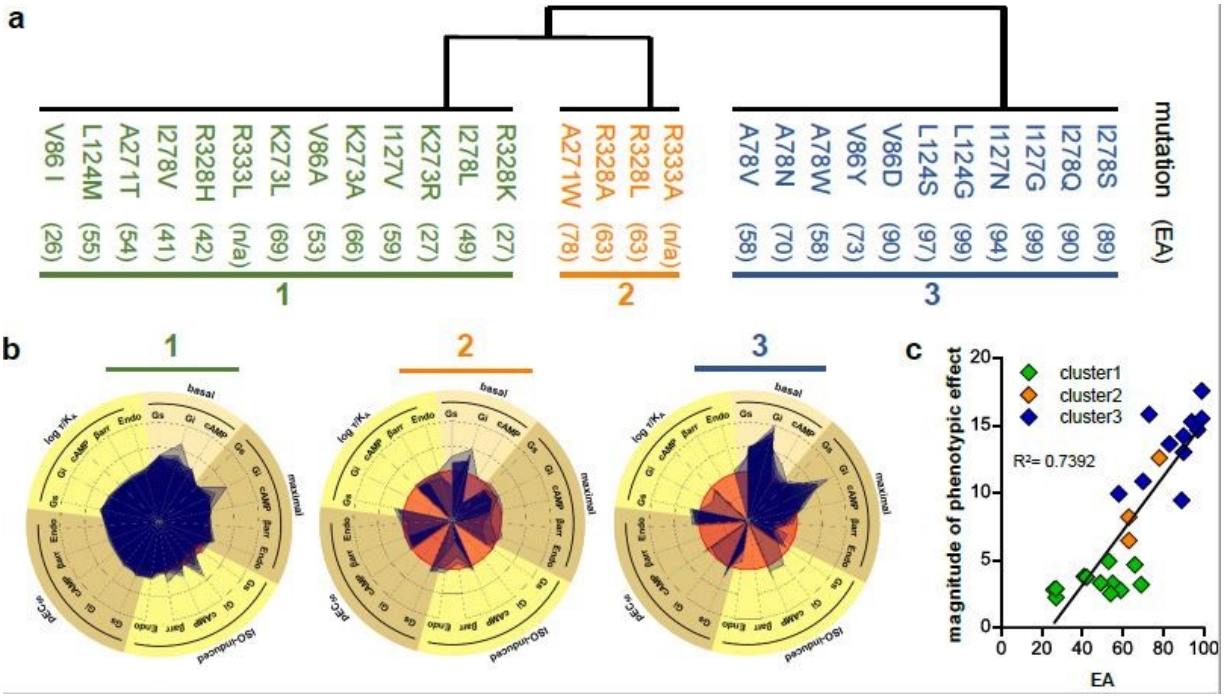
a
mutation (EA)
V86 I (26)
L124M (55)
A271T (54)
I278V (41)
R328H (42)
R333L (n/a)
K273L (69)
V86A (53)
K273A (66)
I127V (59)
K273R (27)
I278L (49)
R328K (27)
R333A (n/a)
R328L (63)
R328A (63)
A271W (78)
A78V (58)
A78N (70)
A78W (58)
V86Y (73)
V86D (90)
L124S (97)
L124G (99)
I127N (94)
I127G (99)
I278Q (90)
I278S (89)
1
2
3
b
1
2
3
basal
maximal
Gs
Gi
cAMP
βarr
Endo
log τ/K
ISO-induced
PEC50
c
cluster1
cluster2
cluster3
R²= 0.7392
magnitude of phenotypic effect
EA
0
5
10
15
20
0
20
40
60
80
100

Figure 5

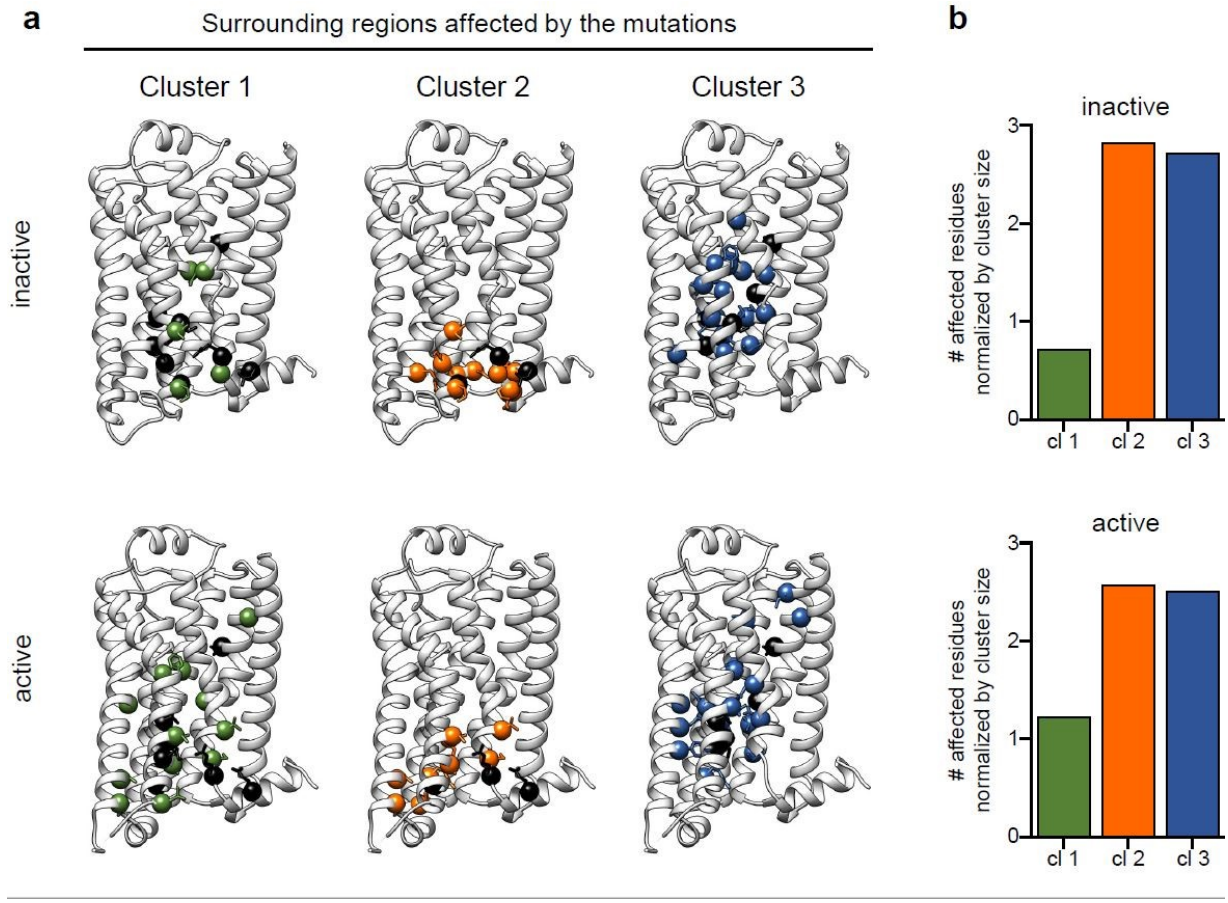
a
Surrounding regions affected by the mutations
Cluster 1
Cluster 2
Cluster 3
inactive
active
b
inactive
active
affected residues
normalized by cluster size
0
1
2
3
cl 1
cl 2
cl 3

Figure 6

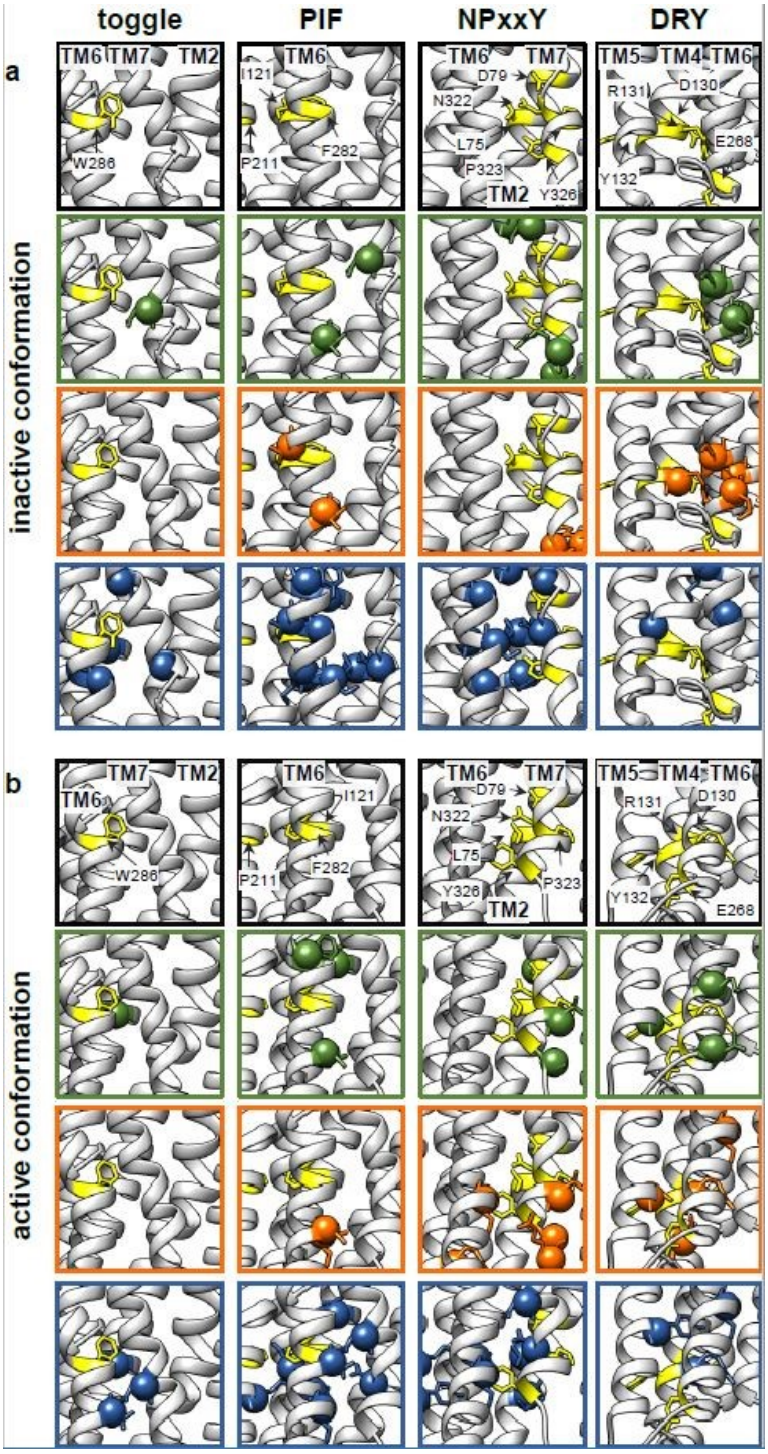
toggle
PIF
NPxxY
DRY
a
inactive conformation
TM6 TM7 TM2
W286
I121 TM6
P211 F282
TM6 TM7
D79
N322
L75
P323
TM2
Y326
TM5 TM4 TM6
R131
D130
E268
Y132
b
active conformation
TM7 TM2
TM6
W286
TM6
I121
P211 F282
TM6 TM7
D79
N322
L75
Y326
P323
TM2
TM5 TM4 TM6
R131
D130
Y132
E268

Supplementary Figure 1

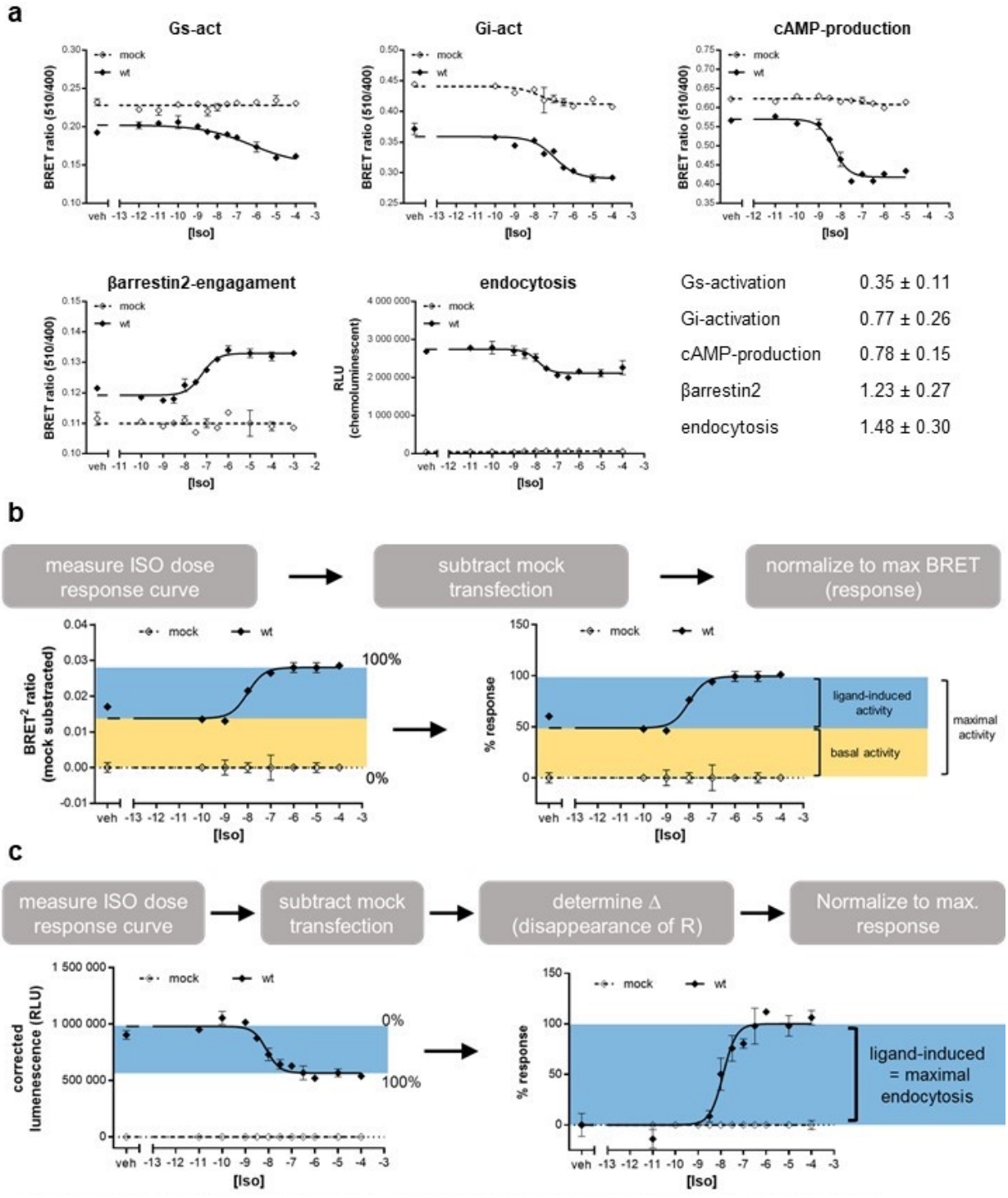

Supplementary Figure2

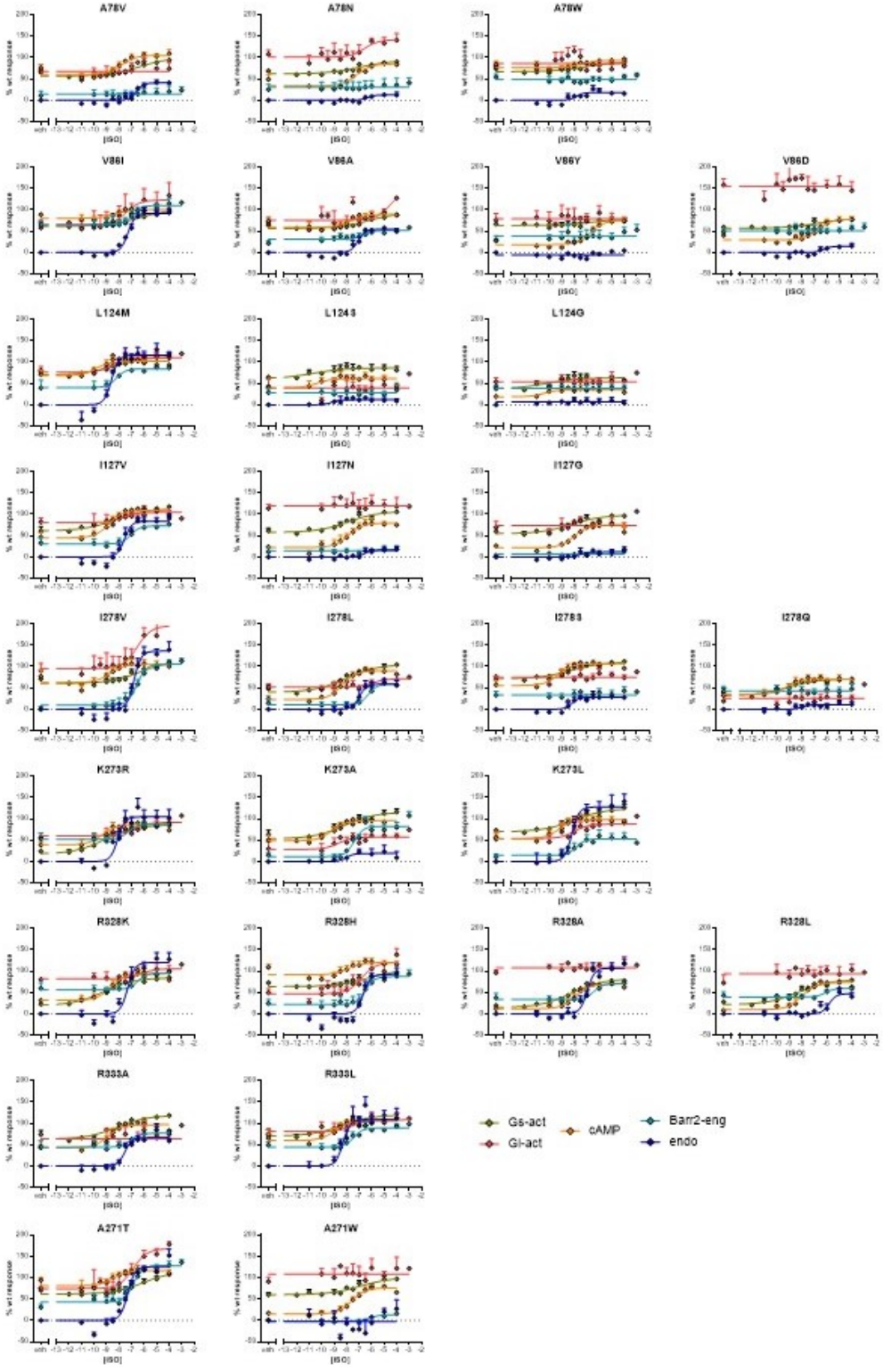

Supplementary Figure 3

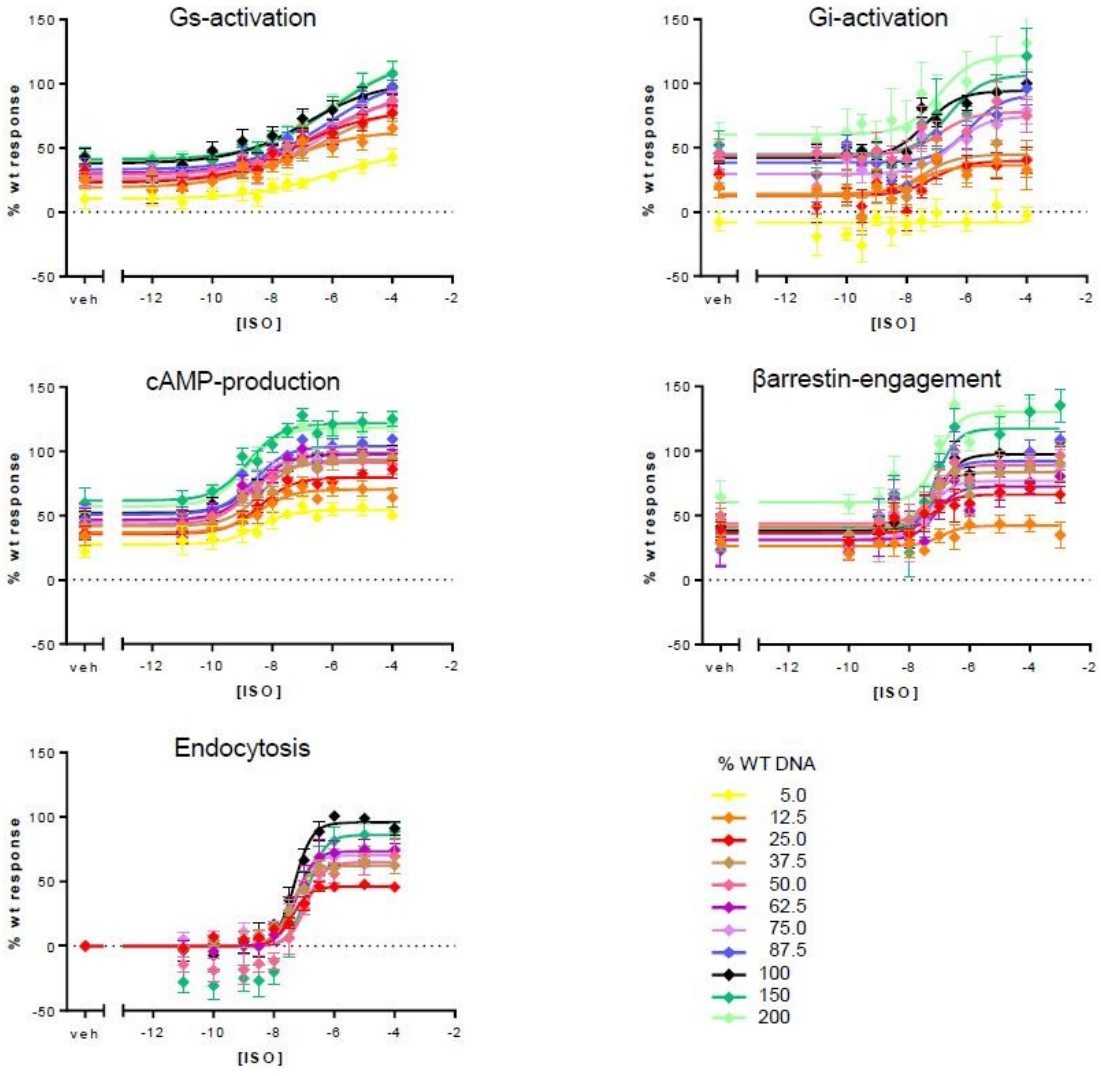

Supplementary Figure 4

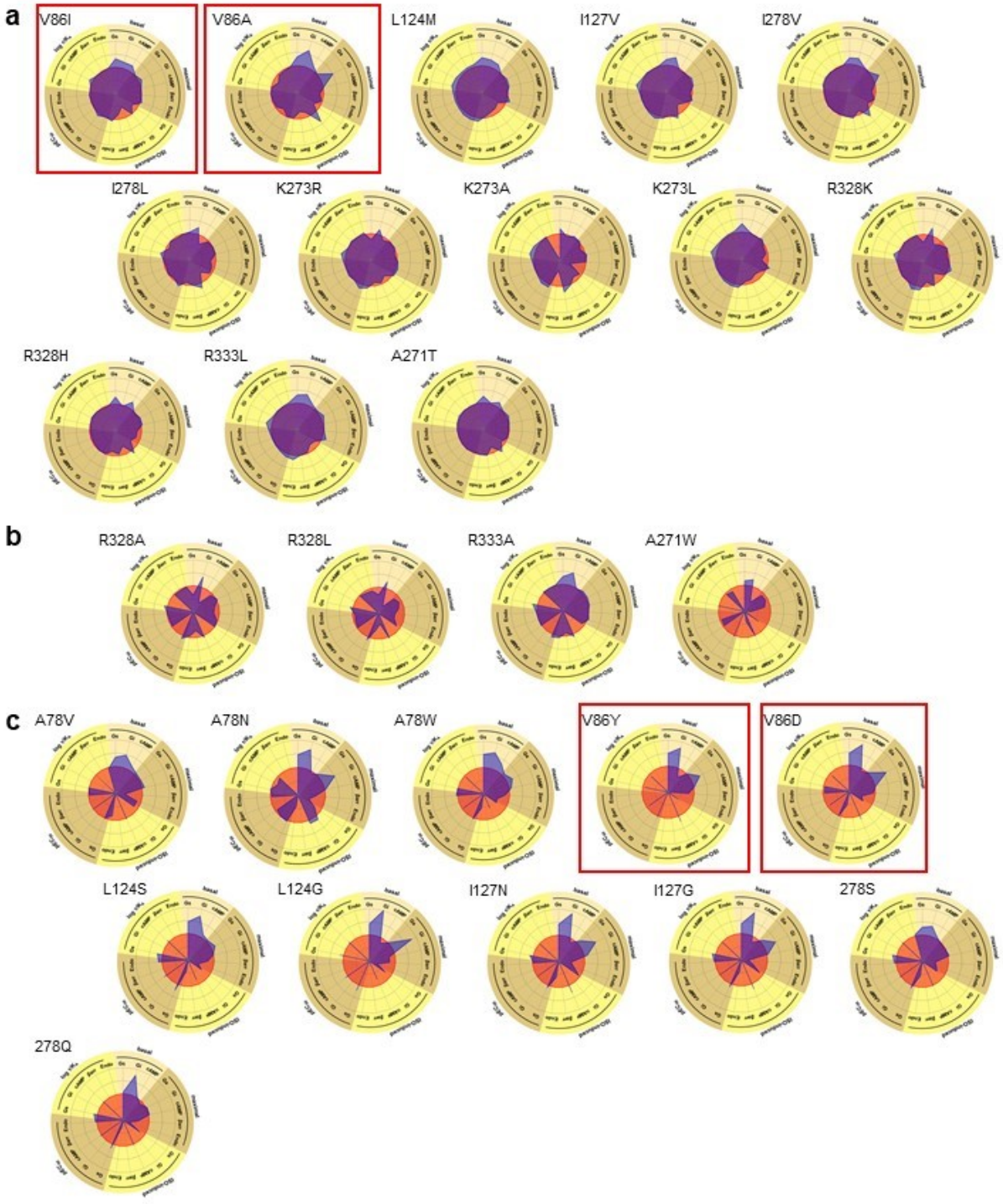

Supplementary Figure 5

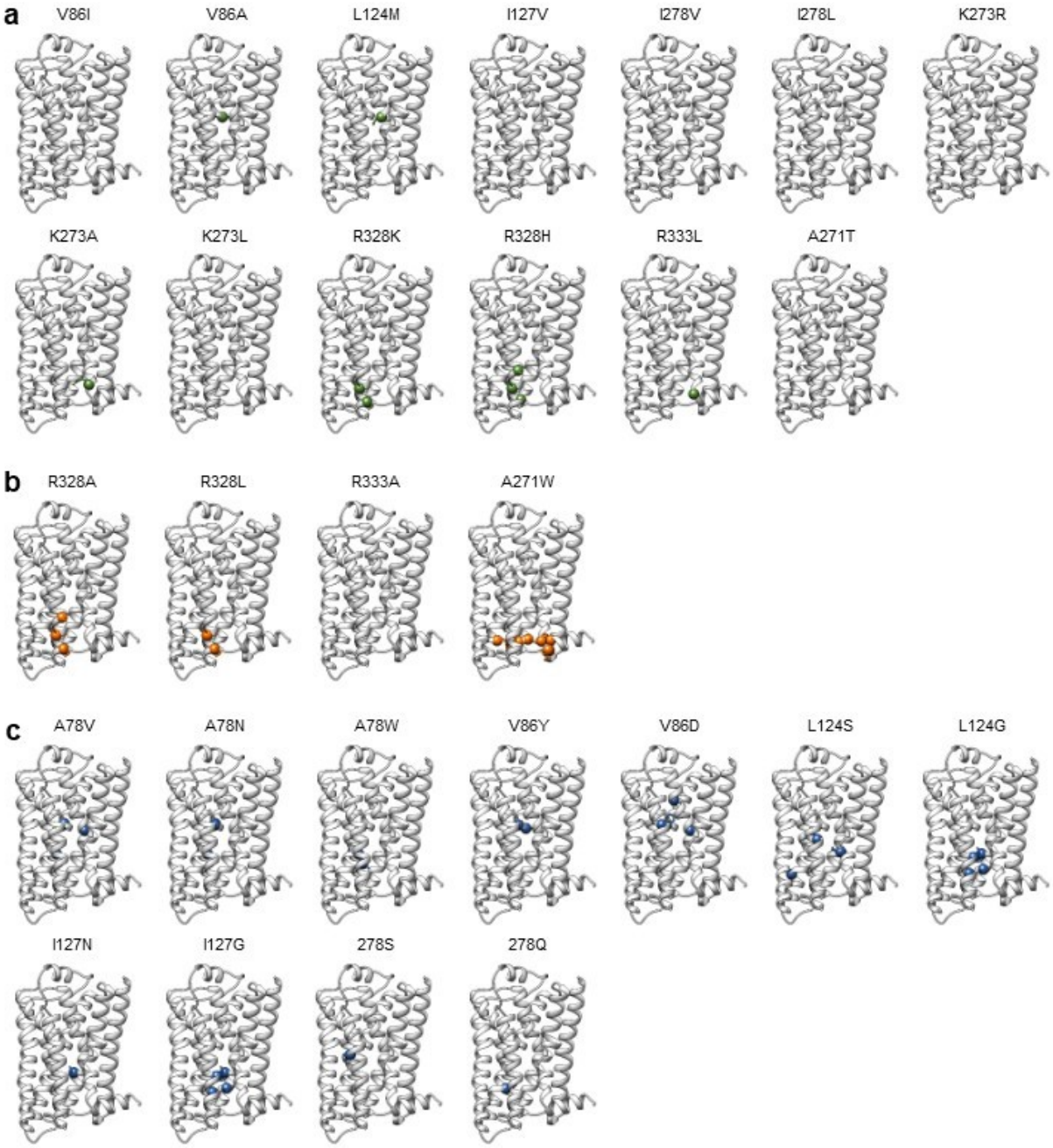

Supplementary Figure 6

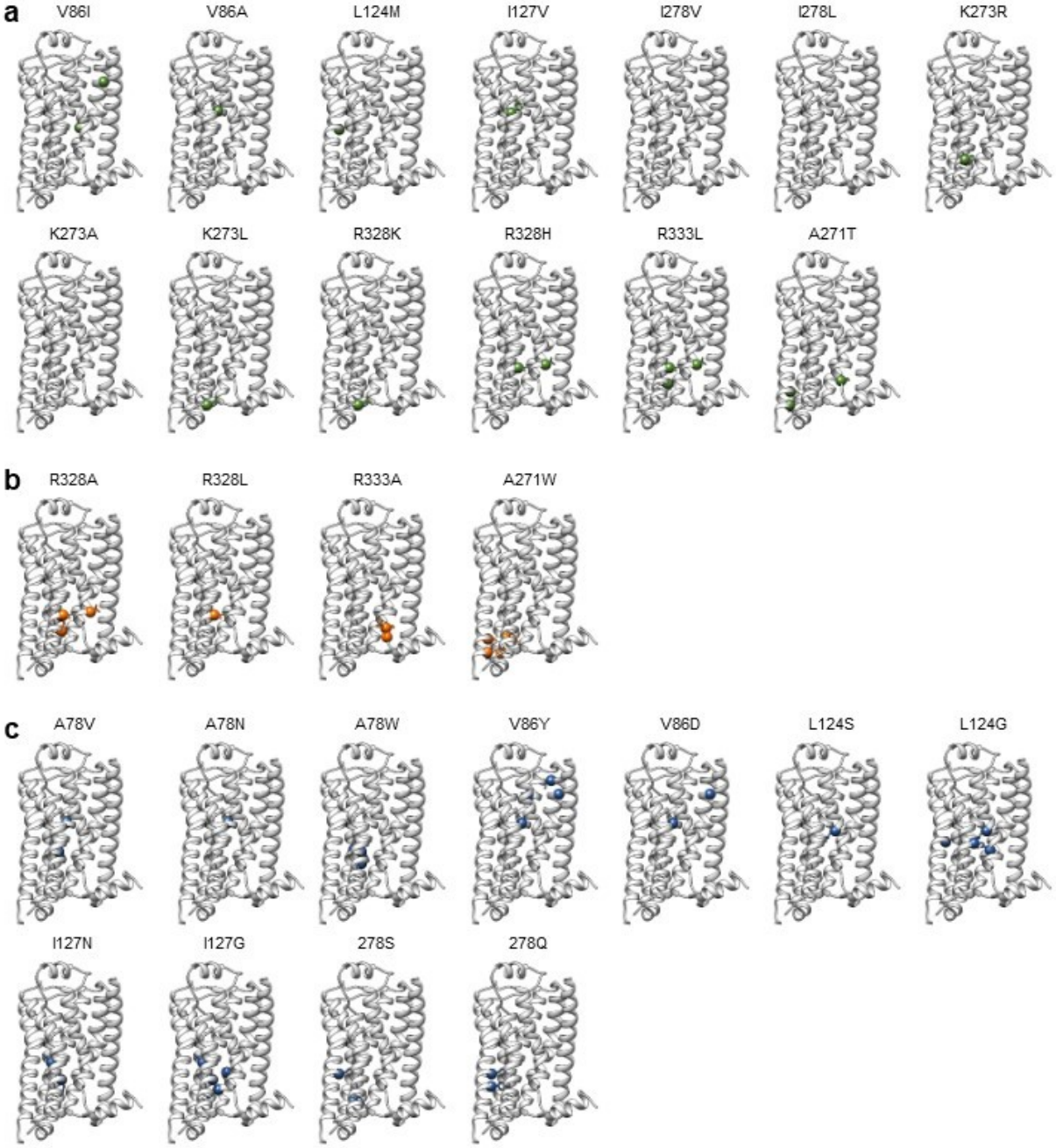

Supplementary Figure 7

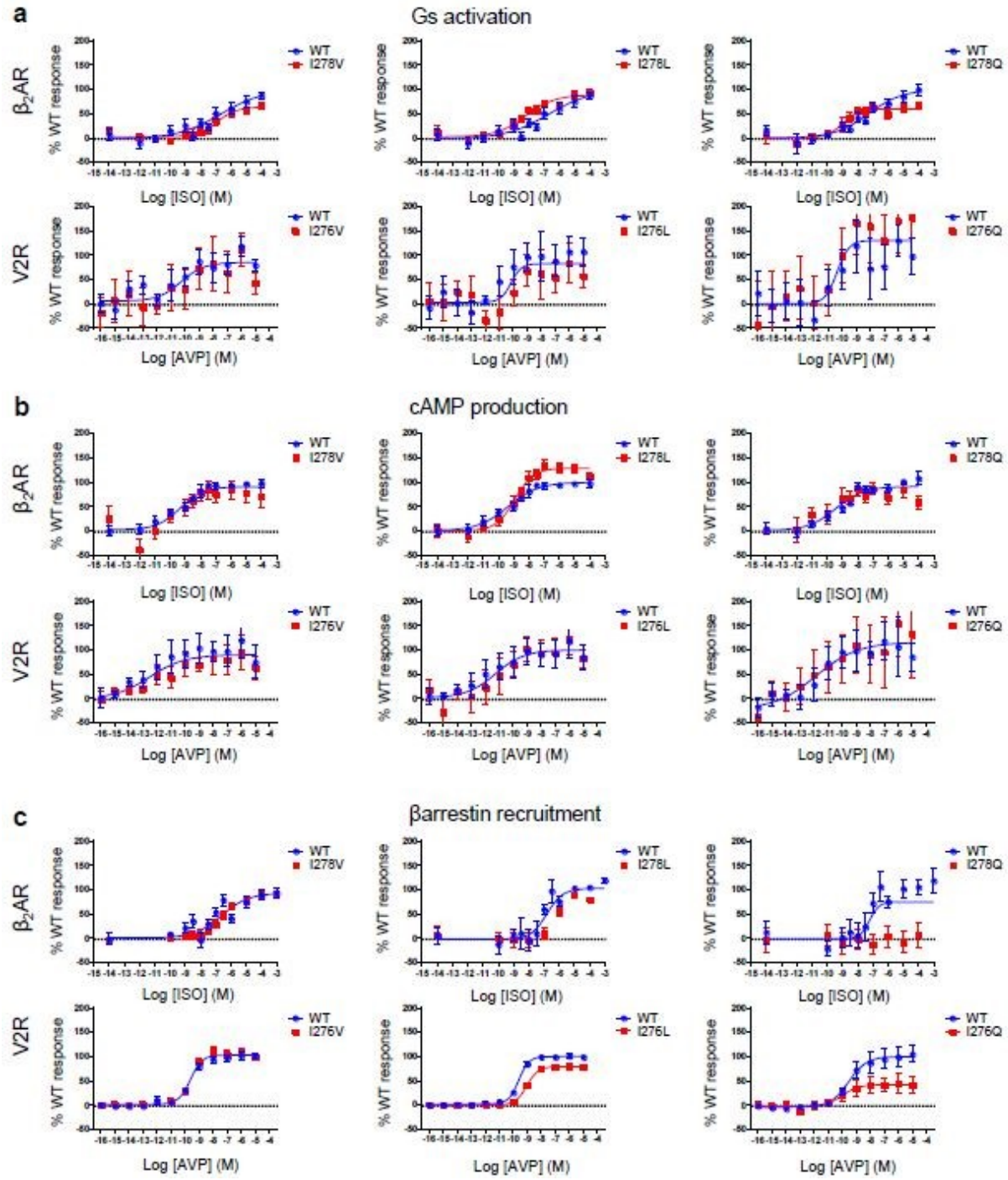

Supplementary Figure 8

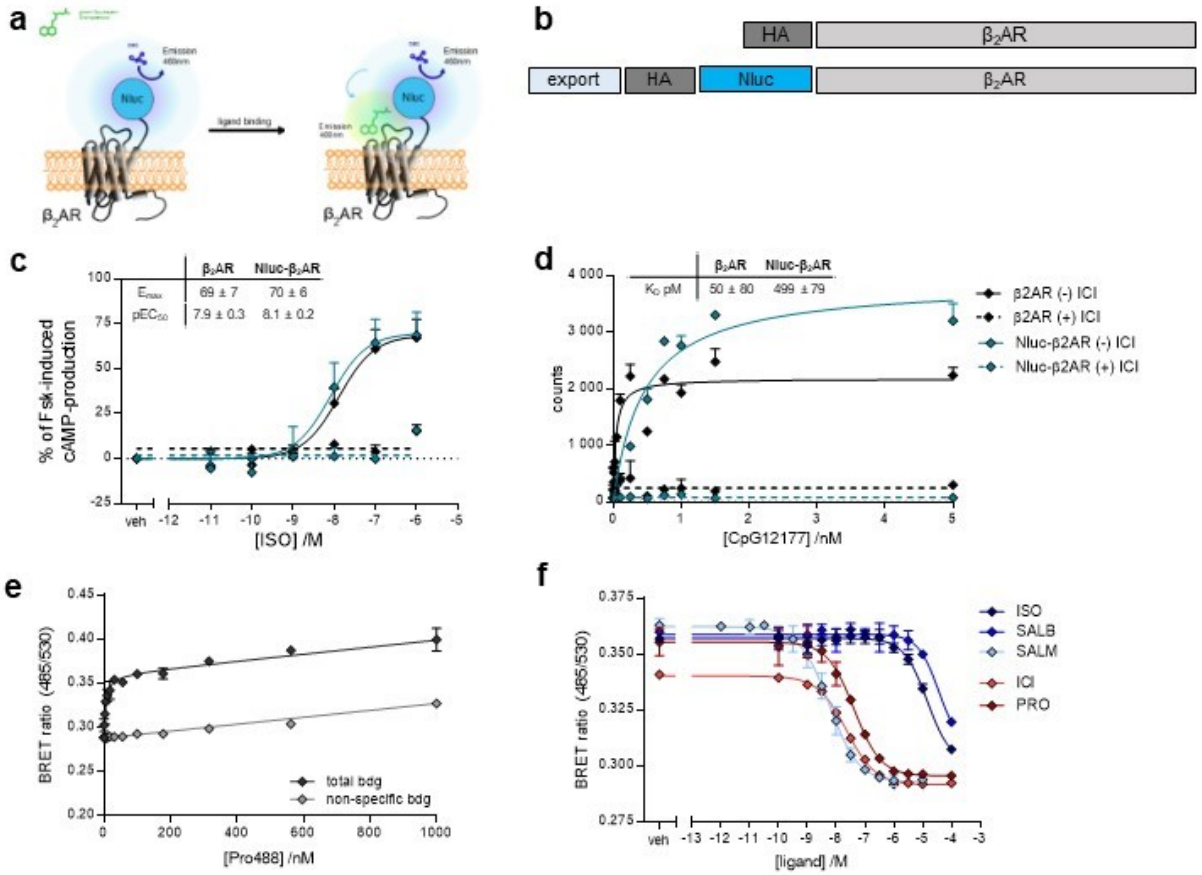

Supplementary Table 1 | Evolutionary importance (ET), distance to the ligand and to the nearest water molecule and substituted amino acid with evolutionary action score (EA) for each mutational target.

	ET score	dist to ligand Å	dist to water Å	Mutation (EA-score)
A78$^{2.49}$	24	10.4	6.4	V (58) N (70) W (58)
V86$^{2.57}$	33	5.9	9.3	I (26) A (53) Y (73) D (90)
L124$^{3.43}$	7	12.7	5.5	M (55) S (97) G (99)
I127$^{3.46}$	7	17.7	7.4	V (59) N (94) G (99)
I278$^{6.40}$	18	15.7	2.9	V (41) L (49) S (89) Q (90)
K273$^{6.35}$	37	23.9	9.8	R (27) L (69) A (66)
R328$^{7.55}$	39	25.1	9.3	K (27) H (42) L (63) A (63)
R333$^{8.51}$	n. d.	30.7	10.2	L (n. d.) A (n. d.)
A271$^{6.33}$	31	25.7	6.0	T (54) W (78)

n. d., not determined; Ballesteros-Weinstein numbering[42] is given in superscript

Supplementary Table 2 | Signaling parameters of Gs-activation of 28 β_2AR variants.

	basal	max	ISO	pEC_{50}	logT/Ka
WT (13)	46 ± 2	104 ± 4	58 ± 4	7.2 ± 03	6.7 ± 0.2
A78V (6)	57 ± 2	100 ± 5	43 ± 4	6.4 ± 0.4	5.9 ± 0.4
A78N (5)	62 ± 2	93 ± 4	31 ± 4	6.9 ± 0.5	6.1 ± 0.5
A78W (5)	67 ± 2	89 ± 4	22 ± 4	7.2 ± 0.8	6.0 ± 0.7
V86I (6)	62± 3	102 ± 7	40 ± 7	6.3 ± 0.7	5.6 ± 0.3
V86A (6)	56 ± 2	93 ± 5	37 ± 5	6.3 ± 0.5	5.5 ± 0.4
V86Y (5)	63 ± 3	78 ± 7	15 ± 7	6.7 ± 2.0	4.9 ± 1.1
V86D (5)	57 ± 2	81 ± 5	24 ± 5	6.7 ± 0.9	5.3 ± 0.7
L124M (3)	70 ± 4	112 ± 4	42 ± 5	8.4 ± 0.6	8.4 ± 0.6
L124S (3)	61 ± 8	86 ± 3	25 ± 8	10.7 ± 1.4	8.6 ± 1.0
L124G (3)	38 ± 6	63 ± 3	25 ± 6	10.1 ± 1.2	7.6 ± 0.9
I127V (3)	61 ± 3	113 ± 3	51 ± 4	8.4 ± 0.3	8.4 ± 0.4
I127N (3)	58 ± 3	107 ± 4	49 ± 5	7.9 ± 0.4	7.5 ± 0.4
I127G (3)	55 ± 3	98 ± 4	44 ± 4	8.2 ± 0.5	7.6 ± 0.4
I278V (6)	61 ± 3	115 ± 7	55 ± 7	6.3 ± 0.5	6.4 ± 0.3
I278L (3)	40 ± 3	105 ± 4	65 ± 4	8.1 ± 0.3	7.6 ± 0.3
I278S (3)	72 ± 3	111 ± 3	39 ± 4	8.2 ± 0.5	8.0 ± 0.5
I278Q (3)	32 ± 4	71 ± 3	40 ± 4	9.1 ± 0.6	7.6 ± 0.5
K273R (3)	18 ± 4	86 ± 3	68 ± 4	9.1 ± 0.3	8 2 ± 0.3
K273L (3)	53 ± 4	116 ± 5	62 ± 6	8.2 ± 0.4	8.4 ± 0.3
K273A (3)	70 ± 4	124 ± 5	54 ± 5	8.0 ± 0.5	8.9 ± 0.5
R328K (3)	19 ± 3	85 ± 2	65 ± 3	9.2 ± 0.3	8.2 ± 0.3
R328H (6)	64 ± 2	104 ± 7	40 ± 6	6.3 ± 0.7	5.6 ± 0.3
R328L (3)	15 ± 3	82 ± 3	67 ± 3	8.2 ± 0.2	7.4 ± 0.3
R328A (3)	22 ± 3	80 ± 3	58 ± 4	8.3 ± 0.3	7.3 ± 0.3
R333L (3)	63 ± 3	119 ± 4	56 ± 5	8.2 ± 0.4	8.6 ± 0.4
R333A (3)	70 ± 3	120 ± 4	49 ± 4	8.4 ± 0.4	9.0 ± 0.5
A271T (6)	62 ± 3	116 ± 9	54 ± 9	6.0 ± 0.6	6.2 ± 0.3
A271W (3)	60 ± 3	101 ± 5	40 ± 5	6.9 ± 0.6	5.9 ± 0.4

Basal, maximal (max) and ISO-induced (ISO) activity are given as % of WT maximal activity. Potency (pEC50) is expressed as -log EC50 M. Signaling efficiency (logT/Ka) was calculated as described in Methods. All data are given as average ±s.e.m. of at least 3 independent experiments performed in duplicate. n for each receptor variant is given in brackets. Note: data in this table are not corrected for expression levels.

Supplementary Table 3 | Signaling parameters of Gi-activation of 28 β_2AR variants.

	basal	max	ISO	pEC_{50}	logT/Ka
WT (22)	28 ± 3	96 ± 5	68 ± 5	7.3 ± 0.2	6.7 ± 0.2
A78V (4)	67 ± 3	67 ± 3	0	n. d.	n. d.
A78N (3)	101 ± 6	142 ± 14	41 ± 14	6.6 ± 0.9	4.1 ± 0.6
A78W (4)	85 ± 4	85 ± 4	0	n. d.	n. d.
V86I (7)	66 ± 13	115 ±13	49 ± 17	8.2 ± 0.9	7.5 ± 0.4
V86A (3)	76 ± 5	148 ±53	72 ± 52	4.5 ± 1.1	3.9 ± 0.4
V86Y (3)	79 ± 4	79 ± 4	0	n. d.	n. d.
V86D (3)	147 ± 7	147 ± 7	0	9.9 ± 2.5	n. d.
L124M (4)	76 ± 8	110 ± 4	34 ± 8	8.5 ± 0.6	7.7 ± 1.1
L124S (3)	39 ± 4	39 ± 4	0	n. d.	n. d.
L124G (3)	54 ± 3	54 ± 3	0	n. d.	n. d.
I127V (3)	81 ± 6	105 ± 5	24 ± 7	7.7 ± 0.7	6.6 ± 1.5
I127N (3)	120 ± 5	120 ± 5	0	n. d.	n. d.
I127G (4)	74 ± 3	74 ± 3	0	n. d.	n. d.
I278V (5)	95 ± 9	196 ± 17	100 ± 18	6.6 ± 0.5	6.6±0.3
I278L (4)	52 ± 3	72 ± 6	19 ± 7	5.9 ± 0.9	4.7 ± 1.7
I278S (4)	75 ± 3	75 ± 3	0	n. d.	n. d.
I278Q (3)	25 ± 3	25 ± 3	0	n. d.	n. d.
K273R (4)	60 ± 6	92 ± 7	31 ± 8	6.9 ± 0.6	5.8 ± 0.9
K273L (4)	28 ± 9	57 ± 5	29 ± 10	8.7 ± 0.9	7.6 ± 1.3
K273A (4)	54 ± 8	88 ± 6	34 ± 9	8.0 ± 0.6	7.0 ± 0.9
R328K (4)	82 ± 5	105 ± 8	24± 9	6.3± 0.9	5.3 ± 1.3
R328H (5)	47 ± 6	121 ± 10	74 ± 11	6.8 ± 0.4	6.3 ± 0.4
R328L (4)	107 ± 3	107 ± 3	0	n. d.	n. d.
R328A (5)	94 ± 4	94 ± 4	0	n. d.	n. d.
R333L (4)	64 ± 5	64 ± 5	0	n. d.	n. d.
R333A (4)	81 ± 7	108 ± 6	28 ± 9	7.6 ± 0.8	6.6 ± 1.1
A271T (5)	61 ± 9	141 ±15	80 ± 16	6.9 ± 0.5	6.6 ± 0.4
A271W (4)	108 ± 5	108 ± 5	0	n. d.	n. d.

Basal, maximal (max) and ISO-induced (ISO) activity are given as % of WT maximal activity. Potency (pEC50) is expressed as -log EC50 M. Signaling efficiency (logT/Ka) was calculated as described in Methods. All data is given as average ±s.e.m. of at least 3 independent experiments performed in duplicate. n for each receptor variant is given in brackets. Note: data in this table is not corrected for expression levels. n. d., not determined

Supplementary Table 4 | Signaling parameters of cAMP-production of 28 β_2AR variants.

	basal	max	ISO	pEC_{50}	logT/Ka
WT (23)	58 ± 2	99 ± 1	41 ± 2	8.8 ± 0.1	8.5 ± 0.1
A78V (5)	60 ± 4	105±4	45 ± 6	7.8 ± 0.3	7.5 ± 0.2
A78N (4)	34 ± 3	85 ± 4	51 ± 4	7.3 ± 0.3	6.9 ± 0.3
A78W (5)	76 ± 3	93 ± 4	17 ± 5	7.5 ± 0.8	7.0 ± 0.7
V86I (5)	80 ± 4	100 ± 3	20 ± 4	8.3 ± 0.6	7.9 ± 0.6
V86A (5)	59 ± 4	90 ± 4	31 ± 5	7.7 ± 0.4	7.3 ± 0.4
V86Y (5)	18 ± 3	76 ± 4	57 ± 5	6.7 ± 0.2	6.3 ± 0.2
V86D (5)	29 ± 3	78 ± 5	49 ± 6	6.7 ± 0.3	6.3 ± 0.2
L124M (6)	68 ± 5	102 ± 2	34 ± 5	9.8 ± 0.4	9.6 ± 0.4
L124S (4)	40 ± 7	61 ± 3	21 ± 7	10.4 ± 0.9	9.5 ± 0.9
L124G (4)	19 ± 5	36 ± 2	17 ± 5	10.4 ± 1.2	9.3 ± 1.2
I127V (6)	45 ± 4	110 ± 3	65 ± 5	8.8 ± 0.2	8.7 ± 0.2
I127N (4)	23 ± 5	79 ± 5	57 ± 6	7.9 ± 0.3	7.5 ± 0.2
I127G (7)	22 ± 3	76 ± 2	54 ± 3	8.0 ± 0.2	7.6 ± 0.2
I278V (7)	63 ± 7	105 ± 4	43 ± 7	8.7 ± 0.3	8.4 ± 0.2
I278L (6)	23 ± 3	90 ± 3	68 ± 4	8.3 ± 0.2	8.1 ± 0.2
I278S (6)	56 ± 5	107 ± 3	51 ± 5	9.2 ± 0.3	9.0 ± 0.2
I278Q (4)	35 ± 5	70 ± 3	35 ± 6	9.1 ± 0.5	8.5 ± 0.5
K273R (6)	39 ± 5	87 ± 2	48 ± 5	9.3 ± 0.3	8.9 ± 0.3
K273L (9)	48 ± 4	96 ± 2	47 ± 5	9.2 ± 0.3	8.9 ± 0.2
K273A (7)	53 ± 6	98 ± 3	45 ± 7	9.2 ± 0.3	9.0 ± 0.2
R328K (6)	32 ± 4	94 ± 3	63 ± 5	8.6 ± 0.2	8.4 ± 0.2
R328H (5)	91 ± 5	120 ± 4	29 ± 6	7.9 ± 0.5	8.3 ± 0.6
R328L (3)	12 ± 3	70 ± 3	58 ± 3	7.9 ± 0.3	7.5 ± 0.2
R328A (4)	10 ± 2	73 ± 2	64 ± 3	8.0 ± 0.3	7.6 ± 0.3
R333L (9)	43 ± 4	97 ± 3	54 ± 4	8.9 ± 0.2	8.7 ± 0.2
R333A (6)	60 ± 5	105 ± 3	45 ± 5	9.0 ± 0.2	8.8±0.2
A271T (7)	81 ± 5	117 ± 4	36 ± 6	8.5 ± 0.3	8.7±0.3
A271W (8)	15 ± 3	76 ± 3	61 ± 4	7.6 ± 0.2	7.2±0.1

Basal, maximal (max) and ISO-induced (ISO) activity are given as % of WT maximal activity. Potency (pEC50) is expressed as -log EC50 M. Signaling efficiency (logT/Ka) was calculated as described in Methods. All data is given as average ±s.e.m. of at least 3 independent experiments performed in duplicate. n for each receptor variant is given in brackets. Note: data in this table is not corrected for expression levels.

Supplementary Table 5 | Signaling parameters of βarrestin2-engagement of 28 β_2AR variants.

	max	ISO	pEC_{50}	logT/Ka
WT (27)	98 ± 2	69 ± 3	7.0 ± 0.1	7.0 ± 0.1
A78V (6)	15 ± 3	0	n. d.	n. d.
A78N (6)	31 ± 4	0	n. d.	n. d.
A78W (4)	49 ± 2	0	n. d.	n. d.
V86I (5)	110 ± 5	44 ± 6	6.9 ± 0.3	6.5 ± 0.2
V86A (5)	52 ± 3	20 ± 4	6.6 ± 0.4	6.2 ± 0.6
V86Y (4)	38 ± 3	0	n. d.	n. d.
V86D (9)	51 ± 2	0	n. d.	n. d.
L124M (4)	84 ± 4	43 ± 7	8.2 ± 0.3	8.1 ± 0.5
L124S (4)	28 ± 3	0	n. d.	n. d.
L124G (4)	39 ± 2	0	n. d.	n. d.
I127V (4)	73 ± 5	42 ± 6	7.1 ± 0.3	6.9 ± 0.4
I127N (4)	15 ± 2	0	n. d.	n. d.
I127G (4)	7 ± 1	0	n. d.	n. d.
I278V (6)	105 ± 5	96 ± 6	6.6 ± 0.1	6.6 ± 0.1
I278L (4)	59 ± 5	49 ± 6	6.3 ± 0.2	6.1 ± 0.4
I278S (5)	34 ± 3	0	n. d.	n. d.
I278Q (4)	44 ± 3	0	n. d.	n. d.
K273R (4)	87 ± 5	35 ± 6	7.3 ± 0.4	7.1 ± 0.6
K273L (4)	82 ± 4	70 ± 6	7.4 ± 0.2	7.3 ± 0.2
K273A (8)	53 ± 4	38 ± 6	7.8 ± 0.3	7.6 ± 0.4
R328K (4)	95 ±5	38 ± 6	6.5 ± 0.4	6.4 ± 0.5
R328H (9)	87 ± 6	65 ± 7	6.5 ± 0.2	6.4 ± 0.1
R328L (4)	71 ± 4	37 ± 4	6.4 ± 0.3	6.2 ± 0.6
R328A (4)	60 ± 4	20 ± 4	6.1 ± 0.4	5.7 ± 0.9
R333L (8)	77 ± 5	32 ± 7	7.1 ± 0.4	6.9 ± 0.6
R333A (4)	89 ± 3	45 ± 5	7.4 ± 0.2	7.3 ± 0.3
A271T (6)	128 ± 6	85 ± 7	6.9 ± 0.2	6.9 ± 0.1
A271W (4)	14 ± 3	15 ± 3	6.1 ± 0.4	5.4 ± 1.2

Basal, maximal (max) and ISO-induced (ISO) activity are given as % of WT maximal activity. Potency (pEC50) is expressed as -log EC50 M. Signaling efficiency (logT/Ka) was calculated as described in Methods. All data is given as average ±s.e.m. of at least 3 independent experiments performed in duplicate. n for each receptor variant is given in brackets. Note: data in this table is not corrected for expression levels. n. d., not determined

Supplementary Table 6 | Signaling parameters of endocytosis of 28 β_2AR variants.

	max	ISO	pEC_{50}	logT/Ka
WT (19)	96 ± 3	96 ± 3	7.5 ± 0.1	7.5 ± 0.1
A78V (7)	41 ± 4	41 ± 4	6.6 ± 0.2	6.5 ± 0.2
A78N (4)	13 ± 2	13 ± 2	6.3 ± 0.3	n. d.
A78W (5)	18 ± 3	18 ± 3	7.8 ± 0.3	n. d.
V86I (4)	92 ± 3	92 ± 3	7.3 ± 0.1	7.3 ± 0.1
V86A (7)	54 ± 3	54 ± 3	7.1 ± 0.1	7.0 ± 0.2
V86Y (8)	-5 ± 1	0	n. d.	n. d.
V86D (5)	15 ± 3	15 ± 3	6.3 ± 0.3	n. d.
L124M (7)	117 ± 5	117 ± 5	8.6 ± 0.1	8.6 ± 0.1
L124S (6)	12 ± 2	12 ± 2	9.2 ± 0.5	n. d.
L124G (6)	6 ± 1	0	n. d.	n. d.
I127V (6)	84 ± 5	84 ± 5	7.6 ± 0.1	7.6 ± 0.1
I127N (6)	17 ±2	17 ± 2	6.6 ± 0.3	n. d.
I127G (6)	12 ±2	12 ± 2	7.5 ± 0.5	n. d.
I278V (8)	137 ± 8	137 ± 8	6.8 ± 0.1	6.8 ± 0.1
I278L (6)	59 ± 5	59 ± 5	7.0 ± 0.2	6.9 ± 0.2
I278S (8)	28 ± 2	28 ± 2	8.2 ± 0.2	7.9 ± 0.4
I278Q (6)	10 ± 2	10 ± 2	8.0 ± 0.5	n. d.
K273R (5)	105 ± 6	105 ± 6	8.1 ± 0.1	8.2 ± 0.1
K273L (4)	19 ± 4	19 ± 4	8.0 ± 0.5	n. d.
K273A (3)	134 ± 7	134 ± 7	8.2 ± 0.1	8.2 ± 0.1
R328K (5)	120 ± 8	120 ± 8	7.3 ± 0.2	7.2 ± 0.1
R328H (5)	92 ± 6	92 ± 6	6.7 ± 0.1	6.7 ± 0.1
R328L (5)	107 ± 6	107 ± 6	7.0 ± 0.1	7.0 ± 0.1
R328A (8)	47 ± 5	47 ± 5	5.8 ± 0.2	5.7 ± 0.3
R333L (6)	67 ± 4	67 ± 4	7.5± 0.1	7.5 ± 0.2
R333A (6)	109 ± 7	109 ± 7	8.3± 0.2	8.4 ± 0.1
A271T (4)	126 ± 5	126 ± 5	7.3± 0.1	7.3 ± 0.1
A271W (5)	-2 ± 4	0	n. d.	n. d.

Basal, maximal (max) and ISO-induced (ISO) activity are given as % of WT maximal activity. Potency (pEC50) is expressed as -log EC50 M. Signaling efficiency (logT/Ka) was calculated as described in Methods. All data is given as average ±s.e.m. of at least 3 independent experiments performed in duplicate. n for each receptor variant is given in brackets. Note: data in this table is not corrected for expression levels. n. d., not determined

Supplementary Table 7 | Mutation similarity matrix derived from the non-negative matrix factorization/K-means clustering method

	V86I	V86A	L124M	I127V	A271T	K273R	K273A	K273L	I278V	I278L	R328K	R328H	R333L	A271W	R328A	R328L	R333A	A78V	A78N	A78W	V86Y	V86D	L124S	L124G	I127N	I127G	I278Q	I278S
V86I	1	0.998	1	0.994	1	0.965	0.997	0.999	1	0.876	0.808	1	1	0	0	0	0.142	0	0	0	0	0	0	0	0	0	0	0
V86A	0.998	1	0.998	0.992	0.998	0.963	0.995	0.997	0.998	0.874	0.806	0.998	0.998	0.002	0.002	0.002	0.144	0	0	0	0	0	0	0	0	0	0	0
L124M	1	0.998	1	0.994	1	0.965	0.997	0.999	1	0.876	0.808	1	1	0	0	0	0.142	0	0	0	0	0	0	0	0	0	0	0
I127V	0.994	0.992	0.994	1	0.994	0.971	0.991	0.995	0.994	0.882	0.814	0.994	0.994	0.006	0.006	0.006	0.148	0	0	0	0	0	0	0	0	0	0	0.003
A271T	1	0.998	1	0.994	1	0.965	0.997	0.999	1	0.876	0.808	1	1	0	0	0	0.142	0	0	0	0	0	0	0	0	0	0	0
K273R	0.965	0.963	0.965	0.971	0.965	1	0.962	0.966	0.965	0.887	0.843	0.965	0.965	0.035	0.035	0.035	0.173	0	0	0	0	0	0	0	0	0	0	0.008
K273A	0.997	0.995	0.997	0.991	0.997	0.962	1	0.996	0.997	0.879	0.811	0.997	0.997	0.003	0.003	0.003	0.145	0	0	0	0	0	0	0	0	0	0	0
K273L	0.999	0.997	0.999	0.995	0.999	0.966	0.996	1	0.999	0.877	0.809	0.999	0.999	0.001	0.001	0.001	0.143	0	0	0	0	0	0	0	0	0	0	0
I278V	1	0.998	1	0.994	1	0.965	0.997	0.999	1	0.876	0.808	1	1	0	0	0	0.142	0	0	0	0	0	0	0	0	0	0	0
I278L	0.876	0.874	0.876	0.882	0.876	0.887	0.879	0.877	0.876	1	0.83	0.876	0.876	0.124	0.124	0.124	0.26	0	0	0	0	0	0	0	0	0	0	0.018
R328K	0.808	0.806	0.808	0.814	0.808	0.843	0.811	0.809	0.808	0.83	1	0.808	0.808	0.192	0.192	0.192	0.29	0	0	0	0	0	0	0	0	0	0	0.023
R328H	1	0.998	1	0.994	1	0.965	0.997	0.999	1	0.876	0.808	1	1	0	0	0	0.142	0	0	0	0	0	0	0	0	0	0	0
R333L	1	0.998	1	0.994	1	0.965	0.997	0.999	1	0.876	0.808	1	1	0	0	0	0.142	0	0	0	0	0	0	0	0	0	0	0
A271W	0	0.002	0	0.006	0	0.035	0.003	0.001	0	0.124	0.192	0	0	1	1	1	0.857	0.001	0	0	0	0	0	0	0	0	0	0.167
R328A	0	0.002	0	0.006	0	0.035	0.003	0.001	0	0.124	0.192	0	0	1	1	1	0.857	0.001	0	0	0	0	0	0	0	0	0	0.167
R328L	0	0.002	0	0.006	0	0.035	0.003	0.001	0	0.124	0.192	0	0	1	1	1	0.857	0.001	0	0	0	0	0	0	0	0	0	0.167
R333A	0.142	0.144	0.142	0.148	0.142	0.173	0.145	0.143	0.142	0.26	0.29	0.142	0.142	0.857	0.857	0.857	1	0.002	0.001	0.001	0.001	0.001	0.001	0.001	0.001	0.001	0.001	0.163
A78V	0	0	0	0	0	0	0	0	0	0	0	0	0	0.001	0.001	0.001	0.002	1	0.999	0.999	0.999	0.999	0.999	0.999	0.999	0.999	0.999	0.834
A78N	0	0	0	0	0	0	0	0	0	0	0	0	0	0	0	0	0.001	0.999	1	1	1	1	1	1	1	1	1	0.833
A78W	0	0	0	0	0	0	0	0	0	0	0	0	0	0	0	0	0.001	0.999	1	1	1	1	1	1	1	1	1	0.833
V86Y	0	0	0	0	0	0	0	0	0	0	0	0	0	0	0	0	0.001	0.999	1	1	1	1	1	1	1	1	1	0.833
V86D	0	0	0	0	0	0	0	0	0	0	0	0	0	0	0	0	0.001	0.999	1	1	1	1	1	1	1	1	1	0.833
L124S	0	0	0	0	0	0	0	0	0	0	0	0	0	0	0	0	0.001	0.999	1	1	1	1	1	1	1	1	1	0.833
L124G	0	0	0	0	0	0	0	0	0	0	0	0	0	0	0	0	0.001	0.999	1	1	1	1	1	1	1	1	1	0.833
I127N	0	0	0	0	0	0	0	0	0	0	0	0	0	0	0	0	0.001	0.999	1	1	1	1	1	1	1	1	1	0.833
I127G	0	0	0	0	0	0	0	0	0	0	0	0	0	0	0	0	0.001	0.999	1	1	1	1	1	1	1	1	1	0.833
I278Q	0	0	0	0	0	0	0	0	0	0	0	0	0	0	0	0	0.001	0.999	1	1	1	1	1	1	1	1	1	0.833
I278S	0	0	0	0.003	0	0.008	0	0	0	0.018	0.023	0	0	0.167	0.167	0.167	0.163	0.834	0.833	0.833	0.833	0.833	0.833	0.833	0.833	0.833	0.833	1

The mutation similarity matrix derived from the 1000 replicates of the nnmf-Kmeans clustering method enables quantification of clustering robustness for k =3.
Specifically, similarities with frequencies close to 0 and 1 indicate very robust assignments as these β2AR variants always demonstrate the same non-random clustering pattern in relation to one another.
Clusters are color-coded (cluster 1 – green, cluster 2 – orange, cluster 3 – blue).

Supplementary Table 8 | Ligand binding parameters determined by BRET-based binding.

	pK_i (ISO)
WT (5)	6.2 ± 0.3
A78V (4)	5.8 ± 0.1
A78N (5)	5.9 ± 0.5
A78W (5)	6.6 ± 0.5
V86I (4)	6.1 ± 0.2
V86A	n. d.
V86Y	n. d.
V86D	n. d.
L124M (4)	6.3 ± 0.3
L124S (5)	8.1 ± 0.6
L124G (5)	n. d.
I127V (4)	6.5 ± 0.2
I127N (5)	7.7 ± 0.4
I127G (5)	6.2 ± 0.7
I278V (4)	5.6 ± 0.2
I278L (4)	7.3 ± 0.1
I278S (4)	7.3 ± 0.1
I278Q (4)	8.3 ± 0.5
K273R (4)	6.5 ± 0.2
K273L (4)	6.5 ± 0.1
K273A (4)	6.0 ± 0.3
R328K (4)	5.9 ± 0.1
R328H (4)	5.9 ± 0.1
R328L (4)	5.9 ± 0.2
R328A (4)	6.2 ± 0.3
R333L (5)	6.4 ± 0.3
R333A (4)	6.3 ± 0.1
A271T (5)	5.8 ± 0.3
A271W (4)	5.8 ± 0.1

The K_D of the fluorescent ligand (S)-Propranolol-green was determined by saturation binding for each variant of the β_2AR and was followed by the determination of pK_i for ISO by competition binding studies. Data is given as average ±s.e.m. of at least 3 independent experiments performed in duplicate. n for each receptor variant is given in brackets. n. d., not determined